Wrocław University
of Science and Technology

Paweł Trybała

3D Surveying of Mining Environments using Simultaneous Localization and Mapping

Wrocław, February 2024

WUST
Politechnika Wrocławska
Wrocław University of Science and Technology
Faculty of Geoengineering, Mining and Geology
Department of Geodesy and Geoinformatics

FBK
Fondazione Bruno Kessler
Bruno Kessler Foundation
3D Optical Metrology unit

Thesis for the Degree of Philosophiae Doctor
Field of Science: Engineering and Technology
Discipline of Science: Environmental Engineering, Mining and Energy

Supervisors
Jan Blachowski, PhD, DSc, Eng
Prof. Fabio Remondino

Abstract

In the 21st century, Mobile Mapping Systems (MMSs) have undergone substantial advancements, driven by progress in sensors, software, and robotics. Although nowadays they are being successfully deployed in diverse scenarios, some sectors' conditions still pose a challenge to reliably obtain high-quality 3D data. One of the most promising industries for benefiting from mobile mapping is mining, where complex and GNSS-denied environments are common. Despite gaining more momentum in recent years in the scientific community, the surveying-related aspects of underground applications of such systems have not yet been well researched. Thus, this thesis aims to fill the gap by developing and validating a low-cost mobile mapping system capable of robustly performing 3D reconstructions in mining environments. The study adopts an iterative approach, evaluating various aspects of the system's performance against state-of-the-art methods, including comparisons with traditional surveying techniques like TLS (Terrestrial Laser Scanning). Different measures were explored to assess the quality of point clouds in subterranean conditions to ensure resilient and reliable operation.

Based on a scientific literature meta-analysis, several research objectives were established, addressing the identified scientific gaps. They include carrying out comprehensive quantitative evaluations of 3D reconstruction quality in mining conditions, establishing an open dataset for further development in mobile mapping methods, and improving open-source SLAM solutions while tailoring measurement approaches for mining environments and 3D reconstruction requirements.

A series of six scientific articles presents the progression from basic measurement systems to advanced SLAM implementations and comprehensive data quality analyses. Each publication provides unique insights and advancements to the field, tackling issues ranging from 3D data quality assessments at various underground sites to publishing an open dataset, and developing several diverse mobile mapping systems. In the final study, these efforts resulted in the creation of a universal and robust handheld mapping system capable of producing high-quality 3D reconstructions. The performance of the system was validated in diverse environments, including underground tunnels, where it matched or outperformed the quality of the results provided by commercial solutions.

The findings contribute to the broader field of research on mobile mapping technologies, particularly in challenging GNSS-denied, unstructured environments like mining areas. Overall, this dissertation not only enhances state-of-the-art SLAM algorithms and develops open-source datasets but also demonstrates the feasibility and effectiveness of using SLAM-based low-cost MMSs in mining surveying, providing a versatile, transparent, reliable and affordable solution for acquiring accurate 3D spatial data for various needs of the mining industry.

Streszczenie

W XXI wieku mobilne systemy pomiarowe (ang. *Mobile Mapping Systems, MMS*), napędzane postępem w dziedzinie czujników, oprogramowania i robotyki, znacząco się rozwinęły. Choć obecnie są skutecznie wykorzystywane w różnych zastosowaniach, warunki panujące w niektórych obiektach i obszarach wciąż stanowią wyzwanie dla zapewnienia niezawodności uzyskiwania wysokiej jakości danych 3D. Jedną z najbardziej obiecujących branż, mogących skorzystać z systemów MMS, jest górnictwo, gdzie częste są obiekty o złożonej geometrii i środowiska pozbawione sygnału GNSS. Pomimo, iż tematyka ta zyskuje w ostatnich latach popularność w społeczności naukowej, aspekty związane z pomiarami w podziemnych zastosowaniach tych systemów nie zostały jeszcze dobrze zbadane. Niniejsza praca ma na celu wypełnienie tej luki poprzez wykonanie i walidację niskobudżetowego systemu pomiarów mobilnych zdolnego do niezawodnego wykonywania rekonstrukcji 3D w środowiskach górniczych. Badania przeprowadzone zostały w podejściu iteracyjnych, oceniając różne aspekty działania systemu w porównaniu z najnowocześniejszymi metodami, w tym porównania z tradycyjnymi technikami pomiarowymi, takimi jak naziemny skaning laserowy (ang. *Terrestrial Laser Scanning, TLS*). Zbadane zostały różne miary oceny jakości uzyskiwanych chmur punktów w warunkach podziemnych, aby zapewnić niezawodną pracę systemu.

Na podstawie metaanalizy literatury naukowej ustalono cele pracy, adresując zidentyfikowane luki badawcze. Obejmują one przeprowadzenie wyczerpujących, ilościowych analiz jakości rekonstrukcji 3D w warunkach górniczych, stworzenie otwartego zbioru danych do dalszego rozwoju metod MMS oraz poprawę otwartych rozwiązań Symultanicznego Lokalizowania i Mapowania (ang. *Simulataneous Localization and Mapping, SLAM*), dostosowując podejścia pomiarowe do środowisk górniczych i wymagań dotyczących rekonstrukcji 3D.

Seria sześciu artykułów naukowych przedstawia postęp badań od podstawowych systemów pomiarowych do zaawansowanych implementacji SLAM i kompleksowych analiz pozyskiwanych przez nie jakości danych 3D. Każda publikacja dostarcza unikalnych spostrzeżeń w dziedzinie, podejmując zagadnienia począwszy od oceny jakości danych 3D w różnorodnych podziemnych polach testowych, poprzez publikację otwartego zbioru danych, aż do opracowania kilku systemów pomiarów mobilnych. W końcowym badaniu te

wysiłki prowadzą do stworzenia uniwersalnego i solidnego systemu mapowania ręcznego zdolnego do generowania wysokiej jakości rekonstrukcji 3D. Wydajność systemu została zweryfikowana w różnych środowiskach, w tym w tunelach podziemnych, gdzie dorównała lub przewyższyła jakość wyników uzyskiwanych przez komercyjne rozwiązania.

Przedstawione wyniki przyczyniają się do rozwoju szerszej dziedziny badań nad technologiami mobilnych systemów pomiarowych, zwłaszcza w trudnych warunkach pozbawionych sygnału GNSS, takich jak kopalnie. Podsumowując, niniejsza praca doktorska nie tylko wprowadza usprawnienia do najnowszych algorytmów SLAM i wzbogaca otwarte zbiory danych, ale także demonstruje wykonalność i skuteczność stosowania MMS opartych na algorytmach SLAM w pomiarach w warunkach górniczych, zapewniając wszechstronne, przejrzyste, niezawodne i niskokosztowe rozwiązanie do uzyskiwania danych przestrzennych 3D o wysokiej dokładności dla różnych potrzeb przemysłu górniczego.

Acknowledgements

This thesis is not the solitary achievement of an individual working in isolation. It is the culmination of years of learning, collaboration, passionate discussions, vigorous brainstorming, field experiments, and teamwork. Therefore, I would like to extend my sincere gratitude to all those who have directly and indirectly contributed to my research and personal development during my PhD studies. This encompasses researchers, professionals, students, and enthusiasts in the fields of surveying, robotics, geoscience, and related areas with whom I have had the privilege to interact. While undoubtedly I will overlook some individuals (I am sorry!), I would like to acknowledge those to whom I owe the most:

My supervisors, Jan and Fabio, for their guidance, unwavering support in all aspects and gentle introduction into the world of science.

The numerous coauthors of my articles, for their collaboration and for fostering an environment where I could grow and flourish amidst multidisciplinary challenges.

My friends from the PhD studies: Ania(s), Darek, Marek, Michał, Monika, Natalia, Ola(s), Karolina, Paulina, for many thought-provoking conversations and creating a flawless, supportive atmosphere during stressful times.

My colleagues from Digital Mining Center, for the years of teamwork and the blood, sweat and tears shared during the field tests; special acknowledgment to Prof. Zimroz and Dr. Szrek, whose leadership and vigor propelled numerous scientific endeavors during this period.

My colleagues from Fondazione Bruno Kessler, especially Elisavet, Fabbio and Luca, for a warm welcome to the group and many brainstorming sessions in the realm of surveying and photogrammetry.

My colleagues from Technische Universität Bergakademie Freiberg, especially Prof. Benndorf and Jing, for the fruitful collaboration and bringing the mining surveying expertise into our discussions.

Lastly, I extend my heartfelt thanks to my family, especially my partner Gabriela and my father Piotr, without whom none of this would have been possible.

Nothing ages as fast as the future.
Nic się teraz nie starzeje tak szybko, jak przyszłość.
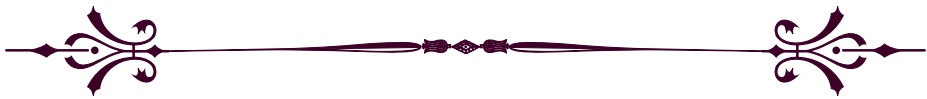
- Stanisław Lem,
Summa Technologiae

Nomenclature

Below is a list of common abbreviations, mostly from fields of geomatics and robotics, used in this thesis. For more in-depth explanations and definitions, the reader is advised to look into the works by Granshaw (2020) and Thrun (2002).

ACRONYMS

AI	Artificial Intelligence	GPS	Global Positioning System
ARE	Absolute Rotation Error		
ATE	Absolute Translation Error	GSD	Ground Sampling Distance
BA	Bundle Adjustment	IMU	Inertial Measurement Unit
CML	Concurrent Mapping and Localization; see SLAM	INS	Inertial Navigation System
CNN	Convolutional Neural Network	LiDAR	Light Detection and Ranging
CSIRO	Commonwealth Scientific and Industrial Research Organisation	MLS	Mobile Laser Scanning
		MMS	Mobile Mapping System
		MMT	Mobile Mapping Technique; see MMS
DARPA	Defense Advanced Research Projects Agency	MVS	Multi-View Stereo
DEM	Digital Elevation Model	NDT	Normal Distributions Transform
DL	Deep Learning		
DoF	Degrees of Freedom	NeRF	Neural Radiance Fields
DSLR	Digital Single-Lens Reflex Camera	PGO	Pose Graph Optimization
DSM	Digital Surface Model	ROS	Robot Operating System
DTM	Digital Terrain Model; see DEM	RRE	Relative Rotation Error
		RTE	Relative Translation Error
FoV	Field of View		
GNSS	Global Navigation Satellite System	RTK	Real-Time Kinematics

SE(x) x-dimensional Special Euclidean Group

SLAM   Simultaneous Localization and Mapping

TLS   Terrestrial Laser Scanning

ToF   Time-of-Flight

UAV   Unmanned Aerial Vehicle

UWB   Ultra Wideband

V-SLAM   Visual Simultaneous Localization and Mapping

Contents

Part II   Publications P1–P6   71

Part I

SCIENTIFIC CONTEXT AND CONTRIBUTIONS

CHAPTER 1

Introduction

Mobile mapping, a concept that can be traced back in the scientific geomatics community at least to the early 1990s (Bossler et al., 1991; Bossler and Toth, 1995), has undergone remarkable evolution fueled by technological advancements in sensors, mobile platforms and computing capabilities. The term *mobile mapping system* has been broadly defined in the literature as (Al-Bayari, 2019): "an integrated system of surveying sensors mounted on a vehicle" or more generally as (Elhashash et al., 2022): "an integrated system of mapping sensors mounted on a moving platform to provide the positioning of the platform while collecting geospatial data". However, as highlighted even earlier in the review study of (Grejner-Brzezinska et al., 2004):

> "mobile mapping that originally emerged as a purely mapping technology, has started its transition from rather exclusive data acquisition applications supported by high quality GPS/INS, to multitasking information systems capable of acquiring, storing, manipulating, and displaying spatially referenced information to provide a variety of mobile services related to spatial analysis, data management, decision making, etc."

In the article, the complex nature and diversity of solutions used for different purposes of acquiring and processing geospatial data are further described. Almost twenty years later, those words still remain pertinent, with Mobile Mapping Systems (MMSs) being widely adopted by end users in multiple industries, from construction, through city planning, mining, to forestry. Not only is metric 3D reconstruction becoming accessible with readily available tools and frameworks, but more advanced topics, such as semantic segmentation, scene understanding and autonomous operation in multiple environments are being successfully explored by researchers (Behley et al., 2019; Kümmerle et al., 2015; Li et al., 2020; Tranzatto et al., 2022).

   Another aspect of Mobile Mapping Technologies (MMTs) that has advanced greatly over the years is sensor fusion. The introduction of concepts known from probabilistic robotics (Thrun, 2002) and the growing availability of relatively low-cost sensors enabled the creation of methods capable of long-term,

reliable and robust mobile mapping in GNSS-denied areas. The prospect of automating the process of performing high-precision and dense 3D reconstruction opens new frontiers in metric 3D data acquisition, making these technologies immensely attractive in various domains. Moreover, novel sensors and approaches, such as event cameras, UWB- or signal-of-opportunity-based localization methods are actively being explored, promising to enhance the reliability of MMSs in the future. Collectively, these innovations are becoming integral to modern technologies in the currently thriving artificial intelligence (AI) applications in multiple sectors, including mobile robotics and highly detailed 3D city modeling. They form the backbone of specialized systems tailored to specific industrial use cases.

Given the enormous value generated, the mining sector emerges as one of the main possible beneficiaries of MMSs. The harsh conditions present in mining environments, the imperative to reduce workers' on-site presence and limit the manual labor, extensive operational scale, and the prevalent use of spatial data in mining surveying and mining operation monitoring and planning make it particularly appealing for MMS integration due to the possibility to greatly shorten (or automate) the 3D reconstruction process with portable or robotic solutions. The complexity of underground spaces, coupled with the necessity to ensure robustness and safety in industrial facilities, naturally creates interest and demand for research efforts that focus on those aspects. The performance of MMTs commercially available nowadays, as well as their open-source counterparts, degrades greatly in challenging, GNSS-denied environments, such as underground mines. Carrying out reliable and accurate 3D reconstructions in such conditions is still deemed an unsolved task in the scientific community. Moreover, the introduction of low-cost 3D sensors to the market, such as LiDARs and RGB-D cameras, considerably boosted the progress in the research field of mobile mapping and made it possible to democratize the access to 3D measurements for enthusiasts and smaller companies. This thesis strives to address these needs, presenting a practically oriented and heavily test-driven study of performing 3D mobile mapping with SLAM algorithms in subterranean sites.

Mobile Mapping for Mining Applications

## 2.1 AN OVERVIEW OF 3D DATA ACQUISITION METHODS

3D reconstruction, sometimes called also **3D mapping**, is a broad collective term that, in the context of surveying, could be described as an overall set of measurement methods used to determine the shape of an object or area in the three-dimensional metric space. For its simplest form, sometimes referred to as a "2.5D map" or an "elevation/height map", where for every planar point only one unique elevation value exists, mentions of the first representation of height difference depiction can be traced back to the Turin Papyrus map from ancient Egypt (Harrell and Brown, 1992). However, at this stage, the hills and mountains were depicted only symbolically. The first measurement-based maps appeared much later. Interestingly, the first known contour map did not convey information about elevation, but depth: a navigation map of the Dutch River from 1584 by Pieter Bruinsz represented a constant-depth line in the form of an isobath (as given by Rann and Johnson (2019)). However, the first mention of a contour map of the ground elevation comes from 1778, from the survey of a mountain in Scotland (Hutton, 1778). The idea of mapping being of great interest of mining sector is stressed by the fact that both the Hutter's map and the earlier Turin Papyrus map both acted simultaneously as geological maps due to the users' interest in the locations of mineral deposits.

Today, large-scale DEMs or DSMs can be relatively easily obtained by various means, from terrestrial methods (Ozhygin et al., 2021; Piermattei et al., 2019; Vaaja et al., 2011), through aerial and UAV surveys (Nex and Remondino, 2014; Rock et al., 2012), to satellite-based measurements (Moreira et al., 2004). Depending on specific use requirements, such as GSD (Ground Sampling Distance), desired accuracy, texturization or survey frequency, an appropriate strategy of performing a survey can be selected. However, in the mining context, the application of DEMs is limited mainly to open pit mining (Chen et al., 2015; Wang et al., 2020; Xiang et al., 2018; Yu et al., 2010) or surface subsidence monitoring of active and post-mining areas of underground deposit exploitation (Figure 2.2) (Ćwiąkała et al., 2020; Dong et al., 2022; Ignjatović Stupar et al.,

2020; Lian et al., 2021; Owczarz, 2020; Ren et al., 2019a; Zhang et al., 2017). Thus, a much more attractive but challenging concept is performing a full volumetric 3D reconstruction, which enables flexible and proper representation of both underground and overground mining scenes (Singh et al., 2022).

FIGURE 2.1. Perspective view of a photogrammetric 3D reconstruction of an open pit mine (Chen et al., 2015)
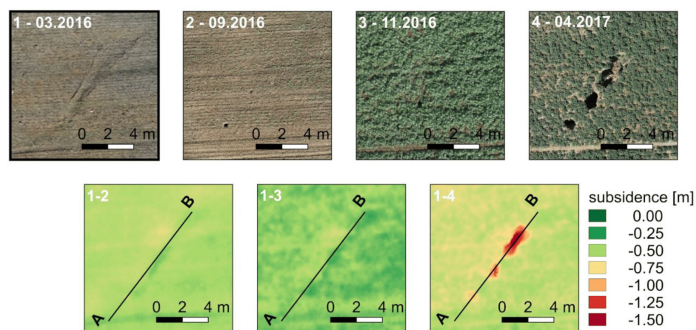
FIGURE 2.2. Results of subsidence monitoring through UAV photogrammetric surveying (Ćwiąkała et al., 2020)

Independently of the means of transportation of the sensor acquiring data, required to describe the target object shape, in the context of modern 3D reconstruction, two main groups of methods can be distinguished. The first, older, is **photogrammetry**, which encompasses all methods of performing measurements on image(s) and their interpretations to describe an object's geometry and location in space (Luhmann et al., 2023), of which the first mention can be found in the 19th century (Meydenbauer, 1867). In this extensive group, several subgroups of different approaches to estimate the target's shape exist. For large-scale 3D reconstruction, stereo vision and MVS can be considered the main pillars. In essence, these traditional methods are based on matching and triangulating features found in pairs or sets of multiple images for the so-called sparse reconstruction to estimate the camera poses, followed by a dense

reconstruction to actually obtain the dense 3D point cloud of the surveyed area.

However, photogrammetry faces multiple challenges in the conditions of an underground mine (Gurgel and Preusse, 2021). In unstructured environments, especially with weak lighting, the lack of natural light sources causes the need to use artificial illumination, which is also often not present in the scene. This can negatively impact the data acquisition process, resulting in poorly illuminated images (see Figure 2.3). In addition, commonly encountered elongated and narrow structures in underground mines, such as vertical shafts and tunnels, hinder the ability to construct a well-defined camera network, with a favorable network geometry for accurate 3D reconstruction.

To a limited extent, because of the common challenges mentioned above, photogrammetric solutions are also seldom applied in underground mining environments. Examples include the monitoring of rock mass and short-term excavation progress (Benton et al., 2016), geological documentation (Sturzenegger and Stead, 2009) and displacement monitoring (Benton et al., 2017; Slaker, 2015). An example of photogrammetry application in underground conditions is shown in Figure 2.4.

FIGURE 2.3. Example of a poorly illuminated underground scene with artificial lighting source (Trybała et al., 2023d)

One of the currently emerging methods of 3D reconstruction in computer vision involves the use of neural radiance fields (NeRFs; Mildenhall et al. (2021)). Those methods utilize different deep learning architectures to learn the 3D volumetric representation of the scene on the basis of images taken from known camera poses (often estimated with, e.g. SfM) and behavior of the light rays. Similarly, Gaussian splats have been proposed as an alternative to represent the scene geometry from radiance fields (Kerbl et al., 2023). Such methods are more focused on reconstructing objects than large-scale scenes, more common in mining applications, and their accuracy and reliability has yet to be proven in diverse scenarios. Nevertheless they should be closely followed in the near future, as they can already be a valuable complementary approach to
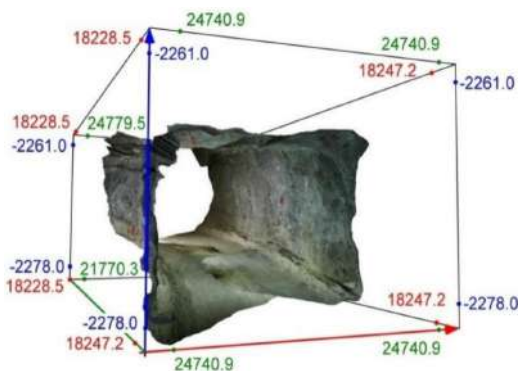
FIGURE 2.4. Photogrammetric 3D reconstruction of a small part of an underground mine tunnel (Benton et al., 2017)

photogrammetric processing in cases where traditional methods struggle (e.g., low-textured objects, reflective surfaces) (Mazzacca et al., 2023; Remondino et al., 2023).

For the second large group of methods, based on **laser scanning**, two distinct sensor categories can be discerned: those measuring distances using the time-of-flight (ToF) principle and those using phase-shift estimation technique. Although this distinction does not influence the standard data processing workflow (i.e., excluding the case of full waveform analysis), they are important in survey planning due to their different characteristics. In general, ToF scanners tend to have longer maximum ranges (up to a few kilometers) at the trade-off of reaching slightly lower accuracy and precision of distance measurement, and thus the final 3D point position compared to the phase-shift-based scanners (Suchocki, 2020). Nevertheless, the data acquisition process is carried out in the same way through obtaining overlapping dense point clouds of the surroundings from different scanner positions and coregistering them in the same reference frame using either clearly identifiable artificial targets (plates, circles, spheres) or in a cloud-to-cloud approach (if a sufficient overlap between point clouds is provided). Both methods can suffer from ubiquitous dust present in the industrial mines.

TLS has been extensively used in mine surveying for the past 15 years. Despite a fairly heavy workload, it has been applied to multiple use cases, including dense 3D reconstruction of underground tunnels (Kajzar et al., 2015), geological structure localization (Kasza, 2018), investigating conditions of different elements of mining infrastructure (Gallwey et al., 2021; Trybała et al., 2020) and displacement monitoring (Slaker, 2015).

Both laser scanning and photogrammetry suffer from different inconveniences of underground mining conditions. The resulting 3D point cloud of

laser scanning is already properly scaled, even if not georeferenced with ground control points. This needs to be addressed in photogrammetric surveys, and if the control point network is already present at the site, it is usually not very dense and easy to include in the survey. Some dedicated solutions have been developed to address this problem (García-Luna et al., 2019). Although photogrammetry has a potentially higher physical accuracy limit in close-range applications than TLS (with currently available hardware solutions), difficulties in dense reconstruction of textureless areas and usually short baselines caused by restricted movement and constrained space in underground corridors often contribute to the quality degradation of the final photogrammetric product.

For the laser scanning, constrained spaces cause multiple occlusions and severely extend the length of the data acquisition process in the common multi-station data acquisition approach. Apart from the 3D geometry, both methods can provide additional information about the surveyed surroundings. The TLS data contains reflectance values of the laser beam and the images convey RGB information. They cannot be directly compared and both have been shown to enrich the data, especially for classification purposes (Li and Cheng, 2018). The main advantage of RGB data is the possibility of texturization with real object colors, which is the most natural way to perceive them for humans and could be the preferred solution for visualization purposes. However, a similar effect can be obtained with a TLS paired with a digital camera (Figure 2.5).

FIGURE 2.5. TLS point cloud of an underground tunnel textured with an DSLR image (Trybała, 2021)

Alternatively to the well-established surveying methods described above, mobile mapping methods emerged in the 90s of the 20th century (Grejner-Brzezinska et al., 2004) in the geomatics community. Those efforts were preceded by similar research interests of the robotic community investigating first simultaneous localization and mapping methods in the late 1980s (Durrant-

Whyte and Bailey, 2006). Their core idea lies in substituting tedious stop-and-go acquisition strategy of high-volume data (e.g., a single TLS station scan) with collecting higher-frequency measurements with a sensor in motion. Moreover, while mobile mapping can still be performed with high-precision, survey-grade instruments, new methods are emerging that allow using low-cost sensors (industry-grade LiDAR scanners, simple digital cameras, MEMS IMUs) to achieve satisfactory results of 3D reconstruction. As these concepts are in great agreement with the aim of this thesis and the challenges of 3D surveys in mining environments, those methods will be described in detail in Sections 2.2 and 2.3.

Moreover, although not used directly to map the environment due to the type of data they acquire, several other sensors are very relevant to mobile mapping methods. Those devices generally lack the means to convey dense information about the environment, but can provide useful information for estimating the sensor position or motion in the approach called *sensor fusion*, in the end improving the mapping results (Alatise and Hancke, 2020; Xu et al., 2022b). Those sensors include global positioning systems, such as GNSS receivers (Jende et al., 2018), radio-based local positioning systems (Chehri et al., 2009) and sources of relative position information, such as mapping vehicle wheel odometry and IMUs (Thrun, 2002).

Even though the topic of 3D reconstruction is also relevant in e.g. reverse engineering, manufacturing, medical imaging, where some additional relevant methods exist (e.g., photometric stereo, structure light and triangulation scanners, X-ray imaging, or computer tomography), the scope of this thesis does not cover them due to their irrelevance to the large-scale mining applications.

2.2   Simultaneous Localization and Mapping

The topic of Simultaneous Localization and Mapping (SLAM), also known as Concurrent Mapping and Localization (CML), emerged in the late 1980s, when the robotic community started adapting probabilistic methods in the research fields of mobile robot control and perception (Durrant-Whyte and Bailey, 2006). The problem raises the issue of localization of the robot (or in generalized form, an agent with capabilities of sensing some geometrical features of its surroundings) in the unknown environment while simultaneously building and expanding its map, without any knowledge of it available a priori. From surveying techniques, it is known that the task of localization requires information about the map (i.e. coordinates of known and identifiable landmarks) and the task of mapping requires knowledge of the sensor position, thus turning SLAM into a "chicken and egg problem" requiring an iterative and concurrent approach to solve it (Będkowski, 2022). Developing a single "correct" solution to SLAM is further hindered by numerous issues such as the natural tendency of relative positioning methods (i.e., odometry, integrating inertial measurements) to accumulate errors in time (so-called *drift*), variety of challenges in different environments, a rapidly growing dimensionality of the feature space as the map expands and the challenge of data association (Bailey and Durrant-Whyte, 2006).

As solving SLAM inherently involves processing various noisy measurement data, a probabilistic approach is usually used to define the *full SLAM* problem as (2.1) (Grisetti et al., 2010):

$$p(x_{1:T}, m | z_{1:T}, u_{1:T}, x_0) \qquad (2.1)$$

which can be read as estimating the full posterior probability of the environment map $\mathbf{m}$ and the sensor trajectory $x_{1:T} = \{x_1, \ldots, x_T\}$ at timestamps $\{1, \ldots, T\}$ given the subsequent pose change estimates (i.e., odometry) $u_{1:T} = \{u_1, \ldots, u_T\}$ and a set of observations connected to the surveyed environment $z_{1:T} = \{z_1, \ldots, z_T\}$.

A simple graphical representation of the problem is shown in Figure 2.6. For continuous SLAM, the $x_{1:T}$ is approximated directly as a continuous smooth function, e.g., a spline, while for a pose graph approach, it is a set of discrete $SE(2)$ or $SE(3)$ poses (Droeschel and Behnke, 2018). Moreover, the problem can be limited to the so-called *online SLAM*, which limits the computational effort, but estimates only the last agent pose x_T, discarding or at least not optimizing previous poses (Grisetti et al., 2010).
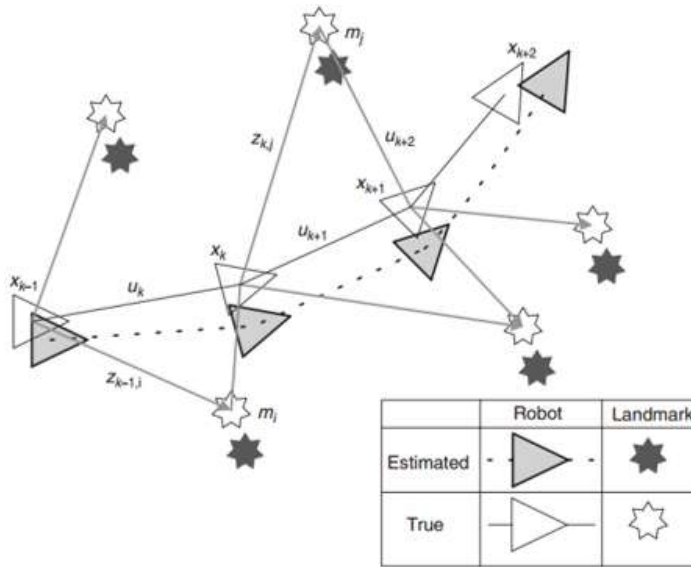
FIGURE 2.6. SLAM problem definition (Bailey and Durrant-Whyte, 2006)

Despite the theoretical foundations of the solvability of the SLAM problem being laid in the early 2000s (Dissanayake et al., 2001) and the publication of the 3 DoF SLAM algorithms now regarded as stable and reliable in practical robotic applications in planar environments (Grisetti et al., 2005, 2007), changing the problem space from SE(2) manifolds (3 DoF poses) to SE(3) (6 DoF poses) greatly increases its difficulty. However, the enticing possibility of rapidly capturing all three geometrical dimensions of objects and large-scale scenes opened up opportunities for SLAM to enable 3D metric reconstructions rivaling photogrammetry and TLS and enter the surveying market. Such a chance is also of great interest for the robotics community, since robust 3D perception is an essential requirement for increasing robot and drone autonomy in challenging applications.

Nonetheless, in general, metrology-related fields are much more strict and demanding in terms of the required quality of 3D reconstruction. In mobile robotics, the essential characteristics of robust SLAM in most applications include: correct topology, smooth and qualitatively correct localization allowing the mobile robot to reliably navigate and operate in its target environment and possibility of subsequent localization on a map created with SLAM. In contrast, in surveying sector, the core characteristics of the desired output of SLAM are map-centric, not agent-centric. A high quality and consistency of 3D reconstruction of a scene is sought after, with the essential relevant metrics being accuracy, precision and completeness of the metric representation of a surveyed scene.

Historically, two means of representing the map in SLAM algorithms can be found in the literature, sets of landmarks (keypoints, linear, planar or other features) and grid-based (or, in case of mapping in 3D space, volumetric) representations (Thrun, 2002). Their examples are shown in Figure 2.7. The former one requires additional steps of feature detection, matching and dense reconstruction and assumes the presence and stability of the features in the data of the surveyed area, but in such favorable conditions possibly increases robustness and quality of positioning while limiting the total computational cost of the algorithm. The latter naturally provides a dense 3D reconstruction as an output (in contrast to sparse landmarks), but increases the memory consumption and thus worsens the scaling of the computational cost of loop closure detection.
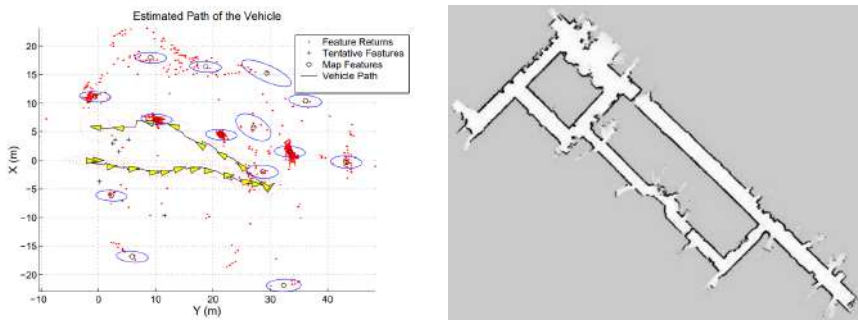

FIGURE 2.7.   A landmark (left) and occupancy grid (right) representations of 3 DoF SLAM maps (Thrun, 2002)

In recent years, a growing number of studies have proposed various approaches to solving the 6 DoF SLAM (Figure 2.8). To identify research trends, prevailing methods and the most important articles and institutes, a meta-analysis of the literature has been carried out on the basis of the *Scinapse* search engine, which supports queries to multiple databases of academic journals (Färber, 2019; Lo et al., 2020; Nature, 2017; White, 2020) and allows advanced filtering and analysis options. Bibliographic information and abstracts were automatically retrieved from the database for queries of study topic relevance with the keyword pair of "SLAM" and 'simultaneous localization and mapping". The results were filtered out by relevant fields, since lookup also returns studies from genetics, where the term "SLAM" means "signalling lymphocyte activation molecule": a specific family of genes.

The DOIs of the articles were used to import the database into the VOS Viewer meta-analysis and visualization software (Van Eck and Waltman, 2010). In total, 9 278 topical works were included. To avoid cluttering up the visualizations and limit the influence of less relevant studies, for further analysis, only the top 100 articles were analyzed according to their citation count. This set the citation threshold at 250.

In the provided visualizations, the size of nodes in the graphs indicates their relative frequency or citation count, while the width of the connection between nodes indicates their co-occurrences, similarity based on references, co-citations or number of joint works. For color coding papers, topics and author affiliations, the clustering algorithm implemented in VOS Viewer was used (Van Eck and Waltman, 2017). Nevertheless, the clustering parameters and chosen number of clusters heavily influenced the process, therefore caution must be kept during their interpretation. It should also be noted that due to setting the citation threshold limit quite hard, the latest publications are naturally put in a disadvantage and are underrepresented. Thereafter, this analysis is not claimed to be exhaustive and only uses the articles' popularity as a proxy of their influence on the field, in practice measurable only after a certain period of time.
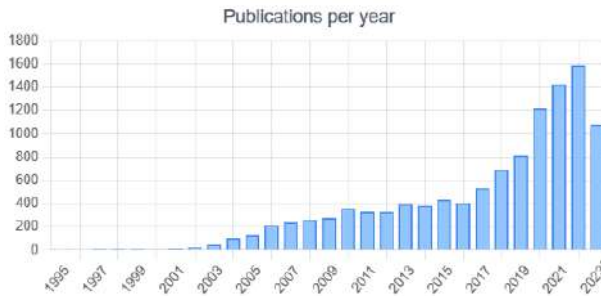
FIGURE 2.8. SLAM-related studies per year based on *Scinapse* multi-database search from 1995 up to October 2023

First, keyword extraction was performed from all reviewed articles, which is presented in Figure 2.9. Several leading topics can be found in the graph:

- particular elements of SLAM systems: loop closure detection, feature extraction, object tracking, visual place recognition, occupancy grid, visual SLAM and odometry, bundle adjustment, convolutional neural network (CNN); also different types of features, i.e., points and lines,

- general areas of research: proposing new approaches and solutions, theoretical investigations of observability, consistency, geometric constraints, experimental evaluation,

- different types of mobile mapping approach: real-time, active, visual, monocular, stereo, RGB-D, semantic, particle, SfM,

- names of popular algorithms ORB-SLAM (Mur-Artal et al., 2015), Hector SLAM (Kohlbrecher et al., 2011) and Fast-SLAM (Montemerlo et al., 2002),

FIGURE 2.9. Term network in the analyzed publications' abstracts and titles for all SLAM-related works. Two terms, "cooperative SLAM" and "wireless sensor network", did not match any cluster

- environments and fields of SLAM application: search and rescue, indoor scenes, GNSS-denied environment, low-cost,

- robotic platforms and sensors targeted in the study: UAV, quadrotor, mobile robots, underwater vehicles.

Two terms, cooperative SLAM and wireless sensor network, created their own clusters likely because both propose significantly different approaches to the SLAM problem.

These clusters indicate the main directions in mobile mapping research. What can be seen is that researchers have been focused mostly on proposing novel SLAM approaches, its particular components or applying them in different fields and with various platforms. The theoretical foundations of SLAM solutions have also been covered by some influential studies (Dissanayake et al., 2001; Huang and Dissanayake, 2007). However, the part of mapping quality and its evaluation have not received much attention. The most cited articles on the topic of SLAM evaluations usually investigate trajectory estimation accuracy and time-wise performance of the algorithm (Endres et al., 2012a;

Geiger et al., 2012a; Huang and Dissanayake, 2007) or in the best case they introduce very simple point cloud comparisons in simulated environments (Handa et al., 2014a).

In the next part, individual influential articles were investigated. The co-citation graph of examined publications is presented as clusters in Figure 2.10.

Bibliographic coupling of the same set of articles is presented in Figure 2.11 as clusters and in Figure 2.12 by year of publication. These graphs examine which pairs of articles reference similar studies. This characteristic indicates the correlation between the foundations of both paired works.

The first graph in Figure 2.10 shows which articles are often referenced jointly in other works. Thus, it informs of the similarity of those studies. In the clusters, we can see some groupings of works regarding:

- monocular visual SLAM, in red Davison et al. (2007); Leutenegger et al. (2013); Mur-Artal et al. (2015); Strasdat et al. (2012),

- frameworks dealing with RGBD SLAM, in yellow (Endres et al., 2012b; Handa et al., 2014b; Kerl et al., 2013; Whelan et al., 2015b, 2016),

- visual SLAM in dynamic environments, in violet (Bescos et al., 2018; Li and Lee, 2017; Sun et al., 2017; Yu et al., 2018),

- SLAM backend, focusing on strategies of fusing and smoothing information gained in time, in blue and cyan (Bosse et al., 2004; Dellaert and Kaess, 2006; Estrada et al., 2005; Grisetti et al., 2010; Guivant and Nebot, 2001; Kaess et al., 2012; Kümmerle et al., 2011; Thrun et al., 2004),

- more heterogeneous green cluster, containing theoretical works on SLAM consistency and solvability (Bailey et al., 2006; Dissanayake et al., 2001; Huang and Dissanayake, 2007), but also stereo SLAM (Cummins and Newman, 2008, 2011; Gomez-Ojeda et al., 2019; Konolige and Agrawal, 2008) and others.

Review works span across multiple clusters due to their wide scope (Bailey and Durrant-Whyte, 2006; Bresson et al., 2017; Cadena et al., 2016; Durrant-Whyte and Bailey, 2006; Fuentes-Pacheco et al., 2015; Saeedi et al., 2016; Taketomi et al., 2017). Furthermore, the only studies that strictly focus on the LiDAR SLAM by Shan and Englot (2018) and by Hess et al. (2016) do not fit any group.

A related graph of bibliographic coupling is presented in Figure 2.11. This time, the graph is very dense, which is understandable given the reputation and popularity of those articles. Although it is difficult to clearly delineate the clusters, studies on the left side of the figure predominantly present theoretical
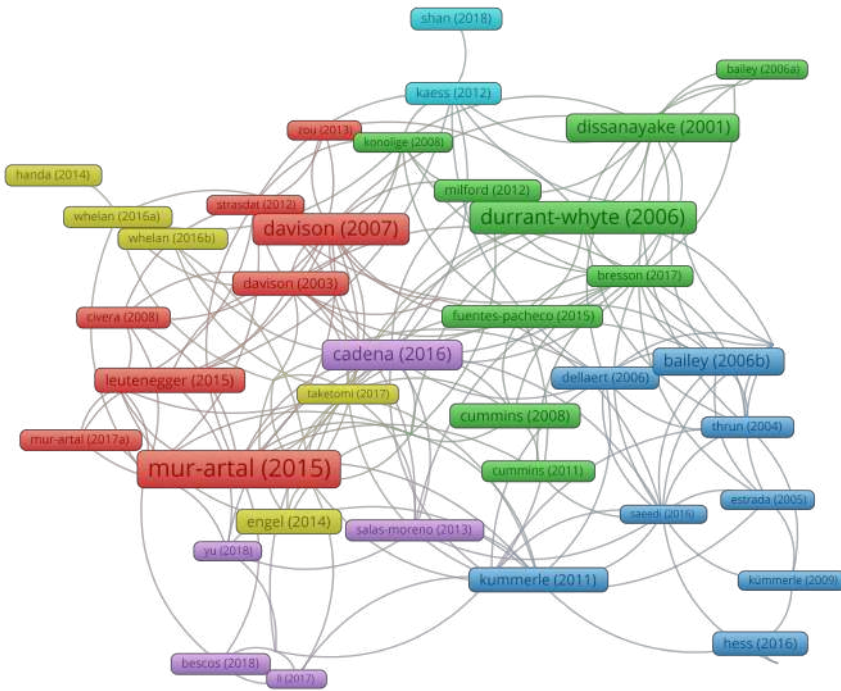
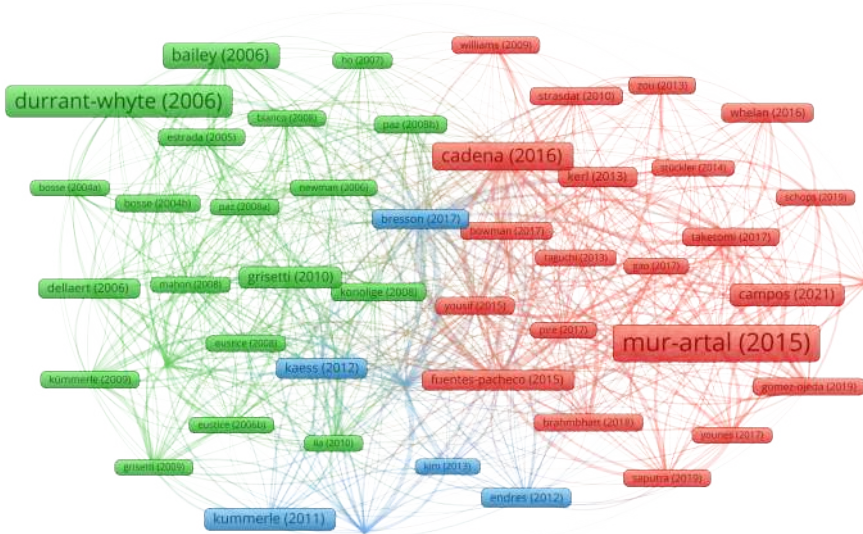**FIGURE 2.10.** Co-citation network of the most cited SLAM works

FIGURE 2.11. Bibliographic coupling by article for all SLAM-related works

or high-level solutions for the SLAM problem. In the center, the review studies are located. Finally, the rightmost cluster cover specific frameworks and applications of SLAM.

The last visualization of the bibligraphic coupling of publications (Figure 2.12) targets the issue of whether the similarity of references in the studies is caused by their setting in time, which is confirmed by the smooth color transition of most works in the network. Notable exceptions are articles that present a highly influential ORB-SLAM framework (Mur-Artal et al., 2015), foundations of semantic SLAM (Bowman et al., 2017) and survey papers of Cadena et al. (2016) and Bresson et al. (2017).
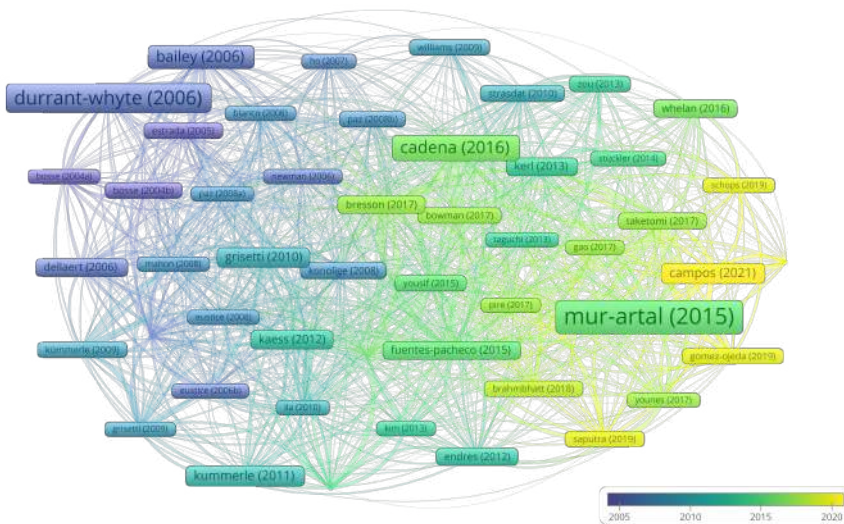
FIGURE 2.12. Bibliographic coupling by year for all SLAM-related works

Finally, the bibliographic coupling has been examined by drawing connections between the affiliated institutions of the authors of all analyzed articles (Figure 2.13). Even though the graph brings some insight into the collaboration between different institutes, the main output of this analysis is the identification of the most influential research groups. The size of the node provides information on their relative total citation count. The importance of Carnegie Mellon University and ETH Zürich is clearly visible. Several other institutions from China, Japan and the USA are also present. Germany, Peru and Taiwan are all represented by single institutions.

As mentioned earlier, the abovementioned analysis has been constrained by number of citations to try to objectively identify trends in the field. Moreover, some important studies were not included due to the usage of different words, which did not match the keywords of the query (e.g., Labbé and Michaud
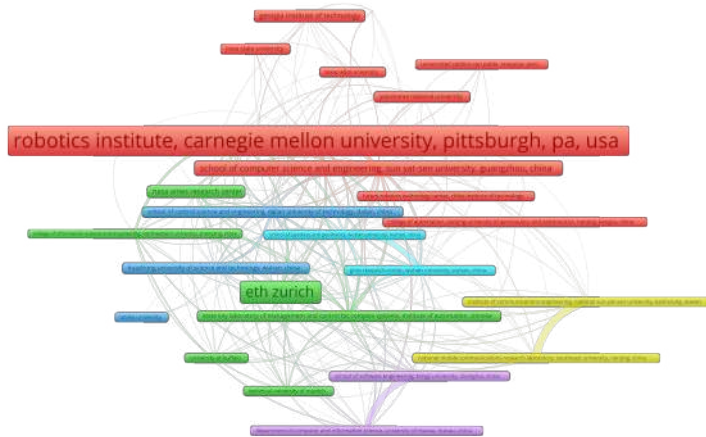
FIGURE 2.13. Bibliographic coupling by institutions for all SLAM-related works

(2019)). To fill this gap, a look into the available, more recent open source SLAM frameworks was taken. An author's subjective list of approaches used in various applications was compiled and last updated in October 2023. The exploration was based on the examination of articles from the most influential research groups listed above and the search on *github.com* open code repository.

The relevant algorithms are divided into *odometry* and *SLAM* frameworks, depending on whether they are capable of performing pose estimation using only sequential data or are able to adjust the odometry drift by applying other methods (e.g., detecting loop closures and integrating them in a pose graph or applying frame-to-map global feature matching approach). For each group, frameworks are listed in chronological order of publishing the article describing their latest major version.

- LiDAR odometry:
    - LiDAR Odometry and Mapping: LOAM (Zhang and Singh, 2014) and its variations, LeGO-LOAM (Shan and Englot, 2018) and FLOAM (Wang et al., 2020),
    - LiDAR-Inertial Odometry and Mapping: LIO-Mapping (Ye et al., 2019)
    - Livox Lidar Odometry and Mapping: LiLi-OM (Li et al., 2021),
    - Direct Lidar Odometry: DLO (Chen et al., 2022),
    - Lidar Odometry for Consistent operation in Uncertain Settings: LOCUS (Reinke et al., 2022),
    - FAST-LIO (Xu et al., 2022a),

- LiDAR SLAM:
    - Google Cartographer (Hess et al., 2016),
    - High-Density Graph LiDAR SLAM: HDL-Graph-SLAM (Koide et al., 2019),
    - Semantic Surfel-based Mapping: SuMa++ (Chen et al., 2019),
    - Multi-Metric Linear Least Square (Pan et al., 2021),
    - Contonous-time ICP (Dellenbach et al., 2021),
    - SC-LiDAR SLAM (Kim et al., 2022)
    - Large-scale Autonomous Mapping and Positioning: LAMP (Chang et al., 2022),

- Visual odometry:
    - Semidirect Visual Odometry (Forster et al., 2016)
    - Direct Visual Odometry (Engel et al., 2017),
    - OpenVINS (Geneva et al., 2020),
    - Tracking and Dense Mapping: TANDEM (Koestler et al., 2022),

- Visual SLAM (V-SLAM):
    - Parallel Tracking and Mapping: PTAM (Klein and Murray, 2007),
    - RGB-D SLAM (Endres et al., 2013),
    - Large-scale Direct SLAM: LSD-SLAM (Engel et al., 2014),
    - Open Keyframe-based Visual-Inertial SLAM: OKVIS (Leutenegger et al., 2015),
    - Kintinuous (Whelan et al., 2015a),
    - ElasticFusion (Whelan et al., 2016),
    - Bundle-Adjusted Direct SLAM: BAD SLAM (Schops et al., 2019),
    - DROID-SLAM (Teed and Deng, 2021),
    - ORB-SLAM3 (Campos et al., 2021),
    - Kimera (Tian et al., 2022),
    - HyperSLAM (Hug et al., 2022),
    - Colmap-SLAM (Morelli et al., 2023a),

- LiDAR-visual SLAM:
    - Real-Time Appearance-Based Mapping: RTAB-Map (Labbé and Michaud, 2019),
    - maplab (Cramariuc et al., 2022),
    - R3LIVE (Lin and Zhang, 2022),
    - Swarm-SLAM (Lajoie and Beltrame, 2023).

On the basis of the meta-analysis, a progression of the prevailing methods used in the literature can be seen. Traditionally, in the early 2000s, 3 DoF

SLAM solutions based on Kalman filters (EKF and UKF), information filters or particle filters were the predominant type of approaches used by researchers (Aulinas et al., 2008). Nowadays, the prevailing approach in most state-of-the-art solutions, especially for LiDAR-centric SLAM algorithms, involves the use of **factor graphs** for fusing the observations and creating an optimized map. Their principle is based on representing unknown variables as nodes in the graph and functions acting on a (typically small) subset of the variables, i.e., factors, as its edges. In SLAM, a specific type of factor graph can be created: a **pose graph**. It expresses subsequent SE(2) or SE(3) poses of the agent as nodes of the graph. Measurement-based constraints are represented by edges connecting poses associated with them (Będkowski, 2022). Common constrain types include relative transformations between poses (e.g., estimated using LiDAR, visual or wheel odometry) or loop closures, preintegrated IMU readings, motion model estimates, relative landmark poses or GNSS positions.

The use of pose graphs allows one to greatly sparsify the information matrix of the system and thus limiting the computational effort required to solve the problem, in turn enabling processing high-frequency image or LiDAR data (Grisetti et al., 2010). A graphical example of a typical LiDAR-centric factor graph representation of a pose graph SLAM, used to fuse LiDAR odometry estimates with other auxiliary measurements and information associations, is taken from the LIO-SAM article (Shan et al., 2020) and presented in Figure 2.14.
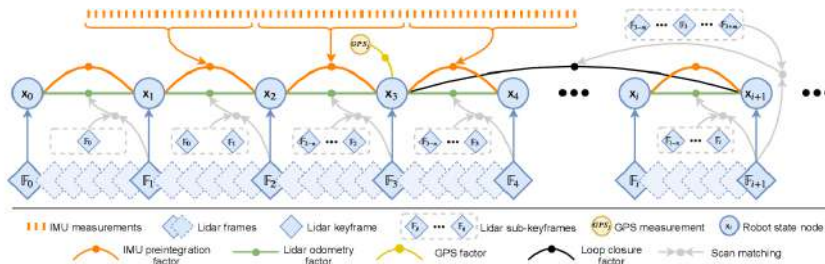
FIGURE 2.14. Multi-sensor pose graph SLAM structure using LIO-SAM architecture as an example (Shan et al., 2020)

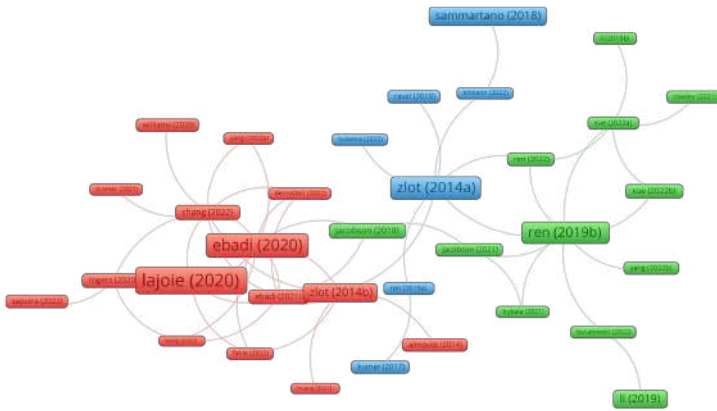## 2.3 Application of SLAM in the Mining Context

The first use of 3D mobile mapping of underground scenes was presented by researchers from one of the most important mobile mapping research units, Carnegie Mellon University and University of Freiburg (Hähnel et al., 2002; Thrun et al., 2003). Although very limited due to available hardware and software at the time, researchers succeeded in creating a topologically correct 3D point cloud of an underground tunnel network using multi-LiDAR sensor setups on a mapping cart and a mobile robot. However, they did not actually solve a 6 DoF SLAM, but rather took the assumption of completely planar sensor movement and used ICP-based scan matching to solve a planar, 3 DoF SLAM problem and then used the estimated trajectory to transform the point clouds from a vertically mounted 2D LiDAR scanner into a common reference frame. This approach, while successful, clearly is not correct from the surveying point of view. The study lacks a reliable assessment of the accuracy of the results. Only a comparison of a planar section of the SLAM-derived map with a hand-drawn map is presented, but some discrepancies of tunnel shapes can still be seen (Figure 2.15).

In the following years, Tsubouchi et al. (2004) and Fairfield et al. (2006) further studied the topic, but then the field of research stagnated. A few years later, several technological advancements helped to continue the advances in the area of 3D SLAM in challenging conditions: introducing affordable and portable 3D LiDAR sensors and RGB-D cameras, edge computing devices capable of SLAM processing (e.g., Nvidia Jetson board) and development of a standardized open source software middleware: Robot Operating System (ROS; Quigley et al., 2009). Together with the introduction of cheaper and more accessible mobile robotic platforms and the increasing interest in autonomous vehicles and robots, they created perfect conditions to push the research field further.

Although nowadays great progress has been made, enabled especially by the Subterranean Challenge funded by the American Defense Advanced Research Projects Agency (DARPA), where several top-tier research groups competed in deploying fleets of autonomous robots in underground conditions for mapping and search & rescue applications, which took place in the years 2018-2021 (Rogers et al., 2020). Multiple solutions developed in its scope have been already released as open source contributions and position articles, published by consortia of robotic teams who participated in the competition. Those works stress the progress of SLAM in unstructured environments and lessons learnt, but also the remaining challenges of SLAM applications (Ebadi et al., 2023; Tranzatto et al., 2022). In the paper of Ebadi et al. (2023), core issues such as maintaining robustness of robot perception, especially using low-cost sensors,

FIGURE 2.15. Comparison of the 2D SLAM grid map constructed by a mapping cart (a) with a hand-drawn map (b) (Thrun et al., 2003)

distributed computing and utilizing alternative sensors (e.g., radar) are given.

Similarly to Section 2.1, a meta-analysis of published work on MMTs and SLAM solutions has been performed, this time narrowing the subject to mapping applications in mining-related applications, containing the keywords "underground" or "subterranean". The query returned 103 articles.

First, popular research directions explored in this particular context were examined. A relevant graph is presented in Figure 2.16. The main topics, not well-clustered by the VOS Viewer algorithm, which can be identified in the graph are:

- V-SLAM and its related issues and features (vision, fisheye camera, monocular camera, texture, lighting),

- some issues or desired characteristic of SLAM (low-drift, failure, real time, complex environment, robustness, effectiveness),

- LiDAR and LiDAR-inertial SLAM-related topics (LeGO-LOAM, LIO,

laser scanner),

- experiment-related terms (underground tunnel, underground mine, underground environment, experimental results, implementation, test),

- graph SLAM and graph optimization are also specifically mentioned.

Some generic, not mentioned above, SLAM keywords are also present in the graph. The trends identified in the word map differ from the previous analysis of all SLAM solutions. This time, the studies are much more practical, with stronger stress on implementation, robustness of the solution and challenges of the subterranean environments. An interesting observation is the appearance of multiple terms related to graph SLAM and LiDAR SLAM, including two specific LiDAR-centric frameworks, while no V-SLAM approach is mentioned. This further underlines of the difficulties of applying vision-based mapping methods in underground conditions.

FIGURE 2.16. Term network in the analyzed publications' abstracts and titles regarding SLAM applications in underground conditions

The next graph in Figure 2.17 illustrates co-citations of article pairs. To limit the number of works analyzed and declutter the visualization, studies without any citations were discarded from this analysis. Three clusters can be identified:

FIGURE 2.17. Co-citation network of the most cited works about SLAM applications in underground environments

- green cluster, describing different, mostly LiDAR-based approaches for mapping underground tunnels with robotic platforms, with the central work of Ren et al. (2019b),

- blue cluster, examining handheld MMTs and autonomous vehicle applications in underground mines, with the most important works of Zlot and Bosse (2014) and Sammartano and Spanò (2018),

- red cluster, with studies mostly related to the DARPA Subterranean Challenge, with the leading works of Lajoie et al. (2020) and Ebadi et al. (2020), both being earlier versions of their subsequent developments in Lajoie and Beltrame (2023) and Chang et al. (2022).

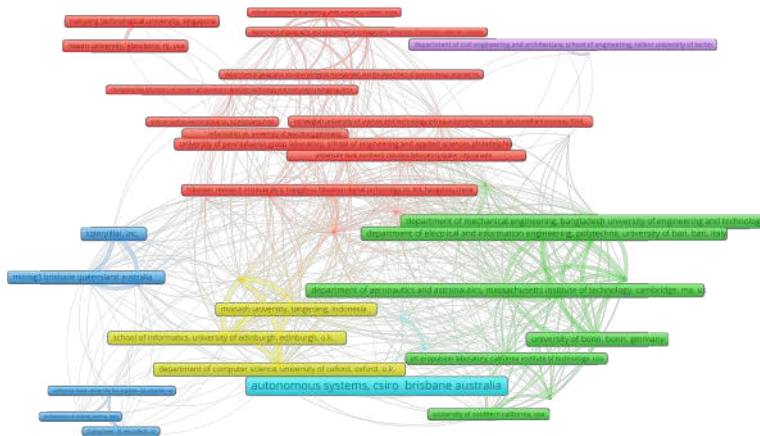The bibliographic coupling graph in Figure 2.18 illustrates trends in referencing similar studies. Although for all SLAM research papers this analysis shows a clear trend with few exceptions, limiting its scope to only underground applications conveys a different message. Because the early studies from 2014-2019 did not have much relevant source material on which to build on, there is generally weak bibliographic coupling between them. Only for very recent works, from 2020-2023, a higher homogeneity of references can be seen. This highlights rapid progress in this specific field of application in the aforementioned period.

Similarly, different trends emerge in the bibliographic coupling graph of research units shown in Figure 2.19 compared to the broader scope of the general SLAM analysis. There is a higher diversity observed in terms of countries, attributed in part to less demanding citation count requirements. Notably,
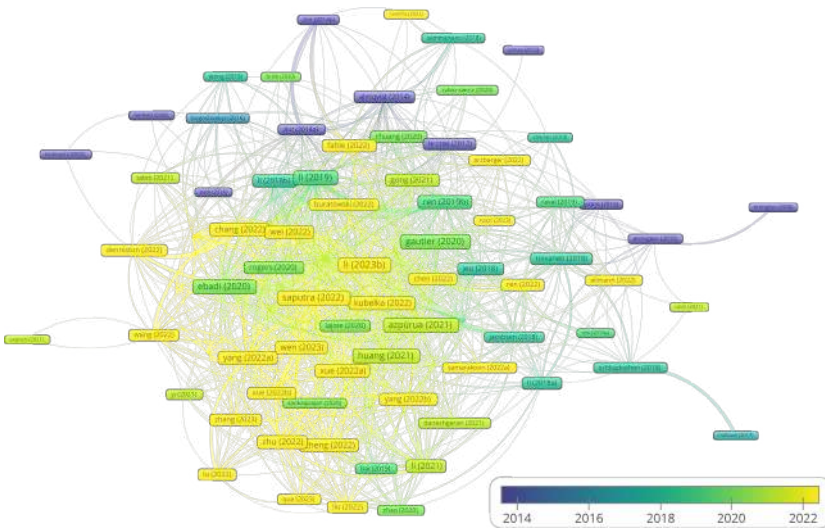
Figure 2.18. Bibliographic coupling by year for SLAM applications in underground environments

Figure 2.19. Bibliographic coupling by institutions for SLAM applications in underground environments

institutions from the United States, China and Germany continue to be the most represented. However, this time, multiple units from Australia, Canada, and Italy also appear in the results, with the Australian CSIRO unit having the highest total citation count. Furthermore, the interest of the mining industry in SLAM is evident through the participation of coauthors affiliated with major companies such as Caterpillar and TransPower.

The survey, extended with studies found independently from other sources, provided valuable insight into various aspects of developments in SLAM for 3D reconstruction of underground sites. Several distinct and important research directions emerged. The first one is associated with robotics and mostly encompasses developments in various technical aspects of SLAM, predominantly based on the DARPA Subterranean Challenge. Rogers et al. (2020) provided first results of benchmarking MMS 3D point cloud quality based on the initial circuit of the Challenge. (Kramer et al., 2021) describes V-SLAM solution developed for this purpose, and Tranzatto et al. (2022) gives an insight into the technologies used by the Challenge-winning team, Cerberus.

Several works concentrate on improving specific system components affected by the degraded geometry and perception in subterranean environments: loop closure detection (Denniston et al., 2022), LiDAR odometry (Reinke et al., 2022), and path planning (Dang et al., 2019). Finally, Lajoie and Beltrame (2023) and Khedekar et al. (2022) propose distributed SLAM systems for mobile mapping in underground conditions with robot swarms. Ebadi et al. (2023) provides an overview of different solutions and lessons learned from various teams participating in the Challenge. The research works of Wang et al. (2022) and Bogoslavskyi et al. (2016) should be mentioned as other relevant studies that were not developed within the scope of the Challenge. The former proposes an approach for loop closure detection in degraded environments and the latter studies the robust robot navigation in the underground conditions.

The topics of multiple examined articles revolve around various applications of SLAM in underground conditions. In addition to the already discussed robotic solutions, there are studies showcasing practical applications. They include advances towards increasing the autonomy of mining vehicles (Jacobson et al., 2018, 2021; Kumar et al., 2017; Park and Myung, 2014), performing inspection tasks in underground conditions with mobile robots (Azpúrua et al., 2021; Marangi et al., 2019; Menendez et al., 2019) and mine search & rescue operations (Li et al., 2023b; Zimroz et al., 2021). Some initial work has been done in the field of UAV application in underground conditions (Jones et al., 2019; Samarakoon, 2022), but this area cannot be considered mature for practical large-scale applications yet. Multiple works focus on digitizing subterranean cultural heritage sites with MMSs (Di Stefano et al., 2021; Gautier et al., 2020; Menna et al., 2022; Torresani et al., 2022).

Ultimately, a group of the most relevant studies was compiled. They cover the topics of evaluating MMS-derived 3D point cloud quality in underground facilities or propose specific solutions to improve those results. Zlot and Bosse (2014), Sammartano and Spanò (2018) and Ellmann et al. (2021) investigate the GeoSLAM commercial MMS system capability for 3D reconstruction of subterranean spaces. They obtain best 3D point position errors in the range

of 5-10 cm, but in favorable conditions (e.g., multiple loop closures, slow and steady movement, relatively large and structured tunnels). For failure cases with strong drift, reported errors reach from 20 cm to 60 cm. For open source-based solution using a Livox LIDAR scanner, Wang et al. (2023) achieves errors reaching from 20 cm to 80 cm in the worst cases. Li et al. (2023a), using a similar solution, but mounted on a helmet, stresses high failure rate of popular LiDAR and LiDAR-inertial odometry algorithms, which rely on feature extraction and matching, in underground conditions. The authors mention FAST-LIO as the algorithm least affected by these problems. A use case in an open pit mine was presented by Vassena et al. (2018). Although the study did not contain a comprehensive accuracy analysis, presented compliance with a TLS point cloud in the range of a few centimeters appears to be satisfactory.

Some studies try to address these issues through developments of a dedicated SLAM approach. (Xue et al., 2022) modified the LeGO-LOAM framework, adding loop closure detection support with the Scan Context algorithm Kim et al. (2022). Although its target environment is an underground coal mine, the tests were performed only in an underground parking lot. Despite showing an improvement, taking into the account conclusions of other, previously mentioned studies, the actual performance in the mining conditions can be considerably lower.

An interesting approach is presented by Yang et al. (2023). Although again a feature-dependant LiDAR SLAM framework is proposed, the authors introduce a degeneration factor, based on the imbalance of spatial distribution of linear and planar features detected in the point clouds. They point out that this disparity is the cause of the increased drift errors of feature-based LiDAR SLAM in degenerated scenes. This factor is utilized to introduce additional IMU-based orientation features into the pose graph in the occurence of such degradation. The results of the experiments carried out in a real underground tunnels show a considerable improvement of the trajectory errors compared to LeGO-LOAM and LIO-SAM. A limitation of the study is the lack of analysis of the 3D reconstruction errors, since only the ATE of the robot returning to the starting point was examined. Moreover, the proposed framework does not support loop closure detections.

The study of Ren et al. (2019b) contrary to the popular feature-based LiDAR SLAM propose a featureless approach (with optional ground plane detection) based on robustifying GICP algorithm. The approach is similar to another popular open source framework, HDL-Graph-SLAM (Koide et al., 2019). However, this work is subject to limitations similar to those discussed in the previous article. Although the proposed algorithm does support loop closures, only ARE and ATE metrics of the trajectory are analyzed and the final point cloud is evaluated only qualitatively.

Concluding from the literature review, one could state that the overwhelming majority of MMTs deployed in underground survey scenarios use LiDAR or LiDAR-inertial systems. Especially LiDAR odometry approaches that are point-based and not feature-based, such as those utilizing GICP or NDT, appear to be an appropriate approach. Analogously to general SLAM algorithms, the prevailing method for incorporating other factors into an optimization workflow is pose graph SLAM. However, the lack of V-SLAM-oriented studies underline the severity of the problems vision-based methods face in practical applications of mapping underground sites, which were described in 2.1. Despite excluding vision systems in this study, in the future, further investigation of fusion methods, leveraging the strengths of both approaches, is envisioned, since visual sensors could bring valuable features to 3D reconstruction results, such as texturization and photogrammetric methods of internal quality control.

Due to these facts and the available hardware, the scope of this thesis has been limited to LiDAR SLAM approaches. Although this approach was deemed to have a high potential to provide sufficient mapping quality, the literature review highlighted several scientific gaps and prospects of introducing novel improvements to existing frameworks, developing a quality-oriented approach. Those possibilities were investigated in this research.

CHAPTER 3

Main Contributions

3.1 AIM AND OBJECTIVES

This thesis seeks to explore the surveying aspect of applying different mobile mapping technologies in the mining environments. The main aim of my research was to **develop and exhaustively test an MMS capable of operating robustly in adverse underground conditions**, which will be able to provide metric 3D point cloud data reaching **survey level quality**. Since the success of completing such a complex task cannot be easily evaluated with a single objective metric (or a closed set of them), the study required adapting a research strategy of **iterative system developments**, which led to performing multiple analyses, focusing on various aspects of the quality of the 3D data produced by the investigated systems.

Furthermore, achieving this goal required exploring **various measures of assessing point cloud quality and adapting them** in the specific context of mapping constrained underground spaces. These evaluation methods had to be used for **number of comparisons** of the systems analyzed **with state-of-the-art MMSs and traditional methods** (e.g., survey-grade TLS) working in various conditions to assess both the shortcomings of the selected evaluation approach and the current stage of development of the proposed MMS. Using this knowledge, the solutions had to be then iteratively improved and fine-tuned to **ensure a system capable of resilient and reliable operation in subterranean environments**, together with a **set of guidelines** for selecting an appropriate method for a specific type of environment and the main purpose of acquiring the point cloud.

Thus, the research thesis of the study is that *SLAM algorithms can be successfully applied to process 3D measurement data to perform high-quality 3D reconstructions of mining environments.* In this context, the term *high-quality 3D reconstructions* should be understood as point clouds characterized by quality measures, such as accuracy, precision, completeness and data density, which can challenge well-established survey-grade methods (although, taking into account the inevitable disparities in the quality of raw measurements due to

vastly different hardware capabilities) and provide output quality sufficient for different mining-related use cases.

Based on the literature review, the identified scientific gap and initial tests of openly available noncommercial SLAM solutions, but also on discussions with mining surveying experts on the current capabilities and desired characteristics of existing commercial mobile mapping systems, three objectives have been established to achieve the aim of this research:

[O1]   Perform comprehensive quantitative evaluations of the 3D reconstruction quality of state-of-the-art LiDAR-SLAM methods in mining conditions (both underground and open pit). A key element in this concept lies in using well-established surveying methods to obtain the reference data and carrying out an in-depth quality assessment analysis of the investigated data.

[O2]   Establish an open data set to facilitate further developments in mobile mapping methods for mining-related applications by the scientific community. The dataset will significantly enrich other available data through simultaneous acquisitions of data from multiple sensors (cameras, LiDAR scanners, IMUs) on a common mobile robotic platform.

[O3]   Improve selected open source state-of-the-art SLAM solutions based on the results of performed evaluations and propose a strategy for choosing and tailoring a measurement approach for a specific type of mining environments and final 3D reconstruction requirements.

Although most of the works included in this thesis at least indirectly supported my advancements to accomplish all of the objectives listed above, for each article a main objective towards which it contributes is given. The summary of these connections is presented in Table 3.1. However, for the last objective, [O3], an important contribution constitutes the conclusions from the entire series of articles, contained in Section 4.1.

TABLE 3.1.   Mapping of the thesis objectives to the articles contributing to them

Objective	Contributing Study
O1	P1, P2, P4, P6
O2	P5
O3	P2, P3, P6

3.2   LIST OF PUBLICATIONS

Contributions made in this thesis are presented in six scientific articles listed below. Since the series shows the progression from a basic measurement system and simple quality evaluation methods towards advanced software and hardware SLAM implementation paired with more comprehensive, complex data quality analyses, the papers are listed in the chronological order of appearance in press. Their short summaries, importance and my personal contributions are detailed in Section 3.3.

[P1]   Trybała, P. (2021). LiDAR-based Simultaneous Localization and Mapping in an underground mine in Złoty Stok, Poland. In *IOP Conference Series. Earth and Environmental Science*, volume 942. IOP Publishing

[P2]   Wajs, J., Trybała, P., Górniak-Zimroz, J., Krupa-Kurzynowska, J., and Kasza, D. (2021). Modern Solution for Fast and Accurate Inventorization of Open-Pit Mines by the Active Remote Sensing Technique—Case Study of Mikoszów Granite Mine (Lower Silesia, SW Poland). *Energies*, 14(20):6853

[P3]   Trybała, P., Szrek, J., Dębogórski, B., Ziętek, B., Blachowski, J., Wodecki, J., and Zimroz, R. (2023c). Analysis of Lidar Actuator System Influence on the Quality of Dense 3D Point Cloud Obtained with SLAM. *Sensors*, 23(2):721

[P4]   Trybała, P., Kasza, D., Wajs, J., and Remondino, F. (2023a). Comparison of Low-Cost Handheld LIDAR-based SLAM Systems for Mapping Underground Tunnels. *The International Archives of the Photogrammetry, Remote Sensing and Spatial Information Sciences*, XLVIII-1/W1-2023:517–524

[P5]   Trybała, P., Szrek, J., Remondino, F., Kujawa, P., Wodecki, J., Blachowski, J., and Zimroz, R. (2023d). MIN3D Dataset: MultI-seNsor 3D Mapping with an Unmanned Ground Vehicle. *PFG – Journal of Photogrammetry, Remote Sensing and Geoinformation Science*

[P6]   Trybała, P., Kujawa, P., Romańczukiewicz, K., Szrek, A., and Remondino, F. (2023b). Designing and Evaluating a Portable LiDAR-based SLAM System. *The International Archives of the Photogrammetry, Remote Sensing and Spatial Information Sciences*, XLVIII-1/W3-2023:191–198

3.3 Summary of the Results

One of the common aspects of all my research works presented as part of this thesis is transparency in terms of free access to all the underlying components of the implementation of each of the SLAM methods tested. This is in contrast to currently prevailing commercial mobile mapping solutions on the market, which allow their user only a limited access to the data, technical details and mathematical methods involved in processing the measurements in their SLAM-based software. Those in my opinion conflict with one of the core principles of surveying: providing the end user of the 3D data a trustworthy quality assurance through transparency, traceability and verifiability of the mathematical process involved in constructing the final point cloud from the raw measurements (e.g. scan registration, pose graph optimization, measurement error model). Because of that, all works carried out by me in the scope of this thesis are based on open source implementations, where each aspect of the data processing pipeline could be analyzed and, in case of necessity, adjusted to the specific needs of the available hardware configuration or survey site characteristics.

An important concept, recurring in the majority of the listed studies, is the point cloud quality assessment. In surveying and photogrammetry, three distinct key terms are usually used in this context. **Accuracy** of the measurements is defined as their compliance with the true values. Since real *true* geometry is usually impossible to obtain, it is estimated with data acquired with instruments of established much higher quality. **Precision**, on the other hand, is a measure of the internal coherence of the data. This quality informs about the repeatability and reliability of the measurements and has an impact on the usable spatial resolution of the 3D reconstruction. Finally, **completeness** indicates the extent to which the geometry of the object is captured. Usually, the metric is estimated at a given spatial resolution due to the discrete nature of the measurements (Knapitsch et al. (2017); Nocerino et al. (2020)).

Most of the software used and developed in the listed articles was performed in a ROS environment (Quigley et al., 2009), which allowed seamless data acquisition with multiple different sensors and the custom-made wheeled mobile robot *Jaroszek* used in many studies, as well as running the actual SLAM processing in an efficient manner. Several analytical tools were additionally written in Python. For vizualizations, data preprocessing and partly also quality evaluation, the Cloud Compare open software was utilized (Girardeau-Montaut, 2016) together with its *M3C2* plugin (DiFrancesco et al., 2020).

The specific contributions of each described article are given in subsections 3.3.1 - 3.3.6. However, in short, the scientific novelty of the entire series can be summarized as follows:

- performing 3D data acquisitions in multiple open-pit and underground mining sites, using in-house build SLAM systems,

- processing the abovementioned data with implementations of state-of-the-art approaches, gradually extended with novel improvements, based on the experience from the previous field tests,

- carrying out exhaustive 3D data quality analyses, providing insights into the performance of the selected SLAM frameworks in mining conditions and pinpointing specific issues for streamlining the algorithms' enhancement process,

- sharing a unique dataset, acquired in the underground conditions, aimed at facilitating SLAM developments for mining applications by the scientific community,

- developing an advanced version of a MMS, comprising hardware and software, for high-quality 3D reconstructions of mining sites.

3.3.1 *P1: Robotic Mapping of an Underground Mine*

Trybała, P. (2021). LiDAR-based Simultaneous Localization and Mapping in an underground mine in Złoty Stok, Poland. In *IOP Conference Series. Earth and Environmental Science*, volume 942. IOP Publishing

The first publication in the series documents the first analysis of the results of performing a 3D reconstruction of a former underground mine tunnel with a multiline LiDAR scanner mounted on a remotely controlled mobile robot. The paper explores the first impressions of using a SLAM algorithm to map an area with challenges typical for underground conditions: a tunnel of an elongated shape, with uneven ground and varied geometry of the walls and roof.

Due to the total lack of availability of open SLAM datasets collected in underground conditions by industrial grade LiDAR sensors (see the review of the literature in the study summarized in Section 3.3.5: Trybała et al. (2023d), a data collection using available simple hardware (a Velodyne VLP-16 LiDAR on a wheeled mobile robot) had to be performed by myself. These tests were carried out in September 2020 in a former gold and arsenic mine in Złoty Stok, Poland. A TLS survey has been performed at the test site to obtain a ground truth (GT) point cloud. The raw data collected was used to test multiple SLAM algorithms, most of which failed the task of performing a topologically correct 3D reconstruction of the approximately 120 m tunnel. Thus, in this very first step of qualitative analysis, they were discarded.

Finally, the algorithm that performed the best, HDL-Graph-SLAM (Koide et al., 2019), was selected for further parameter tuning and used to perform the final 3D tunnel reconstruction. This relatively simple approach employs an ICP-based scan matching, proximity-based loop closure detectors and g2o-based PGO (Kümmerle et al., 2011). The approach is depicted in Figure 3.1, although for the tunnel use case the constraints of GNSS poses and planar ground were disabled on purpose. The 3D data quality has been investigated qualitatively, inspecting the completeness, data density and precision through an interactive visualization, and quantitatively, with the use of the TLS reference data. Both point clouds were coregistered in a common reference frame and the unsigned cloud-to-cloud distances were calculated. The distribution of their values, representing estimates of measurement accuracy, and their spatial distribution were analyzed, which allowed to draw consensus on further system developments, but also proved the suitability of the general surveying approach to obtain 3D point cloud with a SLAM method in an underground tunnel.
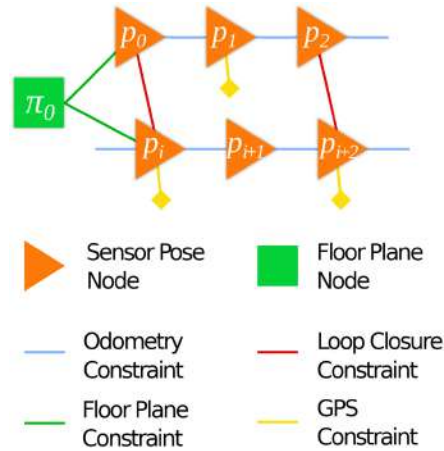
FIGURE 3.1.   HDL-Graph-SLAM pose graph approach overview (Koide et al., 2019)

The positive result of the first algorithm evaluation was the basis for using a similar but extended approach in the next work, described in Section 3.3.2: Wajs et al. (2021). The issues that arose during the data analysis in this study, namely uneven point cloud coverage (low completeness of the ceiling reconstruction), were addressed directly in later works (Section 3.3.3: Trybała et al. (2023c).

Worth mentioning is the fact that, concurrently, other researchers also tackled the issue of performing quality evaluation of the HDL-Graph-SLAM framework point clouds, however, in simpler conditions and with a less elaborated accuracy evaluation method. The work of Milijas et al. (2021) reported a failure of 3D reconstruction, while the study of Akpınar (2021) the evaluation was based only on the comparison of a few distances measured in the reconstructed point cloud and at the real site. Furthermore, a later work of Koval et al. (2022) used this algorithm in underground conditions, with a similar setup as in my study. Although no map accuracy analysis was performed, they similarly reported achieving good accuracy of robot trajectory estimation.

Since the article is a single-author publication, all of its contributions, from system configuration, data acquisition, processing and analysis, as well as manuscript preparation, were done by the author of this thesis. Work contributes mainly to the achievement of the objective [O1].

3.3.2   *P2: Handheld Mapping in an Open-Pit Mine*

Wajs, J., Trybała, P., Górniak-Zimroz, J., Krupa-Kurzynowska, J., and Kasza, D. (2021). Modern Solution for Fast and Accurate Inventorization of Open-Pit Mines by the Active Remote Sensing Technique—Case Study of Mikoszów Granite Mine (Lower Silesia, SW Poland). *Energies*, 14(20):6853

The second study investigates the application of a similar simple SLAM system as in Section 3.3.1, but in a handheld mode. Nevertheless, the same LiDAR sensor, held approximately in a horizontal position, was used to perform the data acquisition. A similar approach was presented in the work of (Vassena et al., 2018). However, a more expensive LiDAR sensor was used there to perform mobile mapping of an open-pit mine and even though survey-grade reference data was available, no exhaustive data quality metrics are given.

Processing was done again with HDL-Graph-SLAM. However, this time, the workflow has been enhanced with postprocessing of the SLAM initial trajectory estimation, because the acquisition in more open area than a single tunnel provided the opportunity to better exploit loop closures to minimize the drift errors and obtain a higher quality point cloud.

A framework proposed by (Koide et al., 2020) was adopted to further optimize the initial estimate of a SLAM solution, calculated with HDL-Graph-SLAM. First, several ground planes were fitted in the raw point clouds. Similarly, a few nodes with clearly identifiable overlap, but without the loop being automatically detected in the first run of real-time SLAM processing, were connected by an edge, with the relative transformation estimated with standard ICP-based scan matching. Then, an additional step of more extensive, but slower, automatic loop detection and scan matching was carried out to densify node connections and strengthen the relationships between nearby pose estimates. Lastly, an iterative process of manual loop verification and automatic graph edge refinement enabled obtaining the final optimized pose graph and retrieving the globally coherent point cloud. The final workflow is presented in Figure 3.2.

The results of handheld mobile mapping were georeferenced to a 3D point cloud obtained with a survey-grade GNSS RTK-supported LiDAR mobile mapping system by Riegl, mounted on a car. The signed distances between the SLAM point cloud and the reference mesh model were calculated and the distribution of their values and spatial concentrations were further analyzed to assess the applicability of the method for mapping open-pit mine areas. Since the coauthors of the article, who have extensive experience in the mining mapping field, deemed the results acceptable from a practical point of view of

the requirements of mapping an open-pit mine, the developed SLAM workflow has been accepted as valid for open-pit mining areas and the focus of further research has been put on challenges of applying SLAM in confined underground spaces.

In this article, my main contributions revolved around performing data acquisitions with the handheld SLAM system, developing and applying the improved data processing workflow, and writing relevant parts of the manuscript. The comparative data analysis, discussion and conclusions were carried out jointly with other coauthors of the paper. The article contributes to the realization of objectives [O1] and [O3].
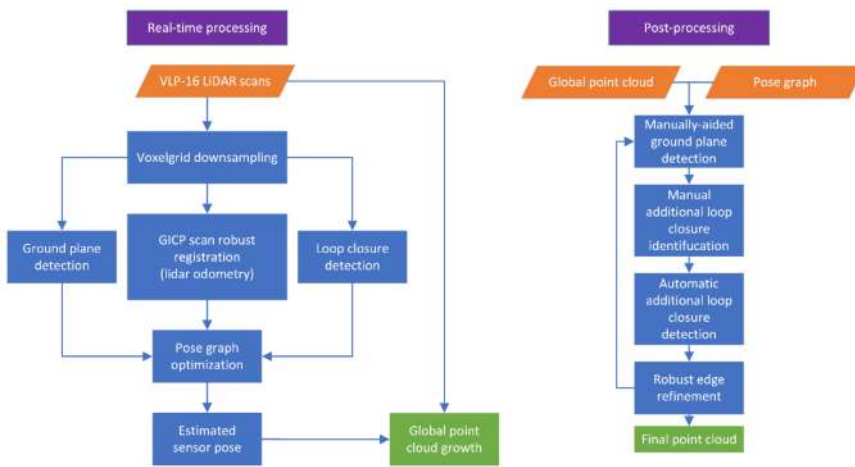
FIGURE 3.2. Data processing workflow for mobile mapping segment of the study (Wajs et al., 2021)

3.3.3 P3: Analyzing Different Aspects of 3D Data Quality from a Robotic Mapping System

Trybała, P., Szrek, J., Dębogórski, B., Ziętek, B., Blachowski, J., Wodecki, J., and Zimroz, R. (2023c). Analysis of Lidar Actuator System Influence on the Quality of Dense 3D Point Cloud Obtained with SLAM. *Sensors*, 23(2):721

In this article, published in *Sensors*, a different aspect of the quality of point cloud data, produced by SLAM, is examined. As discussed earlier, although commonly in the robotics community SLAM algorithms are benchmarked using trajectory-derived metrics, such as ATE, ARE, RTE, RRE (Geiger et al., 2012b; Grupp, 2017; Sturm et al., 2012) or more sophisticated approaches Kümmerle et al. (2009). On the other hand, surveying applications of 3D reconstruction are focused on mapping, i.e., point cloud quality. However, in some benchmarks, comparative analyses using survey-grade reference point clouds or meshes, are still limited. They tend to focus on a single metric, accuracy, estimating it with the computation of cloud-to-cloud or cloud-to-model distances (Helmberger et al., 2022; Knapitsch et al., 2017; Schops et al., 2017). Precision or completeness are rarely investigated. Even in such a case, these metrics do not always give a complete picture of the performance of the 3D reconstruction method performance in confined spaces.

The experiments performed in the first work of the series (Section 3.3.1: (Trybała, 2021)) underlined the issues arising from employing the common strategy of mounting the multi-line LiDAR horizontally on the vehicle. While the accuracy of the SLAM-derived point cloud was rather satisfactory, its completeness was low due to multiple occlusions, small field-of-view (FoV) and proximity of the walls in a narrow tunnel. To improve the system in this aspect, an actuated system for continuously rotating the LiDAR scanner was developed to overcome those flaws Figure 3.3 and several indoor experiments were carried out in a tight corridor to quantitatively evaluate the improvements in mapping quality, using several novel metrics for the evaluation of SLAM systems, such as spatial data density, surface variation, voxel count and 3D points spatial distribution.

The initial tests of the previously utilized framework, HDL-Graph-SLAM, lead to the conclusion that the algorithms do not perform well with the data from continuously rotating sensor. Because of that, the SLAM software backbone was switched to the SC-A-LOAM framework (Kim et al., 2022), which upon qualitative evaluation was able to correctly reconstruct the corridor and all objects located in it. Additional steps of preprocessing (point cloud undistortion based on constant velocity motion model (Będkowski, 2022)) and post-
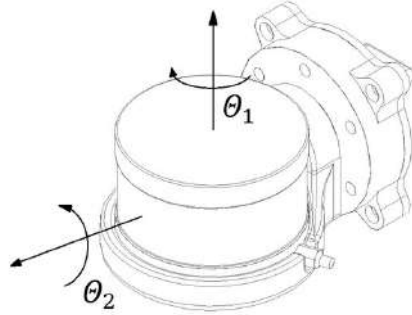
FIGURE 3.3. A scheme of the developed actuated multi-line LiDAR system (Trybała et al., 2023c)

processing (point cloud noise removal (Kim and Kim, 2020) were added to the open-source software. At this point, the SLAM backend was moved from g2o to GTSAM due to, subjectively, its better adaptability and readability to pose graph structure manipulation (Dellaert, 2012). An overview of the applied SLAM pose graph solution is depicted in Figure 3.4.
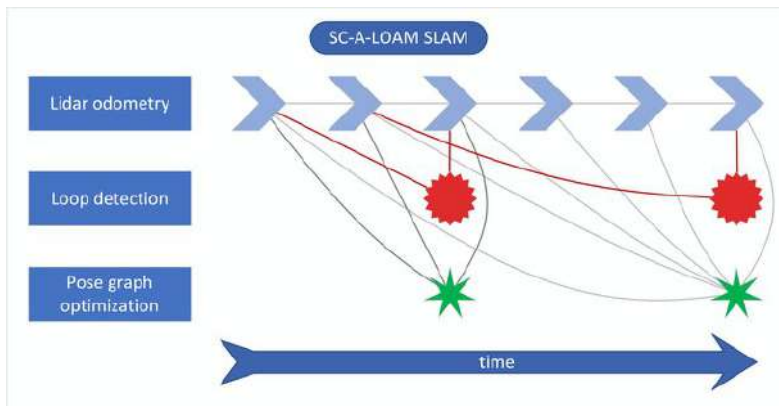
FIGURE 3.4. A scheme of a pose graph SLAM Used in (Trybała et al., 2023c)

The metrics derived from experiments of reconstructing the corridor with a horizontally mounted LiDAR sensor on a mobile robot, a scanner rotating in a limited range and in a full range (180° of rotation) clearly proved the advantages of the proposed solution over the most widespread placement of the LiDAR scanner. Very high completeness and more optimal 3D point distribution were achieved due to the scanning coverage of approximately hemispherical view (combining measurements from a few frames).

The hardware and software solutions developed in the scope of this work

were then used in the next studies described in Sections 3.3.4 and 3.3.5. Since in this work tests were performed only in an indoor site, resembling the conditions of an underground facility, the objective which was targeted was [O3].

My contributions in this multi-author research paper are: conceptualization, developing the study methodology, involvement in hardware developments, low- and high-level programming of the SLAM system, performing the data acquisition, processing and analyses.

3.3.4   P4: Handheld Mobile Mapping in the Underground Tunnels: A Comprehensive 3D Reconstruction Quality Analysis

Trybała, P., Kasza, D., Wajs, J., and Remondino, F. (2023a). Comparison of Low-Cost Handheld LIDAR-based SLAM Systems for Mapping Underground Tunnels. *The International Archives of the Photogrammetry, Remote Sensing and Spatial Information Sciences*, XLVIII-1/W1-2023:517−524

The work described in this Section introduces a rigorous test of developed two mobile mapping solutions, utilizing different hardware and software solutions, in a challenging underground tunnel of varied and complex geometry. Sequences inside of a loop area of a partly collapsed adit were collected with the evaluated systems and a commercial SLAM system GeoSLAM Zeb Horizon. The results were compared to a survey-grade TLS ground truth point cloud.

For SLAM processing, two different solutions investigated were a handheld version of an actuated multi-line LiDAR scanner from the previous work (Trybała et al., 2023c) and a new LiDAR-inertial system, using a Risley prism-based Livox scanner (with a non-repetitive pattern, but limited FoV). For the former, the processing pipeline remained unchanged, while the latter utilized another approach inside the same framework, developed for this type of LiDARs: FAST-LIO-SLAM (Kim et al., 2022; Xu et al., 2022a). All 3D reconstructions of the surveyed area are shown in Figure 3.5.
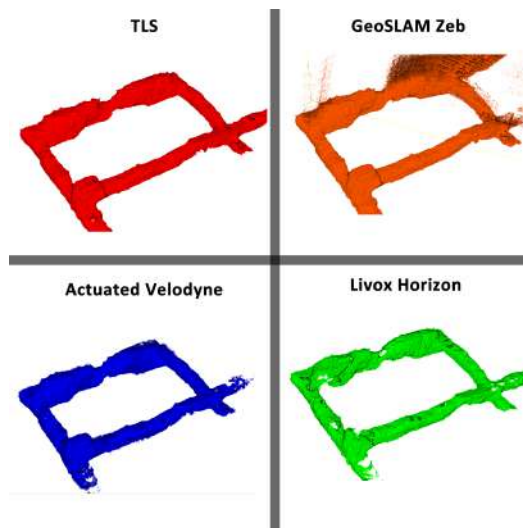
FIGURE 3.5. Perspective views of all point clouds of the surveyed adit area used in the study (Trybała et al., 2023c)

In this publication, the point cloud data quality was assessed with an analysis focusing on several different criteria, building on the metrics proposed in widely used 3D reconstruction benchmarks (Knapitsch et al., 2017; Schops et al., 2017). Accuracy, precision and completeness metrics were calculated for all 3 SLAM methods and analyzed in detail and in summary plots. Moreover, due to the unique characteristic of SLAM-based 3D reconstructions, global drift, a standard method of completeness calculation may lead to incorrect results (see example in Figure 3.6). For the photogrammetric methods evaluated in (Knapitsch et al., 2017) this is corrected using trajectory alignment with the ground truth. Utilizing a TLS-based reference data, this is not possible. Thus, a novel method to perform an approximate SLAM-derived point cloud non-rigid correction was developed to enable correct completeness estimation. Finally, a novel voxel-based visualization and summarization method for the computed metrics is presented.
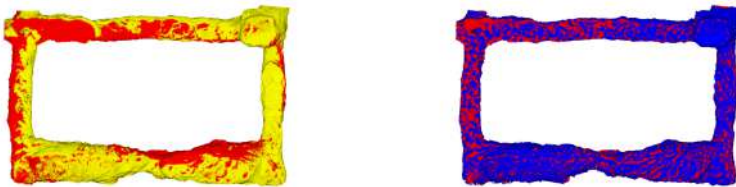
FIGURE 3.6. The SLAM point cloud distorted by a global drift (yellow, left) and the same point cloud corrected by proposed methods for estimating its completeness (blue, right) overlapped with the TLS ground truth (red) (Trybała et al., 2023a)

The results of the evaluation of the SLAM systems in difficult conditions stressed their diverse strengths. Notably, both system based on open-source software were competitive with the much more expensive commercial solution, indicating a high potential for more widespread practical applications. Another remarkable conclusion of the research is the great performance of the non-repetitive scanner, which was previously not available on the market. Those results and addressing identified issues pushed the authors to improve the handheld system, which was reported in the last work (Section 3.3.6: Trybała et al. (2023b).

This study made significant contributions to the objective [O1]. My work in its scope involved conceptualization, formulating the methodology, preparing hardware and software for both open-source-based SLAM systems and performing all the analyzes described above.

3.3.5   P5: Multi-sensor Robotic Mapping in Challenging Conditions: A Public Dataset

Trybała, P., Szrek, J., Remondino, F., Kujawa, P., Wodecki, J., Blachowski, J., and Zimroz, R. (2023d). MIN3D Dataset: MultI-seNsor 3D Mapping with an Unmanned Ground Vehicle. *PFG – Journal of Photogrammetry, Remote Sensing and Geoinformation Science*

The penultimate article published in this series directly aimed to address the lack of publicly available datasets and benchmarks containing appropriate data for evaluating different SLAM algorithms performance in the underground conditions. Therefore, it fulfills the goal of the objective [O2]. Moreover, building on previous developments of a multi-sensor mobile robot (Trybała et al., 2022), this research utilizes the mobile robotic platform to collect a rich multi-modal data set.

The manuscript contains a detailed review of the literature in the area of public datasets relevant to the problem of mobile mapping in subterranean environments. Thus, such a review was not included in Section 2.3. The advantages and disadvantages of other works are given and lead to the conclusion that the proposed MIN3D dataset will have unique characteristics and should be of interest to the scientific community working on mobile mapping solutions, especially those dedicated to the mining sector. The study also comprises the thorough report on the data collection process, structure of the shared dataset and preliminary results of both data processing with SLAM algorithms and an example of an auxiliary data analysis Figure 3.7. Possible ways to utilize the datasets are given as a starting point for the scientific community.
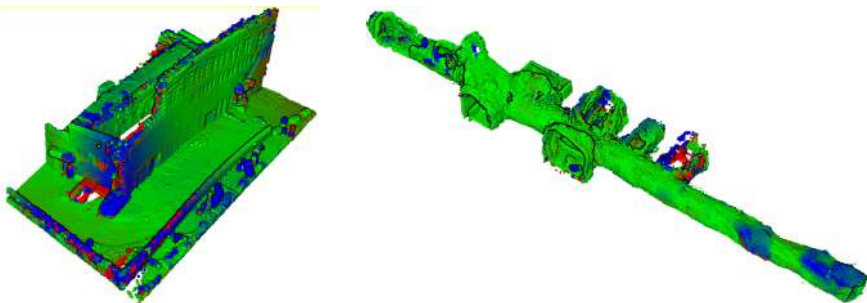
FIGURE 3.7.   Example visualizations from the accuracy analysis of the SLAM results on the MIN3D dataset using a University sequence (left) and an Underground sequence (right) (Trybała et al., 2023a)

In total, 8 sequences were collected with simultaneous recordings of the data coming from 7 cameras, 2 LiDAR scanners and 3 IMUs Figure 3.8. Such variety in devices and types of available data was selected to encourage developments in the areas of sensor fusion methods and facilitate comparisons between results obtained with approaches processing data from different sensors. The dataset is split into two parts by the location of data collection. It encompasses 3 sequences recorded at the university and 5 obtained at a real underground site. Such split allowed us to test the system in more controlled environment, where several challenging factors common in mining applications (e.g., textureless surfaces, indoor-outdoor transitions) could be easily simulated. Additionally, it could be used for evaluating the quality degradation of the results between the "test" and the "real" environment, which is especially critical for learning-based methods.
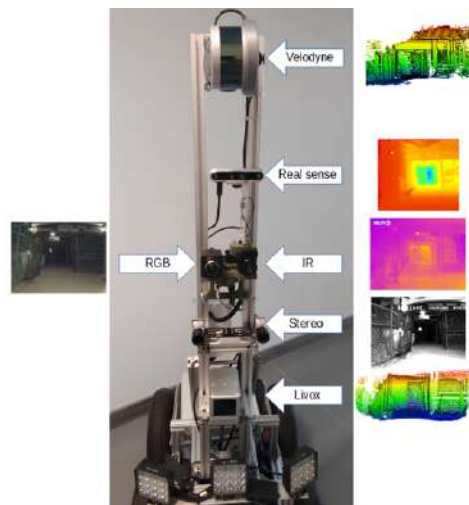
FIGURE 3.8. The mobile robot with its sensor setup used for data collection in this research (Trybała et al., 2023d)

In this work, my contributions spanned from conceptualization, developing the methodology, data collection software preparation, data curation and publication, data processing for 3D reconstruction and evaluation of its results, as well as carrying out the literature review, participating in hardware development and writing the manuscript.

3.3.6   *P6: Developing a Universal and Robust Handheld Mobile Mapping System*

Trybała, P., Kujawa, P., Romańczukiewicz, K., Szrek, A., and Remondino, F. (2023b). Designing and Evaluating a Portable LiDAR-based SLAM System. *The International Archives of the Photogrammetry, Remote Sensing and Spatial Information Sciences*, XLVIII-1/W3-2023:191–198

The last research article in this series takes all the experience from the previous works to create an ultimate version of the MMT solution for mining environments. This does not diminish the value and usefulness of previously developed and tested systems, as each of them has various levels of complexity and diverse strengths that can be leveraged in different scenarios. This aspect is elaborated further in Section 4.1.

Several improvements have been made to an open-sourced LiDAR SLAM framework, based on the FAST-LIO LiDAR odometry: one of the best performing SLAM algorithms in numerous benchmarks and studies (Cramariuc et al., 2022; Koval et al., 2022). Their details are given in the article and include enhancing loop matching accuracy and reliability, robustifying the pose graph optimization and improving the flexibility of the framework. The software side of the proposed PoLiMap system Figure 3.9 leverages its assumptionless approach (i.e., not relying on strong assumptions about the sensor motion and feature presence in the scene) to obtain the most accurate 3D reconstruction of the underground tunnels. where the highly unstructured geometry can hinder the performance of other SLAM approaches, relying on those assumptions. Therefore, the system is characterized by a great versatility and is capable of achieving state-of-the-art performance not only in mining areas, but also other contexts, as proven through successful tests in urban and forest landscapes.

The crucial aspect of the thesis, 3D surveying of subterranean structures, constituted the main part of the research. A cultural heritage site from the First World War, located near Trento, in Northern Italy, served as the primary testing site. The main part of the object is a narrow tunnel, leading through an irregular, carved in stone staircase to a vertical shaft at its dead end. The conditions on the site are similar to those common in touristic mining sites and natural caves. The site has been subject to research on 3D reconstruction methods in the past (Perfetti et al., 2022a; Torresani et al., 2022) and due to that 3D point clouds from several other mapping systems were available. Comparisons with well-known commercial solutions of GeoSLAM Zeb Horizon and Leica BLK2GO, as well as the dedicated multi-camera portable photogrammetric system ANT3D (Perfetti et al., 2022b) were made to assess the quality of the 3D reconstruction results

Figure 3.9. The proposed mobile mapping system PoLiMap (Trybała et al., 2023b)

with the proposed mapping system Figure 3.10. The quality of the results is on par with the reference data of other modern cutting-edge mobile mapping systems.
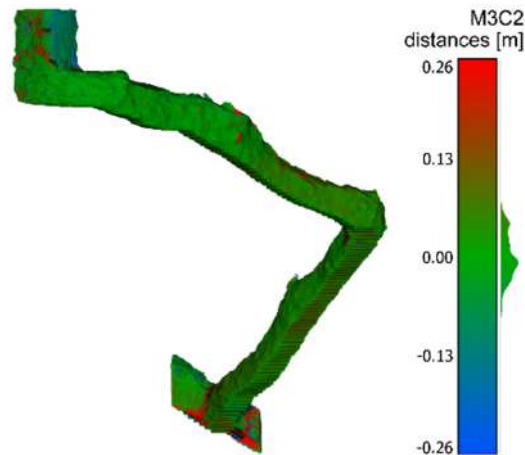
Figure 3.10. The accuracy evaluation of the PoLiMap system at the 100 Scallini: a narrow underground tunnel near Trento, Italy (Trybała et al., 2023b)

This work is the final and most advanced contribution to the objective [O3] and also strives to fulfill the objective [O1]. My personal involvement to this study includes conceptualization, preparation of the research methodology, programming the PoLiMap system, conducting the measurements at the underground site, processing the data and carrying out the 3D reconstruction quality evaluation.

3.4   OTHER CONTRIBUTIONS

During my studies, I explored several other aspects of novel techniques of spatial data processing and robotics in the mining sector. Those topics range from employing machine learning algorithms for various purposes, such as satellite image processing and TLS-based mining machinery condition monitoring, through metrological evaluation of radio-based robot localization techniques, assessing the quality of NeRF-based 3D reconstruction and neural network-based monocular depth estimation, to exploring a search & rescue application of a mini UAV in the underground mine. Although not directly related to this thesis, they underscore the increasing importance and rapid development of robotic and geodata-related applications in multiple, mostly but not exclusively, mining-related fields. The full list of published articles, to which I contributed during my PhD studies, but which are not in the main scope of my thesis, is presented below in chronological order of their publication:

[1]   Kopeć, A., Trybała, P., Głąbicki, D., Buczyńska, A., Owczarz, K., Bugajska, N., Kozińska, P., Chojwa, M., and Gattner, A. (2020). Application of Remote Sensing, GIS and Machine Learning with Geographically Weighted Regression in Assessing the Impact of Hard Coal Mining on the Natural Environment. *Sustainability*, 12(22):9338

[2]   Trybała, P., Blachowski, J., Błażej, R., and Zimroz, R. (2020). Damage Detection Based on 3D Point Cloud Data Processing from Laser Scanning of Conveyor Belt Surface. *Remote Sensing*, 13(1):55

[3]   Szrek, J., Trybała, P., Góralczyk, M., Michalak, A., Ziętek, B., and Zimroz, R. (2020). Accuracy Evaluation of Selected Mobile Inspection Robot Localization Techniques in a GNSS-Denied Environment. *Sensors*, 21(1):141

[4]   Trybała, P. and Gattner, A. (2021). Development of a Building Topological Model for Indoor Navigation. *IOP Conference Series: Earth and Environmental Science*, 684(1):012031

[5]   Zimroz, P., Trybała, P., Wróblewski, A., Góralczyk, M., Szrek, J., Wójcik, A., and Zimroz, R. (2021). Application of UAV in Search and Rescue Actions in Underground Mine—A Specific Sound Detection in Noisy Acoustic Signal. *Energies*, 14(13):3725

[6]   Trybała, P., Kaczan, W., and Górecki, A. (2021). Mining Waste Volume Estimation Using Airborne Lidar Data and Historical Maps: A Case Study of Tailing Piles in Szklary, Lower Silesia. *Environmental Sciences Proceedings*, 9(1):32

[7]   Wróblewski, A., Wodecki, J., Trybała, P., and Zimroz, R. (2022). A Method for Large Underground Structures Geometry Evaluation Based on Multivariate Parameterization and Multidimensional Analysis of Point Cloud Data. *Energies*, 15(17):6302

[8] Trybała, P., John, A., Köhler, C., Benndorf, J., and Blachowski, J. (2022). Towards a mine3D dense mapping mobile robot: a system design and preliminary accuracy evaluation. *Markscheidewesen*, 129(1):18–24

[9] Trybała, P., Szrek, J., Remondino, F., Wodecki, J., and Zimroz, R. (2022). Calibration of a Multi-sensor Wheeled Robot for the 3D Mapping of Underground Mining Tunnels. *The International Archives of the Photogrammetry, Remote Sensing and Spatial Information Sciences*, XLVIII-2/W2-2022:135–142

[10] Wróblewski, A., Wodecki, J., Trybała, P., and Zimroz, R. (2023b). Large underground structures geometry evaluation based on point cloud data analysis. In *IOP Conference Series: Earth and Environmental Science*, volume 1189, page 012005. IOP Publishing

[11] Wróblewski, A., Trybała, P., Banasiewicz, A., Zawiślak, M., Walerysiak, N., and Wodecki, J. (2023a). Possibilities of 3D laser scanning data utilization for numerical analysis of airflow in mining excavations. In *IOP Conference Series: Earth and Environmental Science*, volume 1189, page 012009. IOP Publishing

[12] Blachowski, J., Hajnrych, M., Trybała, P., and Tankielun, M. (2023). Multicriteria methodology for evaluating university campus facilities using the AHP approach. *Zeszyty Naukowe Politechniki Poznańskiej seria Organizacja i Zarządzanie*, 86:57–72

[13] Mazzacca, G., Karami, A., Rigon, S., Farella, E. M., Trybala, P., and Remondino, F. (2023). NeRF for Heritage 3D Reconstruction. *The International Archives of the Photogrammetry, Remote Sensing and Spatial Information Sciences*, XLVIII-M-2-2023:1051–1058

[14] Padkan, N., Trybala, P., Battisti, R., Remondino, F., and Bergeret, C. (2023). Evaluating Monocular Depth Estimation Methods. *The International Archives of the Photogrammetry, Remote Sensing and Spatial Information Sciences*, XLVIII-1/W3-2023:137–144

[15] Yan, Z., Mazzacca, G., Rigon, S., Farella, E. M., Trybala, P., and Remondino, F. (2023). NERFBK: A Holistic Dataset for Benchmarking NeRF-based 3D Reconstruction. *The International Archives of the Photogrammetry, Remote Sensing and Spatial Information Sciences*, XLVIII-1/W3-2023:219–226

[16] Szrek, A., Romańczukiewicz, K., Kujawa, P., and Trybała, P. (2024). Comparison of TLS and SLAM technologies for 3D reconstruction of objects with different geometries. In *IOP Conference Series: Earth and Environmental Science*, volume 1295, page 012012. IOP Publishing

Chapter 4

## *Closing remarks*

4.1   Conclusions

In this thesis, the problem of performing surveys with MMSs in mining environments to obtain their 3D reconstructions was studied. A comprehensive literature study of MMS applications in relevant conditions, carried out in a top-down approach, was presented. Several in-house developed systems, utilizing open source-based SLAM algorithms and different hardware, were tested in multiple real underground sites of various complexity. Both handheld scanners and mobile robots were investigated as a means of acquiring raw data. Field tests and data processing to produce final 3D point clouds as the output of the SLAM-based system were succeeded by extensive analyses of the 3D reconstruction quality. Different aspects and metrics associated with it were examined and compared to baselines of survey-grade TLS surveys and high-quality commercial MMT solutions.

The results of multiple studies show that currently available SLAM frameworks indeed face some challenges in the unstructured underground environment, but upon extending them with several improvements proposed by presented works, can meet or even surpass the 3D data quality provided by the solutions available on the commercial market. Moreover, the point clouds generated by proposed SLAM systems show high compliance with survey-grade measurements. Although the precision and density of the raw data from industrial grade LiDAR sensors used cannot match TLS instruments, the SLAM-based surveys could still be successfully adopted by multiple use cases in mining industry, which do not require millimeter-level precision, but rather need for centimeter-level data.

Although the last solution, developed within the scope of work described in Section 3.3.6: (Trybała et al., 2023b) could generally be considered the best and most advanced, others have specific advantages and can be preferred in selected use cases. A simplified workflow that could be used for selecting the most appropriate approach of applying SLAM for 3D reconstruction in mining environments for different use cases is presented in Figure 4.1 and the details

of each solution are given below:

- The simplest system composed of only a rotating mechanical LiDAR scanner provided satisfactory results for large-scale open-pit mining 3D reconstruction. The high FoV and long range of the sensor in occlusion-less conditions enabled the acquisition of a highly complete point cloud with sufficient accuracy for open-pit mining needs. Simplicity of the system could be beneficial for practical real-life applications,

- Actuated LiDAR system, while more expensive and complex, greatly increases the data coverage and enables achieving much better complete-ness of 3D reconstruction in constrained spaces compared to a standard horizontal sensor placement. This solution could also be of high inter-est for robotized solutions, since obtaining high completeness of the 3D reconstruction can be challenging for LiDAR scanners with limited FoV without applying more sophisticated, dedicated survey planning methods,

- First version of the Livox-based MMS already provided a substantial improvement in terms of accuracy, while still retaining low complexity and real-time performance even in large-scale tunnels. A low cost of building the system is its additional advantage. However, those come
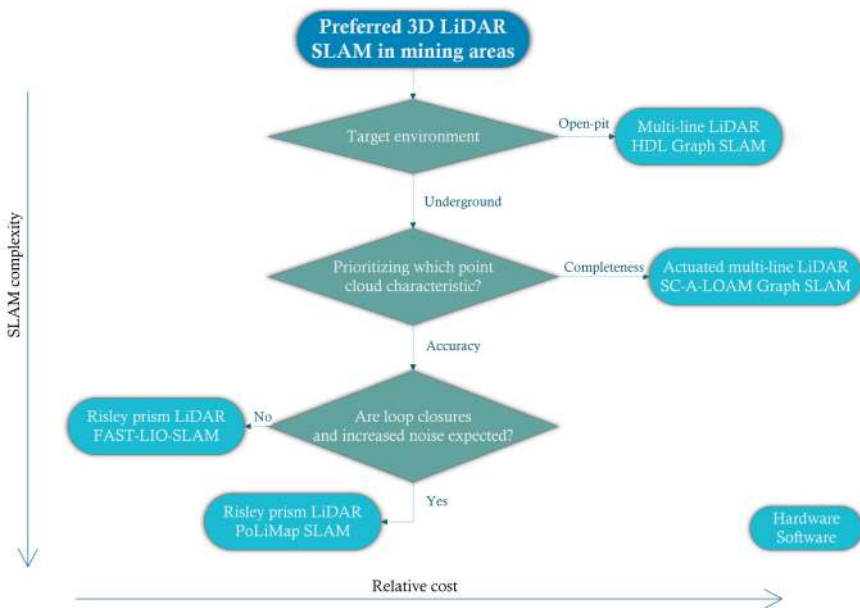
FIGURE 4.1. Flowchart of optimal LiDAR SLAM system selection strategy for mining environments

at a price of point cloud completeness highly dependant on the manual data acquisition strategy and do not perform loop closures very well,

- The final PoLiMap system provided the best accuracy and reliability, better coverage and stability due to employing a gimbal stabilization, but at a cost of quite high complexity of the system. Even though the process of data acquisition and processing with generic parameters is still simple, perfecting the tuning of 3D reconstruction parameters to achieve the best possible accuracy requires some domain-specific knowledge.

Three objectives were set at the start of this work, described in-depth in Section 3.1. All of them (introducing novel developments into state-of-the-art SLAM algorithms, building the open-source dataset collected for mining-related use cases and performing numerous field tests of developed MMTs in open-pit and underground facilities of varying difficulty) were accomplished in a series of six publications. Their specific contributions are presented in 3.3. All of the research activities carried out in this thesis allow to finally draw the conclusion that the thesis stated at the beginning of this work that *SLAM algorithms can be successfully applied to process 3D measurement data to acquire high-quality 3D reconstructions of mining environments* has been proven.

4.2   FUTURE RESEARCH DIRECTIONS

Based on the findings of this study, as well as technological solutions developed in its scope, several future research directions will be sought. Since both the pose graph approach and the FAST-LIO LiDAR-inertial odometry proved to be universal and reliable solutions, incorporating more factors would be a feasible strategy to further improve the final 3D reconstructions results obtained with this system. One such element could be provided by efficient loop closure detectors. Despite a substantial improvement of loop closure matching accuracy and reliability, introduced in Section 3.3.6: (Trybała et al., 2023b), for long acquisitions the time performance of detecting possible loops between graph nodes could start to be an issue. An enticing possibility is the use of DL-based point cloud descriptors.

Further hardware integration is envisioned. The integration of visual sensors for creating visual-LiDAR-inertial sensors could bring benefits not only from capability to add texture information to LiDAR points, but also from robustifying the system with inputs of visual odometry and visual place recognition for loop closure detection. SLAM solutions developed within the scope of this thesis can also be integrated with mobile robotic solutions for autonomous exploration and navigation tasks. Novel sensors, such as recently introduced

360° FoV Risley-prism LiDARs will be another interesting candidate topics to benefit from the developments of this study.

Finally, extending postprocessing options would potentially bring improvements in accuracy achievable with proposed SLAM systems. Features such as automatic hyperparameter tuning and the introduction of bundle adjustment concepts to jointly optimize the 3D point cloud and the sensor trajectory could be investigated. An example of such approach can be found in the study by Di Giammarino et al. (2023).

4.3 LIMITATIONS

Even though the presented dissertation provides extensive analyses on the topic of applying mobile mapping systems in mining environments, as in every study, it has some limitations to its scope related to the practical aspects of carrying out time- and resource-constrained research. In light of the rigorous data requirements inherent in my methodology, which involves the utilization of survey-grade reference data combined with robotic and handheld sensors within specific environments (and adhering to fully open access to the raw data), the feasibility of employing public datasets became impossible at the start of my work. Consequently, data acquisition required a hands-on approach, which led to limitations in both the number of test sites and the diversity of sensors used. New hardware appearing on the market can also greatly influence the quality of results that can be obtained with examined SLAM methods.

Given the plethora of algorithms available across various sensors, a strategic decision was made to narrow the focus to a specific subgroup. This subgroup, characterized by its superior performance in preliminary tests, centers around LiDAR-centric SLAM. This selective approach aimed to streamline the investigation, enhance the depth of understanding of the results and improve the likelihood of applicability of developed methods in real scenarios.

Furthermore, the ongoing DARPA Subterranean Challenge played a pivotal role in propelling research within this domain. Although contributing novelty to the field, the challenge also stressed the interest among researchers and demonstrated the inherent complexities involved in subterranean 3D mapping. This research, carried out in parallel, but clearly with more limitations, resources and slightly different focus, can be seen as a complementary input into the newest developments in underground site mobile mapping from the surveying point of view.

Formerly, simulation studies were also incorporated in initial phases of my research, although they were not published. However, these tests revealed a considerable simulation-to-reality gap, particularly concerning algorithm

performance in simulated environments versus their real-world counterparts shown in the articles. Furthermore, a paper of Kadian et al. (2020) shows that closing the so-called *sim2real* gap even for simple tasks still needs a substantial computational effort for parameter tuning. These discrepancies were observed not only in traditional algorithms but were even more apparent in DL-based solutions. Despite the low applicability of end-to-end DL-based SLAM methods in practical use cases, recent developments in DL features for V-SLAM (Morelli et al., 2023b) have shown promising results in different scenarios.

References

Akpınar, B. (2021). Performance of Different SLAM Algorithms for Indoor and Outdoor Mapping Applications. *Applied System Innovation*, 4(4).

Al-Bayari, O. (2019). Mobile mapping systems in civil engineering projects (case studies). *Applied Geomatics*, 11(1):1–13.

Alatise, M. B. and Hancke, G. P. (2020). A review on challenges of autonomous mobile robot and sensor fusion methods. *IEEE Access*, 8:39830–39846.

Aulinas, J., Petillot, Y., Salvi, J., and Lladó, X. (2008). The SLAM problem: a survey. *Artificial Intelligence Research and Development*, pages 363–371.

Azpúrua, H., Rezende, A., Potje, G., Júnior, G. P. d. C., Fernandes, R., Miranda, V., Filho, L. W. d. R., Domingues, J., Rocha, F., de Sousa, F. L. M., de Barros, L. G. D., Nascimento, E. R., Macharet, D. G., Pessin, G., and Freitas, G. M. (2021). Towards semi-autonomous robotic inspection and mapping in confined spaces with the EspeleoRobô. *J. Intell. Robot. Syst.*, 101(4).

Bailey, T. and Durrant-Whyte, H. (2006). Simultaneous localization and mapping (SLAM): Part II. *IEEE robotics & automation magazine*, 13(3):108–117.

Bailey, T., Nieto, J., Guivant, J., Stevens, M., and Nebot, E. (2006). Consistency of the EKF-SLAM Algorithm. In *2006 IEEE/RSJ International Conference on Intelligent Robots and Systems*, pages 3562–3568.

Będkowski, J. (2022). *Large-Scale Simultaneous Localization and Mapping*. Springer.

Behley, J., Garbade, M., Milioto, A., Quenzel, J., Behnke, S., Stachniss, C., and Gall, J. (2019). Semantickitti: A dataset for semantic scene understanding of lidar sequences. In *Proceedings of the IEEE/CVF international conference on computer vision*, pages 9297–9307.

Benton, D., Seymour, J., Boltz, M., Raffaldi, M., and Finley, S. (2017). Photogrammetry in underground mining ground control—Lucky Friday mine case study. In *Deep Mining 2017: Proceedings of the Eighth International Conference on Deep and High Stress Mining*, pages 587–598. Australian Centre for Geomechanics.

Benton, D. J., Chambers, A. J., Raffaldi, M. J., Finley, S. A., and Powers, M. J. (2016). Close-range photogrammetry in underground mining ground control. In Ardanuy, P. E. and Puschell, J. J., editors, *SPIE Proceedings*. SPIE.

Bescos, B., Fácil, J. M., Civera, J., and Neira, J. (2018). DynaSLAM: Tracking, Mapping, and Inpainting in Dynamic Scenes. *IEEE Robotics and Automation Letters*, 3(4):4076–4083.

Blachowski, J., Hajnrych, M., Trybała, P., and Tankielun, M. (2023). Multi-criteria methodology for evaluating university campus facilities using the AHP approach. *Zeszyty Naukowe Politechniki Poznańskiej seria Organizacja i Zarządzanie*, 86:57–72.

Bogoslavskyi, I., Mazuran, M., and Stachniss, C. (2016). Robust homing for autonomous robots. In *2016 IEEE International Conference on Robotics and Automation (ICRA)*. IEEE.

Bosse, M., Newman, P., Leonard, J., and Teller, S. (2004). Simultaneous localization and map building in large-scale cyclic environments using the Atlas framework. *Int. J. Rob. Res.*, 23(12):1113–1139.

Bossler, J., Goad, C., Johnson, P., and Novak, K. (1991). GPS and GIS map the nation's highway, GeoInfo System Magazine.

Bossler, J. D. and Toth, C. K. (1995). Accuracies obtained by the GPSVan [TM]. In *GIS LIS-*

INTERNATIONAL CONFERENCE-, volume 1, pages 70–77. American Society for Photogrammetry and Remote Sensing.

Bowman, S. L., Atanasov, N., Daniilidis, K., and Pappas, G. J. (2017). Probabilistic data association for semantic slam. In *2017 IEEE international conference on robotics and automation (ICRA)*, pages 1722–1729. IEEE.

Bresson, G., Alsayed, Z., Yu, L., and Glaser, S. (2017). Simultaneous localization and mapping: A survey of current trends in autonomous driving. *IEEE Transactions on Intelligent Vehicles*, 2(3):194–220.

Cadena, C., Carlone, L., Carrillo, H., Latif, Y., Scaramuzza, D., Neira, J., Reid, I., and Leonard, J. J. (2016). Past, present, and future of simultaneous localization and mapping: Toward the robust-perception age. *IEEE Transactions on robotics*, 32(6):1309–1332.

Campos, C., Elvira, R., Gomez, J. J., Montiel, J. M. M., and Tardós, J. D. (2021). ORB-SLAM3: An Accurate Open-Source Library for Visual, Visual-Inertial and Multi-Map SLAM. *IEEE Transactions on Robotics*, 37(6):1874–1890.

Chang, Y., Ebadi, K., Denniston, C. E., Ginting, M. F., Rosinol, A., Reinke, A., Palieri, M., Shi, J., Chatterjee, A., Morrell, B., et al. (2022). LAMP 2.0: A robust multi-robot SLAM system for operation in challenging large-scale underground environments. *IEEE Robotics and Automation Letters*, 7(4):9175–9182.

Chehri, A., Fortier, P., and Tardif, P. M. (2009). UWB-based sensor networks for localization in mining environments. *Ad Hoc Networks*, 7(5):987–1000.

Chen, J., Li, K., Chang, K.-J., Sofia, G., and Tarolli, P. (2015). Open-pit mining geomorphic feature characterisation. *International Journal of Applied Earth Observation and Geoinformation*, 42:76–86.

Chen, K., Lopez, B. T., Agha-mohammadi, A.-a., and Mehta, A. (2022). Direct LiDAR Odometry: Fast Localization With Dense Point Clouds. *IEEE Robotics and Automation Letters*, 7(2):2000–2007.

Chen, X., Milioto, A., Palazzolo, E., Giguère, P., Behley, J., and Stachniss, C. (2019). SuMa++: Efficient LiDAR-based Semantic SLAM. In *Proceedings of the IEEE/RSJ Int. Conf. on Intelligent Robots and Systems (IROS)*, pages 4530–4537.

Cramariuc, A., Bernreiter, L., Tschopp, F., Fehr, M., Reijgwart, V., Nieto, J., Siegwart, R., and Cadena, C. (2022). maplab 2.0–a modular and multi-modal mapping framework. *IEEE Robotics and Automation Letters*, 8(2):520–527.

Cummins, M. and Newman, P. (2008). FAB-MAP: Probabilistic localization and mapping in the space of appearance. *Int. J. Rob. Res.*, 27(6):647–665.

Cummins, M. and Newman, P. (2011). Appearance-only SLAM at large scale with FAB-MAP 2.0. *Int. J. Rob. Res.*, 30(9):1100–1123.

Ćwiąkała, P., Gruszczyński, W., Stoch, T., Puniach, E., Mocheń, D., Matwij, W., Matwij, K., Nędzka, M., Sopata, P., and Wójcik, A. (2020). UAV applications for determination of land deformations caused by underground mining. *Remote Sensing*, 12(11):1733.

Dang, T., Mascarich, F., Khattak, S., Papachristos, C., and Alexis, K. (2019). Graph-based path planning for autonomous robotic exploration in subterranean environments. In *2019 IEEE/RSJ International Conference on Intelligent Robots and Systems (IROS)*, pages 3105–3112. IEEE.

Davison, A. J., Reid, I. D., Molton, N. D., and Stasse, O. (2007). MonoSLAM: Real-time single camera SLAM. *IEEE transactions on pattern analysis and machine intelligence*, 29(6):1052–1067.

Dellaert, F. (2012). Factor graphs and GTSAM: A hands-on introduction. *Georgia Institute of Technology, Tech. Rep*, 2:4.

Dellaert, F. and Kaess, M. (2006). Square root SAM: Simultaneous localization and mapping via square root information smoothing. *Int. J. Rob. Res.*, 25(12):1181–1203.

Dellenbach, P., Deschaud, J.-E., Jacquet, B., and Goulette, F. (2021). CT-ICP: Real-time Elastic LiDAR Odometry with Loop Closure.

Denniston, C. E., Chang, Y., Reinke, A., Ebadi, K., Sukhatme, G. S., Carlone, L., Morrell, B., and Agha-mohammadi, A.-A. (2022). Loop closure prioritization for efficient and scalable multi-robot SLAM. *IEEE Robot. Autom. Lett.*, 7(4):9651–9658.

Di Giammarino, L., Giacomini, E., Brizi, L., Salem, O., and Grisetti, G. (2023). Photometric LiDAR and RGB-D Bundle Adjustment. *IEEE Robotics and Automation Letters*.

Di Stefano, F., Torresani, A., Farella, E. M., Pierdicca, R., Menna, F., and Remondino, F. (2021). 3D surveying of underground built heritage: Opportunities and challenges of mobile technologies. *Sustainability*, 13(23):13289.

DiFrancesco, P.-M., Bonneau, D., and Hutchinson, D. J. (2020). The implications of M3C2 projection diameter on 3D semi-automated rockfall extraction from sequential terrestrial laser scanning point clouds. *Remote Sensing*, 12(11):1885.

Dissanayake, M., Newman, P., Clark, S., Durrant-Whyte, H., and Csorba, M. (2001). A solution to the simultaneous localization and map building (SLAM) problem. *IEEE Transactions on Robotics and Automation*, 17(3):229–241.

Dong, Y., Wang, D., Liu, F., and Wang, J. (2022). A new data processing method for high-precision mining subsidence measurement using airborne LiDAR. *Frontiers in Earth Science*, 10:858050.

Droeschel, D. and Behnke, S. (2018). Efficient continuous-time SLAM for 3D lidar-based online mapping. In *2018 IEEE International Conference on Robotics and Automation (ICRA)*, pages 5000–5007. IEEE.

Durrant-Whyte, H. and Bailey, T. (2006). Simultaneous localization and mapping: part I. *IEEE robotics & automation magazine*, 13(2):99–110.

Ebadi, K., Bernreiter, L., Biggie, H., Catt, G., Chang, Y., Chatterjee, A., Denniston, C. E., Deschênes, S.-P., Harlow, K., Khattak, S., et al. (2023). Present and future of SLAM in extreme environments: The DARPA subT challenge. *IEEE Transactions on Robotics*.

Ebadi, K., Chang, Y., Palieri, M., Stephens, A., Hatteland, A., Heiden, E., Thakur, A., Funabiki, N., Morrell, B., Wood, S., et al. (2020). LAMP: Large-scale autonomous mapping and positioning for exploration of perceptually-degraded subterranean environments. In *2020 IEEE International Conference on Robotics and Automation (ICRA)*, pages 80–86. IEEE.

Elhashash, M., Albanwan, H., and Qin, R. (2022). A Review of Mobile Mapping Systems: From Sensors to Applications. *Sensors*, 22(11).

Ellmann, A., Kütimets, K., Varbla, S., Väli, E., and Kanter, S. (2021). Advancements in underground mine surveys by using SLAM-enabled handheld laser scanners. *Survey Review*, 54(385):363–374.

Endres, F., Hess, J., Engelhard, N., Sturm, J., Cremers, D., and Burgard, W. (2012a). An evaluation of the RGB-D SLAM system. In *2012 IEEE International Conference on Robotics and Automation*. IEEE.

Endres, F., Hess, J., Engelhard, N., Sturm, J., Cremers, D., and Burgard, W. (2012b). An evaluation of the RGB-D SLAM system. In *2012 IEEE International Conference on Robotics and Automation*. IEEE.

Endres, F., Hess, J., Sturm, J., Cremers, D., and Burgard, W. (2013). 3-D mapping with an RGB-D camera. *IEEE transactions on robotics*, 30(1):177–187.

Engel, J., Koltun, V., and Cremers, D. (2017). Direct sparse odometry. *IEEE transactions on pattern analysis and machine intelligence*, 40(3):611–625.

Engel, J., Schöps, T., and Cremers, D. (2014). LSD-SLAM: Large-scale direct monocular SLAM. In *European conference on computer vision*, pages 834–849. Springer.

Estrada, C., Neira, J., and Tardos, J. (2005). Hierarchical SLAM: real-time accurate mapping of large environments. *IEEE Transactions on Robotics*, 21(4):588–596.

Fairfield, N., Kantor, G., and Wettergreen, D. (2006). Towards particle filter SLAM with three dimensional evidence grids in a flooded subterranean environment. In *Proceedings 2006 IEEE International Conference on Robotics and Automation, 2006. ICRA 2006*. IEEE.

Färber, M. (2019). The microsoft academic knowledge graph: A linked data source with 8 billion triples of scholarly data. In *The Semantic Web–ISWC 2019: 18th International Semantic Web Conference, Auckland, New Zealand, October 26–30, 2019, Proceedings, Part II 18*, pages 113–129. Springer.

Forster, C., Zhang, Z., Gassner, M., Werlberger, M., and Scaramuzza, D. (2016). SVO: Semidirect visual odometry for monocular and multicamera systems. *IEEE Transactions on Robotics*, 33(2):249–265.

Fuentes-Pacheco, J., Ruiz-Ascencio, J., and Rendón-Mancha, J. M. (2015). Visual simultaneous localization and mapping: a survey. *Artif. Intell. Rev.*, 43(1):55–81.

Gallwey, J., Eyre, M., and Coggan, J. (2021). A machine learning approach for the detection of supporting rock bolts from laser scan data in an underground mine. *Tunnelling and Underground Space Technology*, 107:103656.

García-Luna, R., Senent, S., Jurado-Piña, R., and Jimenez, R. (2019). Structure from Motion photogrammetry to characterize underground rock masses: Experiences from two real tunnels. *Tunnelling and Underground Space Technology*, 83:262–273.

Gautier, Q. K., Garrison, T. G., Rushton, F., Bouck, N., Lo, E., Tueller, P., Schurgers, C., and Kastner, R. (2020). Low-cost 3D scanning systems for cultural heritage documentation. *J. Cult. Herit. Manag. Sustain. Dev.*, 10(4):437–455.

Geiger, A., Lenz, P., and Urtasun, R. (2012a). Are we ready for autonomous driving? the kitti vision benchmark suite. In *2012 IEEE conference on computer vision and pattern recognition*, pages 3354–3361. IEEE.

Geiger, A., Lenz, P., and Urtasun, R. (2012b). Are we ready for Autonomous Driving? The KITTI Vision Benchmark Suite. In *Conference on Computer Vision and Pattern Recognition (CVPR)*.

Geneva, P., Eckenhoff, K., Lee, W., Yang, Y., and Huang, G. (2020). OpenVINS: A Research Platform for Visual-Inertial Estimation. In *Proc. of the IEEE International Conference on Robotics and Automation*, Paris, France.

Girardeau-Montaut, D. (2016). CloudCompare. *France: EDF R&D Telecom ParisTech*, 11:5.

Gomez-Ojeda, R., Moreno, F.-A., Zuñiga-Noël, D., Scaramuzza, D., and Gonzalez-Jimenez, J. (2019). PL-SLAM: A Stereo SLAM System Through the Combination of Points and Line Segments. *IEEE Transactions on Robotics*, 35(3):734–746.

Granshaw, S. I. (2020). Photogrammetric terminology. *The Photogrammetric Record*, 35(170):143–288.

Grejner-Brzezinska, D. A., Li, R., Haala, N., and Toth, C. (2004). From Mobile Mapping to Telegeoinformatics. *Photogrammetric Engineering & Remote Sensing*, 70(2):197–210.

Grisetti, G., Kümmerle, R., Stachniss, C., and Burgard, W. (2010). A tutorial on graph-based SLAM. *IEEE Intelligent Transportation Systems Magazine*, 2(4):31–43.

Grisetti, G., Stachniss, C., and Burgard, W. (2005). Improving grid-based slam with rao-blackwellized particle filters by adaptive proposals and selective resampling. In *Proceedings of the 2005 IEEE international conference on robotics and automation*, pages 2432–2437. IEEE.

Grisetti, G., Stachniss, C., and Burgard, W. (2007). Improved techniques for grid mapping with rao-blackwellized particle filters. *IEEE transactions on Robotics*, 23(1):34–46.

Grupp, M. (2017). evo: Python package for the evaluation of odometry and SLAM. https://github.com/MichaelGrupp/evo.

Guivant, J. and Nebot, E. (2001). Optimization of the simultaneous localization and map-building algorithm for real-time implementation. *IEEE Transactions on Robotics and Automation*, 17(3):242–257.

Gurgel, M. J. and Preusse, A. (2021). New opportunities and challenges in surveying underground cavities using photogrammetric methods. *International Journal of Mining Science and Technology*, 31(1):9–13. special issue on ground control in mining in 2020.

Hähnel, D., Montemerlo, M., Ferguson, D., Triebel, R., Burgard, W., and Thrun, S. (2002). A system for volumetric robotic mapping of underground mines. *Submitted for publication*.

Handa, A., Whelan, T., McDonald, J., and Davison, A. J. (2014a). A benchmark for RGB-D visual odometry, 3D reconstruction and SLAM. In *2014 IEEE International Conference on Robotics and Automation (ICRA)*. IEEE.

Handa, A., Whelan, T., McDonald, J., and Davison, A. J. (2014b). A benchmark for RGB-D visual odometry, 3D reconstruction and SLAM. In *2014 IEEE International Conference on Robotics and Automation (ICRA)*. IEEE.

Harrell, J. A. and Brown, V. M. (1992). The World's oldest surviving geological map: the 1150 BC Turin Papyrus from Egypt. *The Journal of Geology*, 100(1):3–18.

Helmberger, M., Morin, K., Berner, B., Kumar, N., Cioffi, G., and Scaramuzza, D. (2022). The hilti slam challenge dataset. *IEEE Robotics and Automation Letters*, 7(3):7518–7525.

Hess, W., Kohler, D., Rapp, H., and Andor, D. (2016). Real-Time Loop Closure in 2D LIDAR SLAM. In *2016 IEEE International Conference on Robotics and Automation (ICRA)*, pages 1271–1278.

Huang, S. and Dissanayake, G. (2007). Convergence and Consistency Analysis for Extended Kalman Filter Based SLAM. *IEEE Transactions on Robotics*, 23(5):1036–1049.

Hug, D., Bänninger, P., Alzugaray, I., and Chli, M. (2022). Continuous-Time Stereo-Inertial Odometry. *IEEE Robotics and Automation Letters*, 7(3):6455–6462.

Hutton, C. (1778). An Account of the Calculations Made from the Survey and Measures Taken at Schehallien, in Order to Ascertain the Mean Density of the Earth. By Charles Hutton, Esq. F. R. S. *Philosophical Transactions of the Royal Society of London*, 68:689–788.

Ignjatović Stupar, D., Rošer, J., and Vulić, M. (2020). Investigation of unmanned aerial vehicles-based photogrammetry for large mine subsidence monitoring. *Minerals*, 10(2):196.

Jacobson, A., Zeng, F., Smith, D., Boswell, N., Peynot, T., and Milford, M. (2018). Semi-supervised SLAM: Leveraging low-cost sensors on underground autonomous vehicles for position tracking. In *2018 IEEE/RSJ International Conference on Intelligent Robots and Systems (IROS)*. IEEE.

Jacobson, A., Zeng, F., Smith, D., Boswell, N., Peynot, T., and Milford, M. (2021). What localizes beneath: A metric multisensor localization and mapping system for autonomous underground mining vehicles. *J. Field Robot.*, 38(1):5–27.

Jende, P., Nex, F., Gerke, M., and Vosselman, G. (2018). A fully automatic approach to register mobile mapping and airborne imagery to support the correction of platform trajectories in GNSS-denied urban areas. *ISPRS journal of photogrammetry and remote sensing*, 141:86–99.

Jones, E., Sofonia, J., Canales, C., Hrabar, S., and Kendoul, F. (2019). Advances and applications for automated drones in underground mining operations. In *Deep Mining 2019: Proceedings of the Ninth International Conference on Deep and High Stress Mining*, pages 323–334. The Southern African Institute of Mining and Metallurgy.

Kadian, A., Truong, J., Gokaslan, A., Clegg, A., Wijmans, E., Lee, S., Savva, M., Chernova, S., and Batra, D. (2020). Sim2real predictivity: Does evaluation in simulation predict real-world performance? *IEEE Robotics and Automation Letters*, 5(4):6670–6677.

Kaess, M., Johannsson, H., Roberts, R., Ila, V., Leonard, J. J., and Dellaert, F. (2012). iSAM2: Incremental smoothing and mapping using the Bayes tree. *Int. J. Rob. Res.*, 31(2):216–235.

Kajzar, V., Kukutsch, R., and Heroldova, N. (2015). Verifying the possibilities of using a 3D laser scanner in the mining underground. *Acta Geodyn. Geomater*, 12(1):51–58.

Kasza, D. (2018). Modelling of underground objects and geological-tectonic structures from a

point cloud: application of the developed models in studies of geodynamic processes. *E3S Web of Conferences*, 55:00014.

Kerbl, B., Kopanas, G., Leimkühler, T., and Drettakis, G. (2023). 3d gaussian splatting for real-time radiance field rendering. *ACM Transactions on Graphics (ToG)*, 42(4):1–14.

Kerl, C., Sturm, J., and Cremers, D. (2013). Dense visual SLAM for RGB-D cameras. In *2013 IEEE/RSJ International Conference on Intelligent Robots and Systems*. IEEE.

Khedekar, N., Kulkarni, M., and Alexis, K. (2022). MIMOSA: A multi-modal SLAM framework for resilient autonomy against sensor degradation. In *2022 IEEE/RSJ International Conference on Intelligent Robots and Systems (IROS)*. IEEE.

Kim, G. and Kim, A. (2020). Remove, then revert: Static point cloud map construction using multiresolution range images. In *2020 IEEE/RSJ International Conference on Intelligent Robots and Systems (IROS)*, pages 10758–10765. IEEE.

Kim, G., Yun, S., Kim, J., and Kim, A. (2022). Sc-lidar-slam: a front-end agnostic versatile lidar slam system. In *2022 International Conference on Electronics, Information, and Communication (ICEIC)*, pages 1–6. IEEE.

Klein, G. and Murray, D. (2007). Parallel tracking and mapping for small AR workspaces. In *2007 6th IEEE and ACM international symposium on mixed and augmented reality*, pages 225–234. IEEE.

Knapitsch, A., Park, J., Zhou, Q.-Y., and Koltun, V. (2017). Tanks and temples: Benchmarking large-scale scene reconstruction. *ACM Transactions on Graphics (ToG)*, 36(4):1–13.

Koestler, L., Yang, N., Zeller, N., and Cremers, D. (2022). Tandem: Tracking and dense mapping in real-time using deep multi-view stereo. In *Conference on Robot Learning*, pages 34–45. PMLR.

Kohlbrecher, S., Von Stryk, O., Meyer, J., and Klingauf, U. (2011). A flexible and scalable SLAM system with full 3D motion estimation. In *2011 IEEE international symposium on safety, security, and rescue robotics*, pages 155–160. IEEE.

Koide, K., Miura, J., and Menegatti, E. (2019). A portable three-dimensional LIDAR-based system for long-term and wide-area people behavior measurement. *International Journal of Advanced Robotic Systems*, 16(2):1729881419841532.

Koide, K., Miura, J., Yokozuka, M., Oishi, S., and Banno, A. (2020). Interactive 3D graph SLAM for map correction. *IEEE Robotics and Automation Letters*, 6(1):40–47.

Konolige, K. and Agrawal, M. (2008). FrameSLAM: From Bundle Adjustment to Real-Time Visual Mapping. *IEEE Transactions on Robotics*, 24(5):1066–1077.

Kopeć, A., Trybała, P., Głąbicki, D., Buczyńska, A., Owczarz, K., Bugajska, N., Kozińska, P., Chojwa, M., and Gattner, A. (2020). Application of Remote Sensing, GIS and Machine Learning with Geographically Weighted Regression in Assessing the Impact of Hard Coal Mining on the Natural Environment. *Sustainability*, 12(22):9338.

Koval, A., Kanellakis, C., and Nikolakopoulos, G. (2022). Evaluation of Lidar-based 3D SLAM algorithms in SubT environment. *IFAC-PapersOnLine*, 55(38):126–131.

Kramer, A., Kasper, M., and Heckman, C. (2021). VI-SLAM for subterranean environments. In *Field and Service Robotics*, pages 159–172. Springer Singapore, Singapore.

Kumar, S. S., Jabannavar, S. S., Shashank, K. R., Nagaraj, M., and Shreenivas, B. (2017). Localization and tracking of unmanned vehicles for underground mines. In *2017 Second International Conference on Electrical, Computer and Communication Technologies (ICECCT)*. IEEE.

Kümmerle, R., Grisetti, G., Strasdat, H., Konolige, K., and Burgard, W. (2011). g 2 o: A general framework for graph optimization. In *2011 IEEE International Conference on Robotics and Automation*, pages 3607–3613. IEEE.

Kümmerle, R., Ruhnke, M., Steder, B., Stachniss, C., and Burgard, W. (2015). Autonomous robot navigation in highly populated pedestrian zones. *Journal of Field Robotics*, 32(4):565–589.

Kümmerle, R., Steder, B., Dornhege, C., Ruhnke, M., Grisetti, G., Stachniss, C., and Kleiner, A. (2009). On measuring the accuracy of SLAM algorithms. *Autonomous Robots*, 27:387–407.

Labbé, M. and Michaud, F. (2019). RTAB-Map as an open-source lidar and visual simultaneous localization and mapping library for large-scale and long-term online operation. *Journal of field robotics*, 36(2):416–446.

Lajoie, P.-Y. and Beltrame, G. (2023). Swarm-SLAM : Sparse decentralized collaborative Simultaneous Localization and Mapping framework for multi-robot systems.

Lajoie, P.-Y., Ramtoula, B., Chang, Y., Carlone, L., and Beltrame, G. (2020). DOOR-SLAM: Distributed, Online, and Outlier Resilient SLAM for Robotic Teams. *IEEE Robotics and Automation Letters*, 5(2):1656–1663.

Leutenegger, S., Furgale, P., Rabaud, V., Chli, M., Konolige, K., and Siegwart, R. (2013). Keyframe-based visual-inertial slam using nonlinear optimization. *Proceedings of Robotis Science and Systems (RSS) 2013*.

Leutenegger, S., Lynen, S., Bosse, M., Siegwart, R., and Furgale, P. (2015). Keyframe-based visual–inertial odometry using nonlinear optimization. *The International Journal of Robotics Research*, 34(3):314–334.

Li, J., Wu, W., Yang, B., Zou, X., Yang, Y., Zhao, X., and Dong, Z. (2023a). WHU-helmet: A helmet-based multisensor SLAM dataset for the evaluation of real-time 3-D mapping in large-scale GNSS-denied environments. *IEEE Trans. Geosci. Remote Sens.*, 61:1–16.

Li, K., Li, M., and Hanebeck, U. D. (2021). Towards High-Performance Solid-State-LiDAR-Inertial Odometry and Mapping. *IEEE Robotics and Automation Letters*, 6(3):5167–5174.

Li, M., Hu, K., Liu, Y., Hu, E., Tang, C., Zhu, H., and Zhou, G. (2023b). A Multimodal Robust Simultaneous Localization and Mapping Approach Driven by Geodesic Coordinates for Coal Mine Mobile Robots. *Remote Sensing*, 15(21):5093.

Li, Q. and Cheng, X. (2018). Comparison of Different Feature Sets for TLS Point Cloud Classification. *Sensors*, 18(12).

Li, S. and Lee, D. (2017). RGB-D SLAM in Dynamic Environments Using Static Point Weighting. *IEEE Robotics and Automation Letters*, 2(4):2263–2270.

Li, Y., Ma, L., Zhong, Z., Liu, F., Chapman, M. A., Cao, D., and Li, J. (2020). Deep learning for lidar point clouds in autonomous driving: A review. *IEEE Transactions on Neural Networks and Learning Systems*, 32(8):3412–3432.

Lian, X., Liu, X., Ge, L., Hu, H., Du, Z., and Wu, Y. (2021). Time-series unmanned aerial vehicle photogrammetry monitoring method without ground control points to measure mining subsidence. *Journal of Applied Remote Sensing*, 15(2):024505–024505.

Lin, J. and Zhang, F. (2022). R3LIVE: A Robust, Real-time, RGB-colored, LiDAR-Inertial-Visual tightly-coupled state Estimation and mapping package. In *2022 International Conference on Robotics and Automation (ICRA)*, pages 10672–10678.

Lo, K., Wang, L. L., Neumann, M., Kinney, R., and Weld, D. (2020). S2ORC: The Semantic Scholar Open Research Corpus. In Jurafsky, D., Chai, J., Schluter, N., and Tetreault, J., editors, *Proceedings of the 58th Annual Meeting of the Association for Computational Linguistics*, pages 4969–4983, Online. Association for Computational Linguistics.

Luhmann, T., Robson, S., Kyle, S., and Boehm, J. (2023). *Close-range photogrammetry and 3D imaging*. Walter de Gruyter GmbH & Co KG.

Marangi, A., Olia, K., Daneshgaran, F., Bruno, N., Lizzio, F., and Mondin, M. (2019). Simultaneous localization and mapping with application to monitoring of underground transportation infrastructure. In *2019 International Symposium on Advanced Electrical and Communication Technologies (ISAECT)*. IEEE.

Mazzacca, G., Karami, A., Rigon, S., Farella, E. M., Trybala, P., and Remondino, F. (2023). NeRF for Heritage 3D Reconstruction. *The International Archives of the Photogrammetry, Remote*

Sensing and Spatial Information Sciences, XLVIII-M-2-2023:1051–1058.

Menendez, E., Martinez De La Casa, S., Marin, M., and Balaguer, C. (2019). uSLAM Implementation for Autonomous Underground Robot. In *2019 IEEE SmartWorld, Ubiquitous Intelligence & Computing, Advanced & Trusted Computing, Scalable Computing & Communications, Cloud & Big Data Computing, Internet of People and Smart City Innovation (SmartWorld/SCALCOM/UIC/ATC/CBDCom/IOP/SCI)*. IEEE.

Menna, F., Torresani, A., Battisti, R., Nocerino, E., and Remondino, F. (2022). A modular and low-cost portable VSLAM system for real-time 3D mapping: from indoor and outdoor spaces to underwater environments. *The International Archives of the Photogrammetry, Remote Sensing and Spatial Information Sciences*, 48:153–162.

Meydenbauer, A. (1867). Die photometrographie. *Wochenblatt des Architektenvereins zu Berlin*, 1(14):125–126.

Mildenhall, B., Srinivasan, P. P., Tancik, M., Barron, J. T., Ramamoorthi, R., and Ng, R. (2021). Nerf: Representing scenes as neural radiance fields for view synthesis. *Communications of the ACM*, 65(1):99–106.

Milijas, R., Markovic, L., Ivanovic, A., Petric, F., and Bogdan, S. (2021). A comparison of lidar-based slam systems for control of unmanned aerial vehicles. In *2021 International Conference on Unmanned Aircraft Systems (ICUAS)*, pages 1148–1154. IEEE.

Montemerlo, M., Thrun, S., Koller, D., Wegbreit, B., et al. (2002). FastSLAM: A factored solution to the simultaneous localization and mapping problem. *Aaai/iaai*, 593598.

Moreira, A., Krieger, G., Hajnsek, I., Hounam, D., Werner, M., Riegger, S., and Settelmeyer, E. (2004). TanDEM-X: A TerraSAR-X add-on satellite for single-pass SAR interferometry. In *IGARSS 2004. 2004 IEEE International Geoscience and Remote Sensing Symposium*, volume 2, pages 1000–1003. IEEE.

Morelli, L., Ioli, F., Beber, R., Menna, F., Remondino, F., and Vitti, A. (2023a). COLMAP-SLAM: a Framework for Visual Odometry. *The International Archives of the Photogrammetry, Remote Sensing and Spatial Information Sciences*, 48:317–324.

Morelli, L., Menna, F., Vitti, A., Remondino, F., and Toth, C. (2023b). Performance Evaluation of Image-Aided Navigation with Deep-Learning Features. In *ION GNSS+, The International Technical Meeting of the Satellite Division of The Institute of Navigation*, GNSS 2023. Institute of Navigation.

Mur-Artal, R., Montiel, J. M. M., and Tardos, J. D. (2015). ORB-SLAM: a versatile and accurate monocular SLAM system. *IEEE transactions on robotics*, 31(5):1147–1163.

Nature, S. (2017). Springer Nature SciGraph: Supporting open science and the wider understanding of research.

Nex, F. and Remondino, F. (2014). UAV for 3D mapping applications: a review. *Applied geomatics*, 6:1–15.

Nocerino, E., Stathopoulou, E. K., Rigon, S., and Remondino, F. (2020). Surface reconstruction assessment in photogrammetric applications. *Sensors*, 20(20):5863.

Owczarz, K. (2020). A review of geodetic and remote sensing methods used for detecting surface displacements caused by mining. In *IOP Conference Series: Earth and Environmental Science*, volume 609, page 012076. IOP Publishing.

Ozhygin, D., Dorokhov, D., Ozhygina, S., Ozhygin, S., Staňková, H., et al. (2021). Terrestrial photogrammetry at the quarry and validating the accuracy of slope models for monitoring their stability. In *IOP Conference Series: Earth and Environmental Science*, volume 906, page 012062. IOP Publishing.

Padkan, N., Trybala, P., Battisti, R., Remondino, F., and Bergeret, C. (2023). Evaluating Monocular Depth Estimation Methods. *The International Archives of the Photogrammetry, Remote Sensing and Spatial Information Sciences*, XLVIII-1/W3-2023:137–144.

Pan, Y., Xiao, P., He, Y., Shao, Z., and Li, Z. (2021). MULLS: Versatile LiDAR SLAM via multi-metric linear least square. In *2021 IEEE International Conference on Robotics and Automation (ICRA)*, pages 11633–11640. IEEE.

Park, B. and Myung, H. (2014). Underground localization using dual magnetic field sequence measurement and pose graph SLAM for directional drilling. *Meas. Sci. Technol.*, 25(12):125101.

Perfetti, L., Elalailyi, A., Fassi, F., et al. (2022a). Portable Multi-Camera System: from Fast Tunnel Mapping to Semi-Automatic Space Decomposition and Cross-Section Extraction. *International Archives of the Photogrammetry, Remote Sensing and Spatial Information Sciences*, 43:259–266.

Perfetti, L., Fassi, F., et al. (2022b). Handheld Fisheye Multicamera System: Surveying Meandering Architectonic Spaces in Open-Loop Mode-Accuracy Assessment. *International Archives of the Photogrammetry, Remote Sensing and Spatial Information Sciences*, 46(2):435–442.

Piermattei, L., Karel, W., Wang, D., Wieser, M., Mokroš, M., Surový, P., Koreň, M., Tomaštík, J., Pfeifer, N., and Hollaus, M. (2019). Terrestrial Structure from Motion Photogrammetry for Deriving Forest Inventory Data. *Remote Sensing*, 11(8):950.

Quigley, M., Conley, K., Gerkey, B., Faust, J., Foote, T., Leibs, J., Wheeler, R., Ng, A. Y., et al. (2009). ROS: an open-source Robot Operating System. In *ICRA workshop on open source software*, volume 3, page 5. Kobe, Japan.

Rann, K. and Johnson, R. S. (2019). Chasing the line: Hutton's contribution to the invention of contours. *Journal of Maps*, 15(3):48–56.

Reinke, A., Palieri, M., Morrell, B., Chang, Y., Ebadi, K., Carlone, L., and Agha-Mohammadi, A.-A. (2022). LOCUS 2.0: Robust and Computationally Efficient Lidar Odometry for Real-Time 3D Mapping. *IEEE Robotics and Automation Letters*, pages 1–8.

Remondino, F., Karami, A., Yan, Z., Mazzacca, G., Rigon, S., and Qin, R. (2023). A critical analysis of nerf-based 3d reconstruction. *Remote Sensing*, 15(14):3585.

Ren, H., Zhao, Y., Xiao, W., and Hu, Z. (2019a). A review of UAV monitoring in mining areas: current status and future perspectives. *International Journal of Coal Science amp; Technology*, 6(3):320–333.

Ren, Z., Wang, L., and Bi, L. (2019b). Robust GICP-based 3D LiDAR SLAM for underground mining environment. *Sensors (Basel)*, 19(13):2915.

Rock, G., Ries, J., and Udelhoven, T. (2012). Sensitivity analysis of UAV-photogrammetry for creating digital elevation models (DEM). *The International Archives of the Photogrammetry, Remote Sensing and Spatial Information Sciences*, 38:69–73.

Rogers, J. G., Gregory, J. M., Fink, J., and Stump, E. (2020). Test Your SLAM! The SubT-Tunnel dataset and metric for mapping. In *2020 IEEE International Conference on Robotics and Automation (ICRA)*. IEEE.

Saeedi, S., Trentini, M., Seto, M., and Li, H. (2016). Multiple-robot simultaneous localization and mapping: A review. *J. Field Robot.*, 33(1):3–46.

Samarakoon, K. Y. (2022). *UAV path planning and multi-modal localization for mapping in a subterranean environment*. PhD thesis.

Sammartano, G. and Spanò, A. (2018). Point clouds by SLAM-based mobile mapping systems: accuracy and geometric content validation in multisensor survey and stand-alone acquisition. *Applied Geomatics*, 10(4):317–339.

Schops, T., Sattler, T., and Pollefeys, M. (2019). Bad slam: Bundle adjusted direct rgb-d slam. In *Proceedings of the IEEE/CVF Conference on Computer Vision and Pattern Recognition*, pages 134–144.

Schops, T., Schonberger, J. L., Galliani, S., Sattler, T., Schindler, K., Pollefeys, M., and Geiger, A. (2017). A multi-view stereo benchmark with high-resolution images and multi-camera videos. In *Proceedings of the IEEE conference on computer vision and pattern recognition*, pages

3260–3269.

Shan, T. and Englot, B. (2018). LeGO-LOAM: Lightweight and Ground-Optimized Lidar Odometry and Mapping on Variable Terrain. In *2018 IEEE/RSJ International Conference on Intelligent Robots and Systems (IROS)*, pages 4758–4765.

Shan, T., Englot, B., Meyers, D., Wang, W., Ratti, C., and Rus, D. (2020). Lio-sam: Tightly-coupled lidar inertial odometry via smoothing and mapping. In *2020 IEEE/RSJ international conference on intelligent robots and systems (IROS)*, pages 5135–5142. IEEE.

Singh, S. K., Banerjee, B. P., and Raval, S. (2022). A review of laser scanning for geological and geotechnical applications in underground mining. *International Journal of Mining Science and Technology*.

Slaker, B. (2015). *Monitoring underground mine displacement using photogrammetry and laser scanning*. PhD thesis, Virginia Tech.

Strasdat, H., Montiel, J. M., and Davison, A. J. (2012). Visual SLAM: why filter? *Image and Vision Computing*, 30(2):65–77.

Sturm, J., Engelhard, N., Endres, F., Burgard, W., and Cremers, D. (2012). A benchmark for the evaluation of RGB-D SLAM systems. In *2012 IEEE/RSJ international conference on intelligent robots and systems*, pages 573–580. IEEE.

Sturzenegger, M. and Stead, D. (2009). Close-range terrestrial digital photogrammetry and terrestrial laser scanning for discontinuity characterization on rock cuts. *Engineering Geology*, 106(3-4):163–182.

Suchocki, C. (2020). Comparison of Time-of-Flight and Phase-Shift TLS Intensity Data for the Diagnostics Measurements of Buildings. *Materials*, 13(2).

Sun, Y., Liu, M., and Meng, M. Q.-H. (2017). Improving RGB-D SLAM in dynamic environments: A motion removal approach. *Robotics and Autonomous Systems*, 89:110–122.

Szrek, A., Romańczukiewicz, K., Kujawa, P., and Trybała, P. (2024). Comparison of TLS and SLAM technologies for 3D reconstruction of objects with different geometries. In *IOP Conference Series: Earth and Environmental Science*, volume 1295, page 012012. IOP Publishing.

Szrek, J., Trybała, P., Góralczyk, M., Michalak, A., Ziętek, B., and Zimroz, R. (2020). Accuracy Evaluation of Selected Mobile Inspection Robot Localization Techniques in a GNSS-Denied Environment. *Sensors*, 21(1):141.

Taketomi, T., Uchiyama, H., and Ikeda, S. (2017). Visual SLAM algorithms: a survey from 2010 to 2016. *IPSJ Trans. Comput. Vis. Appl.*, 9(1).

Teed, Z. and Deng, J. (2021). DROID-SLAM: Deep Visual SLAM for Monocular, Stereo, and RGB-D Cameras. *Advances in neural information processing systems*.

Thrun, S. (2002). Probabilistic robotics. *Communications of the ACM*, 45(3):52–57.

Thrun, S., Hahnel, D., Ferguson, D., Montemerlo, M., Triebel, R., Burgard, W., Baker, C., Omohundro, Z., Thayer, S., and Whittaker, W. (2003). A system for volumetric robotic mapping of abandoned mines. In *2003 IEEE International Conference on Robotics and Automation (Cat. No. 03CH37422)*, volume 3, pages 4270–4275. IEEE.

Thrun, S., Liu, Y., Koller, D., Ng, A. Y., Ghahramani, Z., and Durrant-Whyte, H. (2004). Simultaneous localization and mapping with sparse extended information filters. *Int. J. Rob. Res.*, 23(7-8):693–716.

Tian, Y., Chang, Y., Arias, F. H., Nieto-Granda, C., How, J. P., and Carlone, L. (2022). Kimera-multi: Robust, distributed, dense metric-semantic slam for multi-robot systems. *IEEE Transactions on Robotics*, 38(4).

Torresani, A. et al. (2022). A portable V-SLAM based solution for advanced visual 3D mobile mapping.

Tranzatto, M., Mascarich, F., Bernreiter, L., Godinho, C., Camurri, M., Khattak, S., Dang, T., Reijgwart, V., Loeje, J., Wisth, D., et al. (2022). Cerberus: Autonomous legged and aerial

robotic exploration in the tunnel and urban circuits of the darpa subterranean challenge. *arXiv preprint arXiv:2201.07067*.

Trybała, P. (2021). LiDAR-based Simultaneous Localization and Mapping in an underground mine in Złoty Stok, Poland. In *IOP Conference Series. Earth and Environmental Science*, volume 942. IOP Publishing.

Trybała, P., Blachowski, J., Błażej, R., and Zimroz, R. (2020). Damage Detection Based on 3D Point Cloud Data Processing from Laser Scanning of Conveyor Belt Surface. *Remote Sensing*, 13(1):55.

Trybała, P. and Gattner, A. (2021). Development of a Building Topological Model for Indoor Navigation. *IOP Conference Series: Earth and Environmental Science*, 684(1):012031.

Trybała, P., Kaczan, W., and Górecki, A. (2021). Mining Waste Volume Estimation Using Airborne Lidar Data and Historical Maps: A Case Study of Tailing Piles in Szklary, Lower Silesia. *Environmental Sciences Proceedings*, 9(1):32.

Trybała, P., Kasza, D., Wajs, J., and Remondino, F. (2023a). Comparison of Low-Cost Handheld LIDAR-based SLAM Systems for Mapping Underground Tunnels. *The International Archives of the Photogrammetry, Remote Sensing and Spatial Information Sciences*, XLVIII-1/W1-2023:517–524.

Trybała, P., Kujawa, P., Romańczukiewicz, K., Szrek, A., and Remondino, F. (2023b). Designing and Evaluating a Portable LiDAR-based SLAM System. *The International Archives of the Photogrammetry, Remote Sensing and Spatial Information Sciences*, XLVIII-1/W3-2023:191–198.

Trybała, P., Szrek, J., Dębogórski, B., Ziętek, B., Blachowski, J., Wodecki, J., and Zimroz, R. (2023c). Analysis of Lidar Actuator System Influence on the Quality of Dense 3D Point Cloud Obtained with SLAM. *Sensors*, 23(2):721.

Trybała, P., Szrek, J., Remondino, F., Kujawa, P., Wodecki, J., Blachowski, J., and Zimroz, R. (2023d). MIN3D Dataset: MultI-seNsor 3D Mapping with an Unmanned Ground Vehicle. *PFG – Journal of Photogrammetry, Remote Sensing and Geoinformation Science*.

Trybała, P., Szrek, J., Remondino, F., Wodecki, J., and Zimroz, R. (2022). Calibration of a Multi-sensor Wheeled Robot for the 3D Mapping of Underground Mining Tunnels. *The International Archives of the Photogrammetry, Remote Sensing and Spatial Information Sciences*, XLVIII-2/W2-2022:135–142.

Trybała, P., John, A., Köhler, C., Benndorf, J., and Blachowski, J. (2022). Towards a mine3D dense mapping mobile robot: a system design and preliminary accuracy evaluation. *Markscheidewesen*, 129(1):18–24.

Tsubouchi, T., Tanaka, A., Ishioka, A., Tomono, M., and Yuta, S. (2004). A SLAM based tele-operation and interface system for indoor environment reconnaissance in rescue activities. In *2004 IEEE/RSJ International Conference on Intelligent Robots and Systems (IROS) (IEEE Cat. No.04CH37566)*, volume 2, pages 1096–1102 vol.2.

Vaaja, M., Hyyppä, J., Kukko, A., Kaartinen, H., Hyyppä, H., and Alho, P. (2011). Mapping Topography Changes and Elevation Accuracies Using a Mobile Laser Scanner. *Remote Sensing*, 3(3):587–600.

Van Eck, N. and Waltman, L. (2010). Software survey: VOSviewer, a computer program for bibliometric mapping. *scientometrics*, 84(2):523–538.

Van Eck, N. J. and Waltman, L. (2017). Citation-based clustering of publications using CitNet-Explorer and VOSviewer. *Scientometrics*, 111:1053–1070.

Vassena, G., Clerici, A., et al. (2018). Open pit mine 3D mapping by tls and digital photogrammetry: 3D model update thanks to a slam based approach. *International Archives of the Photogrammetry, Remote Sensing and Spatial Information Sciences*, 42(2):1145–1148.

Wajs, J., Trybała, P., Górniak-Zimroz, J., Krupa-Kurzynowska, J., and Kasza, D. (2021). Modern

Solution for Fast and Accurate Inventorization of Open-Pit Mines by the Active Remote Sensing Technique—Case Study of Mikoszów Granite Mine (Lower Silesia, SW Poland). *Energies*, 14(20):6853.

Wang, H., Wang, C., Chen, C., and Xie, L. (2020). F-LOAM : Fast LiDAR Odometry and Mapping. In *2021 IEEE/RSJ International Conference on Intelligent Robots and Systems (IROS)*.

Wang, J., Tian, B., Zhang, R., and Chen, L. (2022). ULSM: Underground localization and semantic mapping with salient region loop closure under perceptually-degraded environment. In *2022 IEEE/RSJ International Conference on Intelligent Robots and Systems (IROS)*. IEEE.

Wang, J., Wang, L., Jia, M., He, Z., and Bi, L. (2020). Construction and optimization method of the open-pit mine DEM based on the oblique photogrammetry generated DSM. *Measurement*, 152:107322.

Wang, J., Wang, L., Peng, P., Jiang, Y., Wu, J., and Liu, Y. (2023). Efficient and accurate mapping method of underground metal mines using mobile mining equipment and solid-state lidar. *Measurement*, 221:113581.

Whelan, T., Kaess, M., Johannsson, H., Fallon, M., Leonard, J. J., and McDonald, J. (2015a). Real-time large-scale dense RGB-D SLAM with volumetric fusion. *The International Journal of Robotics Research*, 34(4-5):598–626.

Whelan, T., Leutenegger, S., Salas Moreno, R., Glocker, B., and Davison, A. (2015b). ElasticFusion: Dense SLAM without A pose graph. In *Robotics: Science and Systems XI*. Robotics: Science and Systems Foundation.

Whelan, T., Salas-Moreno, R. F., Glocker, B., Davison, A. J., and Leutenegger, S. (2016). ElasticFusion: Real-time dense SLAM and light source estimation. *Int. J. Rob. Res.*, 35(14):1697–1716.

White, J. (2020). PubMed 2.0. *Medical reference services quarterly*, 39(4):382–387.

Wróblewski, A., Trybała, P., Banasiewicz, A., Zawiślak, M., Walerysiak, N., and Wodecki, J. (2023a). Possibilities of 3D laser scanning data utilization for numerical analysis of airflow in mining excavations. In *IOP Conference Series: Earth and Environmental Science*, volume 1189, page 012009. IOP Publishing.

Wróblewski, A., Wodecki, J., Trybała, P., and Zimroz, R. (2022). A Method for Large Underground Structures Geometry Evaluation Based on Multivariate Parameterization and Multidimensional Analysis of Point Cloud Data. *Energies*, 15(17):6302.

Wróblewski, A., Wodecki, J., Trybała, P., and Zimroz, R. (2023b). Large underground structures geometry evaluation based on point cloud data analysis. In *IOP Conference Series: Earth and Environmental Science*, volume 1189, page 012005. IOP Publishing.

Xiang, J., Chen, J., Sofia, G., Tian, Y., and Tarolli, P. (2018). Open-pit mine geomorphic changes analysis using multi-temporal UAV survey. *Environmental earth sciences*, 77:1–18.

Xu, W., Cai, Y., He, D., Lin, J., and Zhang, F. (2022a). Fast-lio2: Fast direct lidar-inertial odometry. *IEEE Transactions on Robotics*, 38(4):2053–2073.

Xu, X., Zhang, L., Yang, J., Cao, C., Wang, W., Ran, Y., Tan, Z., and Luo, M. (2022b). A review of multi-sensor fusion slam systems based on 3D LIDAR. *Remote Sensing*, 14(12):2835.

Xue, G., Wei, J., Li, R., and Cheng, J. (2022). LeGO-LOAM-SC: An improved simultaneous localization and mapping method fusing LeGO-LOAM and scan context for underground coalmine. *Sensors (Basel)*, 22(2):520.

Yan, Z., Mazzacca, G., Rigon, S., Farella, E. M., Trybala, P., and Remondino, F. (2023). NERFBK: A Holistic Dataset for Benchmarking NeRF-based 3D Reconstruction. *The International Archives of the Photogrammetry, Remote Sensing and Spatial Information Sciences*, XLVIII-1/W3-2023:219–226.

Yang, X., Lin, X., Yao, W., Ma, H., Zheng, J., and Ma, B. (2023). A Robust LiDAR SLAM Method for Underground Coal Mine Robot with Degenerated Scene Compensation. *Remote Sensing*, 15(1).

Ye, H., Chen, Y., and Liu, M. (2019). Tightly coupled 3d lidar inertial odometry and mapping. In *2019 International Conference on Robotics and Automation (ICRA)*, pages 3144–3150. IEEE.

Yu, C., Liu, Z., Liu, X.-J., Xie, F., Yang, Y., Wei, Q., and Fei, Q. (2018). DS-SLAM: A Semantic Visual SLAM towards Dynamic Environments. In *2018 IEEE/RSJ International Conference on Intelligent Robots and Systems (IROS)*, pages 1168–1174.

Yu, H., Lu, X., Ge, X., and Cheng, G. (2010). Digital terrain model extraction from airborne LiDAR data in complex mining area. In *2010 18th International Conference on Geoinformatics*, pages 1–6. IEEE.

Zhang, D.-B., Zhang, Y., Cheng, T., Meng, Y., Fang, K., Garg, A., and Garg, A. (2017). Measurement of displacement for open pit to underground mining transition using digital photogrammetry. *Measurement*, 109:187–199.

Zhang, J. and Singh, S. (2014). LOAM: Lidar odometry and mapping in real-time. In *Robotics: Science and systems*, volume 2, pages 1–9. Berkeley, CA.

Zimroz, P., Trybała, P., Wróblewski, A., Góralczyk, M., Szrek, J., Wójcik, A., and Zimroz, R. (2021). Application of UAV in Search and Rescue Actions in Underground Mine—A Specific Sound Detection in Noisy Acoustic Signal. *Energies*, 14(13):3725.

Zlot, R. and Bosse, M. (2014). Efficient Large-scale Three-dimensional Mobile Mapping for Underground Mines. *Journal of Field Robotics*, 31(5):758–779.

Part II

PUBLICATIONS P1–P6

Publication 1: LiDAR-based Simultaneous Localization and Mapping in an underground mine in Złoty Stok, Poland

LiDAR-based Simultaneous Localization and Mapping in an underground mine in Złoty Stok, Poland

P Trybała[1,*]

[1]Department of Mining, Faculty of Geoengineering, Mining and Geology, Wrocław University of Science and Technology, Na Grobli 15, 50-421 Wroclaw, Poland

[*]Corresponding author: `pawel.trybala@pwr.edu.pl`

Abstract.   The mining sector is one of the most promising areas for implementing advanced autonomous robots. The benefits of increased safety, robot actions' repeatability, and reducing human presence in hazardous locations are especially important in underground mines. One of the core functionalities of such a device is the robot's ability to localize and navigate itself in the working environment. To achieve this, simultaneous localization and mapping (SLAM) techniques are used. In selected cases, they also allow the acquisition of dense spatial data in the form of 3D point clouds, which can be utilized for various 3D modeling and spatial analysis purposes. In this work, a mobile robot, equipped only with a compact laser scanner, is used to acquire spatial data in the adit of a closed mine in Złoty Stok, Poland. This data is further processed with selected SLAM algorithms to create a homogeneous 3D point cloud. Results are visualized and compared to a model obtained with a survey-grade laser scanner. Accuracy evaluation shows that employing SLAM algorithms to process data collected by a mobile robot can produce a reasonably accurate 3D geometrical model of an underground tunnel, even without incorporating any additional sensors.

1. Introduction

Automation and robotization of various industrial processes are inevitable steps of the mankind technological advancement [1]. Since they provide an ability to reduce or even totally exclude the direct involvement and physical presence of humans in the place of work, one of their most important advantages is the increased safety of employers. This is a crucial issue especially in sectors such as mining, where in many cases, there is a substantial risk of a serious or even fatal accident. Furthermore, if such an accident happens, an underground mine is arguably one of the most challenging environments for carrying out a rescue mission. Using mobile robots in this circumstance would not only help the rescue team safely reach victims, but also employ more sophisticated techniques of localizing them, utilizing sensors mounted on a robot [2, 3].

Deploying robotic devices in a mine can also facilitate the employment of novel techniques of mining machinery monitoring [4]. This is a rapidly growing field, in which one could find examples of using mobile robots for the acquisition of acoustic signals [5], infrared thermography imagery [6] or LiDAR-based point clouds [7] to evaluate the condition of various belt conveyor parts. Unmanned robots and mobile sensors have been also used for monitoring environmental conditions in an underground mine [8, 9].

One of the basic requirements of allowing an inspection robot to safely operate in a mine is achieving its spatial awareness. It should be a core capability of a robot to localize itself, map

and analyze its surroundings, in turn to be able to navigate to certain places for accomplishing the subsequent goals of a defined mission. Solving those issues is a serious challenge in the environment of an underground mine, where uneven illumination, dust, humidity, high temperature and rough terrain are often present. However, such a solution could simultaneously produce another valuable outcome - 3D geometrical model of the environment, which could be used for various other analytical purposes. Currently, such models are acquired with data collected with survey-grade laser scanners used by mine surveyors. While they can provide superior accuracy and resolution of the resulting point cloud, they are expensive and their usage involves the surveyors' physical presence in the place being measured. In this work, a solution to those problems utilizing Simultaneous Localization and Mapping (SLAM) algorithm to process LiDAR data acquired with a much cheaper, industrial-grade instrument will be presented.

The paper is organized as follows. Section 2 describes the robot and sensors used in the experiment carried out in a closed mine in Złoty Stok, Poland. It also outlines the methodology of processing data from both LiDAR scanners, comparing the results and evaluating the accuracy of SLAM-derived model. Section 3 presents the results of the experiment, including the visualization of the raw data, final geometrical models and outcomes of point clouds' comparison. The last section contains conclusions from this research and indicates plans for future work.

2. Methodology

In this study, a SLAM approach has been tested for creating 3D representations of mine tunnel geometry. A SLAM problem is defined by an observer located in an unknown environment where he must simultaneously determine and update his position on a map of the environment and construct and update the map itself. Many researchers utilized various sensors to solve this issue. The most common types of sensors used for mobile robot localization are cameras [10, 11] (visual SLAM), LiDARs [12, 13, 14], ultra-wideband localization [15, 16] and inertial systems [17]. Regarding the dimensionality of the map and the observer's pose space, a SLAM problem can be considered in 2D or 3D space, leading to a 4 degrees of freedom (DoF) or a 6 DoF problem. A SLAM can be robustly and efficiently performed, taking into account the robot's movement over a perfectly flat ground only and constructing a two-dimensional map [18]. The latter version of the problem is much more problematic, especially in demanding conditions.

Various SLAM versions have been tested in mining environments. In [19], 2D Hector-SLAM has been applied to create a map of the underground tunnel. The possibility of applying various versions of 3D LiDAR SLAM for the purpose of enabling autonomous vehicle operation in the tunnels of an underground mine was examined in [20]. Another study concerned developing a methodology of updating a high-resolution open-pit mine model with a cost-effective and fast 3D SLAM solution [21]. In the work of [22] extensive tests of a SLAM system for autonomous mining vehicles were carried out. However, the study concerns mostly the ability to create a simple 2D map of the mine and localize the vehicle in it. The research of [23] concerned a close-source handheld SLAM system, a GeoSLAM ZebRevo. The instrument was tested in underground conditions and results obtained from handheld scanning and from measurements, when the scanner was mounted on a vehicle, were compared. Authors underline the fact that proper usage in the mining environment should be restricted to short scanning periods and unstructured underground conditions still pose a challenge for SLAM algorithms, indicating the need of further research in this area. The same sensor was utilized in the study of [24] to not only create 3D point cloud of an underground adit, but also construct a local geological model through identification of fault zones.

In this work, an unmanned ground vehicle (UGV), equipped with a Velodyne VLP-16 LiDAR, was used to carry out SLAM tests. The unit is shown in the Figure 1. The measurements were performed in the adit of a closed underground gold mine in Złoty Stok, Poland. The adit is currently used as a geotouristic place, so the ground flatness and lightning conditions are not

as extreme as in an operating underground mine. However, they differ substantially from more structured environments, such as buildings.

Figure 1. Mobile robot in the measured adit

Figure 2. Reference measurements with a Riegl Vz-400i

The data from the LiDAR was acquired using a laptop running Ubuntu 18.04 LTS and Robot Operating System (ROS, [25]), placed on the robot. A SLAM algorithm, High-Density LiDAR SLAM (HDL-SLAM) [26] was chosen for processing this data. It provides vast possibilities of customization (e.g. different methods for scan matching, changeable parameters, ground detection and voxelization) and is compatible with the post-processing interactive tool [27], allowing to verify validity of scan matching, manually edit erroneous connections and refine the pose graph with robust estimation. The above-mentioned software is compatible with ROS and is shared online under a 2-Clause BSD license (HDL-SLAM) and GNU General Public License v3.0 (post-processing tool).

After carrying out measurements with the mobile robot, a survey-grade laser scanner was used to obtain the ground truth 3D model. The instrument employed for the survey was Riegl Vz-400i (shown in Figure 2), providing point cloud accuracy of approximately 5 mm. The instrument was additionally equipped with a Nikon D810 digital camera, which allowed to generate colored point cloud visualizations. The scans were cleaned, registered and transformed into a homogeneous local coordinate system using cloud-to-cloud technique in the Vercator cloud software. The SLAM point cloud was matched to the reference model using the iterative closest point (ICP) algorithm and the unsigned distances from points to the reference model were calculated. To minimize the influence of gaps that could appear in the reference measurements and not in the SLAM-based model, thus distorting its accuracy evaluation, the distances were estimated using local surface modeling of the reference point cloud using the quadric local model. Histogram of those distances was calculated and analyzed, as well as basic statistics. Finally, the spatial distribution of the estimated error values was examined.

3. Results and discussion

The drive through the 130-meter long tunnel took approximately 5 minutes. The robot collected 2978 scans, which were saved to a .rosbag file. The LiDAR's field of view was reduced to 270° due to the hardware mounted on the robot, obstructing the view behind the sensor. The UGV, as shown in Figure 3, was additionally equipped with a compact light source to aid the operator's ability to control the machine in the dark parts of the corridor.

Figure 3. Mobile robot equipped with a Velodyne VLP-16 and a laptop for data collection

In the next part of the experiment, Riegl LiDAR was used to measure the tunnel, which was scanned from 8 positions, totalling 120 949 585 points. The clouds have been manually cleaned using Cloud Compare software. Scans were then registered in the Vercator cloud software, using manual prealignment and cloud-to-cloud method. Average root mean square error (RMSE) of the point-to-point error for each pair of clouds has been calculated during the alignment. Since the expected accuracy of the SLAM point cloud is definitely greater than a centimeter, the resulting error of 1.6 mm is satisfactory and justifies using this point cloud as a reference model for the accuracy evaluation of SLAM. Finally, the reference point cloud has been subsampled to the resolution of 5 mm to homogenize its spatial resolution. Render of a colored point cloud can be seen in Figure 4.

Figure 4. Render of a colored reference point cloud acquired with a survey-grade laser scanner

Scans collected with a mobile robot and stored in a .rosbag file were processed in an offline mode to ensure repeatability and the possibility to test different parameter values and modes of HDL-SLAM. They were, however, replayed as a stream of LiDAR scan data and processed in real time. As for the SLAM settings, the generalized iterative closest point (GICP) algorithm was used as a basis for scan matching and ground plane detection was enabled to aid the correct orientation of subsequent scans with respect to the Z-axis. The obtained graph was optimized with Levenberg–Marquardt algorithm. After the first step of real-time processing, the resulting pose graph was refined and optimized in the post-processing mode, enhancing the graph edges using Huber robust kernel to improve scan registration. The resulting point cloud was cleaned in the same manner as the reference data set by removing distinctive outliers. The final point cloud is shown in Figure 5. The resulting point cloud contained 357 468 points.

Registration of the SLAM-derived point cloud to the reference point cloud was carried out in Cloud Compare software. With the random sampling limit of 100 000 points, the resulting RMSE amounted to 14 cm. Visualizations of both point clouds transformed to the consistent local coordinate system can be seen in Figure 6 (the tunnel interior) and Figure 7 (top view). Nevertheless, the examination of the results shows that the SLAM-derived tunnel geometry is mostly locally consistent with the reference data. The errors are mostly due to the drift of the sensor position estimation, since no loop closure was present in the acquired data.
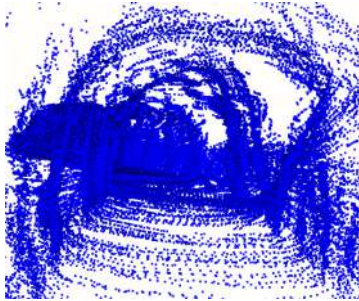
Figure 5. Render of a point cloud produced by the HDL-SLAM algorithm
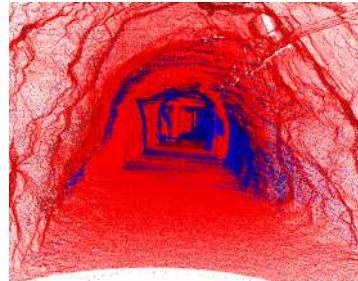
Figure 6. The tunnel interior. SLAM point cloud in blue, reference cloud in red
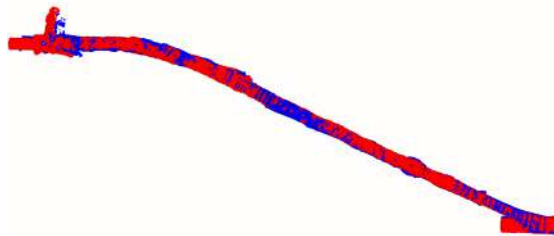
Figure 7. Top view of both point clouds. SLAM point cloud in blue, reference cloud in red

Distances between SLAM point cloud and the ground truth data were calculated. The surface of the reference model was approximated with a local quadric model fitted in the closest neighborhood of each point. The outcome values were used to color the SLAM point cloud according to the estimated errors. The top view of such visualization is depicted in Figure 8. A histogram of distance values was plotted (Figure 9) and the basic summary statistics were calculated (Table 1). Estimated point position errors follow a half-normal distribution, since the unsigned distances were calculated.
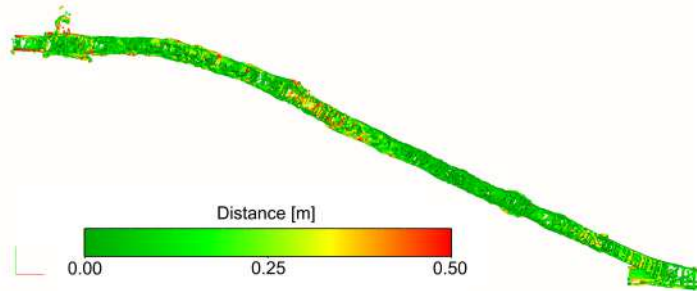
Figure 8. Accuracy evaluation - distances between reference and SLAM point cloud
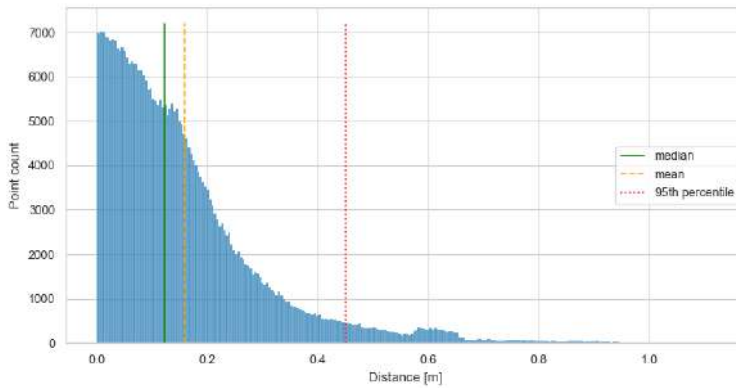
Figure 9. Accuracy evaluation - histogram of distances between reference and SLAM point cloud

Table 1. Summary statistics of SLAM point cloud error distribution

Statistic	Value [cm]
Median	8.3
Mean	11.8
95th percentile	34.0

The obtained results prove that LiDAR SLAM can be successfully used for generating 3D models of the highly unstructured corridors of an underground mine. Uneven ground and irregular geometry of the tunnel, especially the walls and the roof, pose a challenge for correctly matching subsequent, sparse LiDAR scans. However, proper parameter tuning of HDL-SLAM, manual verification and refinement of the pose graph in the post-processing step allowed to obtain reliable results. Gross errors of the final point cloud, caused by a quickly growing cumulative error of the pose or failing to register following scans, showed in [20] in case of applying selected SLAM algorithms in the mining environment, are not present. Accuracy and point cloud density of the tested simple solution is clearly worse than the point cloud data collected with a survey-grade scanner, but the resulting model is still locally consistent and could be used for GIS or robot navigation purposes. Despite this, there are lessons to be learned for the future from the research presented, which could potentially improve the SLAM performance in future applications. Firstly, the main reason of large error values is the drift of robot positioning, gradually skewing its trajectory. To cope with this problem, measurements have to be planned to ensure (optimally several) loop closures. Secondly, as seen in Figures 5 and 6, the highest SLAM point cloud density is concentrated on the lower and middle parts of the corridor walls. This should be attributed to the horizontal placement of LiDAR sensor in the same plane as the robot movement. Because of that, more sparse data is collected about objects located higher up and gaps can appear in the resulting model. A different placement of the sensors with respect to the robot base could be tested to address this issue, e.g. by tilting the LiDAR relative to the robot's main motion plane by a constant angle or by continuously rotating the sensor around its front-facing axis.

4. Conclusions

The conducted experiment shows the possibility of employing SLAM techniques to model the highly irregular geometry of an underground mine tunnel. Even though the relatively simple solution, utilizing only a single LiDAR sensor was tested, the accuracy evaluation of the resulting point cloud indicates that such a model could be used for various purposes, e.g. digital twin creation, flow modeling, volumetric calculations or robot navigation in a mine. In harsh conditions of an underground mine, factors such as dust, rugged terrain or darkness can render SLAM solutions heavily relying on camera vision or IMU readings nonfunctional. For this reason, the ability to rely solely on LiDAR SLAM is very valuable.

Conclusions from this research will allow to enhance the configuration of the demonstrated UGV 3D scanning platform for future applications. Potential works include automation of data acquisition with autonomous exploration of the unknown environment of an underground mine and improving SLAM accuracy with enhanced LiDAR mounting on the robot. Another prospective field of research is testing the proposed solution enhanced with data fusion techniques. Integrated supplementary sensors could include another LiDAR, cameras, IMU or wheel encoders.

References

[1] Johannessen J A 2018 *Automation, innovation and economic crisis: Surviving the fourth industrial revolution* (Routledge)

[2] Murphy R R, Kravitz J, Stover S L and Shoureshi R 2009 Mobile robots in mine rescue and recovery *IEEE Robotics & Automation Magazine* **16** 91–103

[3] Szrek J, Zimroz R, Wodecki J, Michalak A, Góralczyk M and Worsa-Kozak M 2021 Application of the infrared thermography and unmanned ground vehicle for rescue action support in underground mine—the amicos project *Remote Sensing* **13** 69

[4] Zimroz R, Hutter M, Mistry M, Stefaniak P, Walas K and Wodecki J 2019 Why should inspection robots be used in deep underground mines? *Proceedings of the 27th International Symposium on Mine Planning and Equipment Selection-MPES 2018* (Springer) pp 497–507

[5] Skoczylas A, Stefaniak P, Anufriiev S and Jachnik B 2021 Belt conveyors rollers diagnostics based on acoustic signal collected using autonomous legged inspection robot *Applied Sciences* **11** 2299

[6] Szrek J, Wodecki J, Błażej R and Zimroz R 2020 An inspection robot for belt conveyor maintenance in underground mine—infrared thermography for overheated idlers detection *Applied Sciences* **10** 4984

[7] Trybała P, Blachowski J, Błażej R and Zimroz R 2021 Damage detection based on 3d point cloud data processing from laser scanning of conveyor belt surface *Remote Sensing* **13** ISSN 2072-4292

[8] Kasprzyczak L, Szwejkowski P and Cader M 2016 Robotics in mining exemplified by mobile inspection platform *Mining–Informatics, Automation and Electrical Engineering* **54**

[9] Ziętek B, Banasiewicz A, Zimroz R, Szrek J and Gola S 2020 A portable environmental data-monitoring system for air hazard evaluation in deep underground mines *Energies* **13** 6331

[10] Campos C, Elvira R, Rodríguez J J G, Montiel J M and Tardós J D 2021 Orb-slam3: An accurate open-source library for visual, visual–inertial, and multimap slam *IEEE Transactions on Robotics*

[11] Labbé M and Michaud F 2019 Rtab-map as an open-source lidar and visual simultaneous localization and mapping library for large-scale and long-term online operation *Journal of Field Robotics* **36** 416–446

[12] Zhang J and Singh S 2014 Loam: Lidar odometry and mapping in real-time. *Robotics: Science and Systems* vol 2

[13] Zhang J and Singh S 2017 Low-drift and real-time lidar odometry and mapping *Autonomous Robots* **41** 401–416

[14] Droeschel D and Behnke S 2018 Efficient continuous-time slam for 3d lidar-based online mapping *2018 IEEE International Conference on Robotics and Automation (ICRA)* (IEEE) pp 5000–5007

[15] Xu Y, Shmaliy Y S, Ahn C K, Tian G and Chen X 2018 Robust and accurate uwb-based indoor robot localisation using integrated ekf/efir filtering *IET Radar, Sonar & Navigation* **12** 750–756

[16] Szrek J, Trybała P, Góralczyk M, Michalak A, Ziętek B and Zimroz R 2021 Accuracy evaluation of selected mobile inspection robot localization techniques in a gnss-denied environment *Sensors* **21** 141

[17] Skoczylas A and Stefaniak P 2021 Localization system for wheeled vehicles operating in underground mine based on inertial data and spatial intersection points of mining excavations *Intelligent Information and Database Systems: 13th Asian Conference, ACIIDS 2021, Phuket, Thailand, April 7–10, 2021, Proceedings 13* (Springer International Publishing) pp 824–834

[18] Yagfarov R, Ivanou M and Afanasyev I 2018 Map comparison of lidar-based 2d slam algorithms using precise ground truth *2018 15th International Conference on Control, Automation, Robotics and Vision (ICARCV)* pp 1979–1983

[19] Wu D, Meng Y, Zhan K and Ma F 2018 A lidar slam based on point-line features for underground mining vehicle *2018 Chinese Automation Congress (CAC)* pp 2879–2883

[20] Ren Z, Wang L and Bi L 2019 Robust gicp-based 3d lidar slam for underground mining environment *Sensors* **19** 2915

[21] Wajs J, Trybała P, Górniak-Zimroz J, Krupa-Kurzynowska J and Kasza D 2021 Modern solution for fast and accurate inventorization of open-pit mines by the active remote sensing technique—case study of mikoszów granite mine (lower silesia, sw poland) *Energies* **14** 6853

[22] Jacobson A, Zeng F, Smith D, Boswell N, Peynot T and Milford M 2021 What localizes beneath: A metric multisensor localization and mapping system for autonomous underground mining vehicles *Journal of Field Robotics* **38** 5–27

[23] Raval S, Banerjee B P, Kumar Singh S and Canbulat I 2019 A preliminary investigation of mobile mapping technology for underground mining *IGARSS 2019 - 2019 IEEE International Geoscience and Remote Sensing Symposium* pp 6071–6074

[24] Wajs J, Kasza D, Zagożdżon P P and Zagożdżon K D 2018 3d modeling of underground objects with the use of slam technology on the example of historical mine in ciechanowice (ołowiane range, the sudetes) *E3S Web of Conferences* vol 29 (EDP Sciences) p 00024

[25] Quigley M, Conley K, Gerkey B, Faust J, Foote T, Leibs J, Wheeler R, Ng A Y *et al* 2009 Ros: an open-source robot operating system *ICRA workshop on open source software* vol 3 (Kobe, Japan) p 5

[26] Koide K, Miura J and Menegatti E 2018 A portable 3d lidar-based system for long-term and wide-area people behavior measurement *IEEE Trans. Hum. Mach. Syst*

[27] Koide K, Miura J, Yokozuka M, Oishi S and Banno A 2020 Interactive 3d graph slam for map correction *IEEE Robotics and Automation Letters* **6** 40–47
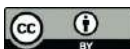
Publication 2: Modern Solution for Fast and Accurate Inventorization of Open-Pit Mines by the Active Remote Sensing Technique—Case Study of Mikoszów Granite Mine (Lower Silesia, SW Poland)

Modern Solution for Fast and Accurate Inventorization of Open-Pit Mines by the Active Remote Sensing Technique—Case Study of Mikoszów Granite Mine (Lower Silesia, SW Poland)

Jaroslaw Wajs *, **Paweł Trybała**, **Justyna Górniak-Zimroz**, **Joanna Krupa-Kurzynowska** and **Damian Kasza**

Faculty of Geoengineering, Mining and Geology, Wrocław University of Science and Technology, Wyb. Wyspianskiego 27 St., 50-370 Wrocław, Poland; pawel.trybala@pwr.edu.pl (P.T.); justyna.gorniak-zimroz@pwr.edu.pl (J.G.-Z.); joanna.krupa-kurzynowska@pwr.edu.pl (J.K.-K.); damian.kasza@pwr.edu.pl (D.K.)

* Correspondence: jaroslaw.wajs@pwr.edu.pl; Tel.: +48-320-6823

Abstract: Mining industry faces new technological and economic challenges which need to be overcome in order to raise it to a new technological level in accordance with the ideas of Industry 4.0. Mining companies are searching for new possibilities of optimizing and automating processes, as well as for using digital technology and modern computer software to aid technological processes. Every stage of deposit management requires mining engineers, geologists, surveyors, and environment protection specialists who are involved in acquiring, storing, processing, and sharing data related to the parameters describing the deposit, its exploitation and the environment. These data include inter alia: geometries of the deposit, of the excavations, of the overburden and of the mined mineral, borders of the support pillars and of the buffer zones, mining advancements with respect to the set borders, effects of mining activities on the ground surface, documentation of landslide hazards and of the impact of mining operations on the selected elements of the environment. Therefore, over the life cycle of a deposit, modern digital technological solutions should be implemented in order to automate the processes of acquiring, sharing, processing and analyzing data related to deposit management. In accordance with this idea, the article describes the results of a measurement experiment performed in the Mikoszów open-pit granite mine (Lower Silesia, SW Poland) with the use of mobile LiDAR systems. The technology combines active sensors with automatic and global navigation system synchronized on a mobile platform in order to generate an accurate and precise geospatial 3D cloud of points.

Keywords: mobile laser scanning; Velodyne LiDAR; Riegl scanning system; open pit mine

1. Introduction

Modern land surveying in the mining industry is based on input data acquired from both classical methods (leveling, tacheometry) and modern solutions: digital photogrammetry, measurements with the use of Global Navigation Satellite Systems (GNSS), and laser scanning. These data allow the preparation of maps documenting the deposit, situational plans illustrating the advancement of mining operations, or 3D visualizations showing planned reclamation forms. Commonly used worldwide, these surveying techniques have both advantages and disadvantages. Their implementation typically depends on the level of detail expected in the mining map, and thus on the accuracy of a particular measurement method and on the duration of the measurement process [1–7].

Classical surveying methods allow highly accurate and precise measurement results. The vertical displacements can be recorded with the use of classical and precise leveling with accuracy levels of several millimeters [8] or under 1 mm [9], respectively. Displace-

ments on the surface of a mining area can be observed in 3D. For this purpose, total station measurements are combined with static GNSS measurements [10].

One of the interesting solutions, which is an extension of satellite measurements, is the use of the so-called pseudolites. Pseudoliths are terrestrial transmitters that are transmitting satellite-like signals to assist satellite navigation in areas depleted in terms of signal availability from traditional satellites. The areas of application of this solution are opencast mines with steep and high slopes, where poor satellite availability due to obscured horizon limits the ability to receive the GNSS signal [11].

Recent years have also been marked by the dynamic development of measurement technology based on ground-based radar. In mining, both underground and opencast, it is mainly used to monitor the stability of slopes or to measure surface deformation [12], rarely to monitor the exploitation progress or build the 3D models of mining area.

Observations in the form of a 3D continuous surface allow the construction of a 3D model from the land or aerial level [13,14]. Such measurements typically involve UAV photogrammetry techniques [15] and LiDAR, mainly ALS, and increasingly often UAV [16]. With the use of such techniques, the model can be quickly reconstructed with an accuracy of below 7 cm [17], which, of course, depends on laser scanner accuracy itself as well as resolution of the scan. In the case of UAVs, the main factor determining the accuracy of the calculated model is so-called ground sampling distance (GSD; it is the distance between pixel centers measured on the ground). Updating 3D mine models does not require as high accuracies as in the case of monitoring subsidence movements or slope stability [18].

Limitations of the above methods also need to be stressed. Most importantly, leveling, total station (excluding situations when prisms are stabilized on the measured points) or photogrammetry survey methods cannot be used without the natural and/or an artificial source of light, which fact practically disqualifies these methods from being used at night or would entail the need to provide prohibitively expensive artificial lighting. Atmospheric conditions (e.g., clouds, wind or atmospheric precipitation) are also a considerable limitation, which may contribute to a lower quality of the measurement results or even prevent the measurements entirely. On the other hand, the GNSS measurements—and more specifically their precision—depend on the availability of satellite constellations, and the use of the so-called differential corrections also increases the cost of the entire procedure. Importantly, in the case of relatively deep open-pit excavations, which may have obstructed views of the satellites, the measurement accuracy is lowered. Recent developments in geomatics have allowed the use of a wide range of sensors to record the geometry of both objects and other features on land [19]. Currently, hybrid sensors such as Mobile LiDAR Systems (MLS) provide additional quality to the inventorying process of mining facilities, as they offer solutions which prove flexible in terms of accuracy, resolution and access to areas which are otherwise inaccessible to vehicles [20].

The aim of this article is to present an MLS-based measurement solution for open-pit mining industry. The proposed technique employs a Riegl VMZ 400i measurement platform and a Velodyne LiDAR sensor in the Simultaneous Localization and Mapping (SLAM) approach to data acquisition and localization. The main concept presented in this paper utilizes a high-resolution, precise geometrical data source (MLS) for creating the initial model of the mine and updating it periodically using low-cost sensor and open-source algorithms. Such solution could provide information about near real-time tracking of the progress of mining works and allow e.g. volumetric calculations of the excavated material.

The measurements from both systems provide data for developing a digital representation (the so-called Digital Twin) of the geometry of a mining excavation, which may be used over the mine life cycle in such applications as monitoring the exploitation state of the mining excavation, performed in the form of cyclical measurements in order to control and optimize (improve) the efficiency of the mining process, constructing a management model of an active or a closed excavation, providing information about the state of the closed excavation and constructing its revitalization model. The methods here proposed

allow quick access to the excavation-related data with a minimum workload required from an operator to acquire and process the data and, as such, they reflect well the principles of Industry 4.0 [21–25].

2. Materials and Methods

The main idea behind this study is based on the use of a point cloud obtained from a RIEGL VMZ commercial hybrid laser-scanning platform equipped with a VZ400i scanner mounted on an off-road vehicle. The system allows a quick acquisition of three-dimensional data about the analyzed object, in this case about a granite quarry. The concept of integrating a high-resolution MLS approach with full georeferencing is a base for further analyses of sensors used in acquisitions of 3D geometrical data related to the mine. The experiment was performed with a low-cost Velodyne scanning sensor was, in a handheld SLAM MLS approach. Tests of such a solution consist in obtaining three-dimensional information about the mine (a point cloud) over a time t_0 and in comparing the results with the results from the Velodyne instrument. Consecutive measurements performed in time t_1, t_2, ... t_n may be in the form of the so-called additional measurements with the use of low-cost handheld MLS sensor. Figure 1 is a schematic diagram of the measurements.
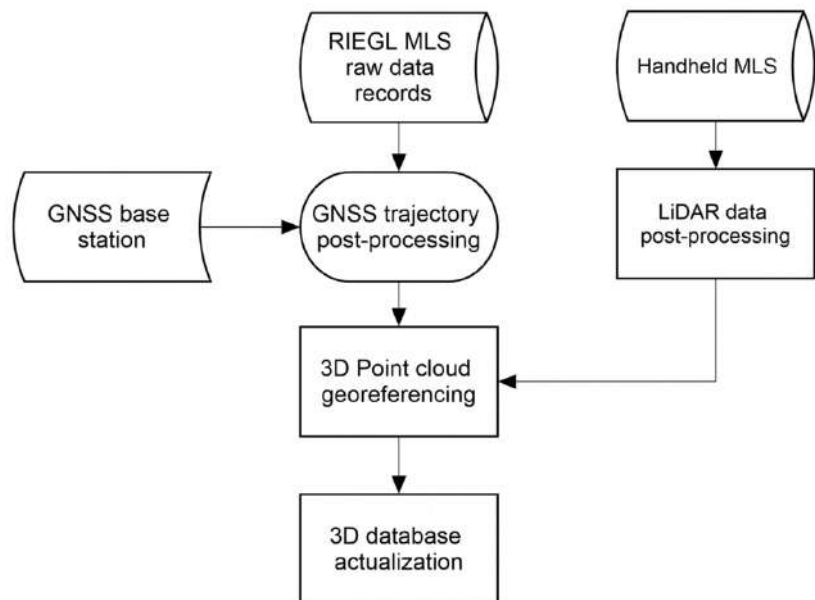
Figure 1. Schematic diagram of the 3D modeling methodology based on two Mobile LiDAR Systems (MLS) systems.

2.1. Description of the Study Area

This experiment was performed on the Mikoszów granite deposit located south-east of the town of Strzelin (Lower Silesia, SW Poland; Figure 2). Based on lease no. 10/2001, until 2016 Mineral Polska Sp. z o.o. mined the deposit for granite and gneiss. The company is planning to renew its lease to mine the deposit with the same technology. The planned output is 800,000 Mg per year. The geological resources of the Mikoszów deposit are 23,249,840 Mg (as per 31 December 2015). Until 2016, the deposit was mined with the use of a mixed wall-shortwall system with parallel advancement of the mining front. The deposit was extracted by drilling and blasting with the use of explosive materials and short and long drillholes. The mined material was loaded with loaders or excavators into mobile hoppers of crushing/sorting machines or into technological vehicles which transported it

to processing devices located outside the mining plant. The processed stone was loaded with a loader from the storage site onto vehicles provided by the clients [26–29].
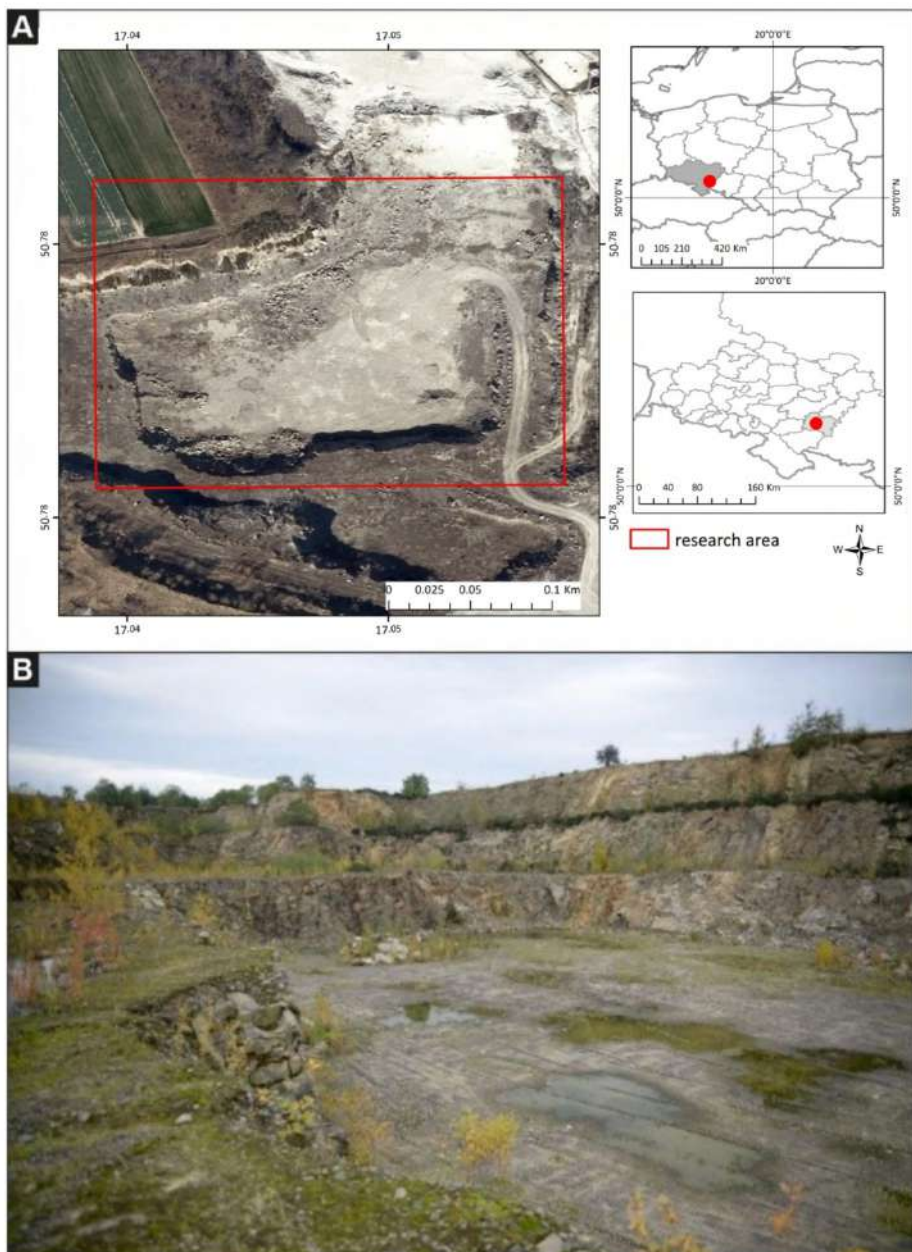
Figure 2. (**A**)—location of the study area; (**B**)—view of the quarry in the NW direction, as of Nov. 2020 (Photo by J. Górniak-Zimroz).

2.2. Mobile Laser Scanning

The literature mentions a number of mobile and autonomous mapping platforms which can collect data form indoor mapping [30]. The main advantage of the MLS system mounted on vehicle lies in the sensor fusion. The mobile mapping platform is equipped

with GNSS, IMU (Inertial Measurement Unit) and DMI (Distance Measurement Indicator) sensors. The GNSS observations are essential in the kinematic mode of Lidar data acquisition. For a perfect trajectory, both static and dynamic alignment is required. If this condition is not met, the derived point clouds are distorted and lose spatial consistency. MLS data acquisition in urban areas may be affected by multipath effects and by signal obstruction due to buildings. This can lead to inaccurate GNSS measurements and, therefore, errors in the estimated trajectory [31]. Kukko et al. (2012) presented on-board sensors integration and MLS platform data acquisition from a vehicle, boat-mounted MLS for mapping fluvial processes and snowmobile application for studying the characteristics of and changes in snow cover. The main advantage of such mobile scanning platforms include fast and smart data collection. In MLS, the slightly elevated point of view gives the advantage of observing vertical surfaces with angle of incidence close to 0°.

The mobile laser scanning technique allows fast and rapid 3D data acquisition in mining areas. In this technique, the measurement is performed with a scanner, and the time-dependent positions of the scanner are also recorded. In comparison to the standard laser scanning technique (Terrestrial Laser Scanning—TLS), in which the measuring instrument is located on an elevating tripod, the MLS has a similar incidence angle of the laser beam with respect to the scanned surface. However, as the system is mobile, it allows the acquisition of data for areas that were not visible from the perspective of the previous location of the scanning platform. The point cloud thus obtained has a relatively smaller number of occlusions and gaps. Examples of the integration of MLS data for the purpose of geological structure mapping were described in [32]. What is more, the recordings of LiDAR MLS datasets provide an alternative point of view. The average height above ground is greater than in the case of TLS scanning stations mounted on tripods. The density of the scan is similar to that of the TLS scan, and the density of the MLS records depends on the movement speed of the scanning platform.

2.2.1. The Riegl VMZ Mobile Scanning Platform

The MLS Riegl VMZ400i system used in the study comprised: a GNSS system based on simultaneous trajectory measurements from two antennas, an IMU, a DMI and a laser scanner (Figure 3).
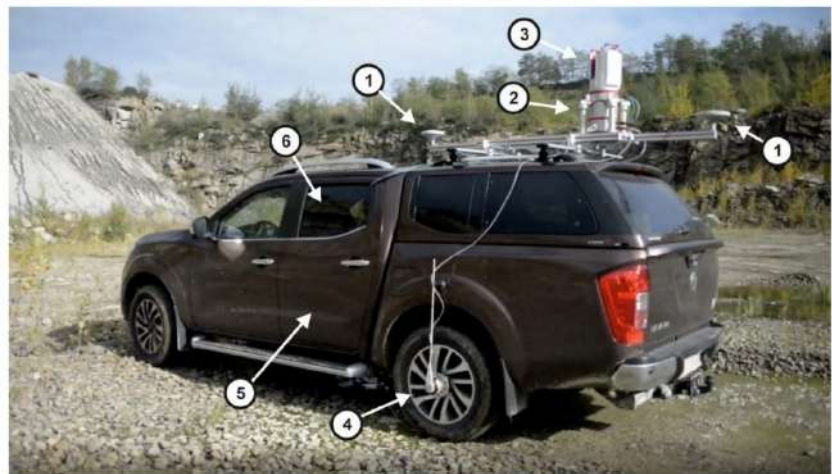
Figure 3. Mobile laser scanning system operated in the excavation: (1) Global Navigation Satellite Systems (GNSS) antenna; (2) Inertial Measurement Unit (IMU); (3) Riegl VZ400i scanner; (4) DMI; (5) power unit (inside the vehicle); (6) driver and control unit—computer with installed software and its operator (inside the vehicle).

2.2.2. Acquisition of MLS Data

The MLS data were recorded for the entire area of the Mikoszów mine and its vicinity. The recording process was performed with the use of the Riegl VMZ 400i hybrid laser scanning system set in the radar mode. The data acquisition process in this mode takes place while the scanner rotates 360° (around it's Z axis) and the whole MLS system drives along the planned trajectory as well. For the purpose of this article, an area of interest (AOI) was defined and indicated in yellow in Figure 4.
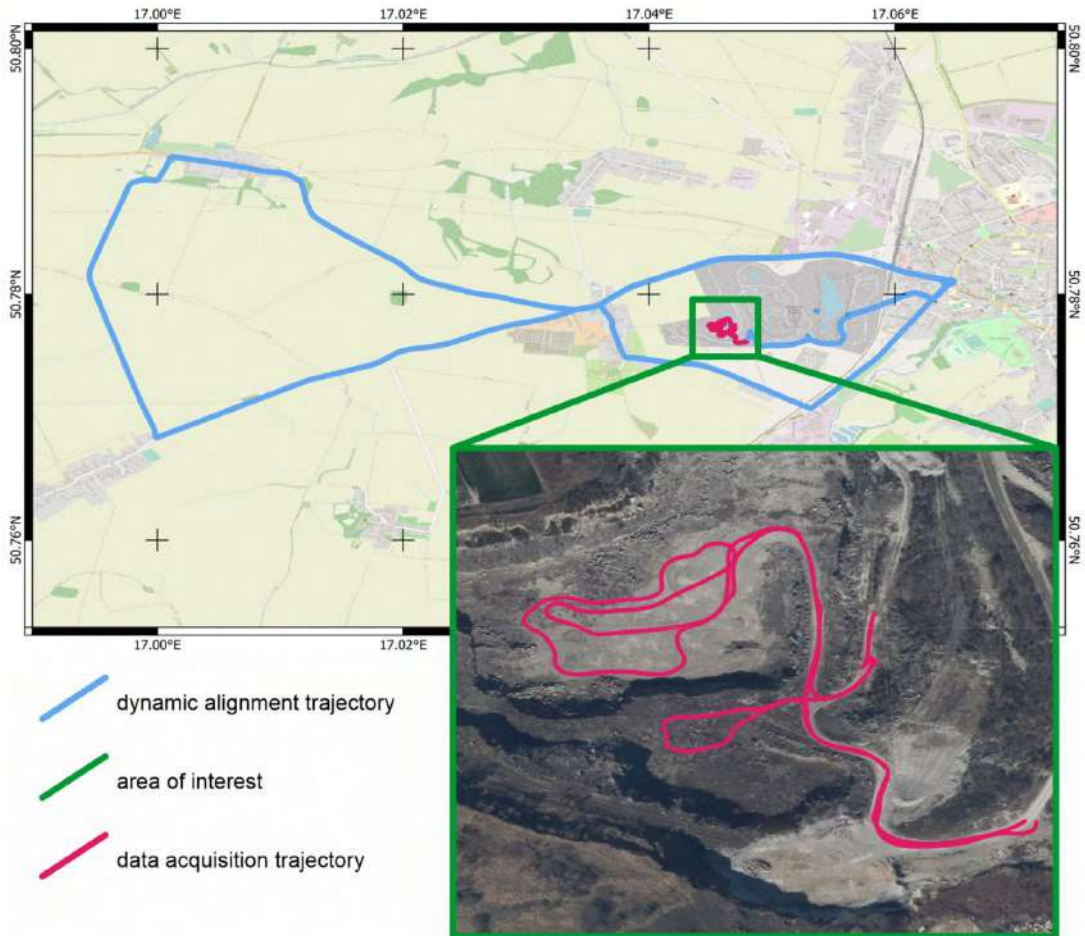
Figure 4. Sketch of the MLS data acquisition trajectory. The presented trajectory (blue line) covers the part of the route of the scanning system used for georeference of the acquired point cloud as well as (purple line) the part of the route within the excavation during the recording process of the data.

The procedure of recording MLS data, which is based on GNSS measurements, required the position of the MLS platform to be acquired around the analyzed mine in the form of a dynamic alignment trajectory loop. All of the works related to the GNSS trajectory measurements were performed in the Applanix PosPac MMS software, using the In-Fusion single base adjustment solution. The procedure allowed the GNSS observations of the platform to be linked with the BASE receiver, which was located in the central part of the mine pit, on its southern slope. The In-Fusion solution integrates the GNSS sensor with displacements recorded by the IMU and the DMI. The DMI allows precise information

on the start and stop of the platform to be obtained from a source different to the GNSS. Figure 5 shows a schematic diagram of the MLS data processing procedure.
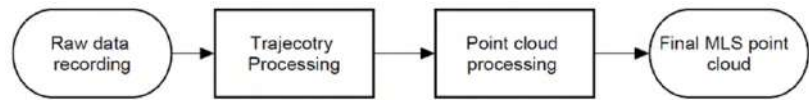
Figure 5. Diagram of MLS data processing.

The MLS measurements and their processing procedure are based on a precise measurement of the time recorded by the measurement system. The processing of a point cloud consists in overlaying individual scan lines on the 3D trajectory in time. The measurement accuracy of the MLS Riegl VMZ 400i is ensured owing to two GNSS antennas that measure the GAMS azimuth (GNSS Azimuth Measurement System). This approach helps eliminate inertial drift errors that are typically produced in a single-antenna approach). GAMS determines the movement direction of the vehicle very accurately regardless of its speed, resulting in the best possible heading accuracy and the best performance in any demanding environment, e.g., with an insufficient number of satellites. The full technical data are shown in Table 1.

Table 1. Riegl VMZ MLS technical data [33].

MLS Parameter	Value
Scanner Min. Range	0.5 [m]
Scanner Max. Range	800 [m]
Accuracy/Precission	5/3 [1] [mm]
Measurement Rate	0.5 M [measurement/s]
Scan field of view—Vertical	100 [°]
Scan field of view—Horizontal	360 [°]
Max Lines per Second (lps)	240 [lps]
GNSS Position Accuracy	20–50 [mm]
Roll/Pith/Heading Accuracy	0.015/0.05 [°]

[1] one sigma @ 100 m.

2.3. Handheld Mobile Laser Scanning

Another MLS technique is based on small mobile laser scanners (originally used in robotics) and on the SLAM technology. The technology consists in simultaneous, iterative determining the position of the observer and in constructing a map (or a 3D model) of the surrounding area. SLAM algorithms are mainly based on data obtained from laser scanners, stereoscopic cameras or monocular cameras. Solutions of this type are normally used in GNSS-denied environments, but if such limitations are not present, the position indicated by the GNSS receiver can be additionally used to improve the quality of SLAM-based positioning [34,35]. The pose of the observation unit and its movement can be additionally determined from the input data provided by other sources, such as IMU sensors [36,37] or wheel odometry [38]. SLAM algorithms are found in numerous implementations and are frequently based on the Kalman filters [35,39], graphs [40,41], or voxels [42].

SLAM functions by solving two basic problems:

- Estimation of consecutive transformations from the coordinate systems (related to the operator), containing point clouds obtained at times t_i and t_{i+1}, into a uniform global coordinate system—this process is referred to as laser odometry,
- Identification of the so-called loop closure, or return visit locations. In the case when point clouds obtained in non-consecutive time points t_i and t_j correspond to identical actual locations, another condition, different than the transformations calculated from

the consecutive scans, can be added to the bundle adjustment of the measurement trajectory. This fact significantly improves the quality and the robustness of the results obtained from the SLAM algorithm, and eliminates errors related to the position drifting in time due to the relative identification of consecutive observing positions.

MLS systems based on small portable laser scanners are now most typically offered as backpack systems, frequently integrated with cameras and GNSS receivers (Figure 6A) or as handheld scanners (Figure 6B). The measurement system can be further simplified by using only a small LiDAR sensor carried by an operator (Figure 6C). Despite a different approach to the sensor arrangement, the systems are, in fact, similar and share the measurement methodology. Therefore, later in this article they will be synonymously referred to as handheld laser scanners.

Figure 6. Examples of LiDAR-based scanning systems: (**A**) GreenValley International LiBackpack DGC50, (**B**) GeoSLAM ZEB Horizon, (**C**) Velodyne VLP-16 with an interface box.

The measurement is performed by an operator who carries a handheld or a backpack scanner and walks around the surveyed area. The latter factor most significantly distinguishes this solution from mobile or stationary laser scanners. On the one hand, it is a limitation, as the range and speed of the measurement is smaller than in the case of mobile scanning performed from a wheeled vehicle, drone or robot. Unlike in the above solutions, the measurement process cannot be automatized. Nevertheless, the operator can easily and naturally adjust the density of the point cloud in desired areas, by prolonging the data acquisition time. Modern SLAM algorithms also allow consecutive scans to be recorded and 3D models of the area to be constructed in real time. In combination with visualization techniques (e.g., on a tablet), this function allows a more effective and precise coverage of the surveyed area. Another advantage lies in the fact that the operator does not have to be highly qualified. Data processing is automatic, and therefore the survey can be performed by a person not familiar with the SLAM technology, or by an autonomous vehicle. Only the post-processing of the data (correctness verification and adding loop closures, georeferencing, improving the quality of defining the measurement trajectory), which allows an improved quality and accuracy of the resultant point cloud, requires higher competences and the ability to use a particular software.

Importantly, the measurement trajectory and thus the resultant point cloud, is biased with a drift error, i.e., a measurement uncertainty which increases with time. As already mentioned, this error is limited by revisiting the previously scanned locations and by allowing the SLAM algorithm to perform loop closure. However, for this to be possible, the measurement path needs to be planned in such a manner that the already surveyed locations are revisited at a sufficient frequency [43,44].

Many of the SLAM algorithms which process 3D data provide lidar odometry with the use of the Generalized Iterative Closest Point (GICP) algorithm. Ren et al. [45] proposed a modification of this algorithm, allowing for the extraction of the ground plane from individual scans and using them as landmarks in order to increase the robustness

of the algorithm. Subsequently, the researchers compared the proposed method with other state-of-the-art algorithms which use a lidar sensor only (VLP-16). These included Lidar Odometry and Mapping (LOAM) [46], Lightweight and Ground-Optimized Lidar Odometry (LeGO-LOAM) [47] and Berkeley Localization and Mapping (BLAM) [48]. The proposed algorithm was designed for the consistent localization of autonomous vehicles in roadways and tunnels of an underground mine. Nevertheless, tests performed on two paths inside a building and on two paths in an underground mine indicate that the results in the mining environment are significantly worse. The authors stress the significance of the loop closure and of introducing plane constraints in obtaining satisfactory results from the tested algorithms.

Vasenna & Clerici [49] introduce a concept of integrating data obtained from classical point cloud construction methods (TLS and UAV photogrammetry) with data from a commercial, backpack SLAM system manufactured by Heron. The aim of the study was to verify the possibility of locating the SLAM operator in an open-pit mine environment previously modeled with the use of classical methods. Having successfully verified this possibility, the authors proposed a methodology for using SLAM in detecting changes of excavation geometry. The estimated accuracy of such detections is above 3–4 cm.

In this study, HDL-SLAM algorithm framework, proposed by Koide et al. [50], has been used. It is based on pose graph optimization and allows a significant elasticity in selecting parameters (for both the LiDAR odometry and the loop closure) and additional conditions in the SLAM algorithm, such as ground plane constraint, GNSS constraint, LiDAR odometry, estimation method and numerous robust kernels. Moreover, the authors provided an interactive graph editing program, which allows the resultant trajectory and point cloud to be improved in the post-processing stage with the use of manual edition tools, loop closure densification and edge refinement. The general concept of the data processing acquired by handheld SLAM is presented in Figure 7. The framework was selected due to its multiple options, which enable adjustments to the conditions of a particular surveyed object, and also due to the open-source implementation in the Robot Operating System (ROS) [51], which allows seamless integration with the LiDAR sensor and with the remaining software installed on a Linux-run laptop computer. The measurements were performed with the use of the Velodyne VLP-16. Its parameters are presented in Table 2.
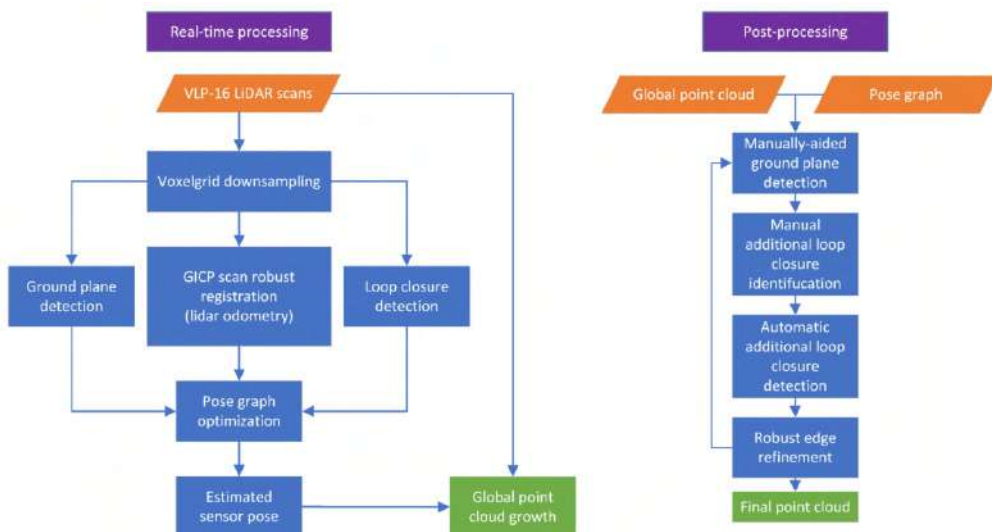
Figure 7. Handheld LiDAR SLAM real-time (**left**) and post-processing (**right**) workflows.

Table 2. Velodyne VLP-16 technical data.

Handheld LiDAR Parameter	Value
Laser Max. Range	100 [m]
Range Accuracy	3 [cm]
Measurement Rate	0.3 M [measurement/s]
Scan Angle Resolution—Vertical	2.0 [°]
Scan Angle Resolution—Horizontal	0.2 [°]
Lines in each scan (channels)	16

3. Results

The fact that the hybrid Riegl VMZ 400i scanner was installed on a Nissan Navara 4×4 off-road vehicle enabled the operator to reach the lowest level of the Mikoszów mine pit, which was the area subjected to further analysis, and to enter the otherwise least accessible locations. The system functions owing to the fact that the scanner was installed above the vehicle and the view of the satellites remained unobstructed. The unfavorable Positional Dilution Of Precision (PDOP) and the insufficient number of satellites visible in the vicinity of the vertical slopes was compensated for by data from IMU and DMI. The geometrical processing of the data was performed in parallel with preliminary filtration. The extraction parameters consisted of such LiDAR signal attributes as reflectance, distance, deviation. The next stage consisted of data filtering. The resultant point cloud represented all classes and comprised above 9.7×10^7 points (Table 3). The resultant point cloud was not filtered in order to classify the point cloud in accordance with the ISPRS .las recommendations. Figure 8 is a visualization in the form of a raster of the measurement range. The recorded MLS point cloud is a set of XYZ 3D data and a series of parameters such as amplitude and reflectance.

The handheld LiDAR measurements were performed by an operator who carried the LiDAR scanner (Velodyne VLP-16) in his hand. The scanner was connected to a laptop in the backpack. The data were recorded on the laptop, in rosbag format in ROS. The measurement covered the area of the lowest level of the open-pit and was performed by an operator walking around the mine. Attention was paid to intentionally form numerous smaller measurement loops and to stop the measurement in the vicinity of the start location in order to achieve a robust point cloud by forming a loop closure. The measurement continued for 16 min and 54 s, during which a total of 10,676 scans were acquired.

The measurement results were subsequently processed offline with the use of SLAM algorithms in order to combine them in a consistent point cloud. The preliminary estimation of the measurement trajectory was performed as the scans were replayed with actual speed. In the next step, the trajectory was manually improved in the post-processing mode by additionally indicating points which correspond to a flat terrain and by indicating clear revisit moments not identified automatically. Subsequently, automatic trajectory improvement methods were used to detect additional loop closures and robust refinement of pose graph edges. This process was iterated until satisfying results were obtained (no deviating observations (at 3 sigma), the trajectory visually corresponds to the actual measurement path). In effect, the obtained trajectory allowed the point clouds to be recorded from all scans. The resultant cloud, comprising 2,241,746 points, was filtered in Cloud Compare to remove measurement noise. The final result comprising a set of 1,968,367 points is shown in Figure 8. The entire post-processing lasted for approximately 30 min.

Table 3. Riegl and Velodyne mls measurement data volume.

| Data Source	Number of Points	Mean Point Density [points/m^2]
MLS Riegl VMZ 400i	97,018,764	1500
Handheld SLAM LiDAR	2,241,746	50
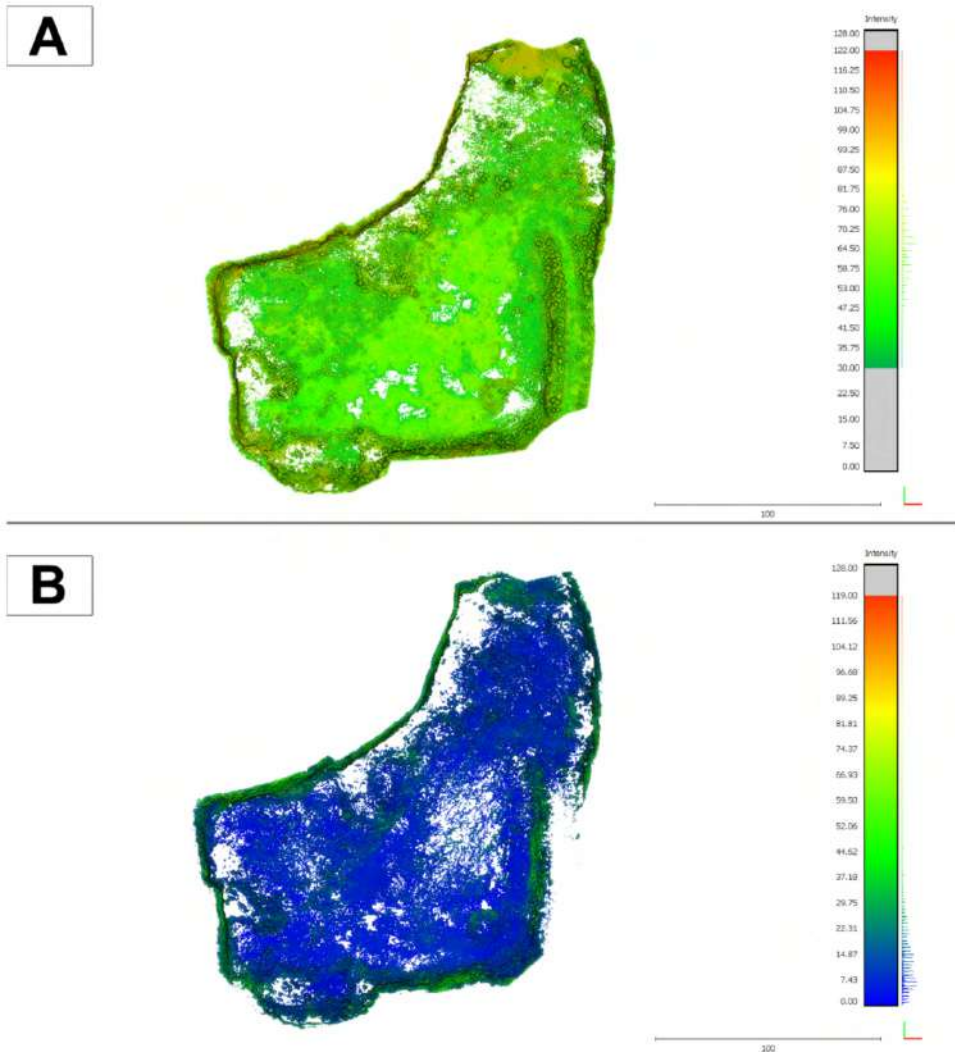
Figure 8. Top view of the point clouds: Riegl MLS VMZ 400i (**A**) and handheld Velodyne SLAM (**B**). Colors represent intensity value in a 7-bit range.

4. Discussion

The analyses demonstrate that mobile LiDAR measurement techniques provide input data that ensure that the constructed 3D mine models are georeferenced. The developed methodology for the processing of SLAM data is based on georeferencing them to the T_0 model built using the MLS Riegl VMZ 400i technique. The results of the experiment also indicate that it is possible to record a point cloud with the Iterative Closest Point (ICP) method, using a low-cost handheld scanner and with reference to the MLS point cloud.

The developed data processing method is based on overlapping the point clouds produced with the use of LiDAR MLS and SLAM techniques. The advantage of the use of MLS Riegl VMZ 400i lies in the fact that the 3D model has a full georeference in the chosen EPSG coordinate system. The SLAM point cloud recorded in the local system allows a continuous representation of the 3D surface in an open-pit mine. The MLS Riegl sensor is also advantageous due to its range, which reaches 800 m, with the SLAM point cloud recording at up to approx. 100 m. Another analyzed aspect is the scanning resolution. As presented in Table 3, average resolution of the MLS measurement was 1500 points/m^2 while the SLAM resolution was at an average of 50 points/m^2. An important part of this study was to verify whether the SLAM technique can be used as a low-cost approach to 3D modeling of mine geometry on ground. The results and the developed methodology clearly demonstrate that the implementation of the SLAM technique allows updates to the 3D model of an open-pit mine. Measurements of the identical ground surface showed the LiDAR data coherence level to be at 0.05 m. Figure 9 shows the spatial distribution of the distances between the points in the SLAM-based cloud, while Figure 10 is their histogram. A more detailed analysis of the locations with the highest individual deviations between the models leads to a conclusion that they occur in areas not covered by the MLS scanning or on areas covered with scattered greenery. In practical applications typical of an active open-pit mine, both cases should not affect the quality of the obtained geometrical data. The obtained accuracy levels (the distance between SLAM point cloud—MLS delivered mesh model is at a level of ± 5 cm) is sufficient to calculate volumes in open-pit mines of similar scale and to update their 3D models, since the geometry changes associated with the periodically monitored advances of the mining operation would usually be in the order of meters.
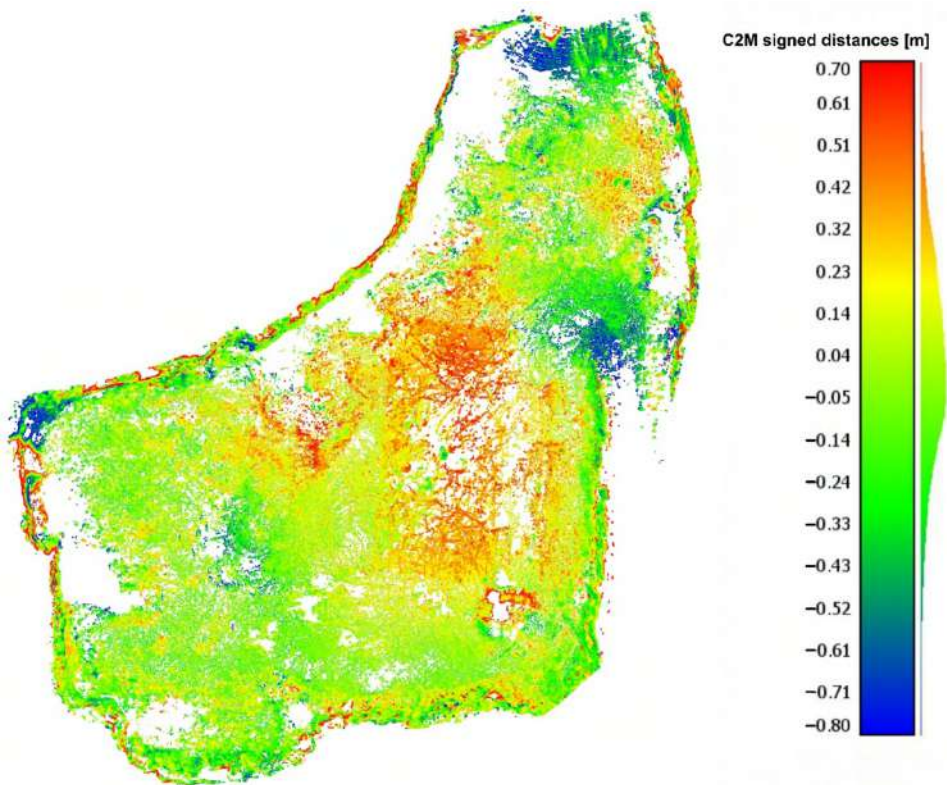
Figure 9. The spatial distribution of the distances between MLS Riegl and Velodyne SLAM points. Colors represent the distances from SLAM cloud to reference mesh.
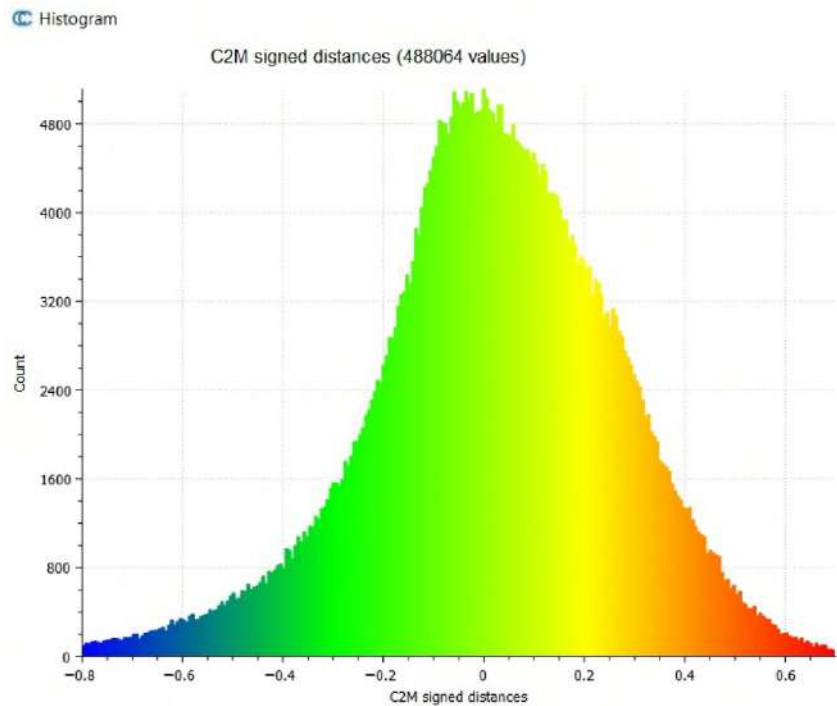
Figure 10. Distribution of the distances from SLAM cloud to reference mesh.

LiDAR observations in the implemented MLS approach allow the angles and distances to be measured from multiple measurement stations represented by the trajectory of the vehicle movement. In comparison to a classic approach to LiDAR measurements, TLS offers a possibility to record a continuous surface in a DSM and to reconstruct it closely representing the 3D surface with high measurement resolution. Importantly, in both the classic TLS approach and the MLS, the measuring instrument has an identical incidence angle at the analyzed object.

The LiDAR MLS method is seemingly limited by the impossibility to acquire data from objects which are covered with water. The observed gaps in the data are due to the absorption of the active LiDAR beam by the air-water medium, which causes the laser beam to become deflected and the LiDAR measurement point not to be recorded (white empty pixels in Figure 11). Another limitation of the LiDAR methods lies in the so-called shadows cast by objects which obstruct the laser beam. The above limitations are minimized by implementing the MLS technique, which allows a continuous measurement along an MLS trajectory.
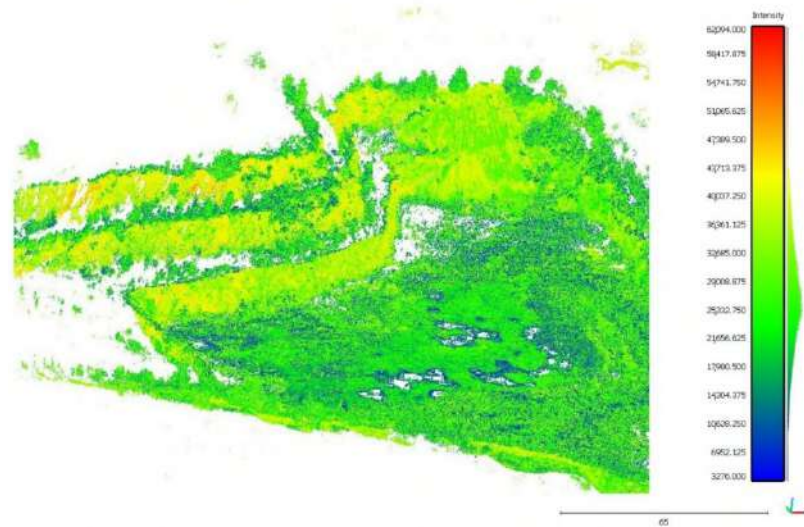
Figure 11. Isometric visualization of intensity MLS LiDAR data with white gaps.

5. Conclusions

Mobile laser scanning technology is experiencing a dynamic growth in surveying. This growth is observed in the precision of the measurements, in the amounts of obtained data (scanning resolution and speed), and in the number of the transport platforms being employed.

The in-field tests performed in the Mikoszów granite mine employed two types of laser scanning systems to demonstrate their usefulness and the potential of using the results in the modeling and monitoring of the geometry changes in an open-pit excavation. The novelty of the presented solution lies in the integration of spatial data acquired with sensors that vary in accuracy, measurement platform and procedure and data processing to optimize the effort and cost of maintaining a time-varying 3D mine model.

The solution proposed by the authors is based on performing the first scan with the use of a precise Riegl VMZ 400i system—this is indicated as state (point cloud) T_0. The most significant advantages of the method include the measurement range, data acquisition speed and the quality of the MLS trajectory adjustment, which allows precision in the order of single centimeters. Moreover, our method does not require the use of ground control points in the measurement area or outside of it. The results of the bundle adjustment of the MLS measurements were similar to the accuracy of RTK GNSS.

Data obtained with the use of this method may be successfully used in 3D modeling the geometry of an excavation, or in planning or monitoring the progress of mining operations, with respect to both compact rock (such as granite in this case, which may be mined in the form of both blocks and aggregate), and bulk minerals.

Consecutive measurement sessions are performed at times $T_1 - \ldots - T_n$ with the use of Velodyne VLP-16, which is a tool operated in the SLAM approach. The experiment, which consisted of acquiring data and then in combining the acquired data into a local point cloud and in georeferencing the data into an MLS cloud, demonstrated that the data are fitted at a precision sufficient to use them in the modeling of the advancement of mining works. From the perspective of mining-related surveying, the data are of adequate quality. Also, the solution proves economical, as it is based on the Velodyne VLP-16 low-cost approach. Importantly, a scanner of this type does not need a highly skilled operator. Additionally, the procedure of data processing and visualization is partially automated (on the basis of low-cost and open-access software solutions), which is a factor limiting the cost related to buying the software and employing a trained operator.

A novel procedure of carrying out 3D measurements was developed that can be applied to the entire life cycle of an open-pit mine. The experiment was successfully carried out to test it in the real mining environment. The core element of the proposed procedure is the creation of a base mine model with a precise MLS platform. Subsequent stages of work, i.e., periodic measurement sessions with a SLAM-based system, are utilized to update the base model and perform calculations of the excavated volume. It is worth noting that the advantage of using Velodyne VLP-16 or similar lidar in the SLAM solution is that there is no need for a highly skilled operator, costly equipment, or software. Such low-cost solution could enable employing digital twin concepts in the small mining companies, e.g., quarries.

Another advantage of the proposed solution is the lack of need to establish the ground control points. The base model is georeferenced using simultaneous GNSS RTK measurements and the subsequent SLAM models are registered to it in cloud-to-cloud manner, since the majority of the mine model is stable over time.

The authors would especially like to emphasize that the results of the experiment performed in the Mikoszów open-pit mine clearly indicate that the integration of the MLS LiDAR technique and of the handheld SLAM LiDAR technique according to the method here described allows a 3D model of the excavation to be constructed and updated in real time. The resultant high-resolution point cloud allows the designing, inventorying, and feeding of big data databases in mines, according to the idea of Industry 4.0. LiDAR techniques used in the analyzed mine enable a fast and comfortable acquisition of 3D information about the excavation over the life cycle of a mine. This information may be used at every stage of the mining operations in open-pit mines, including in prospecting and exploration works, in access and development works, in the exploitation of the mineral, in the reclamation works, and in the management of the post-mining area.

References

1. Battulwar, R.; Winkelmaier, G.; Valencia, J.; Naghadehi, M.Z.; Peik, B.; Abbasi, B.; Parvin, B.; Sattarvand, J. A Practical Methodology for Generating High-Resolution 3D Models of Open-Pit Slopes Using UAVs: Flight Path Planning and Optimization. *Remote Sens.* **2020**, *12*, 2283. [CrossRef]
2. Nieto, J.I.; Monteiro, S.T.; Viejo, D. 3D geological modelling using laser and hyperspectral data. In Proceedings of the 2010 IEEE International Geoscience and Remote Sensing Symposium, Honolulu, HI, USA, 25–30 July 2010. [CrossRef]
3. Werner, T.; Bebbington, A.; Gregory, G. Assessing impacts of mining: Recent contributions from GIS and remote sensing. *Extr. Ind. Soc.* **2019**, *6*, 993–1012. [CrossRef]
4. Deliormanli, A.H.; Maerz, N.H.; Otoo, J. Using terrestrial 3D laser scanning and optical methods to determine orientations of discontinuities at a granite quarry. *Int. J. Rock Mech. Min. Sci.* **2014**, *66*, 41–48. [CrossRef]
5. Buckley, S.J.; Howell, J.; Enge, H.; Kurz, T. Terrestrial laser scanning in geology: Data acquisition, processing and accuracy considerations. *J. Geol. Soc.* **2008**, *165*, 625–638. [CrossRef]

6. Shahbazi, M.; Sohn, G.; Théau, J.; Menard, P. Development and Evaluation of a UAV-Photogrammetry System for Precise 3D Environmental Modeling. *Sensors* **2015**, *15*, 27493–27524. [CrossRef] [PubMed]

7. Keawaram, B.; Dumrongchai, P. Comparisons of Surveying with Terrestrial Laser Scanner and Total Station for Volume Determination of Overburden and Coal Excavations in Large Open-Pit Mine. *World Acad. Sci. Eng. Technol. Int. J. Geol. Environ. Eng.* **2017**, *11*, 964–972.

8. Zaky, K.; Ghonem, A.; El Semary, H. Accuracy, time and cost of different leveling types. *Eng. Res. J.* **2002**, *79*, 55–67.

9. Can, E.; Mekik, C.; Kuşçu, S. Akcın, H. Computation of subsidence parameters resulting from layer movements post-operations of underground mining. *J. Struct. Geol.* **2013**, *47*, 16–24. [CrossRef]

10. Brown, N.; Kaloustian, S.; Roeckle, M. Monitoring of open pit mines using combined GNSS satellite receivers and robotic total stations. In Proceedings of the 2007 International Symposium on Rock Slope Stability in Open Pit Mining and Civil Engineering, Perth, Australia, 12–14 September 2007; Australian Centre for Geomechanics: Crawley, Australia, 2007; pp. 417–429.

11. Einicke, G.; Martin, S.; von Voithenberg, M.V.; Enderle, W. Pseudolite Options for Improved Mining Navigation. In Proceedings of the International Global Navigation Satellite Systems Society IGNSS Symposium 2006, Holiday Inn Surfers Paradise, Gold Coast, QL, Australia, 17–21 July 2006.

12. McHugh, E.L.; Dwyer, J.; Long, D.G.; Sabine, C. *Applications of Ground-Based Radar to Mine Slope Monitoring*; Report of Investigations 9666; NIOSH-Publications Dissemination: Cincinnati, OH, USA, 2006.

13. Wajs, J. Research on surveying technology applied for DTM modelling and volume computation in open pit mines. *Min. Sci.* **2015**, *22*, 75–83. [CrossRef]

14. Xu, Z.; Xu, E.; Wu, L.; Liu, S.; Mao, Y. Registration of Terrestrial Laser Scanning Surveys Using Terrain-Invariant Regions for Measuring Exploitative Volumes over Open-Pit Mines. *Remote Sens.* **2019**, *11*, 606. [CrossRef]

15. Tong, X.; Liu, X.; Chen, P.; Liu, S.; Luan, K.; Li, L.; Liu, S.; Liu, X.; Xie, H.; Jin, Y.; et al. Integration of UAV-Based Photogrammetry and Terrestrial Laser Scanning for the Three-Dimensional Mapping and Monitoring of Open-Pit Mine Areas. *Remote Sens.* **2015**, *7*, 6635–6662. [CrossRef]

16. Jozkow, G.; Totha, C.; Grejner-Brzezinska, D. UAS topographic mapping with Velodyne LiDAR sensor. *ISPRS Ann. Photogramm. Remote Sens. Spat. Inf. Sci.* **2016**, *3*, 201–208. [CrossRef]

17. Toth, C.; Jozkow, G.; Grejner-Brzezinska, D. Mapping with Small UAS: A Point Cloud Accuracy Assessment. *J. Appl. Geod.* **2015**, *9*, 213–226. [CrossRef]

18. Jaboyedoff, M.; Abellán, A.; Carrea, D.; Derron, M.H.; Matasci, B.; Michoud, C. Mapping and monitoring of landslides using LiDAR. In *Natural Hazards*; CRC Press: Boca Raton, FL, USA, 2018; pp. 397–420.

19. Kukko, A.; Kaartinen, H.; Hyyppä, J.; Chen, Y. Multiplatform Mobile Laser Scanning: Usability and Performance. *Sensors* **2012**, *12*, 11712–11733. [CrossRef]

20. Okhotin, A.L. Application of Laser scanning in mine surveying. *Proc. FIG Comm.* **2009**, *6*, 53–62.

21. Bertayeva, K.; Panaedova, G.; Natocheeva, N.; Belyanchikova, T. Industry 4.0 in the mining industry: Global trends and innovative development. In *E3S Web of Conferences*; EDP Sciences: Les Ulis, France, 2019; Volume 135, p. 04026.

22. Lööw, J.; Abrahamsson, L.; Johansson, J. Mining 4.0—The Impact of New Technology from a Work Place Perspective. *Min. Metall. Explor.* **2019**, *36*, 701–707. [CrossRef]

23. Gackowiec, P.; Podobińska-Staniec, M.; Brzychczy, E.; Kühlbach, C.; Özver, T. Review of Key Performance Indicators for Process Monitoring in the Mining Industry. *Energies* **2020**, *13*, 5169. [CrossRef]

24. Sukiennik, M. Challenges Faced by Businesses in the Mining Industry in the Context of the Industry 4.0 Philosophy. *Multidiscip. Asp. Prod. Eng.* **2018**, *1*, 621–626. [CrossRef]

25. Sishi, M.N.; Telukdarie, A. Implementation of industry 4.0 technologies in the mining industry: A case study. In Proceedings of the 2017 IEEE International Conference on Industrial Engineering and Engineering Management (IEEM), Singapore, 10–13 December 2017. [CrossRef]

26. Gruszecki, J. (Geological Company Proxima S.A., Wroclaw, Poland). Geological documentation of the granite and gneiss deposit in category C1 Mikoszow in Strzelin, province. Wroclaw. Unpublished work. 1993.

27. Kominowski, K. (A-Z Geometr s.c., Walbrzych, Poland). Geological documentation of the Mikoszow granite and gneiss deposit in cat. C1, places Mikoszow, commune and over Strzelin, voivodeship Lower Silesia. Unpublished work. 2001.

28. Majkowska, U. (Majkowska Geological Services, Wroclaw, Poland). Appendix No. 1 to the geological documentation of the Mikoszow granite and gneiss deposit in cat. C1 in Strzelin, Strzelin commune, province Wroclaw. Unpublished work. 1996.

29. Szkudlarek, L.; Bernatowicz, W.; Ryng-Duczmal, W.; Bernatowicz, M.; Koltowska, M.; Gil, R.; Filipowska, I. *Renewal of the Mining License for the Mikoszow Deposit*; Environmental Impact Report; Ekovert Szkudlarek: Wroclaw, Poland, 2017.

30. Adán, A.; Quintana, B.; Prieto, S. Autonomous Mobile Scanning Systems for the Digitization of Buildings: A Review. *Remote Sens.* **2019**, *11*, 306. [CrossRef]

31. Hussnain, Z.; Elberink, S.O.; Vosselman, G. Enhanced trajectory estimation of mobile laser scanners using aerial images. *ISPRS J. Photogramm. Remote Sens.* **2021**, *173*, 66–78. [CrossRef]

32. Singh, S.K.; Raval, S.; Banerjee, B.P. Automated structural discontinuity mapping in a rock face occluded by vegetation using mobile laser scanning. *Eng. Geol.* **2021**, *285*, 106040. [CrossRef]

33. Riegl Hybrid Mobile Laser Scanning System Brochure. Available online: http://www.riegl.com/uploads/tx_pxpriegldownloads/RIEGL_VMZ_at-a-glance_brochure_2018-11-28.pdf (accessed on 26 January 2021).

34. Chang, L.; Niu, X.; Liu, T.; Tang, J.; Qian, C. GNSS/INS/LiDAR-SLAM Integrated Navigation System Based on Graph Optimization. *Remote Sens.* **2019**, *11*, 1009. [CrossRef]
35. Hening, S.; Ippolito, C.A.; Krishnakumar, K.S.; Stepanyan, V.; Teodorescu, M. *3D LiDAR SLAM Integration with GPS/INS for UAVs in Urban GPS-Degraded Environments*; AIAA Information Systems-AIAA Infotech@Aerospace; American Institute of Aeronautics and Astronautics: Reston, VA, USA, 2017. [CrossRef]
36. Karam, S.; Lehtola, V.; Vosselman, G. Strategies to integrate imu and lidar slam for indoor mapping. ISPRS Annals of the Photogrammetry. *Remote Sens. Spat. Inf. Sci.* **2020**, *1*, 223–230. [CrossRef]
37. Sadruddin, H.; Mahmoud, A.; Atia, M.M. Enhancing Body-Mounted LiDAR SLAM using an IMU-based Pedestrian Dead Reckoning (PDR) Model. In Proceedings of the 2020 IEEE 63rd International Midwest Symposium on Circuits and Systems (MWSCAS), Springfield, MA, USA, 9–12 August 2020. [CrossRef]
38. Quan, M.; Piao, S.; Tan, M.; Huang, S.S. Tightly-Coupled Monocular Visual-Odometric SLAM Using Wheels and a MEMS Gyroscope. *IEEE Access* **2019**, *7*, 97374–97389. [CrossRef]
39. Brossard, M.; Bonnabel, S.; Barrau, A. Invariant Kalman Filtering for Visual Inertial SLAM. In Proceedings of the 2018 IEEE 21st International Conference on Information Fusion (FUSION), Cambridge, UK, 10–13 July 2018. [CrossRef]
40. Mendes, E.; Koch, P.; Lacroix, S. ICP-based pose-graph SLAM. In Proceedings of the 2016 IEEE International Symposium on Safety, Security, and Rescue Robotics (SSRR), Lausanne, Switzerland, 23–27 October 2016. [CrossRef]
41. Pierzchała, M.; Giguère, P.; Astrup, R. Mapping forests using an unmanned ground vehicle with 3D LiDAR and graph-SLAM. *Comput. Electron. Agric.* **2018**, *145*, 217–225. [CrossRef]
42. Muglikar, M.; Zhang, Z.; Scaramuzza, D. Voxel Map for Visual SLAM. In Proceedings of the 2020 IEEE International Conference on Robotics and Automation (ICRA), Paris, France, 31 May–31 August 2020. [CrossRef]
43. Guclu, O.; Can, A.B. Fast and Effective Loop Closure Detection to Improve SLAM Performance. *J. Intell. Robot. Syst.* **2017**, *93*, 495–517. [CrossRef]
44. Sammartano, G.; Spanò, A. Point clouds by SLAM-based mobile mapping systems: Accuracy and geometric content validation in multisensor survey and stand-alone acquisition. *Appl. Geomat.* **2018**, *10*, 317–339. [CrossRef]
45. Ren, Z.; Wang, L.; Bi, L. Robust GICP-Based 3D LiDAR SLAM for Underground Mining Environment. *Sensors* **2019**, *19*, 2915. [CrossRef] [PubMed]
46. Zhang, J.; Singh, S. Low-drift and real-time lidar odometry and mapping. *Auton. Robot.* **2016**, *41*, 401–416. [CrossRef]
47. Shan, T.; Englot, B. LeGO-LOAM: Lightweight and Ground-Optimized Lidar Odometry and Mapping on Variable Terrain. In Proceedings of the 2018 IEEE/RSJ International Conference on Intelligent Robots and Systems (IROS), Madrid, Spain, 1–5 October 2018. [CrossRef]
48. Nelson, E. Blam—Berkeley Localization and Mapping. Available online: https://github.com/erik-nelson/blam (accessed on 26 January 2021).
49. Vassena, G.; Clerici, A. Open pit mine 3d mapping by tls and digital photogrammetry: 3d model update thanks to a slam based approach. *Int. Arch. Photogramm. Remote Sens. Spat. Inf. Sci.* **2018**, *42*, 1145–1148. [CrossRef]
50. Koide, K.; Miura, J.; Menegatti, E. A portable three-dimensional LIDAR-based system for long-term and wide-area people behaviour measurement. *Int. J. Adv. Robot. Syst.* **2019**, *16*, 172988141984153. [CrossRef]
51. Quigley, M.; Conley, K.; Gerkey, B.; Faust, J.; Foote, T.; Leibs, J.; Bergerm, E.; Wheeler, R.; Ng, A.Y. *ROS: An open-source Robot Operating System*; ICRA: Kobe, Japan, 2009; Volume 3, p. 5.

Publication 3: Analysis of LiDAR Actuator System Influence on the Quality of Dense 3D Point Cloud Obtained with SLAM

Article

Analysis of Lidar Actuator System Influence on the Quality of Dense 3D Point Cloud Obtained with SLAM

Paweł Trybała [1,*], Jarosław Szrek [2], Błażej Dębogórski [1], Bartłomiej Ziętek [1], Jan Blachowski [1], Jacek Wodecki [1] and Radosław Zimroz [1]

[1]   Faculty of Geoengineering, Mining and Geology, Wrocław University of Science and Technology,
     Na Grobli 15, 50-421 Wroclaw, Poland
[2]   Faculty of Mechanical Engineering, Wroclaw University of Science and Technology, Łukasiewicza 5,
     50-371 Wroclaw, Poland
[*]   Correspondence: pawel.trybala@pwr.edu.pl

Abstract: Mobile mapping technologies, based on techniques such as simultaneous localization and mapping (SLAM) and surface-from-motion (SfM), are being vigorously developed both in the scientific community and in industry. They are crucial concepts for automated 3D surveying and autonomous vehicles. For various applications, rotating multiline scanners, manufactured, for example, by Velodyne and Ouster, are utilized as the main sensor of the mapping hardware system. However, their principle of operation has a substantial drawback, as their scanning pattern creates natural gaps between the scanning lines. In some models, the vertical lidar field of view can also be severely limited. To overcome these issues, more sensors could be employed, which would significantly increase the cost of the mapping system. Instead, some investigators have added a tilting or rotating motor to the lidar. Although the effectiveness of such a solution is usually clearly visible, its impact on the quality of the acquired 3D data has not yet been investigated. This paper presents an adjustable mapping system, which allows for switching between a stable, tilting or fully rotating lidar position. A simple experiment in a building corridor was performed, simulating the conditions of a mobile robot passing through a narrow tunnel: a common setting for applications, such as mining surveying or industrial facility inspection. A SLAM algorithm is utilized to create a coherent 3D point cloud of the mapped corridor for three settings of the sensor movement. The extent of improvement in the 3D data quality when using the tilting and rotating lidar, compared to keeping a stable position, is quantified. Different metrics are proposed to account for different aspects of the 3D data quality, such as completeness, density and geometry coherence. The ability of SLAM algorithms to faithfully represent selected objects appearing in the mapped scene is also examined. The results show that the fully rotating solution is optimal in terms of most of the metrics analyzed. However, the improvement observed from a horizontally mounted sensor to a tilting sensor was the most significant.

Keywords: lidar; dense point cloud; SLAM; 3D reconstruction; 3D data quality; surface density

1. Introduction

Simultaneous localization and mapping (SLAM) represents one of the most significant computational problems for any 3D reconstruction. It can be applied to autonomous cars and robotics inspection missions to solve specific tasks, in particular map generation and obstacle detection. The most promising data source for performing these tasks is application of the lidar distance measurement method. Although many 3D-mapping lidar systems have been developed and are used in various applications, the quality and accuracy of the generated 3D point clouds and 3D geometries often remain insufficient, particularly in complex or unstable environments. However, one of the most rapidly growing fields of application for mobile mapping systems is underground mining, as the speed and possible

automation of performing such measurements enables the rapid acquisition of dense 3D data for vast underground structures. For these reasons, constant improvement is needed in measurement system construction and point cloud data processing. New approaches to the analysis and methodological assessment of the 3D data quality are also required. One promising solution, improving the hardware side of the mapping system, is the design of a spinning lidar sensor with an additional module that rotates the sensor around another axis. This actuated lidar design, in which a scanner is combined with an actuation mechanism to scan a 3D volume rather than a single line, has already been used in numerous mobile robot SLAM applications [1].

Therefore, the main objective of our study was to quantitatively and qualitatively assess the influence of a well-known approach using lidar rotation on the accuracy and value of a 3D point cloud using an inspection robot in a test environment mimicking an underground mine tunnel. The paper is structured as follows: first, in Section 2.1, the state of the art is investigated. The scope of the investigation includes use of a rotating lidar in mobile or stationary mapping and point cloud accuracy and quality assessment methods, in particular, with respect to SLAM applications in underground environments. Then, in Section 2.2, the design of an adjustable mapping system, developed for this investigation, is presented. The SLAM data-processing workflow is described in Section 2.3, and our approach to assessing the quality of the results with the metrics utilized for this purpose is explained in Section 2.4. Next, in Section 2.5, the experimental setup used in this study is described. The results obtained from the experiments undertaken are first presented and analyzed in global terms in Section 3.1, and, then, considering local point cloud quality in Section 3.2. Finally, a summary of the research, as well as final thoughts and recommendations for implementing SLAM in underground environments, is presented in Section 4.

2. Materials and Methods

2.1. State of the Art

The data acquisition strategy for autonomous vehicles and inspection robots using the lidar system needs to be based on an understanding of specific environmental parameters, such as the presence of a variety of dynamic or static obstacles, ensuring the highest possible level of accuracy in the scanned data. Measurement systems with rotating lidar sensors enable the capture of dense and close-to-spherical data about the surrounding environment [2]. Thus, numerous research groups and companies have been engaged in the development of methods to increase the resolution of the mapped space with rotating 2D and/or 3D lidar systems. With respect to the academic state-of-the-art, comprehensive reviews can be found in the literature, focusing both on pure lidar SLAM [3] and on more sophisticated, fusion-based, methods [4]. Many commercial, user-oriented devices are also available on the market. An extensive, but not exhaustive, list of such solutions includes handheld scanners, such as GeoSLAM Horizon, GreenValley LiGrip, SatLab Cygnus and Leica BLK2GO, backpack solutions, such as Kaarta Stencil and Leica Pegasus, and complete mapping systems for UGVs and UAVs, such as Emesent Hovermap ST. The wide range of rapidly appearing and evolving SLAM systems on the market makes it difficult to provide a fully comprehensive list.

The design of a dual 2D/3D lidar mapping system and a six-degrees-of-freedom (DOF) interpolated odometry, where 2D lidar is used to enhance 3D solid-state lidar performance used on a ground vehicle platform, can be found in [5]. The design of a spring-mounted 3D range sensor that reduces irregular vibrations of the measurement deck is described in [6]. In [7], a method for focusing on specific regions of interest using a secondary rotation motor to receive high-density measurements of the surroundings with a mobile robot platform is presented. The authors tested how, by decreasing the secondary rotation speed in the specific region, the point density in this area could be increased. The authors of [8] developed a new system (named Art-SLAM) to perform point-cloud-based graph SLAM. The proposed system is capable of achieving real-time performance, maintaining high

accuracy, and can also efficiently detect and close loops in the trajectory, using a three-phase algorithm. A similar method, focusing on the correction of a local point cloud alignment, is described in [9].

Construction of the scanning actuation mechanism can have an impact on different positions of the rotation center of the lidar mirror and construction itself; thus, sufficient calibration methods are needed. The description of an automatic calibration method for the actuated lidar can be found in [10]. An extension of the following calibration methods for multiple spinning laser scanners with the support of inertial/global navigation systems is presented in [11]. The results of the evaluation of an automated algorithm and a spinning/rolling lidar system for continuous-time trajectory estimation, taking into account inter-sample pose errors to handle data distortions, are described in [1]. The drawback of using a high-density dataset is its size; thus, compression frameworks and algorithms are needed. For example, reference [12] describes a detailed investigation of a geometry compression method created for a spinning lidar point cloud.

Point cloud accuracy and data-quality assessment are amongst the most important factors for the creation of reliable, error-free methods used in laser scanning. To tackle the recurrent problems of misregistration, outlier detection and over-completeness, a comparison of several methods is needed. In [13], the use of mobile indoor 3D scanning methods are described, which are applied to a dozen different scanned locations, using five commercial indoor mapping prototypes with respect to error metrics, which do not operate on a manually given proximity scale, but on different proximity scales. High-dense point cloud analyses include simplification methods, which enable significant size reduction, while retaining sufficient variability of the geometry. Well-known algorithms exist that combine incremental/hierarchy clustering or iterative simplification [14]. Surface reconstruction using a robust diagnostic algorithm for more resistant outlier detection and a technique for plane-fitting applying a minimum covariance determinant are presented in [15]. In [16], this is used as an alternative approach for the assessment of local surface damage in civil structures. In the same way, photogrammetry-based 3D mapping of road distress detection is considered for use with unmanned aerial vehicles in [17].

With regard to the underground mining environment being investigated in the present study, SLAM solutions and applications in real or artificial spaces need to be considered. Underground workings are characterized by significant irregularities in the surrounding geometries and by dustiness that can affect the performance of the mobile system and the quality of measurements obtained. The results presented in the studies referred to below confirm that SLAM-enabled laser scanning represents a promising method for underground mining tunnel mapping and examination. One of the first studies that indicated the potential for high-resolution 3D-mapping of an underground mine involved a cart-mounted 3D-laser-scanner setup and an automatic 3D-modeling method [18]. Similarly, reference [19] reported a method for solving the SLAM problem with six DOF for the accurate volumetric mapping of an abandoned mine.

The authors in [20] proposed and tested a graph SLAM optimization method in an underground mine laboratory based on a generalized iterative closest point (GICP). In [21], a system for continuous high-resolution mapping and exploration of underground spaces, with virtual-reality visualization capabilities that can be used in mobile robot rescue operations, was presented. The investigation described in [22] demonstrated a SLAM solution capable of accurately mapping underground mines at kilometer scales, using a spinning 2D-laser scanner and an industrial-grade inertial measurement unit mounted on a light vehicle. Finally, reference [23] analyzed the quality of SLAM-based mobile laser scanner (MLS) data for the accurate and efficient geotechnical monitoring of the underground mine environment. In addition, the applicability of real-time 3D SLAM based on normally distributed transform (NDT) and pose-graph optimization for complex underground space scenarios after disasters was examined in [24]. A broad assessment of handheld laser scanners for mine surveys and the validation of results with terrestrial laser scanners for reference data are presented in [25]. A summary of successful SLAM

approaches for surveying underground environments, based on experiences from the DARPA Subterranean Challenge, is presented in [26].

The literature review highlighted that there are still gaps to be filled with respect to evaluation methods for comparing the results (i.e., 3D point clouds) produced with different SLAM systems, with respect to both the hardware and the software used. Developing such methods would assist in choosing suitable solutions for selected use-case environments, optimizing the cost of scanning, system complexity and data size and quality. This study aims to tackle this challenge.

2.2. Adjustable Mapping System Design

The purpose of developing an adjustable mapping system for this study was to enable additional, controlled rotation of the lidar device around its longitudinal axis. In consequence, the effective field of view (FoV) of the sensor can be gradually increased, almost up to the point of a full-spherical FoV (excluding occlusions caused by the sensor mounting and the robot). The adjustability of the proposed system is controlled by the operator, who can easily change the range of lidar rotation using control software options on the remotely connected tablet. In this research, we utilized these options to emulate three different strategies for lidar head mounting, which have been used in various commercial solutions and research prototypes. The details of the system configuration are presented in the following paragraphs.

In this study, a 16-line Velodyne VLP-16 lidar is used. The sensor is mounted on a rotating module, mounted above the set of sensors designed for inspection purposes Figure 1a. The rotational movement is carried out using a Dynamixel AX-12A servo drive from Robotis. During movement, the desired angle range changes with a resolution of $0.29°$. The supply voltage of the device is 12 V. The feedback signal of the current angular position is used to dynamically generate the rigid body transform between the lidar and the robot base reference frame. This allows the mapping to be performed in the robot frame and provides an initial estimate for transformations between consecutive lidar positions in a global frame of reference, computed by the SLAM algorithm.

(**a**) Sensor suite installed on the robot   (**b**) Data-reading system structure
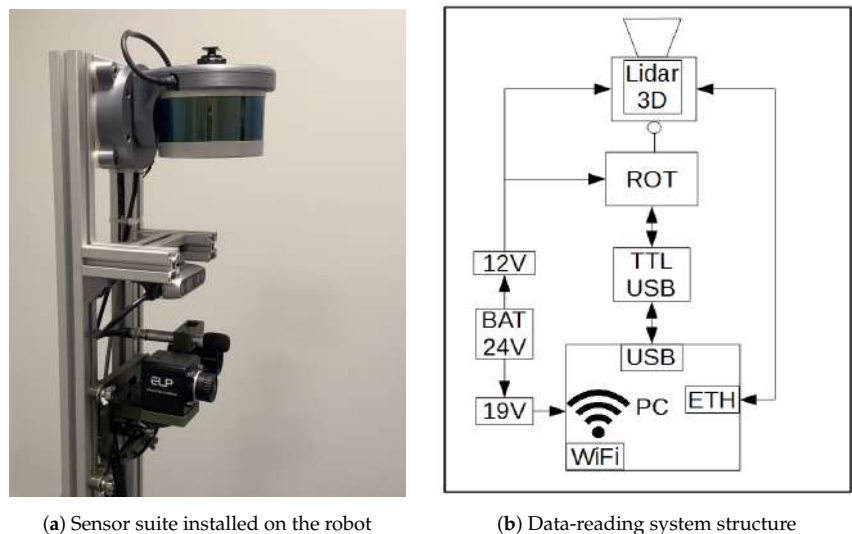
Figure 1. Adjustable mapping system for the mobile robot.

A block diagram of the data-acquisition system with the actuator module is shown in Figure 1. Data from the lidar is sent to a computer via an Ethernet interface using a user datagram protocol (UDP). Simultaneously, the data on the current inclination angle of the

actuator is transferred to the computer via the USB port of the actuator module using a half-duplex UART converter. The system is integrated with the Robot Operating System (ROS) environment and dedicated software was developed for handling the components. The software uses ROS dynamic reconfiguration parameters, which enable the setting of a stable given position of the sensor throughout the measurement session or continuous spinning of the lidar around the longitudinal axis of the robot in a given range. Due to the limitations caused by the wiring, the maximum rotation range was limited to between $-90°$ and $90°$, where the neutral horizontal position of the sensor was considered to be $0°$. The control software was written using the Python language. The power supply of the system was integrated with the robot power system. Suitable voltages for powering the data acquisition computer, the lidar and the actuator module were obtained with DC/DC step-down converters, set to the appropriate output voltage. The scheme of the module is presented in Figure 2.
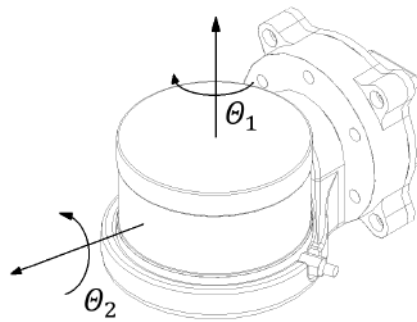
Figure 2. Lidar rotation module scheme. Θ_1 represents inner laser rotation around the vertical axis and Θ_2 denotes external rotation of the entire sensor around its longitudinal axis using an actuator.

2.3. 3D Lidar SLAM

In this study, several steps of point cloud acquisition are taken to obtain coherent and noise-free global point clouds. The aim is to ensure the highest quality of results from the different methods tested so that the comparison outcomes would not be affected by external factors or imperfect execution and repetition of the experiment. The parameter values in each step are universally chosen and kept consistent for each case. Although their method-specific tuning could potentially improve the accuracy of results, it might significantly influence the data density and, thus, introduce bias into one of the most important aspects of the analysis.

First, the robot trajectory is estimated in real time with the SLAM system, consisting of A-LOAM lidar odometry [27], scan context loop closure detection [28,29] and GTSAM-based pose-graph optimization [30–32]. A schematic overview of the method used is presented in Figure 3, where different factor graph elements are denoted as symbols with relevant connections between them. Lidar odometry, as the crucial element of the system, provides transformation estimates between the sensor reference frame and a global reference frame. The transform is calculated with a frequency of 10 Hz (equal to the lidar data acquisition frequency) based on extraction of feature points, creating edge lines and planar patches, and identifying correspondences between features found in consecutive point clouds. An initial guess is provided by the *tf* broadcaster [33], which receives the current actuator inclination angle and uses it to calculate the transform from the lidar frame to the robot base frame. The SLAM workflow is based on open-source implementation of SC-A-LOAM [28,29], with the addition of using rotation module feedback to provide an initial guess of the lidar pose transformation and to prevent distortion of the point clouds.
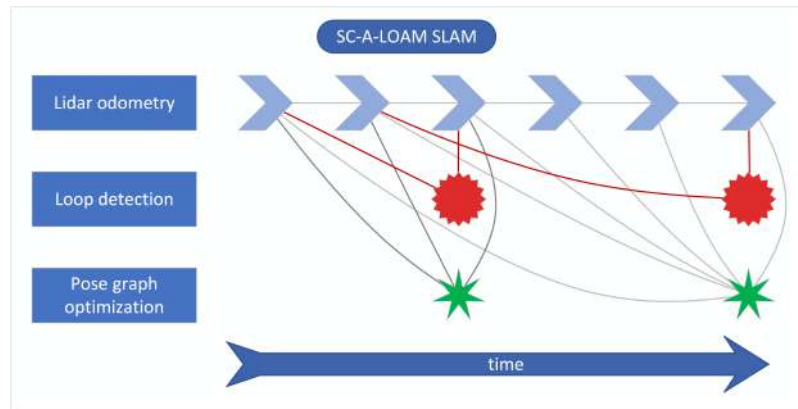
Figure 3. Scheme of utilized SLAM algorithm.

An important part of the applied SLAM algorithm is correction for motion distortion of point clouds. The lidar used in the study acquires 360° 3D point clouds in constant motion, revolving internally around its z-axis. One revolution (a sweep) takes 0.1 s and an aggregated set of point coordinates is sent by the sensor to the PC. However, when the scanner is in motion, the points acquired between the start and the end of the sweep have a slightly different frame of reference. This results in aggregating in each point cloud points acquired from slightly different positions, introducing a systematic error into the measurements (Figure 4). Since the individual point acquisition timestamps are known, it is possible to correct for the sensor ego-motion, provided that at least an approximate motion of the sensor during the sweep is known. Lidar odometry is utilized to reproject the points to the mutual reference frame of the point acquired at the end of the sweep.
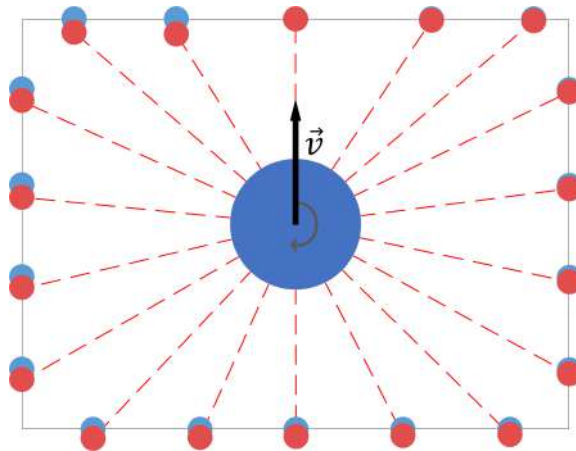
Figure 4. Illustration of point cloud motion distortion in a simple room seen from the top view. Raw point cloud in red; undistorted points in blue.

Lidar odometry provides a quick and constant, but preliminary, sensor pose estimate. It is susceptible to long-term drift, especially with respect to orientation in the 3D space. With a rotating sensor, such as that used in the study, this could cause unacceptable mapping results, with common errors occurring, such as double walls or rotated corridors. To prevent this, loop closure detection and pose-graph optimization are included in the software system. In our test measurements, we did not have explicit loop closures in terms of returning to the same place the robot visited earlier. Therefore, Scan Context++ was

used to additionally bind the trajectory after each full resolution of the actuator. The point clouds acquired at the same actuator inclination angle are/were similar due to the low speed of the robot. The resulting matches between scans are added as a constraint to the pose graph and optimized with GTSAM, reducing the drift of the odometry algorithm.

Then, clusters of points representing dynamic objects are removed in post-processing using removert [34]. This step enables reduction in noise of the point clouds and exclusion of moving objects accidentally appearing in the lidar field of view, such as the robot operator or the robot itself. Although the filtering procedure may slightly influence the density of the analyzed point clouds, due to the different level of robot ego-noise present in the three compared SLAM approaches, this step is necessary to allow comparison of the resulting 3D data. To minimize the influence of this step on the comparison, parameters of the filtration in all three cases were kept consistent. An example of the effect of applying removert to our data is presented in Figure 5. The noisy points are present in the central part of the scanned environment, just above the floor. They are caused by the robot elements occasionally coming into the lidar field of view. After applying the removert algorithms, this noise is successfully eliminated. In the last stage of 3D data preparation, point clouds from every scenario are cropped to the same area of interest to eliminate points that lie outside the surveyed corridor.
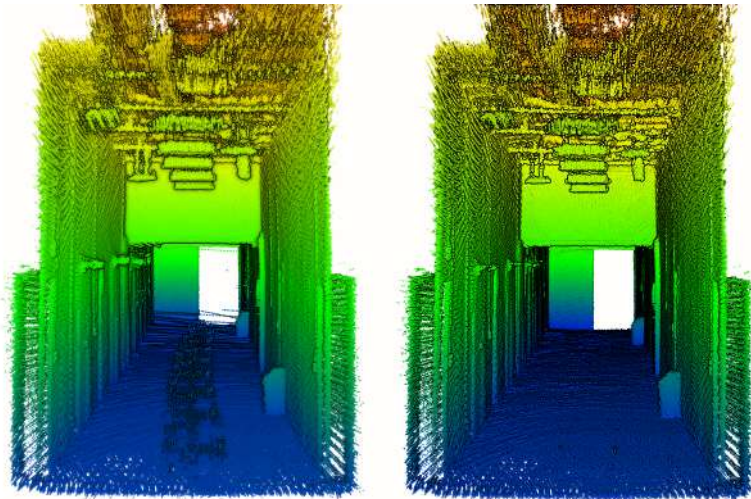
Figure 5. Point cloud before (**left**) and after filtering (**right**).

2.4. Metrics for Quality Assessment of 3D-Scene Reconstruction

Evaluating the quality of 3D point cloud data acquired with a mobile mapping system is not a straightforward task. Many metrics have been proposed and used to assess the accuracy of SLAM measurements, such as the absolute trajectory error (ATE), the relative trajectory error (RTE) and the relative position error (RPE) [35,36]. However, they focus on positioning accuracy in the global context, that is, the angular and linear drift of the algorithm in the long term, and do not convey information regarding the short-term quality of the measurements. Nevertheless, there are other important aspects of 3D-data quality, such as completeness, density and local coherence. In the context of extracting information about specific objects from the point cloud, e.g., during inspection or classification, they provide a more viable insight into the quality of geometry reconstruction [37], and, thus, constitute the centerpiece of this study.

One of the metrics that can be used to estimate the local quality of a point cloud is its density. This simply describes the number of measured points per chosen unit of reference: a volume or a surface. For this study, since the mapped area primarily contains

approximately planar surfaces, surface density was calculated with respect to Equation (1) and analyzed.

$$SD = \frac{N}{\Pi R^2}$$ (1)

where: N—number of neighboring points in the radius R around the analyzed point.

Data density provides information about the spatial distribution of points and their number, characterizing the redundancy of the measured geometry. However, this metric does not convey information on the noise level of the analyzed point cloud. To address this, another component was introduced to the analysis, namely, object reconstruction quality, that is, how accurate the measured geometry is of a single object in the scanned scene.

For evaluating the object reconstruction quality, i.e., the local consistency of a point cloud, several objects were chosen as samples. They were manually identified in each point cloud and compared between different tested lidar SLAM configurations. For planar objects, such as walls, doors or floor, surface variation [38,39] (also named "change of curvature" in other reports [40]) was calculated according to Equation (2). This metric has been utilized in several investigations [15,16] to describe and identify local surface deviations on the basis of point cloud data. The metric uses local descriptors of points in the form of a covariance matrix of their neighborhood, which can be geometrically interpreted as their eigenvectors with associated eigenvalues (Figure 6). The radius, in which the neighboring points were included for calculation of the covariance matrix, was selected as 5 cm to provide detailed information, while still being above the value of the lidar ranging accuracy. Moreover, for perfectly planar objects, it was possible to additionally perform a least-square plane fit to introduce a single-number statistic for evaluation of local geometry consistency [41].

$$SV = \frac{\lambda_3}{\sum_{i=1}^{3} \lambda_i}$$ (2)

where $\lambda_{1,2,3}$—eigenvalues (in descending order) of a covariance matrix calculated for the set of coordinates of neighboring points in radius R.
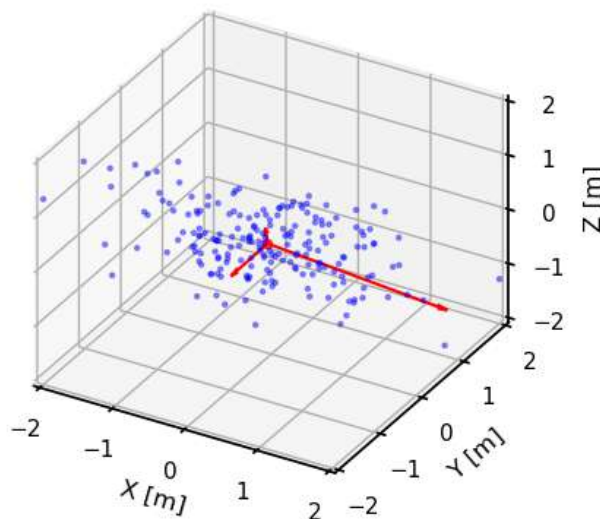

Figure 6. An example subset of a 3D point cloud with corresponding eigenvectors scaled by their eigenvalues.

In the cases of two distinctive objects in the study area, namely a ceiling lamp and a trashcan, such analysis would not be meaningful since their geometry is more complex

than a plane. To account for this, for all objects, point cloud resolution was additionally compared by listing the number of points per object.

The last analyzed aspect of the point clouds acquired with SLAM is their completeness. Since the raw number of points is heavily influenced by noise and redundant measurements, other metrics need to be utilized for this purpose. Such a metric should describe a unique volume of space, containing any measured points. Two data structures commonly used in 3D-data processing have this property: a voxelgrid and an octree. Both divide a 3D space into a regular volumetric grid of boxes. For the voxelgrid, the size of a single voxel is fixed, and an octree contains a multiresolutional representation of the scene, sequentially dividing cells at each level into octants [42,43]. To assess the completeness of scanning the test environment, a number of occupied voxels and octree cells were compared between the tested approaches. Voxelgrid resolution was selected at the levels of 5, 10 and 20 cm based on the expected accuracy of the point cloud acquisition. Octree cells were counted at each of the levels from 1 to 12. An example of an octree volumetric representation is shown in Figure 7.
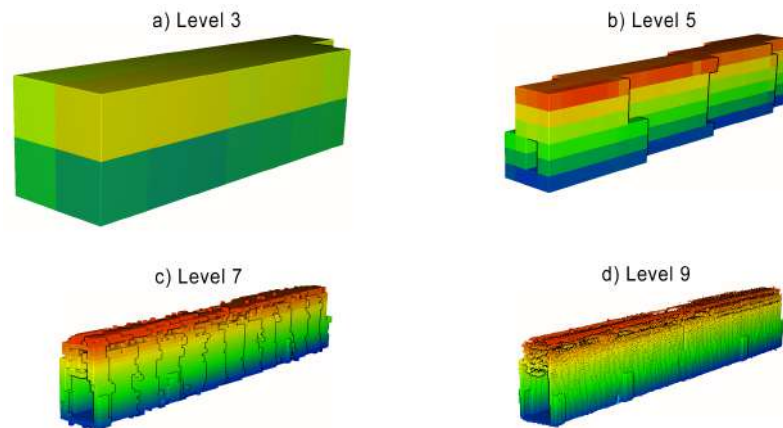
Figure 7. Example volumetric visualizations of an octree at levels: 3, 5, 7 and 9

2.5. Data Acquisition Setup

Several experimental data acquisitions were performed with a wheeled mobile robot (Figure 8, powered by a Robot Operating System (ROS, [44]). Each measurement scenario was carried out in the same corridor, approximately 40 m long, at the Wroclaw University of Science and Technology. The corridor contained several obstructions in front, above and on the sides of the robot, including recesses, doors and the wall above the lintel, creating occlusions for the lidar. Such conditions were chosen to simulate the problems with measurement coverage when scanning narrow linear objects, such as underground tunnels. In each case, the robot followed approximately the same straight path, through the middle of the corridor. Three common ways of utilizing the lidar sensor for SLAM were considered:

1. Sensor in fixed horizontal position, i.e., horizontal lidar;
2. Sensor rotating in the full range from $-90°$ to $90°$, i.e., rotating lidar;
3. Sensor rotating in the limited range from $-45°$ to $45°$, i.e., tilting lidar.

During the tests, the adjustable mapping system was responsible for keeping the stable position of the sensor in the first case and smoothly rotating it in the other cases. The system feedback for the inclination angle was monitored in real time to ensure that no sudden changes in the sensor inclination occurred and that the system worked correctly. Three raw measurement datasets were recorded as *.rosbag* files and later processed with the previously described SLAM workflow. Point sets were prepared for the analysis from consecutive

measurements, with a horizontal, rotating, and tilting lidar containing, respectively, 1.9, 5.9 and 4.1 million points.

Figure 8. Robot during the measurements.

3. Results and Discussion

All the obtained point clouds were visually inspected. The topology and main dimensions of the corridor measured in the point cloud matched the ground truth, which led to the conclusion that the results of each measurement session succeeded in creating a valid 3D representation of the analyzed area. However, further analysis showed discrepancies between the results for different methods.

3.1. Analysis of the 3D Data Density

First, the density of the point clouds was examined. For each point, a value of the density of its surroundings was calculated and represented in a 3D view with an identical color scale. The results are shown in Figures 9–11. The mean densities and corresponding standard deviations were computed and are summarized in Table 1. The histograms with kernel density estimator approximations of the analyzed density values are shown in Figure 12.

Table 1. Density statistics in points per m^2.

No	Point Cloud	Mean Surface Density	Standard Deviation
I	Horizontal lidar	8978	5249
II	Rotating lidar	10,230	5146
III	Tilting lidar	7581	3967

In the 3D visualization of the point clouds (Figure 9), it can clearly be seen that a horizontal lidar did not provide measurements of the whole area due to its limited field of view. The most noticeable difference is located just at the starting point of the test. The density of the point cloud in this case is moderate and slightly higher at the walls at the height of the lidar during the measurements. However, examination of the histogram in Figure 12 shows its great variability. The distribution has three modes, one at a density

of approximately 1000 points per m² (while the mean is roughly equal to 9000 points per m²), which indicates that there are areas with significantly lower data coverage. This phenomenon is not observed in the distributions of the datasets from a rotating lidar or a tilting lidar. These are much smoother and exhibit a left skew towards higher density values. The 3D views in Figures 10 and 11 of point clouds acquired with a rotating sensor and a tilting sensor also indicate good measurement coverage, although the former has a density higher by almost 35%, as illustrated in Table 1.
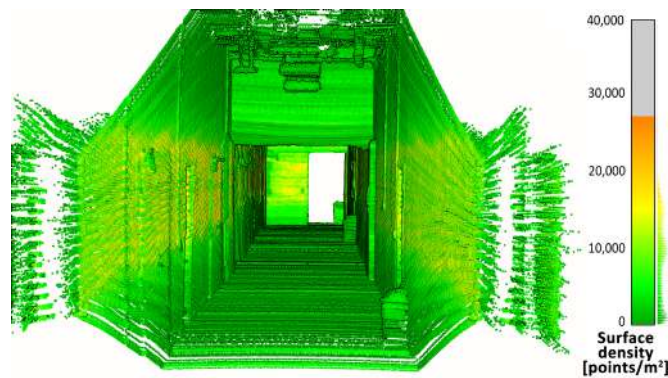
Figure 9. Point cloud density—horizontal lidar.

Figure 10. Point cloud density— rotating lidar.

Figure 11. Point cloud density—tilting lidar.
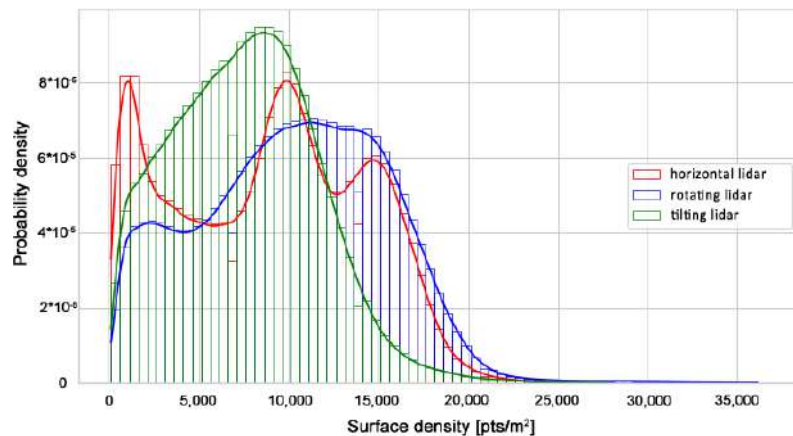
Figure 12. Distributions of surface densities per point.

To further investigate the differences in the density of the point clouds, histograms of the points' z-coordinates were plotted using absolute and relative values. They are shown in Figures 13 and 14. While Figure 13 can be used to directly compare results from different methods to answer the questions such as, "Which method will generate the most dense point cloud and with how large deviations?", Figure 14 is better suited to describe the internal properties of each method, i.e., "How well does the examined method represent different areas, such as the floor, walls and ceiling?". The former question is important in terms of selecting the measurement method for a specific use case, while the latter can be utilized to set expectations and plan measurements with an already selected method, e.g., due to hardware limitations.

The graph in Figure 13 generally indicates lower data density of the horizontal lidar measurements at every height compared to the density of the other point clouds. However, from 1.5 to 2.5 m above the ground level, i.e., at the level of the sensor mounting point, the density is similar to the other methods examined for utilizing the lidar for SLAM. Another mode of distribution is located at the ground level, representing good coverage of the floor area. This peak is not present at the higher elevation, implying weak coverage of the ceiling with the measurements. These issues are further exaggerated in Figure 14, which highlights the limitation of the lidar placed horizontally on the robot. In a narrow, high corridor, this method resulted in an unevenly dense point cloud, where areas of the floor and walls at the level of the sensor position were overrepresented in comparison to areas not well-covered, such as the ceiling. The other two methods, while differing in absolute values (Figure 13), are characterized by very similar distributions of relative point counts per height. This indicates that both methods are suitable for measurements of confined linear spaces, similar to the test corridor, in terms of providing an evenly dense and complete point cloud.

A similar conclusion can be reached when analyzing point clouds downsampled by the voxelgrids and octrees, for which the number of cells occupied for each method are shown in Figures 15 and 16, respectively. At low voxelgrid resolutions and low octree levels, all the point clouds contain a similar number of points, although the dataset acquired with a rotating sensor is always the most numerous, followed by the tilting and horizontal lidar methods. However, the higher the resolution and the octree level, the more visible the difference between each method. At the highest analyzed resolution, the difference between the rotating and tilting lidars also becomes significant: the former dataset contains 17% more 5 cm voxels and 44% more occupied octree cells at its 12th level.
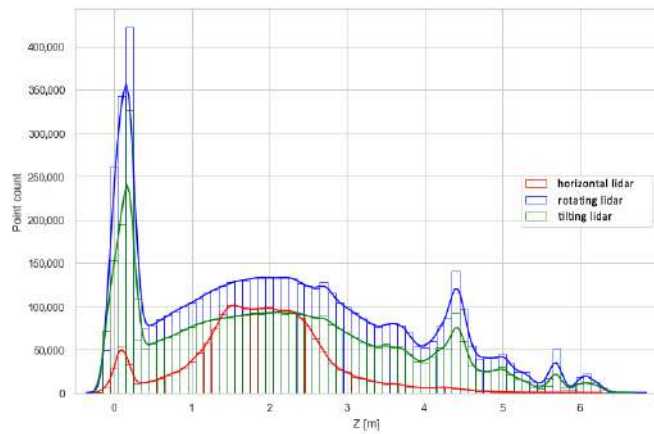
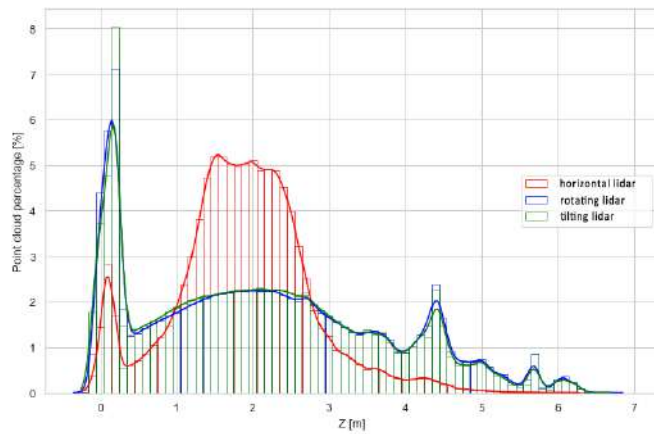**Figure 13.** Distribution of points along the *z*-axis—absolute values.

Figure 14. Distribution of points along the *z*-axis—relative values.
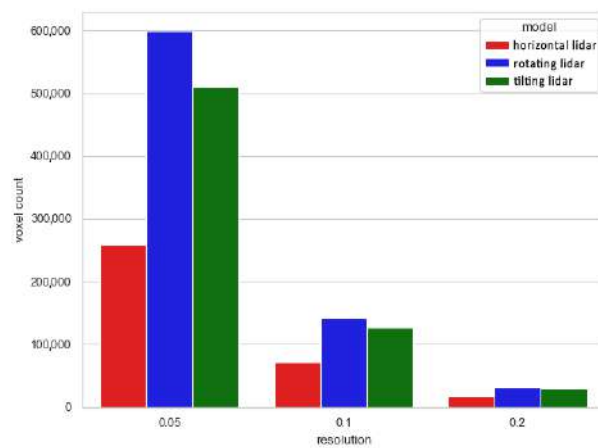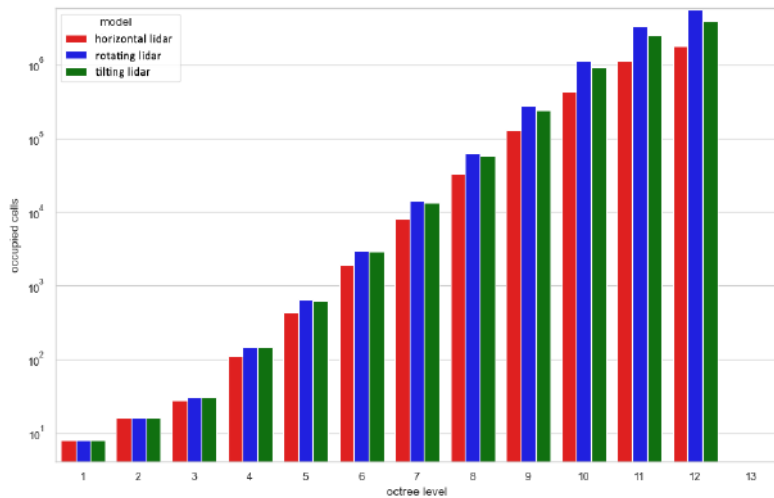

Figure 15. Number of voxels for different voxelgrid resolutions.

Figure 16. Number of occupied octree cells at each level from 1 to 12 (log scale).

3.2. Local Point Cloud Quality

In the previous subsection, the three analyzed point clouds were compared in the global context, i.e., metrics were computed and examined for the whole dataset at once, describing their overall spatial distribution, completeness and density. In contrast, this subsection focuses on the examination of a few selected objects of interest located in the test area. This analysis aims to highlight the deviations in the quality of the 3D reconstruction of these objects between different methods. Six objects chosen for the detailed selective analysis are marked with red boxes, annotated from (a) to (f), in Figure 17.
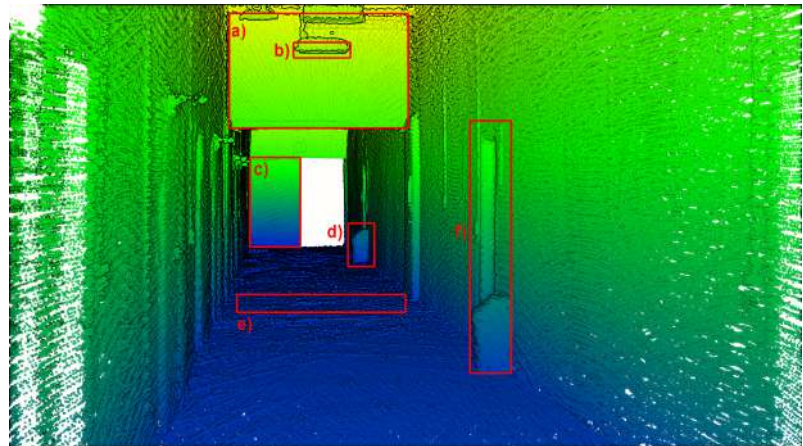
**Figure 17.** Objects selected for point cloud quality evaluation.

To begin with, the reconstruction quality of objects (a), (c), (e), and (f) was investigated, since they consist mostly of planar objects. Consecutively, they are: a vertical surface located high, a vertical surface at the same level as the measurement system, an area of the floor at the mid-section of the measurement area and a door at the side wall in the corridor. Their point clouds, colored by the calculated surface variation per point, are presented in Figures 18–20. For objects (a) and (f) a huge influence of the occlusions is visible in measurements with the horizontal sensor, resulting in parts of the objects not

being mapped. Surface variation values for the above-mentioned objects were similar for all tested methods. Horizontal lidar acquisition was characterized by the most extreme discrepancies of surface variation in most cases, with the areas of values mixed with clusters of moderate and high outlier values. Rotating lidar produced point clouds that had the most coherent surface variation in cases (a), (e), and (f), but the tilting sensor achieved the best results in the case of object (c).
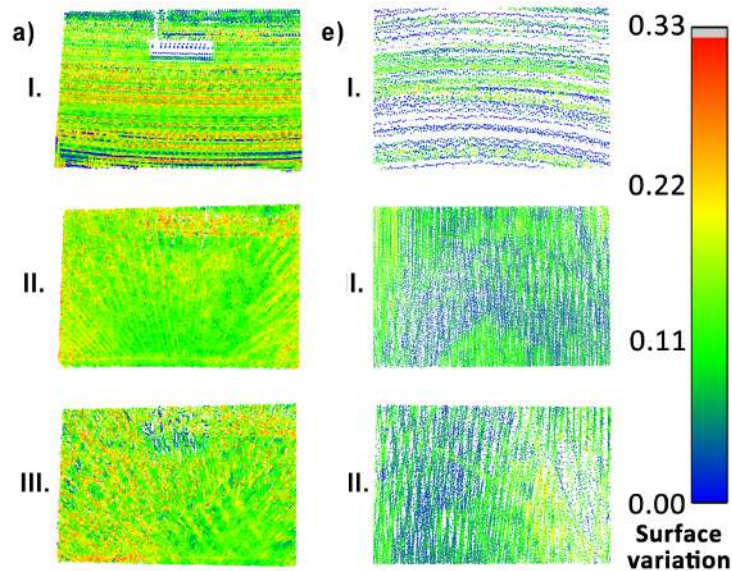
Figure 18. Point cloud surface variation comparison—objects (a) (**left**) and (e) (**right**).
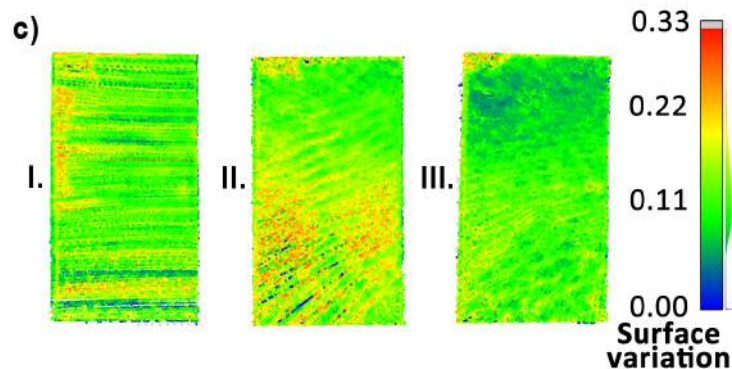
Figure 19. Point cloud surface variation comparison—object (c).

Local accuracy of the final point clouds was assessed using a least-squares plane fit for objects (a), (c) and (e). The results are listed in Table 2. The most consistent method was the rotating lidar, which achieved the maximum standard deviation of plane fit residuals of 36 mm, which is not much greater than the sensor ranging accuracy (30 mm). Although the residuals for horizontal and tilting lidar were also at an acceptable level, each method achieved a roughly 50% increase in the residuals' standard deviation compared to the rotating lidar (for objects (a) and (c)). A noteworthy observation is the high compliance of the results for object (e)—visible in all parts of the floor.
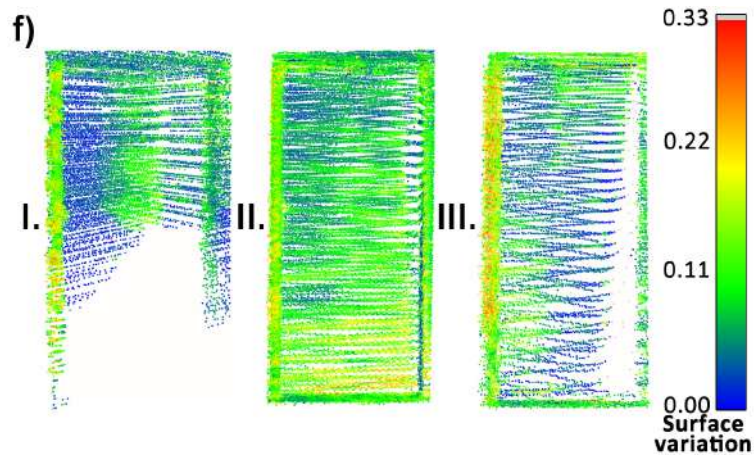
Figure 20. Point cloud surface variation comparison—object (f).

Table 2. Standard deviations of the least-squares plane fit residuals

No	Measurement Type	Plane Fit σ [mm]		
		(a)	(c)	(e)
I	Horizontal lidar	47	28	20
II	Rotating lidar	30	36	12
III	Tilting lidar	42	52	14

Objects (b) and (d), which had more complex geometries, were analyzed only in a simplified context. Their point clouds are shown in Figures 21 and 22, respectively. In the visualizations, the differences between the completeness of the 3D object reconstruction using various methods are clear: the horizontal lidar did not acquire dense and complete point clouds of those objects, while the rotating and tilting lidars successfully provided sufficient 3D data to represent a complete object. For object (b), the difference between the rotating and the tilting sensors is more noticeable than for object (d), which is caused by the unfavorable placement of object (b) for the tilting sensor in the tested configuration (i.e., tilting of the sensor did not direct its field of view much to the ceiling).

Figure 21. Point cloud resolution comparison for object (b)—isometric views.
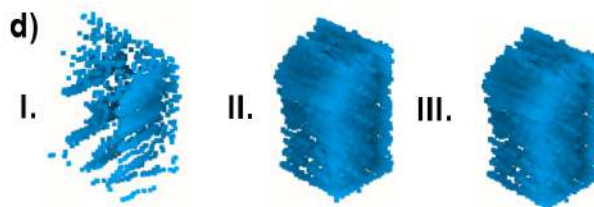

Figure 22. Point cloud resolution comparison for object (d)—isometric views.

The completeness of 3D data in the context of object reconstruction, as well as the point cloud density, can be additionally summed up with a simple metric—the point count

per object. Such an overview is presented in Table 3. Analyzing this metric, it can be seen that the rotating lidar acquired the most points in all cases. Compared to the horizontal lidar, it obtained from 40% more points up to seven times more points in the cases of the complex objects (b) and d)). Compared to the tilt sensor, the rotating lidar acquired roughly 50% more data, but, for object (b), the discrepancy increased to 150% more points in favor of the rotating sensor.

Table 3. Comparison of the number of points per object.

No	Measurement Type	Points per Object					
		(a)	(b)	(c)	(d)	(e)	(f)
I	Horizontal lidar	38,113	836	64,347	1432	6013	23,576
II	Rotating lidar	86,618	5874	90,425	6289	44,671	38,065
III	Tilting lidar	55,151	2286	70,834	4415	25,727	20,222

4. Conclusions

Different aspects of the 3D-data quality of three common hardware solutions utilizing a 3D lidar scanner for the SLAM problem were investigated. Multi-metric comparison was conducted to analyze factors such as local surface density and variation, plane reconstruction accuracy and numbers of octree cells, voxels and points per mapped object. This analysis enabled us to obtain insights into the behavior of SLAM in tunnel-like conditions, especially with respect to key aspects of inspection and mapping robotic missions in constrained, underground environments. Similarly to the method described in [13], in the future, our approach could be extended by performing multi-scale, multi-metric analysis of the presented metrics, using software components with use of the ROS operating system and the hardware setup described. This would enrich the results, especially when carrying out such a comparison for scenes of greater scale.

Increasing the complexity of the system through introduction of an actuator to rotate the spinning lidar around another axis greatly increased the data density and completeness, and did not negatively impact the point cloud local coherence. Although the sensor rotating in its full range generally obtained the best results, a tilting sensor achieved results that were not much worse and provided significant improvement over the static, horizontal placement of the lidar. Depending on the metrics analyzed, generally, the performance of the rotating lidar was from 35% to almost 50% better than that of the tilting lidar. The tilting lidar obtained a smoother data density distribution and almost 200% better completeness (based on voxelgrid and octree cell counts) than the horizontal lidar, while still maintaining comparable plane fit accuracy and mean data density. Choosing the right tool for the selected measurement site will depend on the dimensions of the structure, notably its height and width. The presence of objects causing numerous occlusions, common for underground mining environments, would also favor the selection of one of the actuated lidar mounts.

During inspection missions in underground mines, a massive amount of 3D data is collected with SLAM to be used for both navigation and 3D analysis. In the case of the latter, completeness of different object representations in the point cloud is crucial to enable machine learning algorithms to perform classification successfully and to correctly distinguish different objects of interest, which can then be processed with specialized, use-case-targeted algorithms. Therefore, given the results presented in Section 3.2, sensor solutions providing data denser than regular line scanners are desired. Although in this study an actuated line scanner proved to be effective, similar devices, e.g., solid-state lidars, should provide substantial improvement in data density. On the other hand, their limitations often include a reduced field of view, which may negatively impact coverage of the scanned area.

References

1. Alismail, H.; Baker, L.D.; Browning, B. Continuous trajectory estimation for 3D SLAM from actuated lidar. In Proceedings of the 2014 IEEE International Conference on Robotics and Automation (ICRA), Hong Kong, China, 31 May 2014–7 June 2014; pp. 6096–6101.
2. Neumann, T.; Dülberg, E.; Schiffer, S.; Ferrein, A. A Rotating Platform for Swift Acquisition of Dense 3D Point Clouds. In Proceedings of the Intelligent Robotics and Applications, Tokyo, Japan, 22–24 August 2016; Kubota, N., Kiguchi, K., Liu, H., Obo, T., Eds.; Springer International Publishing: Cham, Switzerland, 2016 ; pp. 257–268.
3. Huang, L. Review on LiDAR-based SLAM Techniques. In Proceedings of the 2021 International Conference on Signal Processing and Machine Learning (CONF-SPML), Stanford, CA, USA, 14 November 2021; pp. 163–168.
4. Xu, X.; Zhang, L.; Yang, J.; Cao, C.; Wang, W.; Ran, Y.; Tan, Z.; Luo, M. A Review of Multi-Sensor Fusion SLAM Systems Based on 3D LIDAR. *Remote Sens.* **2022**, *14*, 2835. [CrossRef]
5. Wei, W.; Shirinzadeh, B.; Nowell, R.; Ghafarian, M.; Ammar, M.M.A.; Shen, T. Enhancing Solid State LiDAR Mapping with a 2D Spinning LiDAR in Urban Scenario SLAM on Ground Vehicles. *Sensors* **2021**, *21*, 1773. [CrossRef] [PubMed]
6. Bosse, M.; Zlot, R.; Flick, P. Zebedee: Design of a spring-mounted 3-d range sensor with application to mobile mapping. *IEEE Trans. Robot.* **2012**, *28*, 1104–1119. [CrossRef]
7. Yoshida, T.; Irie, K.; Koyanagi, E.; Tomono, M. 3D laser scanner with gazing ability. In Proceedings of the 2011 IEEE International Conference on Robotics and Automation, Shanghai, China, 9–13 May 2011; pp. 3098–3103.
8. Frosi, M.; Matteucci, M. ART-SLAM: Accurate Real-Time 6DoF LiDAR SLAM. *IEEE Robot. Autom. Lett.* **2022**, *7*, 2692–2699. [CrossRef]
9. Bosse, M.; Zlot, R. Continuous 3D scan-matching with a spinning 2D laser. In Proceedings of the 2009 IEEE International Conference on Robotics and Automation, Kobe, Japan, 12–17 May 2009; pp. 4312–4319.
10. Alismail, H.; Browning, B. Automatic Calibration of Spinning Actuated Lidar Internal Parameters. *J. Field Robot.* **2015**, *32*, 723–747. [CrossRef]
11. Ravi, R.; Lin, Y.J.; Elbahnasawy, M.; Shamseldin, T.; Habib, A. Bias impact analysis and calibration of terrestrial mobile lidar system with several spinning multibeam laser scanners. *IEEE Trans. Geosci. Remote Sens.* **2018**, *56*, 5261–5275. [CrossRef]
12. Yu, Y.; Zhang, W.; Yang, F.; Li, G. Rate-Distortion Optimized Geometry Compression for Spinning LiDAR Point Cloud. *IEEE Trans. Multimed. (Early Access)* **2022**. [CrossRef]
13. Lehtola, V.V.; Kaartinen, H.; Nüchter, A.; Kaijaluoto, R.; Kukko, A.; Litkey, P.; Honkavaara, E.; Rosnell, T.; Vaaja, M.T.; Virtanen, J.P.; et al. Comparison of the Selected State-Of-The-Art 3D Indoor Scanning and Point Cloud Generation Methods. *Remote Sens.* **2017**, *9*, 796. [CrossRef]
14. Pauly, M.; Gross, M.; Kobbelt, L.P. Efficient simplification of point-sampled surfaces. In Proceedings of the IEEE Visualization, 2002, VIS 2002, Boston, MA, USA, 27 October–1 November 2002; pp. 163–170.
15. Nurunnabi, A.; Belton, D.; West, G. Diagnostic-robust statistical analysis for local surface fitting in 3D point cloud data. *ISPRS Ann. Photogramm. Remote Sens. Spat. Inf. Sci.*, **2012**, *I-3*, 269–274. [CrossRef]
16. Mohammadi, M.E.; Wood, R.L.; Wittich, C.E. Non-temporal point cloud analysis for surface damage in civil structures. *ISPRS Int. J. Geo-Inf.* **2019**, *8*, 527. [CrossRef]
17. Tan, Y.; Li, Y. UAV Photogrammetry-Based 3D Road Distress Detection. *ISPRS Int. J. Geo-Inf.* **2019**, *8*, 409. [CrossRef]
18. Huber, D.F.; Vandapel, N. Automatic three-dimensional underground mine mapping. *Int. J. Robot. Res.* **2006**, *25*, 7–17. [CrossRef]

19. Nuchter, A.; Surmann, H.; Lingemann, K.; Hertzberg, J.; Thrun, S. 6D SLAM with an application in autonomous mine mapping. In Proceedings of the IEEE International Conference on Robotics and Automation, 2004, Proceedings, ICRA '04, 2004, New Orleans, LA, USA, 26 April–1 May 2004. [CrossRef]

20. Ren, Z.; Wang, L.; Bi, L. Robust GICP-based 3D LiDAR SLAM for underground mining environment. *Sensors* **2019**, *19*, 2915. [CrossRef]

21. Ferrein, A.; Scholl, I.; Neumann, T.; Krückel, K.; Schiffer, S. A System for Continuous Underground Site Mapping and Exploration. In *Unmanned Robotic Systems and Applications*; Reyhanoglu, M., Cubber, G.D., Eds.; IntechOpen: Rijeka, Croatia, 2020; Chapter 4.

22. Zlot, R.; Bosse, M. Efficient large-scale three-dimensional mobile mapping for underground mines. *J. Field Robot.* **2014**, *31*, 758–779. [CrossRef]

23. Fahle, L.; Holley, E.A.; Walton, G.; Petruska, A.J.; Brune, J.F. Analysis of SLAM-Based Lidar Data Quality Metrics for Geotechnical Underground Monitoring. *Mining Metall. Explor.* **2022**, *39*, 1939–1960. [CrossRef]

24. Li, M.; Zhu, H.; You, S.; Wang, L.; Tang, C. Efficient Laser-Based 3D SLAM for Coal Mine Rescue Robots. *IEEE Access* **2019**, *7*, 14124–14138. [CrossRef]

25. Ellmann, A.; Kütimets, K.; Varbla, S.; Väli, E.; Kanter, S. Advancements in underground mine surveys by using SLAM-enabled handheld laser scanners. *Surv. Rev.* **2021**, *54*, 363–374. [CrossRef]

26. Ebadi, K.; Bernreiter, L.; Biggie, H.; Catt, G.; Chang, Y.; Chatterjee, A.; Denniston, C.E.; Deschênes, S.P.; Harlow, K.; Khattak, S.; et al. Present and future of slam in extreme underground environments. *arXiv* **2022**, arXiv:2208.01787.

27. Zhang, J.; Singh, S. LOAM: Lidar Odometry and Mapping in Real-time. In Proceedings of the Robotics: Science and Systems, Berkeley, CA, USA, 12–16 July 2014; Volume 2; pp. 1–9.

28. Kim, G.; Kim, A. Scan Context: Egocentric Spatial Descriptor for Place Recognition within 3D Point Cloud Map. In Proceedings of the Proceedings of the IEEE/RSJ International Conference on Intelligent Robots and Systems, Madrid, Spain, 1–5 October 2018.

29. Kim, G.; Choi, S.; Kim, A. Scan context++: Structural place recognition robust to rotation and lateral variations in urban environments. *IEEE Trans. Robot.* **2021**, *38*, 1856–1874. [CrossRef]

30. Lupton, T.; Sukkarieh, S. Visual-Inertial-Aided Navigation for High-Dynamic Motion in Built Environments Without Initial Conditions. *IEEE Trans. Robot.* **2012**, *28*, 61–76. [CrossRef]

31. Carlone, L.; Kira, Z.; Beall, C.; Indelman, V.; Dellaert, F. Eliminating conditionally independent sets in factor graphs: A unifying perspective based on smart factors. In Proceedings of the 2014 IEEE International Conference on Robotics and Automation (ICRA), Hong Kong, China, 31 May–7 June 2014; pp. 4290–4297.

32. Forster, C.; Carlone, L.; Dellaert, F.; Scaramuzza, D. IMU Preintegration on Manifold for Efficient Visual-Inertial Maximum-a-Posteriori Estimation; In: Proceedings of the Robotics: Science and Systems Conference, Rome, Italy, 13–17 July 2015.

33. Foote, T. tf: The transform library. In Proceedings of the 2013 IEEE Conference on Technologies for Practical Robot Applications (TePRA), Woburn, MA, USA, 22–23 April 2013; pp. 1–6.

34. Kim, G.; Kim, A. Remove, then Revert: Static Point cloud Map Construction using Multiresolution Range Images. In Proceedings of the 2020 IEEE/RSJ International Conference on Intelligent Robots and Systems (IROS), Las Vegas, NV, USA, 24 October 2020–24 January 2021; pp. 10758–10765.

35. Olson, E.; Kaess, M. Evaluating the performance of map optimization algorithms. In Proceedings of the RSS Workshop on Good Experimental Methodology in Robotics, Seattle, WA, USA, 28 June 2009; Volume 15.

36. Kümmerle, R.; Steder, B.; Dornhege, C.; Ruhnke, M.; Grisetti, G.; Stachniss, C.; Kleiner, A. On measuring the accuracy of SLAM algorithms. *Auton. Robot.* **2009**, *27*, 387–407. [CrossRef]

37. He, Y.; Hu, Z.; Wu, K.; Wang, R. A Novel Method for Density Analysis of Repaired Point Cloud with Holes Based on Image Data. *Remote Sens.* **2021**, *13*, 3417. [CrossRef]

38. Demantké, J.; Mallet, C.; David, N.; Vallet, B. Dimensionality based scale selection in 3D lidar point clouds. *Int. Arch. Photogramm. Remote Sens. Spatial Inf. Sci.* **2011**, *XXXVIII-5/W12*, 97–102. [CrossRef]

39. Hackel, T.; Wegner, J.D.; Schindler, K. Contour detection in unstructured 3D point clouds. In Proceedings of the IEEE Conference on Computer Vision and Pattern Recognition, Las Vegas, NV, USA, 27–30 June 2016; pp. 1610–1618.

40. Blomley, R.; Weinmann, M.; Leitloff, J.; Jutzi, B. Shape distribution features for point cloud analysis-a geometric histogram approach on multiple scales. *ISPRS Ann. Photogramm. Remote Sens. Spat. Inf. Sci.* **2014**, *2*, 9. [CrossRef]

41. Huang, C.; Tseng, Y.H. Plane fitting methods of LiDAR point cloud. In Proceedings of the 29th Asian Conference on Remote Sensing 2008, ACRS 2008, Colombo, Sri Lanka, 10–14 November 2008; pp. 1925–1930.

42. Meagher, D. Geometric modeling using octree encoding. *Comput. Graph. Image Process.* **1982**, *19*, 129–147. [CrossRef]

43. Xu, Y.; Tong, X.; Stilla, U. Voxel-based representation of 3D point clouds: Methods, applications, and its potential use in the construction industry. *Autom. Constr.* **2021**, *126*, 103675. [CrossRef]

44. Quigley, M.; Conley, K.; Gerkey, B.; Faust, J.; Foote, T.; Leibs, J.; Berger, E.; Wheeler, R.; Ng, A.Y. ROS: An open-source Robot Operating System. In Proceedings of the ICRA Workshop on Open Source Software, Kobe, Japan, 12–17 May 2009; Volume 3, p. 5.

Publication 4: Comparison of Low-Cost Handheld LiDAR-Based SLAM Systems for Mapping Underground Tunnels

COMPARISON OF LOW-COST HANDHELD LIDAR-BASED SLAM SYSTEMS FOR MAPPING UNDERGROUND TUNNELS

P. Trybała [1,2], D. Kasza [2], J. Wajs [2], F. Remondino [1]

[1] 3D Optical Metrology (3DOM) unit, Bruno Kessler Foundation (FBK), Trento, Italy
Web: http://3dom.fbk.eu – Email: <ptrybala><remondino>@fbk.eu
[2] Department of Geodesy and Geoinformatics, Wrocław University of Science and Technology (WUST), Wrocław, Poland
Web: https://wggg.pwr.edu.pl/en/ – Email: <damian.kasza><jaroslaw.wajs>@pwr.edu.pl

Commission II

KEY WORDS: LiDAR SLAM, Low-Cost, Mobile Mapping, Open-Source, Underground Mining, Evaluation, Voxel

ABSTRACT:

The use of mobile mapping technologies (MMT) has become increasingly popular across various applications such as forestry, cultural heritage, mining, and civil engineering. While Simultaneous Localization and Mapping (SLAM) algorithms have greatly improved in recent years with regards to accuracy, robustness, and cooperativity, it is important to understand the limitations and strengths of each metrological measurement method to ensure the provision of 3D data of appropriate quality for the selected application. In this study, we perform a comparative analysis of three LiDAR-based handheld mobile mapping systems with survey-grade reference point clouds in a challenging test area of a partially collapsed underground tunnel. We investigate various aspects of 3D data quality, including accuracy and completeness, and present an improved method for 3D data completeness assessment aimed at evaluating SLAM-derived point clouds. The results demonstrate unique and diverse strengths and shortcomings of the tested mapping systems, which provide valuable guidelines for selecting an appropriate system for subterranean applications.

1. INTRODUCTION

Mobile mapping systems (Nocerino et al., 2019; Otero et al., 2020; Elhashash et al., 2022) are steadily growing in popularity for the 3D reconstruction of indoor spaces. They are becoming more and more available for end-users thanks to their simplicity in use and affordability. They can be a cost- and time-effective alternative for traditional methods such as photogrammetry or Terrestrial Laser Scanning (TLS) in particular for large areas where mobile acquisitions would speed-up the surveying operations. Handheld, backpack and robotic-based vision-(Menna et al., 2022; Perfetti and Fassi, 2022), LIDAR- (Liang et al., 2014; Xie et al., 2022) or hybrid- (Trybała et al., 2022) systems using SLAM (Simultaneous Localization and Mapping) are becoming widely applied in multiple fields, such as cultural heritage documentation (Di Stefano et al., 2021), forestry (Pierzchała et al., 2018) and mining (Jones, 2020; Ebadi et al., 2022). The application of mobile mapping technologies is quite complicated in underground, unstructured environments, since algorithms employed for motion estimation of the sensor have to deal with challenges such as low or uneven lighting, dust, high humidity, rough surfaces and overall lack of distinct visual and geometric features. Thus, a good understanding of the mapping system capabilities in terms of reliability and accuracy is needed for ensuring the compliance with the requirements of specific application. Moreover, in confined, underground spaces, multiple occlusions and a limited field of view of the sensors create other challenges for 3D data acquisition, leading to occurrences of holes and gaps in the resulting point clouds (Trybała et al., 2023).

1.1 Paper's aims

The goal of the work is to assess the quality (geometry compliance with respect to ground truth data) and completeness of 3D point clouds acquired with different handheld LiDAR-based SLAM solutions in unstructured underground conditions. A Livox- and Velodyne-based systems are benchmarked against

a GeoSLAM ZEB Horizon and a TLS reference point cloud. For our analyses, different SLAM approaches are considered whereas a voxel-based point cloud comparison methodology is proposed, together with an improved method for evaluating the completeness of the 3D reconstruction.

The work is part of the EIT-RM project VOT3D which aims to support the raw material sector by introducing modern methods and innovative solutions for the optimization of underground ventilation in mining scenarios based on 3D data. Utilization of mobile mapping technologies in the subterranean conditions, despite constituting a challenge, is an important part of enabling realistic simulations of ventilation system operation in an industrial underground mine. Consequently, understanding limitations and achievable quality of 3D data survey results in such environment is crucial for ensuring the reliability of entire optimization process.

2. MOBILE MAPPING SOLUTIONS IN UNDERGROUND SCENARIOS

2.1 Related works

The issue of assessing accuracy of 3D point clouds for ensuring their suitability for the further analysis has been raised multiple times and for various use cases. Farella (2016) examined a commercial SLAM solution accuracy in the narrow underground corridors using targets measured with a total station. Toschi et al. (2015) performed an in-depth statistical analysis of accuracy of a mobile mapping system, mounted on a car, utilizing ground truth data obtained with a TLS and photogrammetry. Nocerino et al. (2017) similarly examined selected commercial SLAM solutions (a backpack and a handheld scanner) through point cloud comparison with a TLS ground truth data. The tests were performed in indoor and outdoor urban conditions. Lehtola et al. (2017) introduced a multi-scale error metrics for assessing the accuracy of point cloud data and performed the evaluation of multiple SLAM systems in the indoor setting. The works underlines the need of multi-objective 3D data quality

examination for SLAM besides carrying out a raw comparison of geometrical compliance with the reference data. Raval et al. (2019) investigated the ZebRevo SLAM-based mobile mapping system in an underground coal environment to evaluate its potential and identify related challenge. Kim and Choi (2021) proposed an autonomous driving robot to perform 3D mapping of mining tunnels based on two 2D LiDARs placed horizontally and vertically.

2.2 Study area

The test measurements were carried out in the Gontowa adit[1], located in the Owl Mountains in Poland (Figure 1). The tunnels had been carved in sandstone during the World War II by Germans in the scope of the Riese project. Due to several collapses, the site is characterized by irregular geometry, thus being a perfect site to test the performances of mobile mapping units in a complex, uneven, underground scenario.
For the assessment of the SLAM systems (Section 2.3), a part of the surveyed tunnels with a loop shape is considered (ca 120 m in total). This allowed to better check the results of LiDAR odometry, testing the ability of SLAM algorithms to detect loop closures and appropriately adjust the trajectory with a pose graph optimization.
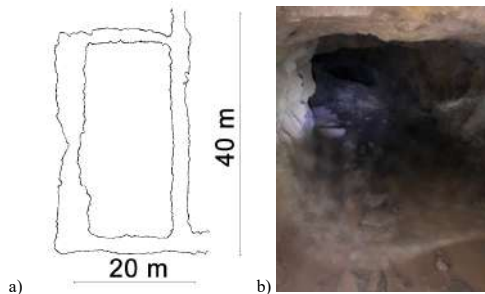

Figure 1: Sketch (a) and a photo (b) of the surveyed tunnel.

2.3 Assessed LiDAR-based mobile mapping systems

Three portable mobile mapping solutions (Table 1) were used during a measurement session in the tunnels:
- a GeoSLAM ZEB Horizon;
- a Livox Horizon LiDAR, coupled with an internal inertial measurement unit (IMU) manually carried during the surveying operations;
- a Velodyne VLP-16 LIDAR sensor coupled with a Dynamixel servomotor.

The Velodyne LiDAR was assembled using open-source libraries and 3D printing rapid prototyping to realized handheld SLAM system (Figure 2a). It was designed for low-cost, fast mapping of unstructured underground environments. Thanks to integration with Robot Operating System (ROS, Quigley et al., 2009), our system is capable of utilizing different SLAM frameworks for LiDAR data, integrating various sources of LiDAR odometry, point cloud ego-motion compensation caused by the LiDAR and actuator rotating motions, as well as online and offline loop closure detection and pose graph optimization. Standardized setup in the ROS environment, using state-of-the-art libraries for point cloud processing and SLAM, such as PCL (Rusu and Cousins, 2011) and GTSAM (Dellaert et al., 2022), allows easy further extensions and improvements or streamlined implementation on a different machine. The setup does not

require IMU unit for mapping, which allows to perform mapping tasks even in high-vibration, industrial areas. However, it comes at a cost of expected slight degradation in mapping quality, comparing to LiDAR-inertial solutions.
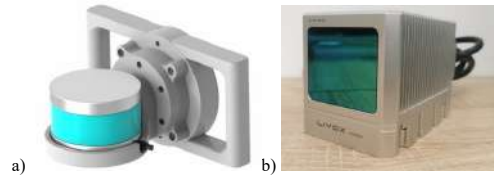

Figure 2: Assessed low-cost LiDAR SLAM systems: in-house 3D design of an actuated Velodyne (a) and a Livox Horizon with an integrated IMU (b).

Sensor	Sensor parameter		
	Measurement speed [pts/s]	Maximum range [m]	Ranging accuracy [mm]
Riegl VZ-400i	500,000	800	5 (@100 m)
GeoSLAM Zeb Horizon	300,000	100	30 (@100 m)
Velodyne VLP-16	300,000	100	30 (@100 m)
Livox Horizon	240,000	90	20 (@25 m)

Table 1: Specification of sensors involved in the study.

2.4 Ground truth data

A dense reference point cloud was acquired with a Riegl VZ-400i TLS, a survey-grade instrument characterized by the ranging precision of 3 mm and accuracy of 5 mm at 100 m distance. First, a field reconnaissance was conducted. The condition and accessibility of the site were assessed and a measurement plan has been prepared. Numerous collapses located mainly at the intersections of the corridors and tight constrictions made the measurements with a heavy TLS significantly more arduous and demanding. Finally, the entire 3D surveying was performed from 60 stations, with the average distance between them being approximately 5 meters. Data acquisition parameters were selected to obtain a scanning grid with a resolution of 9 mm at a distance of 10 m. More than 931 mil points were collected in the entire underground area.
The registration of the 60 individual scans into a single coherent poit cloud was performed with the proprietary RiSCAN PRO software. The employed scans adjustment method is based on plane-to-plane matching of patches extracted from the point clouds, utilizing a solver with a robust kernel. To create the final registered point cloud (Figure 3), some 171,197 patches were used and the final standard deviation of the adjustment was 2.6 mm. The histogram of residuals, indicating their well-balanced, normal distribution, is shown in Figure 4.

Figure 3: Registered reference point cloud of the entire underground complex.
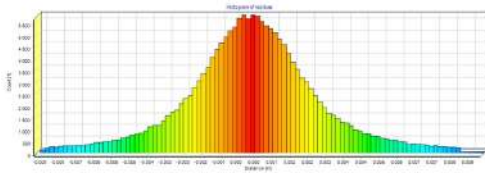
---

[1] from Latin aditus, entrance

Figure 4: Residual distribution of plane-to-plane TLS point clouds registration.

Finally, cropping to the investigated area of interest and subsampling the point cloud to the maximum resolution of 1 mm, the reference dataset size was reduced to some 11 mil points.

2.5 3D data quality evaluation

The assessment of the 3D reconstruction quality can be performed with a focus on particular aspects of the generated 3D data properties. The most important ones are accuracy (i.e., compliance with the ground truth geometry), completeness (a measure of the area of interest coverage) and precision (point dispersion around the averaged location of a mapped object in a 3D space). Nevertheless, abovementioned qualities are still only a simplification of the broad topic and more metrics have been proposed and analyzed in other works (Lehtola et al., 2017; Trybała et al., 2023).

For analyzing datasets acquired both with photogrammetric (Knapitsch et al., 2017) and laser scanning (Schops et al., 2017) methods, common multi-scale metrics of accuracy and completeness are often used (Nocerino et al., 2017). They derive from the classical metrics of precision and recall in classification problems. The ratio of evaluated points aligned to a ground truth model is calculated at different distance thresholds for determining the precision curve shape. On the contrary, completeness is estimated by thresholding the closest distances calculated from reference data to the analyzed point cloud. Different approaches of estimating the precision metric can be found in the literature, with the calculation of the roughness parameter (Santos and Júlio, 2013) and checking the standard deviation of the least-square fit on the planar surfaces (Chen et al., 2018) being the prevailing options. In this paper, due to lack or regular shapes in the underground tunnel, local accuracy, i.e., quality of the 3D data alignment to the reference data calculated for a small subset of points, will be considered as an approximation of precision evaluation.

However, while being appropriate for tasks of small scenes or object 3D reconstruction, the evaluation of the completeness of large-scale indoor mapping can be heavily influenced by the drift error of the SLAM algorithm. The illustration of this problem is shown in Figure 5: although the point cloud acquired with SLAM is topologically correct, the drift errors result in the global shift of the location of the tunnel on the left side of the figure. While the inclusion of this drift error in assessing the point cloud global accuracy is desired, for estimating completeness it can falsely negatively skew the results. A simple co-registration of the evaluated point cloud with the ground truth data, even using a 9-parameter transform, would not solve the issue, since the rotational and translational errors of the SLAM algorithm cannot be expected to accumulate uniformly with the traveled distance, especially in variable and challenging underground conditions. A method of non-rigid and non-uniform point cloud alignment is needed to obtain an accurate fit to the reference data and calculate an accurate completeness metric (Figure 5b).

To tackle this issue, we propose a sequential, voxel-based adjustment method. Its overview is presented in Figure 6.
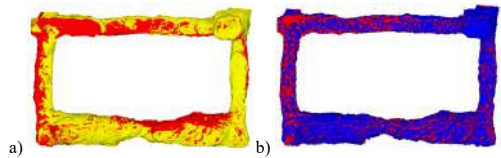

Figure 5: Top view of the point clouds depicting the influence of the global drift on their relative alignment: ground truth (red) overlapped with the original Velodyne SLAM data (yellow) (a) and with its drift-compensated version (blue) (b).

First, we downsample the point clouds and create a common voxel grid for all of the evaluated datasets and the ground truth. We then create voxel models, checking the occupancy of each cell with a set minimum threshold of points to minimize the influence of noisy data. Afterward, we start an iterative process of aligning points inside of each voxel to the ground truth with the iterative closest point algorithm (ICP, Rusinkiewicz & Levoy, 2001), estimating the rotation and translation parameters. We select the initial voxel, e.g., the one populated with the highest number of points, and continue aligning subsequent neighboring voxels until all are transformed. We start the alignments with the initial guesses of the transform based on already calculated transforms of the neighboring voxels, which in turn reduces the drift error of the SLAM algorithm. Finally, all points from the original point cloud are transformed according to the transformation of their parent voxel.
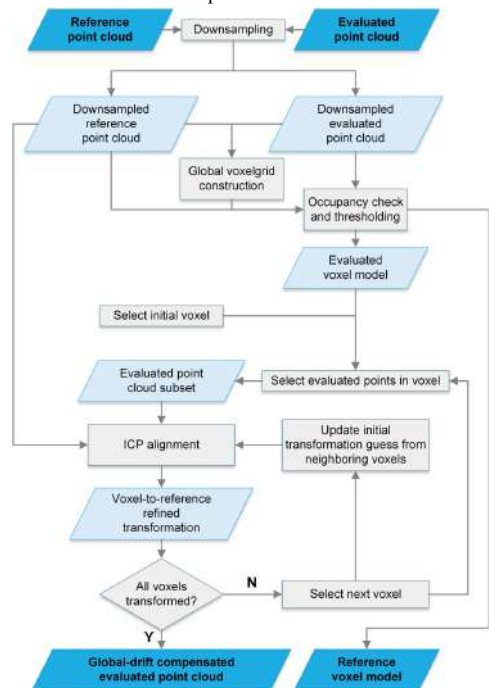

Figure 6: Flowchart of the proposed method for compensating SLAM drift errors and improve the 3D data completeness evaluation.

In our method, we divide the analyzed point clouds regularly in the space domain, i.e., in a voxel grid. Alternatively, a temporal division approach can be used, as presented by Al-Durgham et al. (2021). Nevertheless, this would require the evaluated point clouds to be timestamped or to have the estimated sensor

trajectory with poses corresponding to raw point clouds. This cannot be always achieved, especially with commercial SLAM solutions.

Our approach allows to adjust a whole, single point cloud for the evaluation, without any information on the sensor trajectory, and without artificially reducing the local noise of the point cloud for obtaining accurate completeness and local accuracy estimates.

However, it must be stressed that the presented method does not aim to reduce the SLAM algorithm drift for achieving better mapping results since it utilizes the usually unavailable ground truth data. The presented workflow aims only to improve the process of evaluating the quality of the results obtained with different mobile mapping methods on a test field with reliable reference data.

2.6 Selected metrics

In this case study, results of mapping the underground site with 3 mobile mapping systems are divided into 3 aspects:

  a) global accuracy,
  b) local accuracy,
  c) completeness.

For assessing global and local accuracy, evaluated point clouds registered with a rigid ICP transform to the reference data were used. Global accuracy has been analyzed both using traditional approach (i.e., as percentage of cloud-to-reference unsigned distances below different thresholds) and calculating cloud-to-reference signed distances with M3C2 method available in Cloud Compare software (Lague et al., 2013). Local accuracy has been analyzed through calculating standard deviations of point cloud subset fit in 2 selected areas and 2 cross-sections of the tunnel shown in Figure 7. Completeness metrics has been obtained with point clouds adjusted according to the previously described algorithm, summarized in Figure 6.
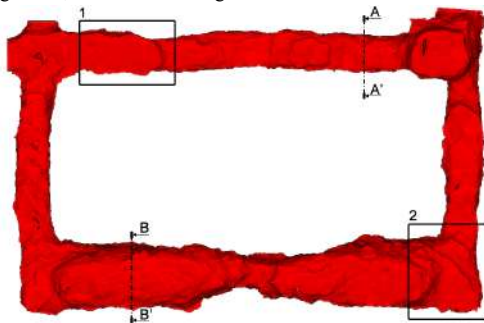

Figure 7: The ground truth point cloud with highlighted regions-of-interest (ROIs) and cross-sections chosen for the selective local accuracy analysis.

3. RESULTS

The SC-LiDAR-SLAM open-source framework (Kim et al., 2022) was adopted for processing the collected LiDAR data. A-LOAM was used as a source of LiDAR odometry for Velodyne and FAST-LIO was selected for Livox. Processing pipelines for both sensors utilized Scan Context++ for loop closure detection and GTSAM for constructing the pose graph. The data collected with the ZEB Horizon were processed with the GeoSLAM proprietary tool.

The perspective views of the resulting point clouds are presented in Figure 8 whereas Figure 9 shows closeup views in one of the more challenging areas, where a passage through the tunnel is

steep and narrow due to the rockfall. From those figures onwards, the uniform color coding is kept consistent for all point cloud data, unless indicated otherwise: TLS data is represented in red, GeoSLAM in orange, Velodyne in blue and Livox in green.
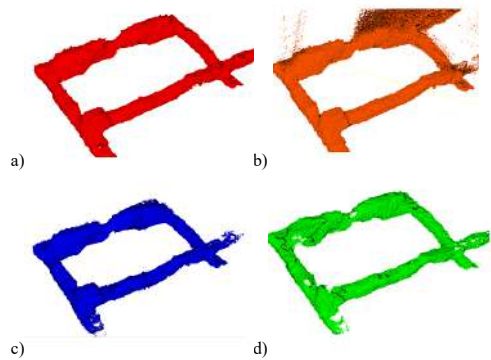

Figure 8: Registered point clouds of the study area: TLS (a), GeoSLAM (b), actuated Velodyne (c) and Livox (d).
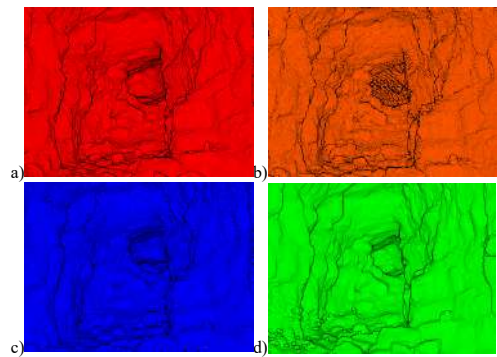

Figure 9: Close view of the collected point clouds of an area with a partly collapsed passage: TLS (a), GeoSLAM (b), actuated Velodyne (c) and Livox (d).

A qualitative investigation of those visualizations reveals some issues with the performance of different tested mapping systems. First, the point cloud from GeoSLAM contains heavy noise, concentrated around the area with the narrow passage of the tunnel. Livox point cloud seems to show the least surface deviation. However, sparse, more apparent erroneous point groups are also visible. The limited field of view of the sensor also caused the presence of visible gaps in the mapping coverage of the tight tunnel spaces. On the other hand, the 3D reconstruction from the actuated Velodyne measurements manifests visibly higher, although more uniformly distributed noise on the surfaces.

In the next step, a quantitative assessment based on metrics selected in Section 2.6 has been performed. First, the local geometry of the mapped areas was examined on the basis of 2 cross-sections and 2 ROIs. Point cloud subsets were registered to the corresponding TLS subset with an ICP algorithm again. This step refines their alignment to the reference data, enabling analyzing the local accuracy of results acquired with tested mapping systems. The resulting aligned point cloud cross-sections and ROIs are shown in Figures 10 and 11, respectively. The standard deviations of each fit are reported in Table 2.
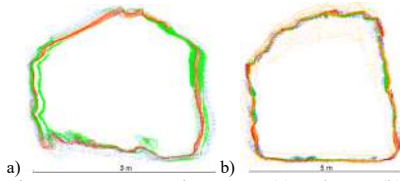
Figure 10: Cross-sections A-A' (a) and B-B' (b) of point clouds acquired with: TLS (red), GeoSLAM (orange), actuated Velodyne (blue) and Livox (green).
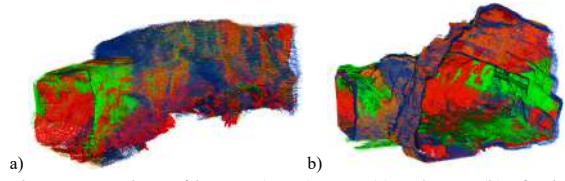

Figure 11: Regions-of-interest (ROIs) No. 1 (a) and No. 2 (b) of point clouds acquired with: TLS (red), GeoSLAM (orange), actuated Velodyne (blue) and Livox (green).
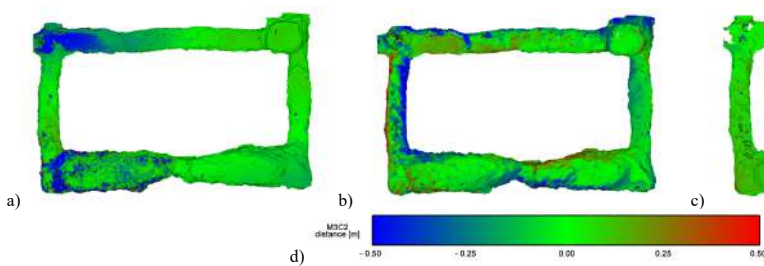

Figure 12: M3C2 signed distances between the ground truth point cloud and GeoSLAM (a), actuated Velodyne (b) and Livox (c) data. Common coloring scheme according to the distance values applied to all point clouds (d).

Sensor	M3C2 distance σ [mm]	Cross-section ICP fit σ [mm]		ROI ICP fit σ [mm]	
		A-A'	B-B'	No.1	No.2
GeoSLAM	364	26	94	49	35
Actuated Velodyne	281	62	59	86	57
Livox Horizon	232	53	24	26	114

Table 2: Standard deviations of comparisons to the ground truth using the entire evaluated datasets (M3C2) and only selected cross-sections and ROIs.

Most notably, a double-wall and double-floor errors is visible for Livox point cloud slice A-A' and ROI No. 2. GeoSLAM exhibits a significantly higher noise level in slice B-B'. Velodyne point cloud fit errors are consistent at a medium level, ranging from 57 to 86 mm. Results from fitting both Livox and GeoSLAM 3D data display higher variability, reaching error extremes from 24 mm to around 100 mm.

Global accuracy was investigated thereafter. Signed distances between each evaluated point cloud were computed and visualized with a common color scheme in Figure 12 to pinpoint the areas of the degradation of the mapping quality due to the drift of the SLAM algorithm. 3D data generated with all mobile mapping systems contain outlier groups in different areas. For the GeoSLAM, they are concentrated in tunnel parts on the left side of Figure 12a, while for the Livox highest error values were estimated for the area on the right side of the Figure 12c. Velodyne point cloud, presented in Figure 12b, differs from the ground truth mostly in the lower and left part of the figures. All of the examined SLAM variations exceeded the standard deviation of the signed distances to the reference data of 200 mm (Table 2). However, this not necessarily indicate the bad quality of the mapping results, but only the expected presence of the drift error since no global positioning source was available in the underground site. This results in numerous groups of outlying points (in terms of global accuracy), which on purpose were not manually removed or corrected. This is further proved by degradation of global accuracy concentrated in the in the lower

left corner of the figure: the area furthest from the mapping starting point (and thus, the loop closure location).

Another aspect of 3D data quality assessment, the completeness, was studied with drift-compensated versions of all evaluated point clouds. However, to showcase the difference between our proposed approach and the original, completeness curves were approximated and plotted with both methods (Figure 13). Noticeable difference can be seen not only in the absolute values, but also in the shape of the curves, indicating that our method provides estimates of the completeness metric in a more reliable and accurate manner.
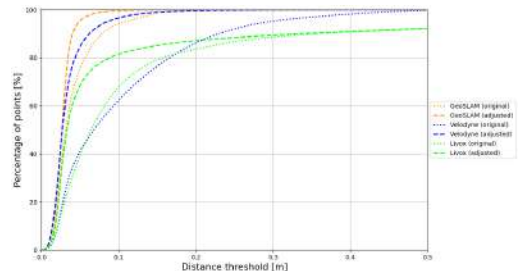
Figure 13: Comparison of completeness curves calculated for the analyzed datasets with the original method and our approach.

Furthermore, accuracy and completeness curves, calculated as described in Section 2.6, are presented in Figure 14. The plot summarized the weaknesses of each tested method. Completeness of Velodyne and GeoSLAM mapping results quickly reaches values close to 100%. The accuracy of GeoSLAM, matching the Livox accuracy for low distance thresholds, plateaus at around 95% due to the presence of highly erroneous points.

On the other hand, Velodyne's accuracy rises considerably slower, but consistently, to almost 100% at the 0.5 m threshold. 3D data generated with Livox achieves superior accuracy of all the tested methods, but due to narrow field of view, its results show an impaired completeness of the measurements even at high distance thresholds.

Figure 14: Resulting estimates of accuracy and adjusted completeness for different distance thresholds for the evaluated SLAM point clouds.
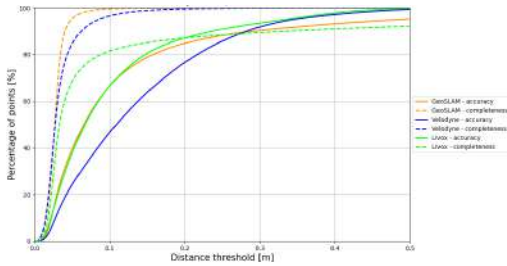
To easily visualize the spatial distribution of areas with lower completeness and local accuracy, a simple voxel-based comparison method was developed. Using the common voxel grid, prepared during the drift-compensation phase of data processing, we compare the occupancy of voxels in each examined model with the reference voxel model. Thus, true positive (*TP*) voxel is occupied both in the examined and the ground truth data; false negative (*FN*) voxel is occupied only in the reference model, and a false positive (*FP*) voxel corresponds to a voxel occupied only in the evaluated dataset. Their percentages have been calculated for 2 voxel sizes (0.2 m and 0.5 m) and listed in Table 3 and the corresponding visualizations are included in Figure 15. Confirming the findings of previous analyzes, the number of incorrectly mapped voxels for GeoSLAM and the number of unmapped voxels for Livox stay high even at lower resolutions, while results from Velodyne scanning generally improve in all aspects.

System	20 cm voxel count [%]			50 cm voxel count [%]		
	TP	*FN*	*FP*	*TP*	*FN*	*FP*
GeoSLAM	61	3	36	82	1	17
Actuated Velodyne	57	25	18	88	5	7
Livox Horizon	49	30	21	74	18	8

Table 3: Ratios of voxels classified according to their occupancy compared to the reference voxel model.

4. CONCLUSIONS

This study presented a comprehensive assessment of the quality of results obtained from different 3D LiDAR-based mobile mapping techniques in an underground environment. We presented 2 in-house built systems, based on popular low-cost 3D LiDAR sensors, manufactured by Velodyne and Livox, and utilizing open-source SLAM frameworks for generating co-registered point clouds. We compared such sensors to the GeoSLAM Zeb Horizon commercial solution and benchmark all systems against reference data collected with survey-grade TLS. Analyzing different aspects of 3D data quality provides insights into the unique strengths and limitations of each examined approach, which need to be considered when selecting the appropriate method for a particular application of 3D reconstruction of complex underground scenes.

Based on our findings and the presented comparison methodology, an optimal mobile mapping system can be chosen according to the desired focus on the particular 3D data quality: accuracy and completeness. A crucial aspect is the determination of their critical values for selected metrics representing them. For example, for the VOT3D project purposes and ventilation simulations at a large scale, systems maximizing the completeness of the measurements, i.e., GeoSLAM and our actuated Velodyne system, would be the most suitable options. While the former has the potential to achieve greater accuracy, the latter might provide more robustness in the industrial mine environment due to not utilizing inertial data. On the other hand, applications requiring high accuracy and providing more room for maneuvering the sensor could benefit from employing a Livox-based mobile mapping system.

The article reported also a dedicated technique for improving the assessment of 3D reconstruction completeness through applying an iterative, voxelized ICP alignment refinement. The proposed method aims to provide a more accurate assessment of real coverage of the 3D scene, obtained with SLAM. We reduced the influence of one of its inherent error sources, the drift, on the resulting completeness estimate. The approach is designed to be versatile due to the fact of requiring only the 3D point cloud data (reference and assessed) as the input.
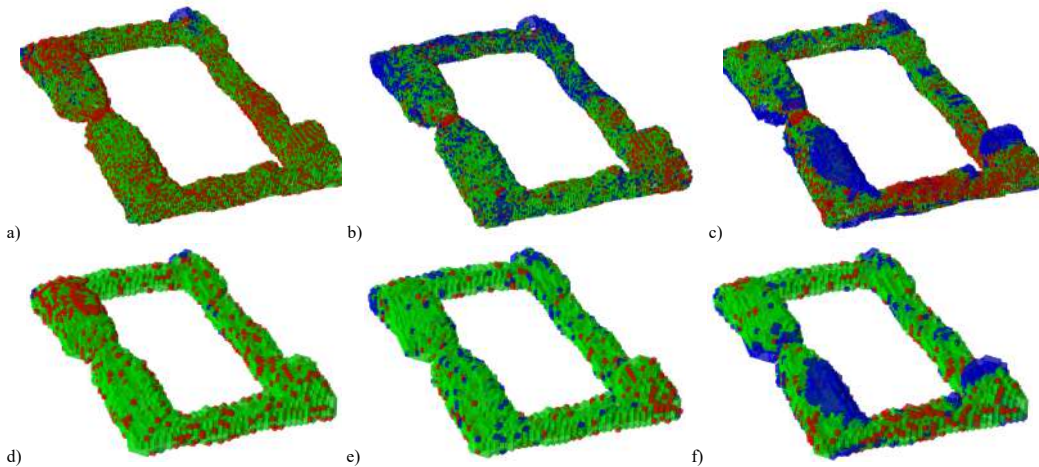

Figure 15: 3D visualizations of the voxel-based point cloud comparison with the reference data: GeoSLAM (a, d), actuated Velodyne (b, e) and Livox (c, f). Voxels compliant with the ground truth data are shown in green, non-mapped areas in blue and incorrect voxels in red. Figures a-c rendered for 0.2 m voxel size, figures d-f for 0.5 m voxel size.

ACKNOWLEDGEMENTS

REFERENCES

Al-Durgham, K., Lichti, D. D., Kwak, E., & Dixon, R., 2021. Automated accuracy assessment of a mobile mapping system with lightweight laser scanning and MEMS sensors. *Applied Sciences*, 11(3), 1007.

Chen, J., Mora, O. E., & Clarke, K. C., 2018. Assessing the accuracy and precision of imperfect point clouds for 3d indoor mapping and modeling. *Int. Ann. Photogramm. Remote Sens. Spatial Inf. Sci.*, 4, pp. 3-10.

Dellaert, F. & GTSAM Contributors, 2022. *Borglab/GTSAM*. 4.2a8, Georgia Tech Borg Lab.

Di Stefano, F., Torresani, A., Farella, E. M., Pierdicca, R., Menna, F., Remondino, F., 2021. 3D surveying of underground built heritage: Opportunities and challenges of mobile technologies. *Sustainability*, 13(23), 13289.

Ebadi, K., Bernreiter, L., Biggie, H., Catt, G., Chang, Y., Chatterjee, A., Denniston, C. E., Deschênes, S.-P., Harlow, K., Khattak, S., Nogueira, L., Palieri, M., Petráček, P., Petrlík, M., Reinke, A., Krátký, V., Zhao, S., Agha-mohammadi, A., Alexis, K., Carlone, L., 2022. Present and future of SLAM in extreme underground environments. *arXiv preprint* arXiv:2208.01787.

Elhashash, M., Albanwan, H., Qin, R., 2022. A review of mobile mapping systems: from sensors to applications. *Sensors*, 22, 4262.

Farella, E. M., 2016. 3D mapping of underground environments with a hand-held laser scanner. *Bollettino della società italiana di fotogrammetria e topografia (SIFET)*, (2), pp. 1-10.

Kim, G., Yun, S., Kim, J. & Kim, A. 2022. SC-LiDAR-SLAM: A Front-end Agnostic Versatile LiDAR SLAM System. *Proc. Int. Conference on Electronics, Information and Communication* (ICEIC), pp. 1-6.

Kim, H., Choi, Y., 2021. Location estimation of autonomous driving robot and 3D tunnel mapping in underground mines using pattern matched LiDAR sequential images. *International Journal of Mining Science and Technology*, 31(5), pp. 779-788.

Knapitsch, A., Park, J., Zhou, Q.Y., Koltun, V., 2017. Tanks and temples: Benchmarking large-scale scene reconstruction. *ACM Trans. Graph. ToG*. 36, pp. 1–3.

Jones, E.W., 2020. Mobile LiDAR for underground geomechanics: learnings from the teens and directions for the twenties. Proc. 2nd *UMT Conference*, pp. 3-26.

Lague, D., Brodu, N., & Leroux, J., 2013. Accurate 3D comparison of complex topography with terrestrial laser scanner: Application to the Rangitikei canyon (NZ*). ISPRS journal of photogrammetry and remote sensing*, 82, pp. 10-26.

Lehtola, V. V., Kaartinen, H., Nüchter, A., Kaijaluoto, R., Kukko, A., Litkey, P., Hyyppä, J., 2017. Comparison of the

selected state-of-the-art 3D indoor scanning and point cloud generation methods. *Remote sensing*, 9(8), 796.

Liang, X., Hyyppa, J., Kukko, A., Kaartinen, H., Jaakkola, A., Yu, X., 2014. The use of a mobile laser scanning system for mapping large forest plots. *IEEE Geosci. Remote Sens. Lett.*, *11*, pp. 1504-1508.

Menna, F., Torresani, A., Battisti, R., Nocerino, E., Remondino, F., 2022: A modular and low-cost portable VSLAM system for real-time 3D mapping: from indoor and outdoor spaces to underwater environments. *Int. Arch. Photogramm. Remote Sens. Spatial Inf. Sci.,* XLVIII-2/W1-2022, pp. 153-162.

Nocerino, E., Menna, F., Remondino, F., Toschi, I., & Rodríguez-Gonzálvez, P., 2017. Investigation of indoor and outdoor performance of two portable mobile mapping systems. In *SPIE Videometrics, Range Imaging, and Applications XIV,* Vol. 10332, pp. 125-139.

Nocerino, E., Rodríguez-Gonzálvez, P. and Menna, F., 2019. Introduction to mobile mapping with portable systems. In Laser Scanning: *An Emerging Technology in Structural Engineering*. In Laser Scanning - An Emerging Technology in Structural Engineering, Chapter 4, CRC Press.

Nocerino, E., Stathopoulou, E. K., Rigon, S., & Remondino, F., 2020. Surface reconstruction assessment in photogrammetric applications. *Sensors*, 20(20), 5863.

Otero, R., Lagüela, S., Garrido, I., Arias, P., 2020. Mobile indoor mapping technologies: A review. *Automation in Construction*, Vol. 120, 103399.

Perfetti, L. and Fassi, F., 2022. Handheld fisheye multicamera system: surveying meandering architectonic spaces in open-loop mode – accuracy assessment. *Int. Arch. Photogramm. Remote Sens. Spatial Inf. Sci.,* XLVI-2/W1-2022, pp. 435-442.

Pierzchała, M., Giguère, P., Astrup, R., 2018. Mapping forests using an unmanned ground vehicle with 3D LiDAR and graph-SLAM. *Computers and Electronics in Agriculture*, 145, pp. 217-225.

Quigley, M., Conley, K., Gerkey, B., Faust, J., Foote, T., Leibs, J., Berger, E., Wheeler, R., Ng, A.Y., 2009. ROS: an open-source robot operating system. *In Proceedings of the ICRA Workshop on Open Source Software,* Vol. 3, pp. 5.

Raval, Banerjee, B.P., Kumar Singh, S., Canbulat, I., 2019. A preliminary investigation of mobile mapping technology for underground mining. Proc. *IEEE IGARSS*, pp. 6071-6074.

Rusinkiewicz, S., & Levoy, M., 2001. Efficient variants of the ICP algorithm. Proc. 3rd *3DIM Conference*, pp. 145-152.

Rusu, R.B., Cousins, S., 2011. 3D is here: Point Cloud Library (PCL). Proc. *IEEE Int. Conference on Robotics and Automation*, pp. 1-4.

Santos, P.M., Júlio, E.N., 2013. A state-of-the-art review on roughness quantification methods for concrete surfaces. *Construct. Build. Mater.*, 38, pp. 912–923.

Schops, T., Schonberger, J.L., Galliani, S., Sattler, T., Schindler, K., Pollefeys, M., Geiger, A., 2017. A multi-view stereo

benchmark with high-resolution images and multi-camera videos. Proc. *CVPR*.

Toschi, I., Rodríguez-Gonzálvez, P., Remondino, F., Minto, S., Orlandini, S., Fuller, A., 2015. Accuracy evaluation of a mobile mapping system with advanced statistical methods. *Int. Arch. Photogramm. Remote Sens. Spatial Inf. Sci.*, 40(5), 245.

Trybała, P., Szrek, J., Remondino, F., Wodecki, J., Zimroz, R., 2022: Calibration of a multi-sensor wheeled robot for the 3d mapping of underground mining tunnels. *Int. Arch. Photogramm. Remote Sens. Spatial Inf. Sci.,* XLVIII-2/W2-2022, pp. 135-142.

Trybała, P., Szrek, J., Dębogórski, B., Ziętek, B., Blachowski, J., Wodecki, J., & Zimroz, R., 2023. Analysis of Lidar Actuator System Influence on the Quality of Dense 3D Point Cloud Obtained with SLAM. *Sensors*, 23(2), 721.

Xie, Y., Yang, T., Wang, X., Chen, X., Pang, S., Hu, J., Wang, A., Chen, L., Shen, Z., 2022. Applying a portable backpack LiDAR to measure and locate trees in a nature forest plot: accuracy and error analyses. *Remote Sensing*, *14*, 1806.

Publication 5: MIN3D Dataset: MultI-seNsor 3D Mapping with an Unmanned Ground Vehicle

ORIGINAL ARTICLE

MIN3D Dataset: MultI-seNsor 3D Mapping with an Unmanned Ground Vehicle

Paweł Trybała[1,3] · Jarosław Szrek[2] · Fabio Remondino[3] · Paulina Kujawa[1] · Jacek Wodecki[1] · Jan Blachowski[1] · Radosław Zimroz[1]

Abstract

The research potential in the field of mobile mapping technologies is often hindered by several constraints. These include the need for costly hardware to collect data, limited access to target sites with specific environmental conditions or the collection of ground truth data for a quantitative evaluation of the developed solutions. To address these challenges, the research community has often prepared open datasets suitable for developments and testing. However, the availability of datasets that encompass truly demanding mixed indoor–outdoor and subterranean conditions, acquired with diverse but synchronized sensors, is currently limited. To alleviate this issue, we propose the MIN3D dataset (MultI-seNsor 3D mapping with an unmanned ground vehicle for mining applications) which includes data gathered using a wheeled mobile robot in two distinct locations: (i) textureless dark corridors and outside parts of a university campus and (ii) tunnels of an underground WW2 site in Walim (Poland). MIN3D comprises around 150 GB of raw data, including images captured by multiple co-calibrated monocular, stereo and thermal cameras, two LiDAR sensors and three inertial measurement units. Reliable ground truth (GT) point clouds were collected using a survey-grade terrestrial laser scanner. By openly sharing this dataset, we aim to support the efforts of the scientific community in developing robust methods for navigation and mapping in challenging underground conditions. In the paper, we describe the collected data and provide an initial accuracy assessment of some visual- and LiDAR-based simultaneous localization and mapping (SLAM) algorithms for selected sequences. Encountered problems, open research questions and areas that could benefit from utilizing our dataset are discussed. Data are available at https://3dom.fbk.eu/benchmarks.

Keywords Robotics · UGV · Underground · Mining · Open dataset · SLAM · Evaluation

✉ Paweł Trybała
ptrybala@fbk.eu; pawel.trybala@pwr.edu.pl

Jarosław Szrek
jaroslaw.szrek@pwr.edu.pl

Fabio Remondino
remondino@fbk.eu

Paulina Kujawa
paulina.kujawa@pwr.edu.pl

Jacek Wodecki
jacek.wodecki@pwr.edu.pl

Jan Blachowski
jan.blachowski@pwr.edu.pl

Radosław Zimroz
radoslaw.zimroz@pwr.edu.pl

[1] Faculty of Geoengineering, Mining and Geology, Wrocław University of Science and Technology (WUST), Wrocław, Poland

[2] Faculty of Mechanical Engineering, Wrocław University of Science and Technology (WUST), Wrocław, Poland

[3] 3D Optical Metrology (3DOM) Unit, Bruno Kessler Foundation (FBK), Trento, Italy

 Springer

1 Introduction

1.1 Mobile Mapping

Mobile mapping (Chiang et al. 2021; Elhashash et al. 2022) is a widely used technique for various applications, such as documenting and inventorying scenes (Vallet and Mallet 2016; Di Stefano et al. 2021), integration of airborne surveying (Toschi et al. 2017), creating computer models for simulations or decisions (Tak et al. 2021; Feng et al. 2022), and guiding robots for navigation (Funk et al. 2021). The integration of localization and mapping into a single process, known as simultaneous localization and mapping (SLAM), is crucial for accurate spatial positioning and navigation. A variety of sensors and devices can be used for mapping, including 2D and 3D LiDAR scanners, cameras, and depth sensors. SLAM algorithms perform well in indoor environments, such as factories and warehouses, allowing for autonomous operation of robots. However, mapping in outdoor and uncontrolled scenarios presents challenges for SLAM algorithms, such as uneven terrain, limited range of 2D LiDAR sensors, dynamic objects and more sources of sensor noise, which can potentially degrade the quality of mapping and render some popular assumptions useless (e.g., presence of the flat ground). In such scenarios, 3D LiDAR scanners and camera-based systems (V-SLAM) are more effective. In open spaces, global navigation satellite systems (GNSS) can provide a reliable location, but in areas where satellite signals are not available, such as tunnels, caves and mines, a more sophisticated SLAM algorithm is needed.

Research and development of mobile mapping solutions for such environments can be traced back to early works of Thrun et al. (2003), which showcased the usage of laser scanners mounted on a robot to carry out a volumetric 3D survey of an underground mine. Future advances in field robotics and increasing availability of open-source solutions resulted in developing a wide selection of robotic (Kanellakis and Nikolakopoulos 2016; Nüchter et al. 2017; Ren et al. 2019; Trybała 2021; Yang et al. 2022), handheld (Zlot and Bosse 2013; Trybała et al. 2023), and wearable (Masiero et al. 2018; Blaser et al. 2019) solutions of varying complexity for mapping subterranean spaces. However, the problem of performing robust SLAM in challenging environments still cannot be considered as fully solved (Ebadi et al. 2022).

1.2 Open Datasets

To advance research in the field of SLAM, multiple open datasets have been collected and made publicly available by scientists from the robotics and geomatics communities (Geiger et al. 2012; Liu et al. 2021; Macario Barros et al. 2022; Helmberger et al. 2022). These datasets allow researchers to investigate various mapping approaches and easily test and evaluate in-house, commercial, or open-source software solutions without the need for access to expensive data acquisition platforms, particularly for robotic systems. The popularity of these datasets has led to the creation of benchmarks, where automated systems evaluate the accuracy of processing methods using standardized metrics and rank them among other submitted solutions.

This approach enables an objective comparison of different SLAM algorithms through use of common metrics, such as absolute and relative trajectory errors (ATE and RTE), to assess localization accuracy. However, there are various other strategies for evaluating the quality of 3D mapping, such as using different metrics for measuring the compliance of point clouds with ground truth (GT), and for aligning the resulting spatial data with reference data, such as using global or local registration methods.

One of the key events that greatly accelerated progress in mobile mapping research were the competitions organized by the US-based Defense Advanced Research Projects Agency (DARPA), such as the DARPA Grand Challenges (starting from 2004) (Seetharaman et al. 2006) and the Subterranean Challenge (held in 2017–2021) (Chung et al. 2023). The former type of competition primarily focused on the needs of the automotive industry, such as localization, mapping, and perception in open, urban areas, and the latter on robot autonomy, perception, and SLAM, respectively. Through dedicated funding, clear goals, and reliable evaluation methods, these events enabled teams from around the world to collaborate and develop innovative SLAM solutions. The by-products of these challenges are also open datasets and benchmarks, which were collected and formed during the field trials of the competitions. Although there are numerous publicly available datasets dedicated to evaluating SLAM algorithms, the diversity of real-world environments in which these algorithms are applied, as well as the various sensor configurations for which mapping solutions are developed, results in a constant need for acquiring more data to evaluate method performance under different conditions. This issue is becoming increasingly critical as learning-based methods gain popularity. Providing them with well-diversified training data with reliable reference data is crucial for their generalization, adaptability, and in consequence usability in real-world scenarios. Furthermore, the universality and uniqueness of a dataset is not only determined by the environment in which the data was collected, but also by the limited set of sensors used. The use of multiple sensors to simultaneously acquire different

types of data not only facilitates the development and testing of data fusion methods, but also provides the most objective way to compare methods based on different sensors, such as visual SLAM (V-SLAM) with LiDAR-based approaches. In recent years, the AMICOS[1] and VOT3D[2] EIT Raw Materials projects, among others, tackled the use of ground/wheeled/handheld robotic platforms, equipped with various imaging and LiDAR devices, to inspect underground mining scenarios and technical infrastructures. Multi-sensors robots (Trybała et al. 2022) or portable stereo-vision systems (Torresani et al. 2021) can be used to search for hot idlers in a conveyor belt, map underground spaces, or automatically search for humans or damages of components (Szrek et al. 2020; Menna et al. 2022; Dabek et al. 2022).

1.3 Paper Contribution

A common aspect of robotics platforms and mobile mapping solutions is the accuracy and robustness evaluation of localization and mapping methods in harsh conditions (Nocerino et al. 2017; Trybała et al. 2023). Despite the availability of various robotic datasets collected in different environments, most of the available datasets do not have redundant sensor suites or accurate and complete 3D ground truth.

To address the above-mentioned issues, we propose a novel set of data collected in (i) an indoor man-made environment (University buildings) and (ii) an underground facility in Walim (Poland) using a wheeled mobile robot (UGV) equipped with multiple low-cost sensors. The dataset comprises data from an exhaustive, redundant sensor system, including two sets of different stereo cameras, inertial measurement units (IMUs), and two independent LiDAR scanners: a spinning Velodyne VLP-16 with an actuator and a solid-state Livox Horizon. To facilitate the evaluation of mapping results by the users, we also provide reliable GT data in the form of a survey-grade point cloud acquired with a Riegl time-of-flight-based terrestrial laser scanner and the parameters of the external calibration of the sensors mounted on the robot. The collected data are processed and a preliminary accuracy assessment of the results obtained with selected SLAM methods, utilizing various sensors, is presented.

The structure of the article is as follows. First, related works and available datasets for testing SLAM methods are discussed. Then, the utilized in-house mobile robot characteristics, dataset structure, and ground truth data acquisition methodology are presented. The collected and shared eight sequences are reported in Sect. 3, together with some results of the performance of selected state-of-the-art SLAM

algorithms. Finally, the directions of challenging research areas and an outlook or the future developments in the context of utilizing the presented dataset close the paper.

2 Related Works

2.1 SLAM Datasets: Common Scenarios

In the general research area of mobile mapping, numerous open datasets have been published, often featuring a dedicated benchmark. The most prominent research groups involved in these studies focus on the applications in the automotive industry, photogrammetry, surveying, and robotics. At the early days of 3D SLAM developments for autonomous systems, datasets being published were dominated by car-based systems in urban areas and did not focus on benchmarking and metrological evaluation of mapping. Thus, they did not provide an accurate reference data for mapping, but only the raw data from sensor systems consisting usually of camera(s), LiDAR scanners, and inertial measurement unit (IMU) (Smith et al. 2009; Blanco-Claraco et al. 2014; Cordts et al. 2015).

The prime example is the Massachusetts Institute of Technology (MIT) DARPA Grand Challenge 2007 dataset (Huang et al. 2010). Despite the lack of full GT, it still marks an important moment of publicly releasing a huge amount of image and point cloud data, acquired with sensors relevant to the automotive industry applications, enabling a wide audience to work on robotic perception-related solutions. Similarly, two Korea Advanced Institute of Science and Technology (KAIST) datasets (Choi et al. 2018; Jeong et al. 2019) include only GNSS-derived trajectories as the reference data, but provide additional data, recorded at day and at night, and extend the sensor selection by a thermal camera.

Among the most influential SLAM datasets, constituting arguably the most popular benchmark, is the Karlsruhe Institute of Technology and Toyota Technological Institute (KITTI) dataset (Geiger et al. 2012, 2013). The data were collected with a sensor system mounted on a roof of a Volkswagen car in the urban area of Karlsruhe, Germany. Apart from providing image, LiDAR point clouds and IMU data, it includes GNSS-based trajectory and an automated benchmarking system for evaluating the performance of submitted solutions. Although it does not contain a reliable reference for mapping, subsequent developments added other challenges to the benchmark suite, such as image depth prediction, object detection, or semantic segmentation. A recent survey of SLAM algorithms (Liu et al. 2021) highlighted the problem of providing the reliable GT for mapping in open SLAM datasets: only 35 out of 97 investigated datasets include 3D reference data for mapping quality evaluation.

In the robotic and photogrammetric communities, three distinct classes of SLAM datasets can be distinguished, based on whether they were acquired with an unmanned aerial vehicle (UAV), unmanned ground vehicle (UGV), or a handheld system. An example of a UAV-based research is the European Robotics Challenge (EuRoC) dataset (Burri et al. 2016), which features visual–inertial system data with GT data consisting of trajectories acquired with a motion capture (MC) system, total station (TS) tracking and terrestrial laser scanner (TLS) point cloud for mapping evaluation. However, the dataset lacks LiDAR scanning data. For UGV systems, the Technical University of Munich (TUM) RGB-D (Sturm et al. 2012) and Mobile Autonomous Robotic Systems lab (MARS) Mapper (Chen et al. 2020) systems should be mentioned. The former one features only the data from depth cameras and only a, MC GT trajectory (further extended by an IMU in a handheld system in the TUM VI dataset (Schubert et al. 2018)), while the latter contains data from multiple LiDAR devices, stereo camera and an IMU, as well as trajectory obtained with a tracking system and a TLS point cloud. In the scope of the ETH3D dataset (Schops et al. 2017), multiple image sequences obtained with a monocular camera and a stereo visual–inertial handheld system are shared. Most of them are recorded indoors, with a GT provided by a MC system. For a few scenes mapped outside, a GT is only reconstructed by a structure-from-motion (SfM) approach. From the most recent developments, interesting SLAM datasets start to include novel sensors such as event cameras (Klenk et al. 2021) and utilize simulation environments to facilitate the need for data acquisition in different conditions, especially for learning-based methods (Wang et al. 2020b). Nevertheless, the final evaluation of SLAM method performance should be assessed on real datasets, since multiple noise sources and possible failure factors present in the real world are extremely hard to reproduce in a simulated environment.

2.2 SLAM Datasets: Challenging Environments

All the above-mentioned datasets are, however, captured in relatively easy indoor, feature-rich environments. For mobile mapping underground sites, especially industrial facilities, conditions are much harder and include a multitude of potential noise sources, such as dust, variable humidity, uneven lighting, lack of distinct visual and geometrical features, vibrations, and uneven ground. These factors negatively affect possible assumptions in SLAM algorithm, e.g., the presence of planar features in the surveyed data. Dynamic conditions of the working machinery and possible rockfalls further contribute to the unpredictability of the environment and dangers that need to be recognized for a mobile robot working in such a facility. Thus, SLAM datasets acquired in such harsh conditions were investigated further: the HILTI

(Helmberger et al. 2022) and ConSLAM (Trzeciak et al. 2023) datasets from a construction site and the S3LI dataset (Giubilato et al. 2022) from Mount Etna in Italy, providing data of featureless, bare rock surface of the volcanic landscape. The HILTI dataset features multiple datasets from different editions, which vary in terms of the sensor suites used. Although the ConSLAM dataset provides data collected with a similar, prototypic sensor setup, it provides data from a periodically repeated measurements at the same construction site. Another challenging natural environment of a botanic garden was investigated by Liu et al. (2023), who share a dataset collected with a wheeled mobile robot with a rich sensor selection and a reliable ground truth 3D point cloud. A different challenging case could be considered for the mapping systems operating in areas with unreliable, partial GNSS signal coverage. An example of a dataset focusing on such conditions is BIMAGE Blaser et al. (2021), which provides raw data from a mobile mapping system collected in urban canyons and forest areas supplemented by ground control points surveyed with a total station.

The first underground SLAM dataset (Leung et al. 2017) was published in 2017 and featured data acquired in a Chilean underground mine recorded using a Clearpath UGV, equipped with a radar, stereo camera, and a Riegl TLS. The TLS was used in two ways: as a reference sensor, performing static scans when the robot was not moving, and similarly to an industrial-grade 3D LiDAR system, continuously scanning during robot's movement. However, utilizing such expensive instrument is not common, since it greatly increases the costs of the measurement system, is not suitable for flying units due to its weight, and the laser scan frequency is low (6 s for one full scan).

The most suitable datasets for evaluating robotic SLAM solutions for mining-related applications were acquired during the DARPA Subterranean (SubT) Challenge. Many teams shared data they collected during at least one of the events, which included a tunnel circuit, a power plant site and a cave system, all of which are relevant to the subject of our study. Datasets were published by the DARPA Army Research Lab (Rogers et al. 2020) and teams: Cerberus (Tranzatto et al. 2022), CoSTAR (Koval et al. 2022; Reinke et al. 2022), MARBLE (Kasper et al. 2019; Kramer et al. 2022), CTU-Cras-Norlab (Petracek et al. 2021; Krátký et al. 2021), Explorer (Wang et al. 2020a). They include UGV- and UAV-based data from stereo cameras, IMUs, and industrial-grade LiDAR scanners, seldom supplemented by thermal cameras and radars. The TLS-based GT was provided by DARPA. Although useful, those datasets usually feature expensive platforms (e.g., Boston Dynamics Spot) and do not have redundant sensors (multiple stereo cameras, LiDAR scanners, IMUs), making them solution dependent. A summary of the above-mentioned relevant open SLAM datasets is presented in Table 1.

Table 1 Comparison of selected relevant, popular SLAM open datasets

Dataset	Setting	LiDAR scanner		Camera		Inertial	Other sensors	GNSS	3D GT point cloud
		Spinning	Solid state	Stereo	RGB-D				
KITTI	Urban	✓	–	✓	✓	✓	–	✓	–
KAIST multispectral	Urban	✓	–	✓	–	✓	Thermal camera	✓	–
EuRoC	Indoor	–	–	✓	–	✓	–	–	✓
TUM VI	Indoor	–	–	✓	–	✓	–	–	–
ETH3D	Indoor and outdoor	–	–	✓	✓	✓	–	–	–
HILTI	Construction site	✓	✓	✓	–	✓	–	–	✓
ConSLAM	Construction site	✓	–	–	–	✓	Monocular and thermal cameras	–	✓
S3LI	Outdoor	–	✓	✓	–	✓	–	✓	–
Chilean underground mine	Underground	–	–	✓	–	–	TLS LiDAR, radar	–	✓
SubT: DARPA Army Research Lab	Underground	✓	–	✓	–	✓	–	–	✓
SubT: Cerberus	Underground	✓	–	✓	–	✓	–	–	✓
SubT: CoSTAR	Underground	✓	–	✓	✓	✓	Thermal camera, event camera, UWB beacons	–	–
SubT: MARBLE (ColoRadar)	Underground, indoor, and urban	✓	–	–	–	✓	Radars	–	–
SubT: CTU-Cras-Norlab	Underground	✓	–	✓	✓	✓	–	–	✓
MIN3D	Indoor and underground	✓	✓	✓	✓	✓	Thermal camera, multiple IMUs	–	✓

To move beyond a simple comparison between different SLAM algorithms (working on the data from the same sensor), we decided to enhance this approach, allowing to compare results from SLAM running on different sensors, acquired during the same sequence (e.g., solid-state and spinning LiDAR sensors, stereo and RGB-D camera). Moreover, utilizing low-cost solutions popular in the robotic community and sharing a survey-grade, TLS-based ground truth data, we allow researchers to evaluate SLAM software and hardware solutions that can be then used by them to create affordable systems for popularizing mobile mapping methods in underground applications.

3 The MIN3D Dataset

The data were collected in interior and exterior areas of the Wroclaw University of Science and Technology (Fig. 1) and within some tunnels of the underground facility "Rzeczka", which is a part of the "Riese" complex (Fig. 2), constructed during the World War II (Stach et al. 2014). Both sites feature varying surfaces and environments, which pose a challenge for SLAM algorithms as they must adapt to varying structural conditions, illumination changes, and the inconsistent level of the presence of distinct visual features.

Fig. 1 The employed multi-sensor UGV near the university building

3.1 Employed Robotic System and Sensor Configuration

The data were collected using a mobile robot equipped with a multi-sensory measuring column (Fig. 3). The robot was equipped with various sensors, as well as a data recording computer, power batteries, and lighting, which featured an adjustable intensity to adapt to the

Fig. 2 Mapped locations: underground tunnel (aka *adit*)

Fig. 3 The mobile robot with its sensors placed along the vertical column bar with the example data frames (adapted from: Trybała et al. 2022)

environmental conditions and enable the recording of image data in low-light environments. The list of utilized devices includes:

- A Velodyne LiDAR scanner, mounted at the top of the measuring column through an additional rotation module, which increases the resolution of the acquired data by rotating the sensor around the horizontal axis.

- An Intel RealSense D455 depth camera, placed below the Velodyne.
- Monocular RGB and IR cameras installed in the middle pair and featuring a similar optical system and field of view.
- A synchronized Basler stereo-rig.
- A Livox LiDAR scanner located at the bottom of the column.
- A NGIMU inertial measurement unit mounted at the robot base.

The data are supplemented by two IMU sensors integrated with an Intel RealSense camera and the Livox LiDAR system as well as an independent NGIMU. The robot was controlled manually from a remote operator panel. Control signals were transmitted in the 2.4 GHz frequency band, while data acquisition control telemetry was obtained from a tablet connected to a computer placed on the robot via a Wi-Fi network. The block diagram of the connected sensors is shown in Fig. 4, while the remote visualization and control
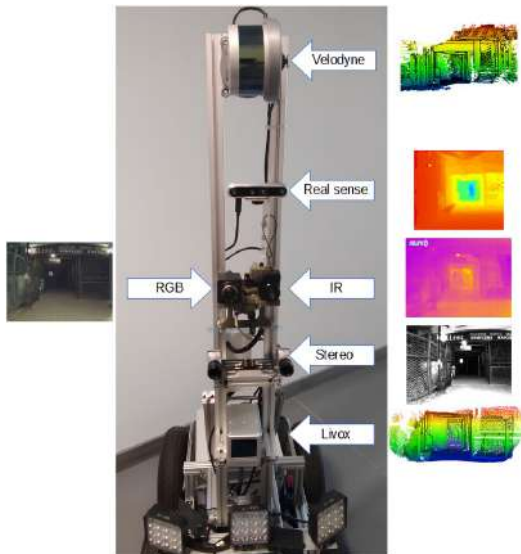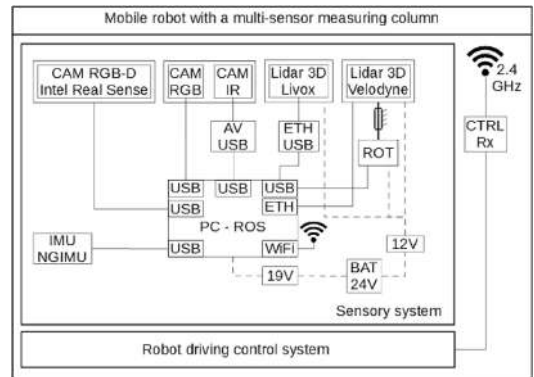

Fig. 4 Block diagram of a robotic multi-sensory measurement system (Trybała et al. 2022)
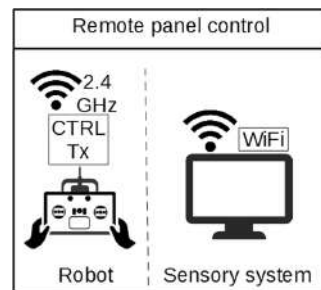

Fig. 5 Remote visualization and control panel (Trybała et al. 2022)

Table 2 Characteristics of the acquired data

Sequence	Path sketch	Size/length	Data acquisition aim	Data samples	Total size
University 1: ground level[a]	Figure 6	60 m×40 m /220 m	Whole area mapping, longer route, reflective surfaces, lack of visual features	53,147 images 10,163 point clouds 130,370 IMU readings	26.1 GB
University 2: indoor/outdoor	Figure 7	50 m×20 m/120 m	Indoor/outdoor transition with changing illumination	26,419 images 5359 point clouds 111,500 readings	22.1 GB
University 3: lab loop closures	Figure 8	20 m×10 m/90 m	Changing illumination in different rooms, multiple loop closures	25,519 images 5093 point clouds 159,215 IMU readings	18.9 GB
Tunnel 1: forward pass[b]	Figure 9	80 m×5 m/80 m	Basic bare rock tunnel mapping, sparse geometrical and visual features	22,244 images 5785 point clouds 180,813 IMU readings	13.2 GB
Tunnel 2: return pass[b]	Figure 10	80 m×5 m/80 m	Basic bare rock tunnel mapping, sparse geometrical and visual features. Possibility of multi-session mapping with previous dataset	19,104 images 4156 point clouds 129,952 IMU readings	10.8 GB
Tunnel 3: main tunnel with loops, part 1[b]	Figure 11	70 m×20 m/120 m	Loop closures in underground conditions, transitions between unstructured/structured geometry	27,198 images 7074 point clouds 221,094 IMU readings	17.9 GB
Tunnel 4: main tunnel with loops, part 2[b,c]	Figure 11	40 m×20 m/60 m	Loop closures in underground conditions, transitions between unstructured/structured geometry. Kidnapped robot problem if analyzed jointly with previous dataset	12,821 images 3336 point clouds 37,303 IMU readings	13.9 GB
Tunnel 5: secondary tunnel[b, c]	Figure 12	90 m×10 m/100 m	Basic bare rock tunnel mapping, transitions between unstructured/structured geometry	19,884 images 5172 point clouds 57,828 IMU readings	22.5 GB

[a]Velodyne LiDAR sensor placed horizontally

[b]Basler stereo with limited frame rate

[c]No RealSense IMU data

panel are shown in Fig. 5. A methodology for system calibration, i.e., estimation of the relative orientation between sensors, was presented in Trybała et al. (2022).

3.2 Data Acquisition

A total of eight datasets were acquired in two different settings:

- Three sequences inside and around the research building of the Faculty of Geoengineering, Mining and Geology at Wrocław University of Science and Technology (Poland).
- Five sequences in the underground site "Rzeczka", part of the "Riese" underground complex (Walim, Poland).

The conditions of the university dataset resemble an industrial environment, with mostly monochromatic colors, scarce visual features, long and uniform corridors, and the presence of reflective surfaces. During the acquisitions in the subterranean environment, the robot was equipped with its own lighting system due to the absence of illumination

in a huge part of the mine. These real underground conditions allowed to illustrate the challenges often encountered in a setting of an industrial mine, where irregular tunnels carved or blasted in rock are mixed with reinforced, more structured areas.

To further increase the level of difficulty for SLAM algorithms, the acquisitions featured illumination changes (robot driving from indoor to outdoor or through a room with light turned off) and frequent revisiting of the same area, often from different perspectives. The specific aims of each acquisition, together with resulting data size, has been summed up in Table 2. Approximate robot trajectories for each sequence, drawn on a 2D projection of the ground truth point cloud cross sections, are shown in Figs. 6, 7, 8, 9, 10, 11, 12.

Due to some problems with the reliability of RealSense internal IMU, an additional NGIMU sensor was added to the measurement system. However, we still provide the incomplete data from the RealSense device, since it may allow some interesting analyses and development in terms of multi-IMU systems, as discussed further in Sect. 4. Similarly, probably due to the challenging environmental
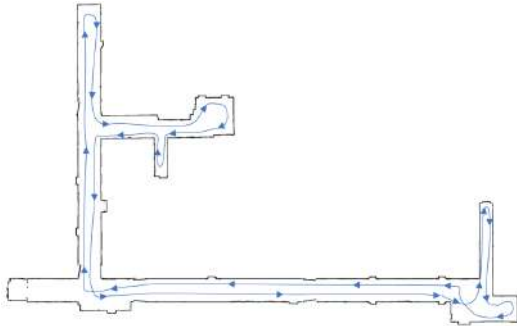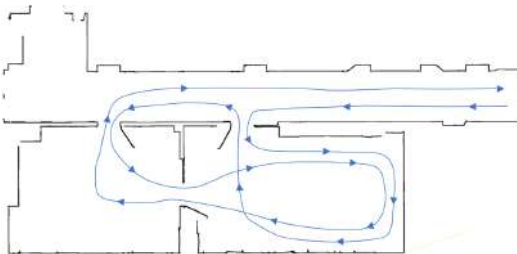
Fig. 6 Sketch of the robot trajectory in the university building (Sequence University 1): textureless ground floor
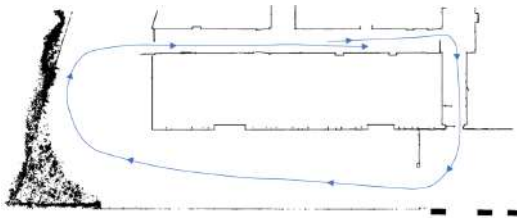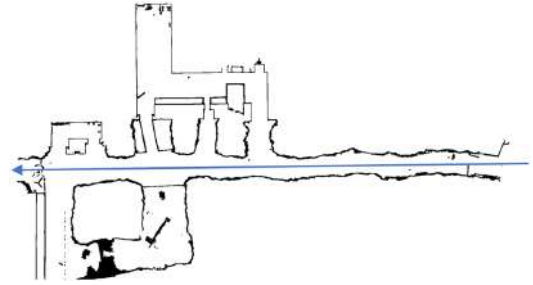

Fig. 7 Sketch of the robot trajectory in the university building (Sequence University 2): indoor–outdoor transitions
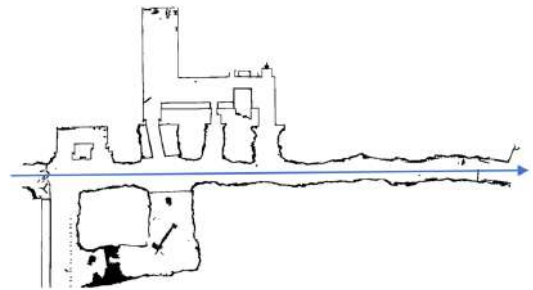

Fig. 8 Sketch of the robot trajectory in the university building (Sequence University 3): ground floor (Sequence 1)

Fig. 9 Sketch of the robot trajectories in the underground tunnel (Sequence Underground 1): main tunnel, forward pass

Fig. 10 Sketch of the robot trajectories in the underground tunnel (Sequence Underground 2): main tunnel, return pass

Fig. 11 Sketch of the robot trajectories in the underground tunnel (Sequences Underground 3 & 4): pass with multiple loops. Route is split into two sequences: before (blue) and after (red) kidnapping a robot (position marked as a red cross)
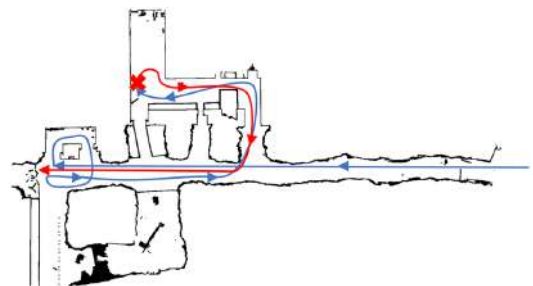
conditions, the Basler stereo camera rig was not able to maintain the desired frame rate during the tunnel tests. Direct processing of this data will result in worse results than for images from other cameras, but might facilitate the development and evaluation of, e.g., AI-based image denoising and frame rate interpolation methods for robustifying mobile robotic applications in challenging environments.

3.3 Dataset Structure

The data were recorded using an Intel NUC machine and, during the measurements, saved in the.rosbag file format using ROS (Robot Operating System) Melodic (Quigley et al. 2009) and common driver packages. In the post-processing operations, the data were unpacked and converted
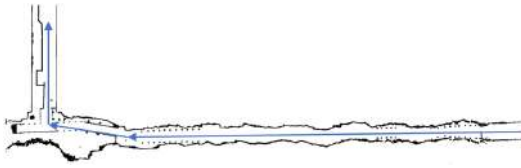
Fig. 12 Sketch of the robot trajectories in the underground tunnel (Sequence Underground 5): secondary tunnel

to open formats suitable for further analyses, as shown in Table 3.

The naming convention of the files is $<ROS\ timestamp> <dot> <extension>$, since all data were time-stamped in a centralized manner, according to the ROS master node clock. However, time stamps of some of the data were already pre-synchronized by the respective device drivers. Time stamps for: RealSense RGB, IR images, depth maps, and IMU are synchronized to each other, as well as

Table 3 Data types and file formats

Source of data	Type of data	File format
Velodyne LiDAR scanner	Point cloud	.ply
Livox LiDAR scanner	Point cloud	.ply
RGB camera	Image	.png
FLIR IR camera	Image	.png
RealSense RGB camera	Image	.png
RealSense stereo IR camera	Images	.png
RealSense precomputed depth map	Image	.png
Basler stereo camera	Images	.png
IMU Livox	Linear acceleration, angular velocity	.csv
IMU RealSense	Linear acceleration, angular velocity	.csv
IMU NGIMU	Linear acceleration, angular velocity	.csv
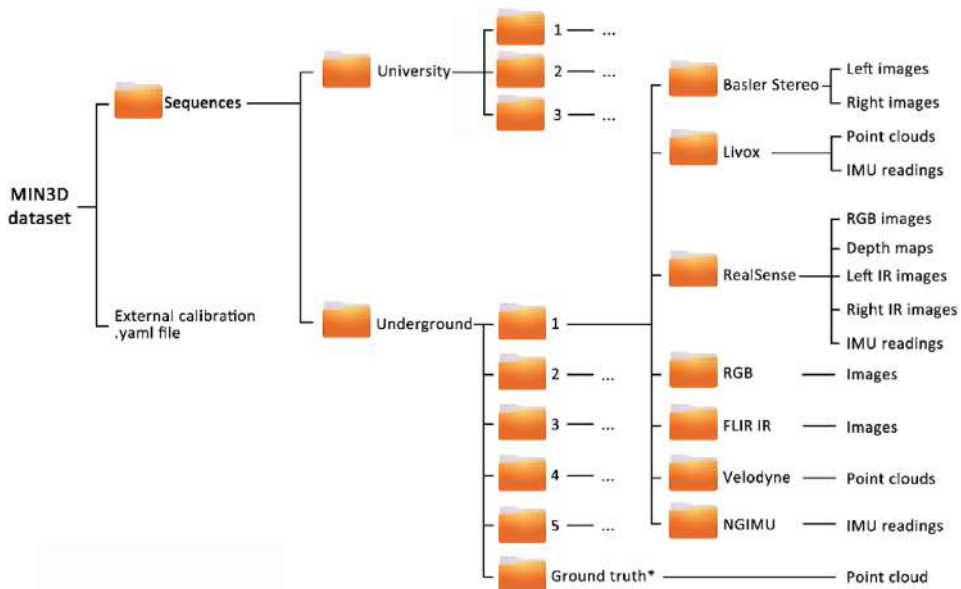
Fig. 13 File structure of the MIN3D dataset. Separate ground truth point clouds are provided for each of the three university sequences, but a single reference point cloud is shared for all five sequences of the underground facility

Basler stereo pairs and Livox point clouds with its internal IMU. The dataset general structure is explained in Fig. 13.

3.4 Ground Truth and Evaluation Methodology

Reference data were acquired using a RIEGL VZ-400i terrestrial laser scanner (Fig. 14). The scanner features a laser pulse repetition rate of 100–1200 kHz, a maximum effective measurement rate of 500,000 points/s, and a measurement range of 0.5 m to 800 m. The scanning angle range is a total of 100° in a vertical line and max. 360° in the horizontal frame. The manufacturer's stated accuracy of resulting single point 3D position is 5 mm and the declared precision is 3 mm (Riegl datasheet 2019).

For both test sites, the distance between consecutive scan positions was about 5–15 m. The scanning parameters used were a laser pulse repetition rate of 1200 kHz, a scanning resolution of 0.05°, and a point cloud resolution characterized by point-to-point distance of 17.5 mm at a distance of 20 m.

The processing of the acquired TLS data was carried out in the dedicated RiSCAN PRO software (RIEGL Laser Measurement Systems GmbH 2019) for point cloud filtering and scan registration. The preliminary scan registration was performed using an automatic registration method based on voxels extraction and fitting. To improve scan position registration, alignment was performed using the multi station adjustment (MSA) procedure. The position and orientation of each scan position were adjusted in a bundle adjustment (BA), which included several iterations to minimize position error between overlapping planes and determine the best fit.

The alignment process resulted in an error (i.e., scanner position standard deviation after BA) of ca 2 mm for both test sites. Control of the alignment of the overlapping first and last positions, creating a loop, showed a spatial matching within 5 mm. This quality control was omitted only for the GT point cloud of the first university sequence, which does not include a loop. The resulting point cloud of the building test site and the underground facility are shown in Figs. 15 and 16, respectively.

To facilitate the proper matching of measurement data with GT, reference points in the form of white spheres with a diameter of 100 mm were placed in the area of interest of both test sites (Fig. 17). The reference targets were selected to be properly visible by all the optical sensors mounted on the robot.

4 Processing and Analyses

The MIN3D dataset could support evaluations of 3D mapping methods, including SLAM. As multiple approaches to assess the quality of the mapping results exist, we do not provide a dedicated benchmarking tool and leave the decision of selecting an appropriate workflow to the readers. Pipelines developed for ETH3D (Schops et al. 2017), 3D Tanks and Temples (Knapitsch et al. 2017), as well as a more sophisticated analysis presented by Toschi et al. (2015) could be mentioned as examples of sound methodologies for carrying out quality evaluation of the 3D reconstruction for the results achieved from processing MIN3D data.

An overview of current state-of-the-art strategies of tackling common problems, based on the research and experiences from the DARPA Subterranean Challenge, in applying SLAM in underground environments can be found in Ebadi et al. (2022). Moreover, we also envision a MIN3D contribution toward the development of specific algorithms for challenging mining environments (Fig. 18), which includes, e.g., dedicated methods for dealing with various structurization levels of geometry, loop closure detection in mostly featureless conditions, or point cloud filtering and optimization approaches.

4.1 Underground Mobile Mapping Accuracy

During the preliminary evaluation of SLAM on our dataset, comparisons of the point clouds obtained with example SLAM algorithms were carried out on representative sequences of the dataset. One sequence has been selected from the indoor part of the dataset (University 2) and two sequences were chosen from the underground tunnels (Underground 1 and 3). Based on the state-of-the-art research, we chose one V-SLAM algorithm, one LiDAR-inertial algorithm, and one pure-LiDAR method. We processed:

- RealSense RGB-D data with ORB-SLAM3 (Campos et al. 2021).
- Livox LiDAR scanner and IMU data with FAST-LIO SLAM (Kim et al. 2021; Xu et al. 2022).
- Actuated Velodyne LiDAR scanner data with SC-A-LOAM (Kim et al. 2022).

As representative statistics, summarizing the mapping performance of each of those methods, we have chosen mean, standard deviation, and $(-3\sigma, 3\sigma)$ range of cloud-to-cloud distance distributions, calculated as signed distances using M3C2 plugin of Cloud Compare software (Lague et al. 2013).
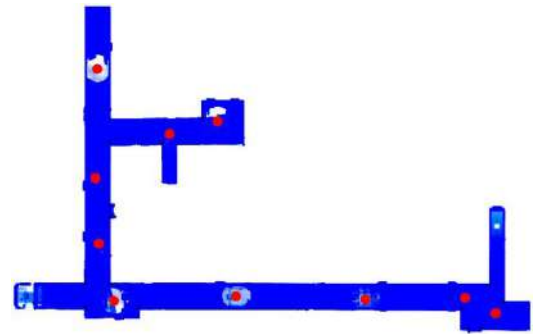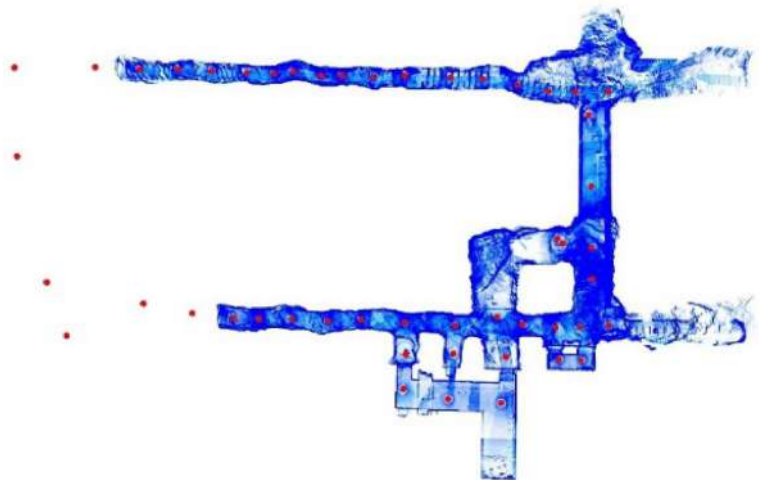
Fig. 14 RIEGL VZ-400i terrestrial laser scanner

Fig. 15 Top view of reference TLS point clouds with the locations of the scan positions (in red): university ground floor, sequence 1

Point clouds based on the simultaneously acquired data from three different sensors were obtained using the previously mentioned state-of-the-art mobile mapping methods. They were then registered to the GT model using iterative closest point (ICP; Besl and McKay 1992) with an initial manual alignment. Mapping errors were estimated as the distances between the point clouds and the local GT model and signed according to their estimated normals. The error distributions were analyzed together with the qualitative analysis of the results (long- and short-term drifts, topology correctness). Summary statistics of the quantitative analysis of the mapping error distributions are presented in Table 4.

The obtained results show that the tested methods were appropriate for 3D mapping of the examined areas. Using a common color-coding scheme (Fig. 19), we compare the results of accuracy evaluation of the three tested SLAM approaches (Figs. 20, 21, 22). Qualitatively analyzing them, the resulting point clouds present the "correct" topology comparing to the GT data. However, in-depth analysis often revealed inconsistencies such as lack of proper loop closures, high short-term rotational drifts, long-term rotational drift around the robot's roll axis, and increased noise near reflective surfaces. Those resulted in point cloud errors such as "ghosting", i.e., not-aligned point clouds of areas measured multiple times or dimension deformation, i.e., shortening of the tunnel length. The above-mentioned issues occurred in both indoor and underground datasets and their example visualizations are presented in Fig. 23. It is worth mentioning

Fig. 16 Top view of reference TLS point clouds with the locations of the scan positions (in red): tunnels of the underground area. Part of the point cloud, representing the outdoor area irrelevant for the dataset, is not displayed

Fig. 17 References object on robot path in the building corridor (left) and in the underground tunnel area (right)
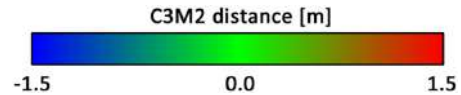

Fig. 18 Challenges for SLAM in the underground environment: uneven illumination, lack of visual features (left); changing types of geometry: passage from an unstructured tunnel to a concrete corridor (right)

Fig. 19 Universal color scale used in all point cloud visualizations in Figs. 20, 21, 22, and 23

that no algorithm was able to properly recover from the simulation of the kidnapped robot problem between sequences Underground 3 and 4 using loop closure detection. Thus, Underground 3 was analyzed only as a standalone sequence.

4.2 Multi-sensor Signal Analysis

Apart from the core issue of improving robustness and reliability of various mobile mapping and localization approaches, we encourage using the proposed MIN3D dataset also for other purposes, such as image enhancement. Conditions in which the data were acquired can challenge state-of-the-art image processing methods. Such methods include, but are not limited to, image deblurring and upscaling, frame interpolation, depth estimation from monocular camera (or improving the quality of depth obtained with the stereo images), and application of different 3D geometry reconstruction methods. Evaluations of deep learning-based techniques are foreseen, since scarcity of the training data from unique, underground conditions may seriously hinder their performance on the MIN3D dataset.

Furthermore, simultaneous acquisition of data from various sensors allows exploration of novel data fusion methods: this could also include methods for improving the quality of the data using multiple devices. As an example, we show a proof of concept of utilizing two IMUs in the context of possible developments in the area of the positioning methods using multiple inertial devices. We compared signals from IMUs installed in Livox and RealSense, with the focus on acceleration data. Figure 24 presents raw data from the sensors expressed in g units.

Firstly, the moving average of the absolute value of the signals was calculated for every channel with the window of 1 s (see Fig. 25). This way, an average variability of vibration strength can be visualized and compared per axis. The main visible difference between devices is expressed as slightly stronger vibrations in the horizontal plane for RealSense compared to Livox. It can be explained by the fact that RealSense was mounted higher on the sensor column, and angular movements of the entire column, with respect

Table 4 Statistics of the mapping error distributions for selected SLAM algorithms

Dataset	Mean mapping error [cm]			Standard deviation [cm]			95% of mapping error distribution range [m]		
	ORB-SLAM3	FAST-LIO-SLAM	SC-A-LOAM	ORB-SLAM3	FAST-LIO-SLAM	SC-A-LOAM	ORB-SLAM3	FAST-LIO-SLAM	SC-A-LOAM
University 2	− 3.5	2.8	− 7.7	101	31	54	(− 2.20, 1.72)	(− 0.65, 0.38)	(− 1.29, 0.85)
Underground 1	− 3.8	0.7	− 8.9	47	23	60	(− 1.26, 0.41)	(− 0.11, 0.14)	(− 1.63, 0.73)
Underground 3	− 3.5	2.5	− 14.6	45	16	81	(− 1.33, 0.46)	(− 0.15, 0.29)	(− 2.30, 1.44)
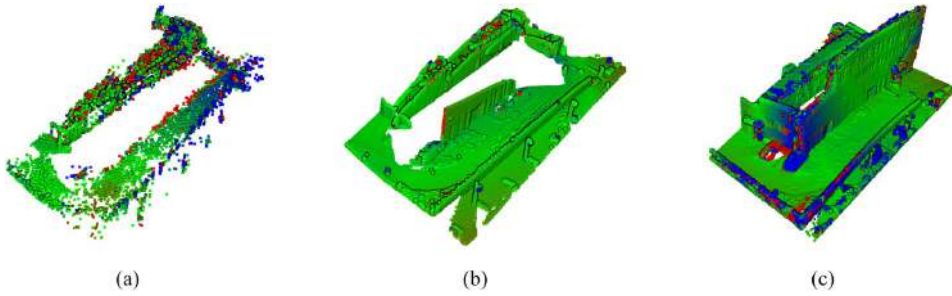
Fig. 20 Examples of SLAM results on the University 2 sequence: **a** ORB-SLAM3 (sparse point cloud); **b** FAST-LIO-SLAM; **c** SC-A-LOAM
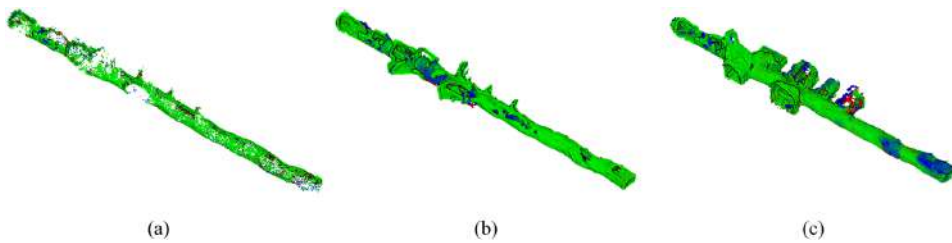
Fig. 21 Examples of SLAM results on the Underground 1 sequence: **a** ORB-SLAM3 (sparse point cloud); **b** FAST-LIO-SLAM; **c** SC-A-LOAM
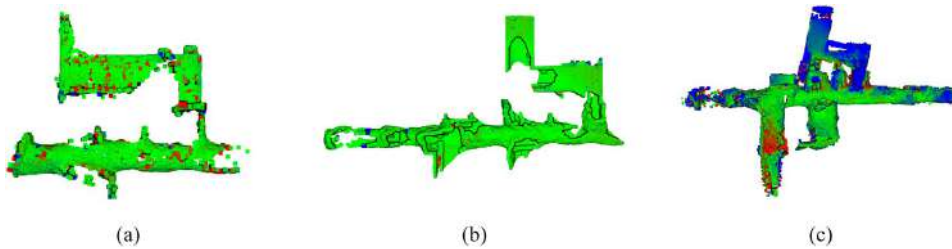
Fig. 22 Examples of SLAM results on the Underground 3 sequence: **a** ORB-SLAM3 (incomplete sparse point cloud); **b** FAST-LIO-SLAM; **c** SC-A-LOAM
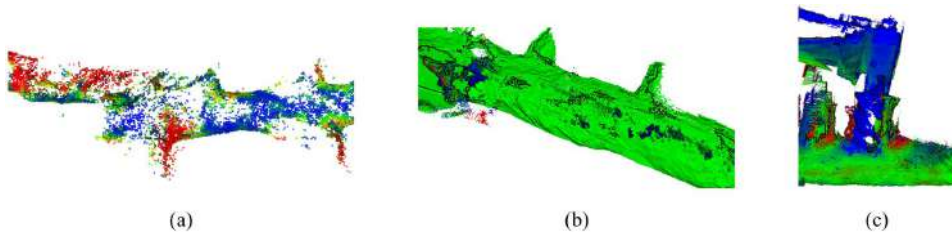
Fig. 23 Issues in various SLAM results: **a** large linear drift error at the straight start of Underground 2 dataset (ORB-SLAM3); **b** double wall error and noisy points in the Underground 1 dataset (FAST-LIO-SLAM); **c** angular drift at the end of Underground 3 dataset (SC-A-LOAM)
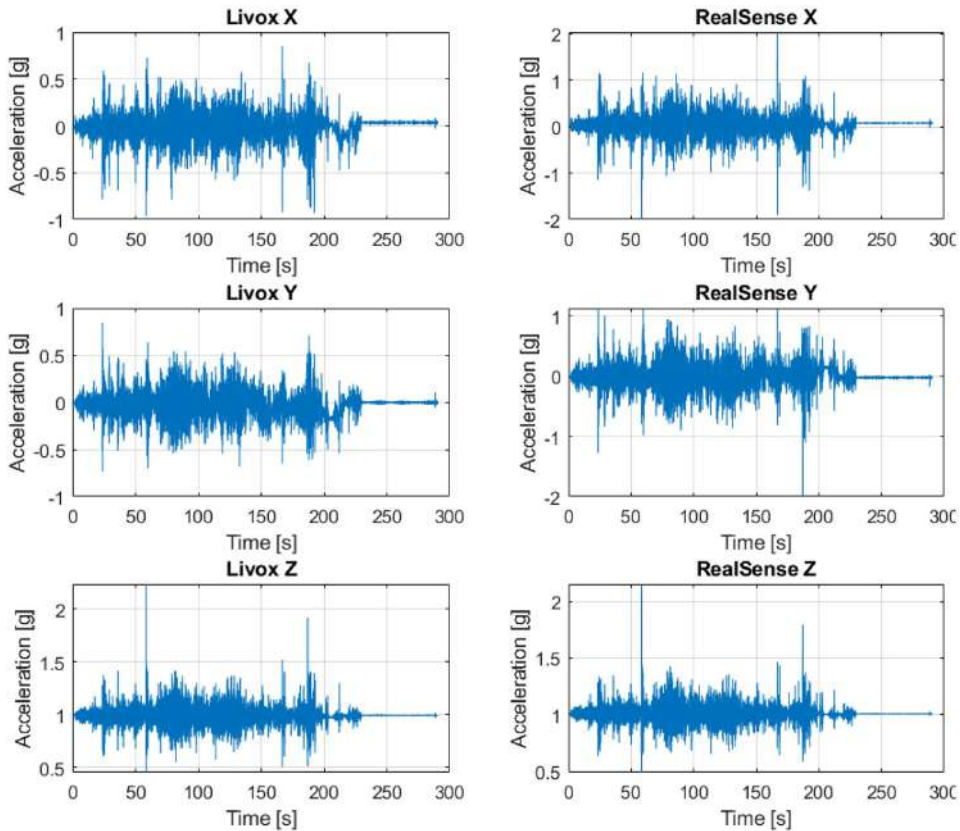
Fig. 24 Raw signals from IMU accelerometers of Livox and RealSense

to the pivot point at the bottom of the column, translate to stronger readings of the RealSense IMU.

In the second step, a moving variance was calculated for all channels, also with the window length of 1 s (see Fig. 26). Comparison of vibrations in the XY directions shows that there is a visible proportional relation between the energy of vibration of each device. It could be explained by the fact that the devices are mounted at different heights on the column, and the angular nature of the vibrations of the column causes the amplification of vibrations in the lateral plane as a function of the height of the column.

The authors attempted to evaluate the relation between vibration energy for the devices. The best achieved fit was a linear model with the ratio of 2.93 at $R^2 = 0.91$ (Fig. 27). It shows that RealSense at its mounting point experiences almost 3 × more energetic vibration in the horizontal plane in relation to Livox due to the angular vibrations of the column. Additionally, the linear nature of the model, as

well as the coefficient of 2.93 can be confirmed by the fact that Livox is mounted 30 cm above the pivot point (bottom mount of the column) and RealSense is placed at 88 cm above the pivot point, which is 2.933 times higher.

5 Conclusions

The paper presented a novel UGV-based dataset for developing and testing mobile mapping solutions (e.g., SLAM) in challenging GNSS-denied conditions, common in mining applications or textureless indoor spaces. We provide data sequences collected simultaneously with multiple sensors, including different LiDAR scanners, cameras, and inertial units. The environments of tests were selected to pose a challenge for state-of-the-art data processing algorithms and feature changing illumination, varying complexity of geometry, and textureless areas. Acquisitions were carried out inside a university building and in an underground historical tunnel,
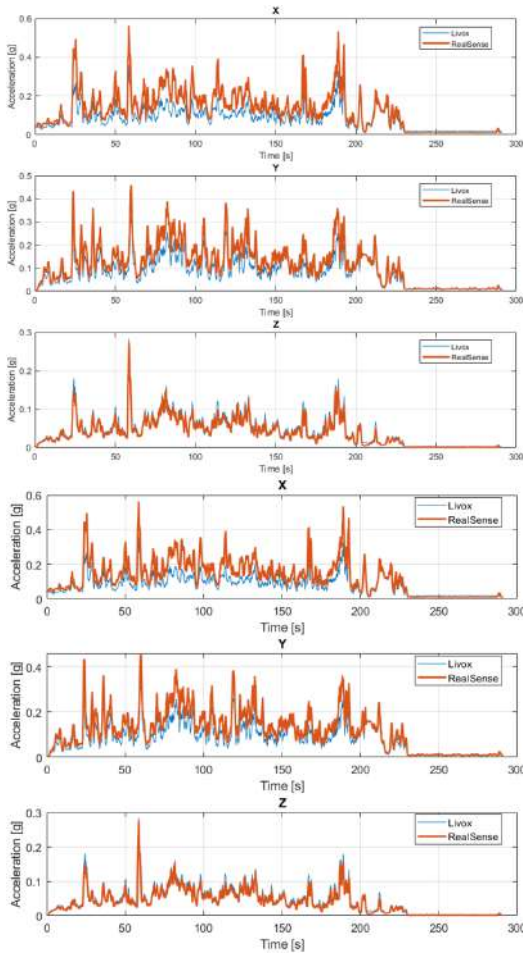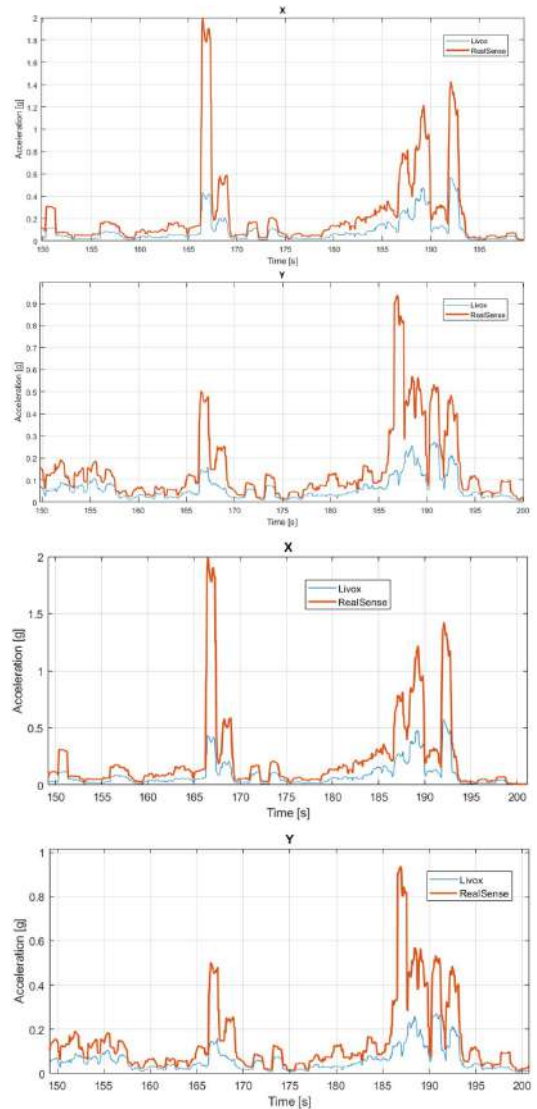
Fig. 25 Moving average of absolute values for all axes with the window of 1 s. Axes X and Y (vibrations on the horizontal plane) show stronger vibration for RealSense, which was mounted higher on the column

Fig. 26 Moving variance for IMU linear accelerations X and Y (comparison per axis) with a window of 1 s. Significant proportional relation between vibration energy is revealed, which is a result of height difference of the mounting points on the column

which allows to also evaluate the performance degradation of developed methods between real and simulated conditions. Such analysis would be especially valuable for learning-based approaches.

We presented quantitative evaluations of selected SLAM methods utilizing data from different sensors (cameras, LiDAR devices, IMU) and showed some shortcomings in their performance when applied to the MIN3D data. Additionally, an analysis of data from the multi-IMU system was performed to showcase the possible directions of research of multi-sensor data fusion.

In summary, it is envisaged that the utilization of the MIN3D dataset has the potential to accelerate

advancements in multiple research domains within the field of robotics, computer vision and geomatics, acknowledging that the list provided below is not exhaustive:

- Testing and improving mapping approaches (visual, LiDAR, fusion) in the challenging underground or indoor conditions.
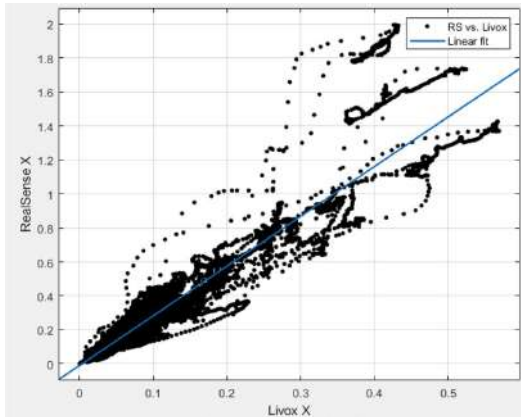
Fig. 27 Relation between vibration energy of the devices evaluated based on the X axis of IMU linear acceleration

- Robustifying V-SLAM in the environments with changing illumination.
- Estimating depth with a monocular camera.
- Developing visual and LiDAR-based loop closure detection algorithms in degraded environments.
- Using multi-sensor odometry and mapping approaches (multi-IMU, multi-camera, multi-LiDAR).
- Online calibration and utilization of multi-sensor suites, including cameras with different spectral responses (e.g., RGB and thermal).

Data Availability Datasets have been published at https://3dom.fbk.eu/benchmarks.

Declarations

Conflict of Interest The authors declare no conflict of interest.

References

Besl PJ, McKay ND (1992) Method for registration of 3-D shapes. In: Sensor fusion IV: control paradigms and data structures. pp 586–606

Blanco-Claraco J-L, Moreno-Duenas F-A, González-Jiménez J (2014) The Málaga urban dataset: high-rate stereo and LiDAR in a realistic urban scenario. Int J Rob Res 33:207–214

Blaser S, Nebiker S, Wisler D (2019) Portable image-based high performance mobile mapping system in underground environments-system configuration and performance evaluation. ISPRS Ann Photogramm Remote Sens Spatial Inform Sci 4:255–262

Blaser S, Meyer J, Nebiker S (2021) Open urban and forest datasets from a high-performance mobile mapping backpack—a contribution for advancing the creation of digital city twins. Int Arch Photogramm Remote Sens Spat Inf Sci 43:125–131

Burri M, Nikolic J, Gohl P, Schneider T, Rehder J, Omari S, Achtelik MW, Siegwart R (2016) The EuRoC micro aerial vehicle datasets. Int J Rob Res 35:1157–1163

Campos C, Elvira R, Rodriguez JJG, Montiel JMM, Tardós JD (2021) Orb-slam3: an accurate open-source library for visual, visual–inertial, and multimap slam. IEEE Trans Rob 37:1874–1890

Chen H, Yang Z, Zhao X, Weng G, Wan H, Luo J, Ye X, Zhao Z, He Z, Shen Y, Schwertfeger S (2020) Advanced mapping robot and high-resolution dataset. Rob Auton Syst 131:103559

Chiang KW, Tsai G-J, Zeng JC (2021) Mobile mapping technologies. Springer

Choi Y, Kim N, Hwang S, Kibaek P, Yoon JS, An K, Kweon IS (2018) KAIST multi-spectral day/night data set for autonomous and assisted driving. IEEE Trans Intell Transp Syst 19:934–948

Chung TH, Orekhov V, Maio A (2023) Into the robotic depths: analysis and insights from the DARPA subterranean challenge. Annu Rev Control Robot Auton Syst 6:477–502

Cordts M, Omran M, Ramos S, Scharwächter T, Enzweiler M, Benenson R, Franke U, Roth S, Schiele B (2015) The Cityscapes Dataset. In: CVPR Workshop on The Future of Datasets in Vision

Dabek P, Szrek J, Zimroz R, Wodecki J (2022) An automatic procedure for overheated idler detection in belt conveyors using fusion of infrared and RGB images acquired during UGV robot inspection. Energies 15:601. https://doi.org/10.3390/en15020601

Di Stefano F, Torresani A, Farella EM, Pierdicca R, Menna F, Remondino F (2021) 3D surveying of underground built heritage: opportunities and challenges of mobile technologies. Sustainability 13:13289

Ebadi K, Bernreiter L, Biggie H, Catt G, Chang Y, Chatterjee A, Denniston CE, Deschênes S-P, Harlow K, Khattak S, Nogueira L, Palieri M, Petráček P, Petrlík M, Reinke A, Krátký V, Zhao S, Agha-mohammadi A, Alexis K, Carlone L (2022) Present and future of slam in extreme underground environments. arXiv preprint arXiv:220801787

Elhashash M, Albanwan H, Qin R (2022) A review of mobile mapping systems: from sensors to applications. Sensors 22:4262

Feng Y, Xiao Q, Brenner C, Peche A, Yang J, Feuerhake U, Sester M (2022) Determination of building flood risk maps from LiDAR mobile mapping data. Comput Environ Urban Syst 93:101759. https://doi.org/10.1016/j.compenvurbsys.2022.101759

Funk N, Tarrio J, Papatheodorou S, Popović M, Alcantarilla PF, Leutenegger S (2021) Multi-resolution 3D mapping with explicit free space representation for fast and accurate mobile robot motion planning. IEEE Robot Autom Lett 6:3553–3560

Geiger A, Lenz P, Urtasun R (2012) Are we ready for autonomous driving? The KITTI vision benchmark suite. In: 2012 IEEE Conference on Computer Vision and Pattern Recognition. IEEE

Geiger A, Lenz P, Stiller C, Urtasun R (2013) Vision meets robotics: the KITTI dataset. Int J Rob Res 32:1231–1237

Giubilato R, Sturzl W, Wedler A, Triebel R (2022) Challenges of SLAM in extremely unstructured environments: the DLR planetary stereo, solid-state LiDAR, inertial dataset. IEEE Robot Autom Lett 7:8721–8728

Helmberger M, Morin K, Berner B, Kumar N, Cioffi G, Scaramuzza D (2022) The Hilti SLAM challenge dataset. IEEE Robot Autom Lett 7:7518–7525

Huang A, Antone M, Olson E, Fletcher L, Moore D, Teller S, Leonard J (2010) A high-rate, heterogeneous data set from the Darpa urban challenge. Int J Rob Res 29:1595–1601. https://doi.org/10.1177/0278364910384295

Jeong J, Cho Y, Shin Y-S, Roh H, Kim A (2019) Complex urban dataset with multi-level sensors from highly diverse urban environments. Int J Rob Res 38:642–657

Kanellakis C, Nikolakopoulos G (2016) Evaluation of visual localization systems in underground mining. In: 2016 24th Mediterranean Conference on Control and Automation (MED). pp 539–544

Kasper M, McGuire S, Heckman C (2019) A benchmark for visual-inertial odometry systems employing onboard illumination. In: 2019 IEEE/RSJ International Conference on Intelligent Robots and Systems (IROS). IEEE

Kim G, Choi S, Kim A (2021) Scan context++: structural place recognition robust to rotation and lateral variations in urban environments. IEEE Trans Rob 38:1856–1874

Kim G, Yun S, Kim J, Kim A (2022) Sc-lidar-slam: a front-end agnostic versatile lidar slam system. In: 2022 International Conference on Electronics, Information, and Communication (ICEIC). pp 1–6

Klenk S, Chui J, Demmel N, Cremers D (2021) Tum-vie: The tum stereo visual-inertial event dataset. In: 2021 IEEE/RSJ International Conference on Intelligent Robots and Systems (IROS). pp 8601–8608

Knapitsch A, Park J, Zhou Q-Y, Koltun V (2017) Tanks and temples: benchmarking large-scale scene reconstruction. ACM Trans Graph (ToG) 36:1–13

Koval A, Karlsson S, Mansouri SS, Kanellakis C, Tevetzidis I, Haluska J, Agha-mohammadi A, Nikolakopoulos G (2022) Dataset collection from a SubT environment. Rob Auton Syst 155:104168. https://doi.org/10.1016/j.robot.2022.104168

Kramer A, Harlow K, Williams C, Heckman C (2022) ColoRadar: the direct 3D millimeter wave radar dataset. Int J Rob Res 41:351–360

Krátký V, Petráček P, Báča T, Saska M (2021) An autonomous unmanned aerial vehicle system for fast exploration of large complex indoor environments. J Field Robot 38:1036–1058

Lague D, Brodu N, Leroux J (2013) Accurate 3D comparison of complex topography with terrestrial laser scanner: application to the Rangitikei canyon (NZ). ISPRS J Photogramm Remote Sens 82:10–26

Leung K, Lühr D, Houshiar H, Inostroza F, Borrmann D, Adams M, Nüchter A, del Solar J (2017) Chilean underground mine dataset. Int J Rob Res 36:16–23

Liu Y, Fu Y, Chen F, Goossens Bart and Tao W, Zhao H (2021) Simultaneous Localization and Mapping related datasets: a comprehensive survey. arXiv preprint arXiv:210204036

Liu Y, Fu Y, Qin M, Xu Y, Xu B, Chen F, Goossens B, Yu H, Liu C, Chen L, Tao W, Zhao H (2023) BotanicGarden: A high-quality and large-scale robot navigation dataset in challenging natural environments. arXiv preprint arXiv:2306.14137

Macario Barros A, Michel M, Moline Y, Corre G, Carrel F (2022) A comprehensive survey of visual SLAM algorithms. Robotics. https://doi.org/10.3390/robotics11010024

Masiero A, Fissore F, Guarnieri A, Pirotti F, Visintini D, Vettore A (2018) Performance evaluation of two indoor mapping systems: low-cost UWB-aided photogrammetry and backpack laser scanning. Appl Sci. https://doi.org/10.3390/app8030416

Menna F, Torresani A, Battisti R, Nocerino E, Remondino F (2022) A modular and low-cost portable VSLAM system for real-time 3D mapping: from indoor and outdoor spaces to underwater environments. Int Arch Photogramm Remote Sens Spat Inf Sci 48:153–162

Nocerino E, Menna F, Remondino F, Toschi I, Rodr\'\iguez-González P (2017) Investigation of indoor and outdoor performance of two portable mobile mapping systems. In: Videometrics, Range Imaging, and Applications XIV. pp 125–139

Nüchter A, Elseberg J, Janotta P (2017) Towards Mobile Mapping of Underground Mines. In: Benndorf J, Buxton M (eds) Proceedings of Real Time Mining - International Raw Materials Extraction Innovation Conference. TU Bergakademie Freiberg, Amsterdam, pp 27–37

Petracek P, Kratky V, Petrlik M, Baca T, Kratochvil R, Saska M (2021) Large-scale exploration of cave environments by unmanned aerial vehicles. IEEE Robot Autom Lett 6:7596–7603

Quigley M, Conley K, Gerkey B, Faust J, Foote T, Leibs J, Wheeler R, Ng AY, others (2009) ROS: an open-source Robot Operating System. In: ICRA workshop on open source software. pp 5–10

Reinke A, Palieri M, Morrell B, Chang Y, Ebadi K, Carlone L, Agha-Mohammadi A-A (2022) LOCUS 2.0: robust and computationally efficient lidar odometry for real-time 3D mapping. IEEE Robot Autom Lett 7:9043–9050

Ren Z, Wang L, Bi L (2019) Robust GICP-based 3D LiDAR SLAM for underground mining environment. Sensors 19:2915

RIEGL Laser Measurement Systems GmbH (2019) RiSCAN PRO Operating & Processing Software

Riegl VZ-400i Datasheet (2019) http://www.riegl.com/uploads/tx_pxprieqldownloads/RIEGL_VZ-400i_Datasheet_2022-09-27.pdf. Accessed 30 Aug 2023

Rogers JG, Gregory JM, Fink J, Stump E (2020) Test Your SLAM! The SubT-Tunnel dataset and metric for mapping. In: 2020 IEEE International Conference on Robotics and Automation (ICRA). IEEE

Schops T, Schonberger JL, Galliani S, Sattler T, Schindler K, Pollefeys M, Geiger A (2017) A multi-view stereo benchmark with high-resolution images and multi-camera videos. In: Proceedings of the IEEE conference on computer vision and pattern recognition. pp 3260–3269

Schubert D, Goll T, Demmel N, Usenko V, Stuckler J, Cremers D (2018) The TUM VI benchmark for evaluating visual-inertial odometry. In: 2018 IEEE/RSJ International Conference on Intelligent Robots and Systems (IROS). IEEE

Seetharaman G, Lakhotia A, Blasch EP (2006) Unmanned vehicles come of age: the DARPA grand challenge. Computer 39:26–29

Smith M, Baldwin I, Churchill W, Paul R, Newman P (2009) The new college vision and laser data set. Int J Rob Res 28:595–599

Stach E, Pawłowska A, Matoga Ł (2014) The development of tourism at military-historical structures and sites–a case study of the building complexes of project riese in the owl mountains. Pol J Sport Tour 21:36–41

Sturm J, Engelhard N, Endres F, Burgard W, Cremers D (2012) A benchmark for the evaluation of RGB-D SLAM systems. In: 2012 IEEE/RSJ International Conference on Intelligent Robots and Systems. IEEE

Szrek J, Wodecki J, Błażej R, Zimroz R (2020) An inspection robot for belt conveyor maintenance in underground MineInfrared thermography for overheated idlers detection. Appl Sci 10:4984. https://doi.org/10.3390/app10144984

Tak AN, Taghaddos H, Mousaei A, Bolourani A, Hermann U (2021) BIM-based 4D mobile crane simulation and onsite operation management. Autom Constr 128:103766. https://doi.org/10.1016/j.autcon.2021.103766

Thrun S, Hahnel D, Ferguson D, Montemerlo M, Triebel R, Burgard W, Baker C, Omohundro Z, Thayer S, Whittaker W (2003) A system for volumetric robotic mapping of abandoned mines. In: 2003 IEEE International Conference on Robotics and Automation (Cat. No. 03CH37422). pp 4270–4275

Torresani A, Menna F, Battisti R, Remondino F (2021) A V-SLAM guided and portable system for photogrammetric applications. Remote Sens 13: 2351 https://doi.org/10.3390/rs13122351

Toschi I, Rodríguez-Gonzálvez P, Remondino F, Minto S, Orlandini S, Fuller A (2015) Accuracy evaluation of a mobile mapping system with advanced statistical methods. Int Arch Photogramm Remote Sens Spatial Inform Sci. https://doi.org/10.5194/isprsarchives-XL-5-W4-245-2015

Toschi I, Ramos MM, Nocerino E, Menna F, Remondino F, Moe K, Poli D, Legat K, Fassi F et al (2017) Oblique photogrammetry supporting 3D urban reconstruction of complex scenarios. Int Arch Photogramm Remote Sens Spatial Inform Sci 42:519–526

Tranzatto M, Dharmadhikari M, Bernreiter Lukas and Camurri M, Khattak S, Mascarich Frank and Pfreundschuh P, Wisth D, Zimmermann S, Kulkarni M, Reijgwart V, Casseau B, Homberger T, De Petris P, Ott Lionel and Tubby W, Waibel G, Nguyen H, Cadena C, Buchanan R, Wellhausen L, Khedekar N, Andersson O, Zhang L, Miki T, Dang T, Mattamala M, Montenegro M, Meyer K, Wu X, Briod A, Mueller M, Fallon M, Siegwart R, Hutter M, Alexis K (2022) Team CERBERUS wins the DARPA Subterranean Challenge: Technical overview and lessons learned. arXiv preprint arXiv:220704914

Trybała P (2021) LiDAR-based Simultaneous Localization and Mapping in an underground mine in Złoty Stok, Poland. In: IOP Conference Series. Earth and Environmental Science

Trybała P, Szrek J, Remondino F, Wodecki J, Zimroz R (2022) Calibration of a multi-sensor wheeled robot for the 3D mapping of underground mining tunnels. Int Arch Photogramm Remote Sens Spatial Inform Sci. https://doi.org/10.5194/isprs-archives-xlviii-2-w2-2022-135-2022

Trybała P, Kasza D, Wajs J, Remondino F (2023) Comparison of low-cost handheld lidar-based slam systems for mapping underground tunnels. Int Arch Photogramm Remote Sens Spat Inf Sci 48:517–524

Trzeciak M, Pluta K, Fathy Y, Alcalde L, Chee S, Bromley A, Brilakis I, Alliez P (2023) ConSLAM: construction data set for SLAM. J Comput Civ Eng 37:4023009

Vallet B, Mallet C (2016) 2—urban scene analysis with Mobile mapping technology. In: Baghdadi N, Zribi M (eds) Land surface remote sensing in urban and coastal areas. Elsevier, pp 63–100

Wang C, Wang W, Qiu Y, Hu Y, Scherer S (2020a) Visual memorability for robotic interestingness via unsupervised online learning. Computer vision—ECCV 2020. Springer International Publishing, Cham, pp 52–68

Wang W, Zhu D, Wang X, Hu Y, Qiu Y, Wang C, Hu Y, Kapoor A, Scherer S (2020b) TartanAir: A dataset to push the limits of visual SLAM. In: 2020 IEEE/RSJ International Conference on Intelligent Robots and Systems (IROS). IEEE

Xu W, Cai Y, He D, Lin J, Zhang F (2022) Fast-lio2: fast direct lidar-inertial odometry. IEEE Trans Rob 38:2053–2073

Yang X, Lin X, Yao W, Ma H, Zheng J, Ma B (2022) A robust LiDAR SLAM method for underground coal mine robot with degenerated scene compensation. Remote Sens 15:186

Zlot R, Bosse M (2013) Efficient large-scale 3D mobile mapping and surface reconstruction of an underground mine. In: Field and service robotics: Results of the 8th international conference. pp 479–493

Publication 6: Designing and Evaluating a Portable LiDAR-Based SLAM System

DESIGNING AND EVALUATING A PORTABLE LIDAR-BASED SLAM SYSTEM

P. Trybała [1,2], P. Kujawa[1], K. Romańczukiewicz[1], A. Szrek[1], F. Remondino[2]

[1] Faculty of Geoengineering, Mining and Geology, Wrocław University of S cience and Technology, Na Grobli 15, 50-421 Wrocław,
Poland - Email: (pawel.trybala, paulina.kujawa, kinga.romanczukiewicz, aleksandra.szrek)@pwr.edu.pl

[2] 3D Optical Metrology (3DOM) unit, Bruno Kessler Foundation (FBK), Trento, Italy – Email: (ptrybala, remondino)@fbk.eu

ABSTRACT

Mobile Mapping Technology (MMT) has evolved rapidly over the past few decades, especially in using low-cost sensors. This progress is primarily attributed to the appearance of innovative simultaneous localization and mapping (SLAM) algorithms. This article focuses on evaluating the efficiency of a new LiDAR-based portable SLAM system for mapping in dynamic real-world environments. The work proposed a technical solution based on a Livox Avia LiDAR sensor enhanced by gimbal stabilization. The system, named Portable Livox-based Mapping system (PoLiMap), is compared to other similar solutions by acquiring data from various environments, including urban sceneries, underground tunnels and forested areas, and processing them using a modified FAST-LIO-SLAM algorithm. The research presented in the article contributes to the understanding of the capabilities of PoLiMap systems under various conditions and offers significant insight into its potential applications. Accuracy evaluation results prove that the proposed MMT system can successfully tackle various demanding environments and challenge the results of other more costly state-of-the-art portable mobile laser scanning methods.

KEY WORDS: Mobile Mapping, 3D reconstruction, Evaluation, Low-Cost, Urban mapping, Forest mapping, Cultural heritage.

1. INTRODUCTION

Advances in currently available technologies have greatly simplified the process of terrestrial 3D mapping in various conditions. However, different factors present in multiple environments, including dynamic objects, limited GNSS coverage, underground passages, reflective surfaces, dense and ever-changing vegetation, varying exposure to sunlight and more, pose a great challenge for developing a universal mobile mapping solution (Ali et al., 2020; Cheng et al., 2022). Achieving efficient 3D data collection and accurate reconstruction is possible with the use of Mobile Mapping Technologies (MMT) Systems. These devices equipped with different sensors, such as LiDARs (Elhashash et al., 2022; Ismail et al., 2022), radars (Rouveure et al., 2021; Glira et al., 2022) or cameras (Kolhatkar and Wagle, 2020; Torresani et al., 2021), enable the generation of precise and dense point clouds providing information about the geometric characteristics of the investigated area. The software backbone of MMTs is a Simultaneous Localization And Mapping (SLAM) method, either based on image or range data. SLAM allows to construct a map of the unknown environment while simultaneously estimating the sensor pose, and thus its trajectory during movement (Debeunne and Vivet, 2020). MMT sensors can be mounted on an autonomous robot (Wang et al., 2018), placed aboard a ground vehicle (Singandhupe and La, 2019) or UAV (Sonugür, 2023), but can also be used as a handheld device (Torresani et al., 2021).

The principle of the currently prevailing pose graph approach to solving the SLAM problem can be split into two main components: LiDAR or visual odometry and graph optimization. The former is responsible for continuous association of the data collected by the sensors at subsequent frames, either through direct methods, or using feature extraction and matching for estimating the relative change of the sensor pose in the analyzed period. Those estimates constitute the main factor in the pose graph, which together with other available data, can be useful for calculating the sensor motion (inertial measurements, GNSS observations, landmark positions) is optimized in the backend to produce the final, adjusted sensor trajectory results and thus, allowing accumulating all measurements in a coherent, global

map (He et al., 2022). In this study, one of the open-source LiDAR-based SLAM frameworks, FAST-LIO-SLAM (Kim et al., 2022a), is revisited, with the focus on improving its accuracy and robustness.

The need of developing such solution is to ensure user-friendly acquisitions and quality mapping results in challenging conditions, such as those of irregular, underground tunnels. This lies in the EIT-RM projects VOT3D - Ventilation Optimizing Technology based on 3D-scanning VOT3D which aims to reform the current ventilation design approach by incorporating accurate and detailed 3D surveying and modeling of airways (Figure 1) in airflow simulations. The introduction of modern methods and innovative solutions for underground optimisation in mining scenarios based on 3D data is crucial for the resources sector. The utilization of MMT in underground environments, despite being a challenge, is a key factor enabling realistic simulations of the ventilation system's operation within an industrial underground mine (Janus and Ostrogórski, 2022; Wróblewski et al., 2023). An understanding of the limitations and achievable quality standards associated with 3D data surveys performed in such peculiar environment is therefore important to guarantee the reliability of the entire optimisation process.
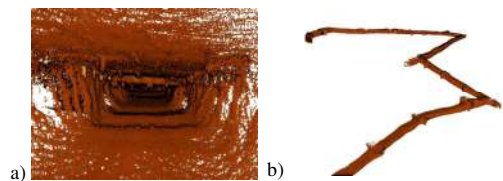
Figure 1. One of the underground test sites of the VOT3D project, surveyed with the proposed MMT system: view from inside the tunnel (a) and side view of the mining tunnel (b).

1.1 Paper aims

In the past, various SLAM systems and algorithms have been tested for 3D reconstruction of cultural heritage objects (Di

The International Archives of the Photogrammetry, Remote Sensing and Spatial Information Sciences, Volume XLVIII-1/W3-2023
2nd GEOBENCH Workshop on Evaluation and BENCHmarking of Sensors, Systems and GEOspatial Data
in Photogrammetry and Remote Sensing, 23–24 October 2023, Krakow, Poland

Stefano et al., 2021; Perfetti and Fassi, 2022), mapping of underground and underwater scenario (Farella, 2016; Menna et al., 2023; Trybała et al., 2023a), or natural environments such as forests (Qian et al., 2016; Hyyppä et al., 2020). However, a rapid progress in the developments in both hardware and software in MMTs has democratised the use of low-cost, reliable and increasingly accurate in-house-built SLAM-based systems. Thus, the aim of this paper is multi-folds:

(i) to assemble a 3D surveying measurement system based on a Livox Avia LiDAR sensor stabilized with a gimbal and designed to be easily carried by an operator or placed on a vehicle;

(ii) to couple the proposed handheld system, based on a solid-state LiDAR, with a state-of the art pose graph SLAM approach for real-time 3D mapping;

(iii) to perform a metrological assessment of the proposed low-cost, lightweight MMT system in different environments (urban space, underground tunnel and forestry), using accurate ground truth data;

(iv) to compare the proposed MMT system with other available mobile mapping solutions (GeoSLAM mobile scanner, multi-camera in-house photogrammetric system).

Data acquired with the proposed setup with and without the laser scanner mounted on a gimbal were also compared. The quality of both IMU signals and resulting point clouds were analyzed with the goal of assessing the extent to which external stabilization of the scanner improves data quality and reduces motion artefacts.

2. RELATED WORKS

Methods for acquiring 3D point clouds and assessing their accuracy to ensure their suitability for further analysis has been discussed repeatedly in the literature (Di Stefano et al., 2021; Tanduo et al., 2022; Trybała et al., 2023). The development of reality-based 3D surveying instruments and methods, and in particular MMT, has represented a significant progress in data acquisition in various environments. Application of MMT using SLAM algorithms in a complex urban environment was presented in Wang et al. (2018). In its review Mobile Laser Scanning (MLS) solutions, GNSS, IMU and applications are presented. Similarly, examination was carried out in the historic part of the urban centre of Venice by Tanduo et al. (2022), involving selected SLAM solutions, using a commercial backpack-mounted system and a handheld scanner. This assessment involved a comparative analysis of point clouds against TLS-derived ground truth data.

The use of a TLS and SLAM-based method in forest area mapping is described in Bienert et al. (2018) whereas Pan et al. (2023), present a system that integrates a dual laser scanners and an IMU system. Similar comparisons and combinations of SLAM-based methodologies with TLS data in forest areas are presented in Pierzchała et al. (2018), and Shao et al. (2020).

Nocerino et al. (2017) evaluated portable MMT in indoor and outdoor scenarios. Comparative analyses of point clouds acquired using commercial LiDAR-based SLAM algorithms and portable, mobile scanning devices are presented in Sesmero et al. (2021), Fasiolo et al. (2023), Trybała et al. (2023a).

Prados Sesmero et al. (2021) introduced an algorithm of graph SLAM applied in diverse environments, with particular emphasis on narrow, longitudinal facilities, especially tunnels, in which missing features and the problematic separation of different positions in the environment create difficulties to answer. Indoor and outdoor mapping studies on the performances of different SLAM algorithms in 3D mapping is presented in Akpınar (2021).

3. PROPOSED SYSTEM

The Portable Livox-based Mapping (PoLiMap) system was designed for convenient mobility during surveying operations. The LiDAR Livox Avia sensor (Table 1) is placed on a gimbal to ensure smooth motion and a secured grip, even when the sensor is used on a high speed vehicle (car, motorcycle). A NVIDIA Jetson Xavier board running Robot Operating System (ROS) as well as the rest of the necessary equipment (power supplies, Livox Converter 2.0, external drive and screen tablet) are placed in a suitcase (Figure 2).

Laser wavelength	905 nm	
Max. detection range (@ 100 klx)	From 190 m @ 10% reflectivity to 320 m @ 80% reflectivity	
Range precision	2 cm @ 100 m	
Angular precision	0.05°	
Scanning rate	10 Hz	
Scanning pattern	Line	Circular
Scanning mode	Repetitive	Non-repetitive
Field of view (horizontal x vertical)	70.4° x 4.5°	70.4° x 77.2°
Point rate	From 240,000 points/s to 720,000 points/s (triple return)	
Beam divergence	horizontal: 0.03° vertical: 0.28°	
Data Latency	$\leq$ 2 ms	
Weight	0.5 kg	

Table 1. Livox Avia specification (Livox Avia Quick Start Guide v1.4, 2021).

Figure 2. Assembled PoLiMap and its equipment.

For processing the LiDAR data, the system runs a FAST-LIO LiDAR odometry (Kim et al., 2022a): it estimates the change in sensor pose based on inertial measurements coupled with subsequent point cloud matching with a point-to-plane iterative closest point (ICP) algorithm in a frame-to-local map manner. Moreover, it utilizes Scan Context++ (Kim et al., 2022b) as a loop closure detector and GTSAM-based pose graph optimization (Dellaert et al., 2022).

The International Archives of the Photogrammetry, Remote Sensing and Spatial Information Sciences, Volume XLVIII-1/W3-2023
2nd GEOBENCH Workshop on Evaluation and BENCHmarking of Sensors, Systems and GEOspatial Data
in Photogrammetry and Remote Sensing, 23–24 October 2023, Krakow, Poland

Due to past critical evaluations of SLAM frameworks (Trybała et al., 2023a) and other internal tests, several improvements have been implemented in FAST-LIO-SLAM librar:

- loop closure improvement: in the original implementation (Kim et al., 2022a), authors assumed constant, a priori assigned covariance values of each constraint in the pose graph. We used real covariance estimates for each measurement component, resulting from point cloud registration results in LiDAR odometry and fast generalized ICP-based (Koide, 2021) loop closures.

- loop candidate identification: we allow using intensity-based Scan Context++ (Kim et al., 2022b) instead of height-based default version to tackle scenarios with huge variations of LiDAR scanner orientation, such as handheld mapping of nnarrow spaces. Moreover relaxed parameter values for accepting a candidate loop detection to make Scan Context++ act as a quick heuristic of finding several reasonable candidates.

- rigorous loop closure verification: first the point clouds around both the historic and previous pose are aggregated in their neighbourhoods using current trajectory estimates and then downsampled with a rough-resolution voxel filter. The alignment is performed using fast voxelized generalized ICP (FastVGICP; Koide, 2021), assuming only a partial overlap between matched point clouds. It allows to reject in real-time multiple incorrect loop closures and provide a good initial guess for the precise registration, which is performed using FastGICP at much finer resolution if the matching error threshold is passed. Pre-aligning the point clouds facilitates achieving final convergence of the algorithm and speeds up the process.

- alternative metric computation: the registration error is usually computed as the root mean square error (RMSE) of the entire aligned point clouds. In our approach we limit the set of points included in the RMSE calculation to the same predefined overlap ratio used for registration or use percentile Hausdorff distance of a corresponding ratio.

Finally, a final check is performed if the loop candidate passes those tests. A hypothetical loop constrain is temporarily added to the pose graph. After optimizing the graph, adjustment error is computed, and if adding the loop causes a severe graph deformation, the hypothesis is rejected. This acts as an additional sanity check and reduces the number of incorrectly detected loops in distant areas similar to each other, which is a risk, e.g., in simple indoor environments.

All these changes aim to achieve centimeter-level loop closure and 3D mapping accuracy even in cases of very different sensor orientations and partial point cloud overlap, while still maintaining a reasonable speed of computations.

Although the implemented changes can add a noticeable overhead to the computation time, the results are obtained in close to real-time and the surveying process is not disturbed. In the worst case of loop closure detection and verification or pose graph optimisation taking too much time, LiDAR odometry with the resulting non-optimized point cloud is still performed in real-time thanks to the original multi-threaded implementation of the framework. This trade-off however allows to obtain more accurate results of 3D mapping through increasing robustness of utilizing loops in the pose graph, as well as improving its accuracy through multi-resolution point cloud registration. Finally, multiple variables, such as selection of a robust kernel for each type of pose graph constraint and variables of abovementioned new elements of the framework, have been additionally exposed as ROS parameters, allowing its easier adaptation to challenging mapping conditions.

4. EVALUATION

4.1 Test scenarios

To exhaustive evaluate the performances of the assembled 3D surveying system, different scenarios are chosen:

- a part of the campus of Wroclaw University of Science and Technology (WUST) in Poland: the scene is particularly interesting because of its buildings of various sizes, geometries, surface types (concrete, glass, etc.) and architectural styles. The scene belongs to the MIN3D dataset (Trybala et al., 2023b):

- a single deciduous tree from the forest area representing the types of tall trees (height of approx. 17 m).

- a tight up-hill underground tunnel ("100 Scalini"), part of a large World War I fortification structure located in Mount Celva, Trento (Italy). The site structure is similar to that found in caves or historical mining areas.

- a small forest area composed of different types of trees and representing a natural environmental scene with varied and irregular geometry.

Additionally, a part of a tree-lined cobblestone street in an urban area was used to perform an ablation study of the proposed PoLiMap system (Section 5.1). The use case was selected for comparison of the system with and without the use of a gimbal to assess the impact of its use in scenarios of mapping environments with heavy vibrations.

4.2 Quality assessment methodology

To evaluate the quality of the data acquired with the proposed 3D surveying system, the SLAM-based points clouds were compared with ground truth (GT) data obtained using terrestrial laser scanning (TLS) or photogrammetry. The summarized scenarios with GT are included in Table 2.

For the campus WUST and single tree case studies, the GT point cloud was acquired with a RIEGL VZ-400i pulse TLS. The manufacturer's declared accuracy of a single point is 5 mm, and the precision is 3 mm. Data processing including scan cloud cleaning, filtering, registration, and adjustment was performed in specialized RiSCAN PRO software.

For the other underground study area, GT data were acquired using a Leica BLK2GO mobile scanner. Additionally, the results were compared to two other point clouds, generated by a GeoSLAM ZEB Horizon and with a portable multi-camera photogrammetric system (Perfetti et al., 2022).

For the quantitative assessment of the produced 3D data, registered with the method proposed in Section 3, the Multiscale Model-to-Model Cloud Comparison (M3C2) method (Lague et al., 2013) against the GT point cloud was used and statistics were calculated to determine mapping error values. Accuracy and completeness analysis was also carried out (Knapitsch et al., 2017; Trybała et al., 2023a).

Scenario	Approx. size	Reference data
Outdoor university campus	60 x 20 m, 15 m height	RIEGL VZ-400i
Single tree	17 m height, 10 m (crown), 0.5 m (trunk) diameter	RIEGL VZ-400i
WWI tunnel	50 m length	BLK2GO, Zeb Horizon, photogrammetry
Forest area	60 x 40 m, 20 m height	BLK2GO

Table 2. Summarized case studies with reference data.

The International Archives of the Photogrammetry, Remote Sensing and Spatial Information Sciences, Volume XLVIII-1/W3-2023
2nd GEOBENCH Workshop on Evaluation and BENCHmarking of Sensors, Systems and GEOspatial Data
in Photogrammetry and Remote Sensing, 23–24 October 2023, Krakow, Poland

5. RESULTS

3D visualizations of the resulting point clouds along with close-ups are shown in Figure 3. The point clouds represent three different environments: urban, underground and natural. Urban environments include dense open spaces with complicated geometry of buildings and urban infrastructure, interspersed with natural elements such as trees, shrubs and plants. Acquiring 3D data for the uppermost parts of high buildings can be a challenge due to the scanner's limited range. In contrast, closed spaces, of which an underground tunnel is an example, do not cause such issues, but the data may be degraded or sparse due to multiple occlusions or lack of geometrical features. The last scenario, represented by a forest, is one of the most difficult environments for 3D reconstruction due to the scattering of points caused by leaves or branches. The resulting point cloud is non-uniform with increased level of random noise in the tree crowns.


(a)   (b)   (c)
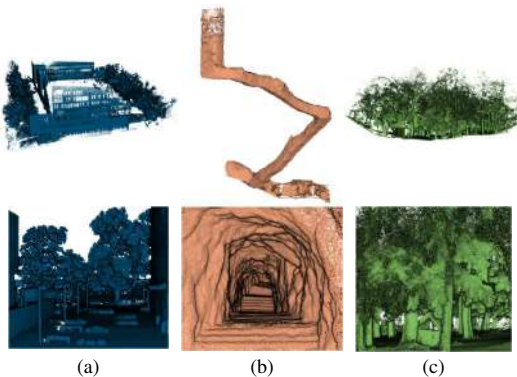
Figure 3. Visual impressions of the point clouds obtained with the proposed 3D surveying system: a fragment of the WUST campus (a), "100 Scalini" cultural heritage site (b) and the foresty area (c).

Figures 4 – 7 present the 3D reconstructions of selected objects acquired with the proposed portable PoLiMap system and their comparison to reference data. Statistics from those comparisons are compiled in Table 3.

For the WUST scenario, an analysis of specific man-made elements, including two building facades and a concrete substrate, reveals the smallest error on the ground level and a relatively larger error on the farther one of the building walls, partially obstructed by a fence. However, 95% of point were within 7 cm distance to the reference point cloud (Figure 4-top). For the tree object, due to occlusions and natural instability, tree foliage contains a lot of noise. The smallest deviations are observed on the outer parts of the crown the trunk, where standard deviation of M3C2 distances reaches 5.5 cm (Figure 4 – ceter ad bottom). Noteworthy to say that the general shape of the tree with its crown can still be distinguished.

For both cases, it can be noticed that the point cloud generated from the PoLiMap system shows a lower point density (approx. 800 points/m^2 for WUST campus and 700 points/m^2 for single tree) compared to the data collected with TLS (6600 points/m^2 and 1500 points per m^2, respectively).
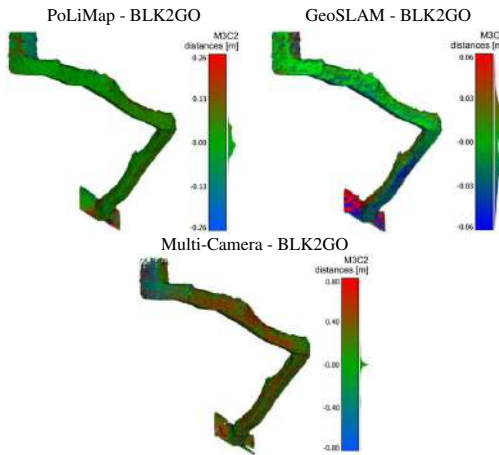
PoLiMap   TLS   COMPARISON
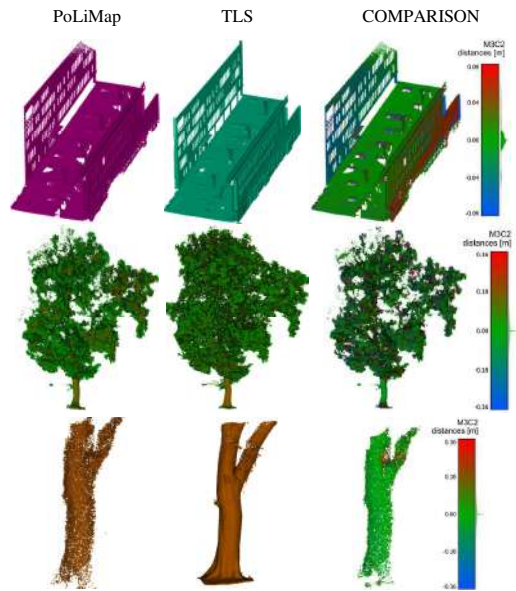
Figure 4. M3C2 comparison of point clouds from PoLiMap and TLS: a part of the WUST campus (top) and a single tree of the forest areas (center and bottom).

For the underground case, data obtained from the PoLiMap system, GeoSLAM and multi-camera photogrammetric solutions were benchmarked against data obtained from Leica BLK2GO mobile scanner. The Leica handheld solution offers a high measurement rate of 420,000 points per second, with a range noise of +/-3 mm and an indoor accuracy of +/-10 mm. Comparison with reference data showed very comparable mapping results of GeoSLAM and Livox. Both of them achieved standard deviations in the M3C2 comparisons (Figure 6) below 4 cm. The photogrammetric solution, although maintaining a correct shape of the tunnel, generated a slightly more noisy point cloud with the trajectory affected by a drift error. The errors were mostly accumulated in the vertical shaft at the end of the tunnel, which due to the constrained space could be captured from very limited perspectives, creating short baselines for the 3D reconstruction. As indicated in Table 3, excluding this part of the tunnel leads to achieving median error at level in line with other tested solutions. For all systems, the biggest differences, amounting to several centimeters, are noticeable at the inlet and outlet of the tunnel.
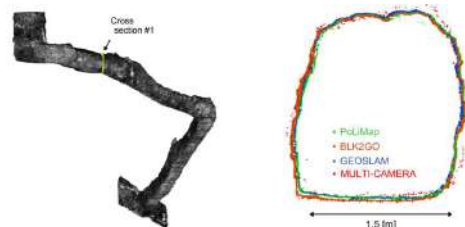

Figure 5. Visualization of the reference point cloud from "100 Scalini" (left) and the compared cross sections (right).

The International Archives of the Photogrammetry, Remote Sensing and Spatial Information Sciences, Volume XLVIII-1/W3-2023
2nd GEOBENCH Workshop on Evaluation and BENCHmarking of Sensors, Systems and GEOspatial Data
in Photogrammetry and Remote Sensing, 23–24 October 2023, Krakow, Poland

Figure 6. M3C2 comparison of point clouds from PoLiMap, GeoSLAM and ANT3D with respect to the BLK2GO for the underground case.

For the forest test site, the smallest M3C2 values occur on the ground and tree trunks. Larger differences are found in tree crowns due to the difficulty in mapping leaf objects and possible dynamics. This park area of approximately 60 x 40 m has been densely mapped with multiple, successfully recognized loop closures and repeated parts of the trajectory. No shadows or double object errors in the point cloud have been observed, despite this being a common issue with processing similar trajectories. Final standard deviation of the M3C2 distances to the reference BLK2GO data reached 13.8 cm, mostly due to the tree crowns. Using a robust error metric such as median absolute deviation, the obtained error was equal to 1.2 cm.
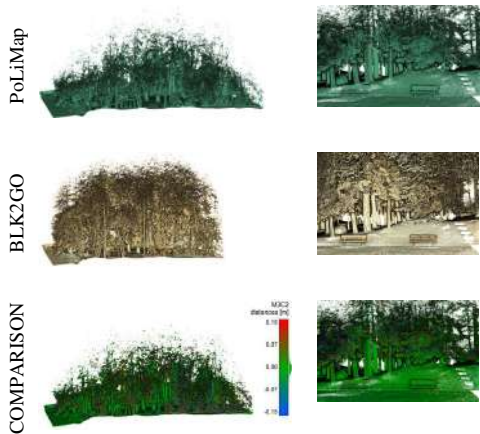

Figure 7. M3C2 comparison of point clouds from PoLiMap and BLK2GO for the forest case.

The quality assessment in the form of completeness and accuracy estimation is provided by Figure 8. Together with previous accuracy analysis, it allows to draw final conclusions from the evaluation of proposed system. Summarizing the achieved errors, it can be seen that the investigated PoLiMap system is well-suited

for mapping both indoor and outdoor environments. Urban spaces were reconstructed with mapping errors not exceeding 5 cm for 95% of points and completeness of above 90% for 10 cm threshold (Figure 8a). For underground environment, the reconstruction accuracy and the mapping completeness of Livox point cloud were similar to results of GeoSLAM. Both methods performed fantastically, approaching close to 100% metrics for distance thresholds of 5-6 cm (Figure 8b). The case study of tree and forest were also mapped with correct topology and a reasonable accuracy, although visibly degraded in foliage of the plants. While the accuracy metric reached 90% for 10 cm and 5 cm thresholds respectively, the completeness plateaued earlier, barely exceeding 80% in both cases for the highest considered threshold of 20 cm (Figures 8c and 8d). Moreover, as seen in Table 3, in almost all analysed cases median absolute deviation of comparisons to reference data was below 2.5 cm (besides foliage-rich single tree example). Considering that the measurement accuracy of a single point of the Livox scanner is 2 cm, the obtained accuracy values can be considered satisfactory and effective in the tested scenarios.

Mapping error [mm]	WUST campus	Underground				Tree		Forest
		PoLi-Map	Geo-SLAM	ANT 3D	ANT3D (without vertical shaft)	All points	Tru-nk	
Mean	1	-1	0	-12	11	1	5	1
Median	0	-1	3	4	4	0	0	0
Standard deviation	61	38	36	152	89	236	55	136
Median absolute deviation	10	24	18	29	21	62	7	11
95th percentile	71	65	52	362	160	53	90	91

Table 3. Mapping error values for the applied LiDAR SLAM algorithm.
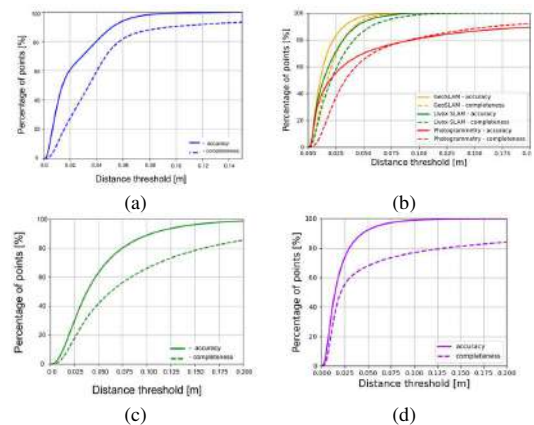

Figure 8. Accuracy and completeness curves for the proposed MMT system in all study sites: (a) WUST campus, (b) underground, (c) tree and (d) forest.

The International Archives of the Photogrammetry, Remote Sensing and Spatial Information Sciences, Volume XLVIII-1/W3-2023
2nd GEOBENCH Workshop on Evaluation and BENCHmarking of Sensors, Systems and GEOspatial Data
in Photogrammetry and Remote Sensing, 23–24 October 2023, Krakow, Poland

5.1 Ablation study

An ablation study is performed to evaluate whether the gimbal stabilization is bringing benefit to the final SLAM-based 3D point clouds.

Therefore additional measurements were taken in two scenarios: with and without the gimbal. The PoLiMap system was mounted on a vehicle which followed the same route two times. The 3D data captured in both scenarios were examined extracting various fragments from the data, visually comparing and calculating the root mean square error (RMSE) of fitting geometric primitives to point cloud subsets, representing several clearly distinguishable objects (tree trunks, flat elements of a facade). A set of the cross-sections is shown in Figure 9. It is noticeable that the noise level is slightly lower in the point clouds acquired with the scanner coupled to the gimbal, which proves that the device has successfully fulfilled its main function. In addition, RMSE were calculated using the fitted circle or plane and point clouds obtained with and without the stabilization device. The results in Table 4 show that smaller values are consistently observed in all cases where the gimbal was used.
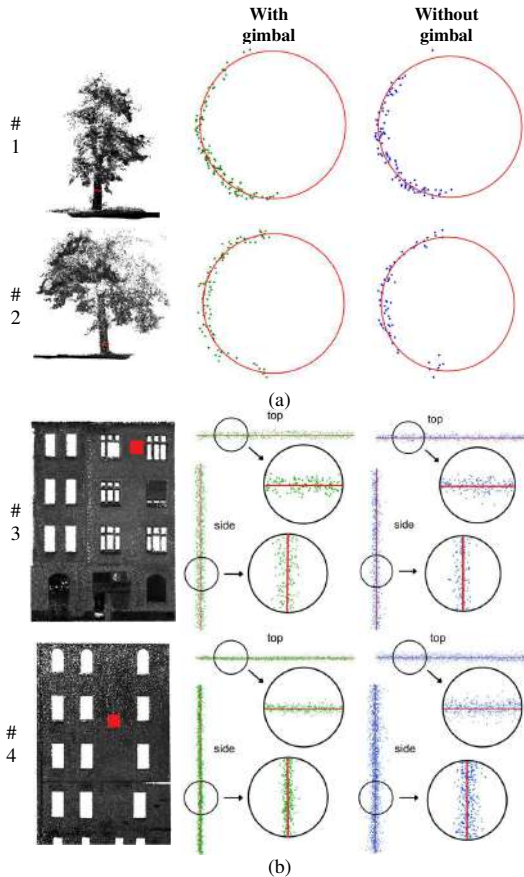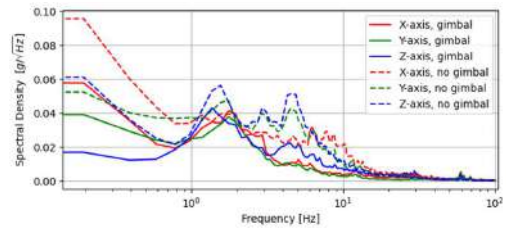
Object	With gimbal	Without gimbal
#1	15	19
#2	17	20
#3	14	15
#4	8	16

Table 4. The value of the RMSE [in mm] between the fitted circle/plane and the point cloud.

Moreover, within the ablation study, we decided to quantify the difference in IMU noise levels using Power Spectral Density (PSD) analysis, which is one of the common metrics for this purpose and allows comparison of different signals in terms of their energy (Nirmal et al., 2016). PSDs were calculated using Welch's method (Welch, 1967). Resulting plots for accelerometer and gyroscope data are presented in Figures 10 and 11. Mean noise densities are compiled in Table 5. All signals from unstabilized scanner case exhibit clearly higher energy levels, especially considering higher frequencies. While the difference in mean noise values for the accelerometer varies from 50% to 100% of higher noise for the scenario without gimbal, the increase in the gyroscope mean noise density reaches over 600%. Since IMU measurements quality degradation can influence both short-term trajectory estimation and correction of point cloud distortion caused by the sensor motion, the use of a stabilization solution in conditions with possible external sources of vibrations or shaking (vehicle moving on an uneven ground, heavy machinery, etc.) can clearly contribute to improving accuracy, precision and stability of the mobile mapping system.

Figure 10. Power Spectral Density of the acceleration measurements in the ablation study: with gimbal (solid lines) and without gimbal (dashed lines). Frequency in a log scale.

Figure 11. Power Spectral Density of the gyroscopic measurements in the ablation study: with gimbal (solid lines) and without gimbal (dashed lines). Frequency in a log scale.

Figure 9. Examples of point cloud cross sections: trees with fitted trunk circles (a) and building walls with fitted planes (b).

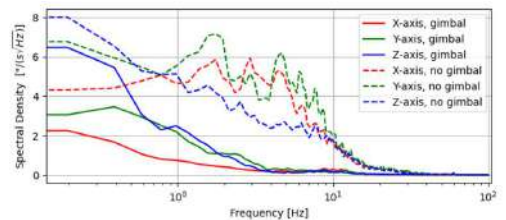The International Archives of the Photogrammetry, Remote Sensing and Spatial Information Sciences, Volume XLVIII-1/W3-2023
2nd GEOBENCH Workshop on Evaluation and BENCHmarking of Sensors, Systems and GEOspatial Data
in Photogrammetry and Remote Sensing, 23–24 October 2023, Krakow, Poland

Data	Axis	Mean noise density	
		Linear acceleration $[\frac{g}{\sqrt{Hz}}]$	Angular velocity $[\frac{\circ}{s\sqrt{Hz}}]$
With gimbal	X	0.0027	0.07
	Y	0.0022	0.10
	Z	0.0031	0.11
Without gimbal	X	0.0050	0.50
	Y	0.0044	0.60
	Z	0.0045	0.42

Table 5. Mean noise densities in the ablation study obtained with PSD analysis.

6. CONCLUSIONS

The research conducted in this article presents an evaluation of the proposed PoLiMap system in different environments (urban, natural and underground). The developed low-cost MMT solution consists of a Livox Avia LiDAR sensor and a gimbal for stabilization purposes. The acquired data for the various scenarios were processed using an improved SLAM algorithm and then compared with reference data from terrestrial laser scanning and other high-quality mobile mapping systems. The effectiveness of the stabilization tool was also proved by comparing quality of raw IMU and resulting 3D data collected with and without its use.

The comprehensive evaluation of the derived 3D data in the selected use cases shows how well the proposed system can perform in different conditions. The statistics obtained from the comparison with ground truth data highlight the potential and limitations of the system for accuracy and completeness when mapping a specific environment. In all use cases the obtained metrics show satisfactory performance of the system, with great results of mapping man-made structures and reasonable results of reconstructing geometry of natural, more dynamic objects.

Worth considering how the proposed MMT portable system can be applied in practice: industrial engineering, architecture or environmental monitoring. Prospects for future advances in PoLiMap system may include a comparative analysis between a configuration utilising a sensor affixed to a handheld gimbal and an alternative setup including portable, mobile scanning devices integrated into a backpack, widely used in case-studies. Even lower costs and high customization possibilities could facilitate easy adoption of the proposed system in different industries.

ACKNOWLEDGEMENTS

REFERENCES

Akpınar, B., 2021: Performance of different SLAM algorithms for indoor and outdoor mapping applications. *Applied System Innovation*, 4(4), 101.

Ali, I., Durmush, A., Suominen, O., Yli-Hietanen, J., Peltonen, S., Collin, J., Gotchev, A., 2020: FinnForest dataset: A forest landscape for visual SLAM. *Robotics and Autonomous Systems*, 132, 103610.

Bienert, A., Georgi, L., Kunz, M., Maas, H.-G., Von Oheimb, G., 2018: Comparison and Combination of Mobile and Terrestrial Laser Scanning for Natural Forest Inventories. *Forests*, 9, 395.

Cheng, J., Zhang, L., Chen, Q., Hu, X., Cai, J., 2022: A review of visual SLAM methods for autonomous driving vehicles. *Engineering Applications of Artificial Intelligence*, 114, 104992.

Debeunne, C., Vivet, D., 2020: A Review of Visual-LiDAR Fusion based Simultaneous Localization and Mapping. *Sensors*, 20(7).

Dellaert, F., GTSAM Contributors. Borglab/GTSAM. 4.2a8, Georgia Tech Borg Lab, 2022.

Di Stefano, F., Torresani, A., Farella, E. M., Pierdicca, R., Menna, F., Remondino, F., 2021: 3D Surveying of Underground Built Heritage: Opportunities and Challenges of Mobile Technologies. *Sustainability*, 13(23), 13289.

Elhashash, M., Albanwan, H., Qin, R., 2022: A Review of Mobile Mapping Systems: From Sensors to Applications. *Sensors*, 22(11), 4262.

Farella, E. M., 2016: 3D mapping of underground environments with a hand-held laser scanner. *Bollettino della società italiana di fotogrammetria e topografia*, (2), 1–10.

Fasiolo, D. T., Scalera, L., Maset, E., 2023: Comparing LiDAR and IMU-based SLAM approaches for 3D robotic mapping. *Robotica*, 1-17.

Glira, P., Weidinger, C., Kadiofsky, T., Pointner, W., Olsbock, K., Zinner, C., Doostdar, M., 2022: 3D mobile mapping of the environment using imaging radar sensors. *2022 IEEE Radar Conference (RadarConf22)*, IEEE.

He, X., Gao, W., Sheng, C., Zhang, Z., Pan, S., Duan, L., Zhang, H., Lu, X., 2022: LiDAR-Visual-Inertial Odometry Based on Optimized Visual Point-Line Features. *Remote Sensing*, 14(3).

Hyyppä, E., Yu, X., Kaartinen, H., Hakala, T., Kukko, A., Vastaranta, M., Hyyppä, J., 2020: Comparison of Backpack, Handheld, Under-Canopy UAV, and Above-Canopy UAV Laser Scanning for Field Reference Data Collection in Boreal Forests. *Remote Sensing*, 12(20).

Ismail, H., Roy, R., Sheu, L.J., Chieng, W. H., Tang, L. C., 2022: Exploration-Based SLAM (e-SLAM) for the Indoor Mobile Robot Using Lidar. *Sensors*, 22(4).

Janus, J., Ostrogórski, P., 2022: Underground Mine Tunnel Modelling Using Laser Scan Data in Relation toManual Geometry Measurements. *Energies*, 15(7), 2537.

Kim, G., Yun, S., Kim, J., Kim, A., 2022a: SC-LiDAR-SLAM: A Front-end Agnostic Versatile LiDAR SLAM System. *Proc. Int. Conference on Electronics, Information and Communication* (ICEIC), 1-6.

Kim, G., Choi, S., Kim, A., 2022b: Scan Context++: Structural Place Recognition Robust to Rotation and Lateral Variations in Urban Environments. *IEEE Transactions on Robotics*, 38(3), 1856-1874.

Knapitsch, A., Park, J., Zhou, Q. Y., Koltun, V., 2017: Tanks and temples: Benchmarking large-scale scene reconstruction. *ACM Transactions on Graphics (ToG)*, 36(4), 1-13.

The International Archives of the Photogrammetry, Remote Sensing and Spatial Information Sciences, Volume XLVIII-1/W3-2023
2nd GEOBENCH Workshop on Evaluation and BENCHmarking of Sensors, Systems and GEOspatial Data
in Photogrammetry and Remote Sensing, 23–24 October 2023, Krakow, Poland

Koide, K., Yokozuka, M., Oishi, S., Banno, A., 2021: Voxelized GICP for fast and accurate 3D point cloud registration. *IEEE International Conference on Robotics and Automation (ICRA),* 11054-11059.

Kolhatkar, C., Wagle, K., 2020: Review of SLAM algorithms for indoor mobile robot with LIDAR and RGB-d camera technology. *Lecture Notes in Electrical Engineering, Springer Singapore,* 397–409.

Lague, D., Brodu, N., Leroux, J., 2013: Accurate 3D comparison of complex topography with terrestrial laser scanner: Application to the Rangitikei canyon (N-Z). *ISPRS Journal of Photogrammetry and Remote Sensing*, 82, 10-26.

Livox Avia Quick Start Guide v1.4, 2021. Brochure. Accessed 25.09.2023:
https://terra-1-g.djicdn.com/65c028cd298f4669a7f0e40e50ba1131/Download/Avia/Livox%20Avia_Quick%20Start%20Guide_V1.4.pdf

Menna, F., Battisti, R., Nocerino, E., Remondino, F., 2023: FROG: a portable underwater mobile mapping system. Int. Arch. Photogramm. Remote Sens. Spatial Inf. Sci., XLVIII-1/W1-2023, 295–302

Nirmal K., Sreejith A. G., Mathew, J., Sarpotdar, M., Suresh, A., Prakash, A., Safonova, M., Murthy, J., 2016: Noise modeling and analysis of an IMU-based attitude sensor: improvement of performance by filtering and sensor fusion, *Proc. SPIE 9912,* 99126W.

Nocerino, E., Menna, F., Remondino, F., Toschi, I., Rodríguez-Gonzálvez, P., 2017: Investigation of indoor and outdoor performance of two portable mobile mapping systems. SPIE Proc. 10332.

Pan, D., Shao, J., Zhang, S., Zhang, S., Chang, B., Xiong, H., Zhang, W. 2023: SLAM-based Forest Plot Mapping by Integrating IMU and Self-calibrated Dual 3D Laser Scanners. *IEEE Transactions on Geoscience and Remote Sensing*.

Perfetti, L., Elalailyi, A., Fassi, F., 2022: Portable Multi-Camera System: from Fast Tunnel Mapping to Semi-Automatic Space Decomposition and Cross-Section Extraction. *International Archives of the Photogrammetry, Remote Sensing and Spatial Information Sciences*, 43, 259-266.

Perfetti, L. and Fassi, F., 2022: Handheld fisheye multicamera system: surveying meandering architectonic spaces in open-loop mode – accuracy assessment. *Int. Arch. Photogramm. Remote Sens. Spatial Inf. Sci.*, XLVI-2/W1-2022, 435–442.

Pierzchała, M., Giguère, P., Astrup, R., 2018: Mapping forests using an unmanned ground vehicle with 3D LiDAR and graphSLAM. *Computers and Electronics in Agriculture*, 145, pp. 217- 225.

Qian, C., Liu, H., Tang, J., Chen, Y., Kaartinen, H., Kukko, A., Zhu, L., Liang, X., Chen, L., Hyyppä, J., 2016: An Integrated GNSS/INS/LiDAR-SLAM Positioning Method for Highly Accurate Forest Stem Mapping. *Remote Sensing*, 9(1), 3.

Rouveure, R., Faure, P., Monod, M. O., 2021: Terrestrial mobile mapping based on a microwave radar sensor. Application to the localization of mobile robots. *ISPRS Annals of the Photogrammetry, Remote Sensing and Spatial Information Sciences*, V-1-2021, 73–80.

Sesmero, C. P., Lorente, S. V., Castro, M. D., 2021: Graph SLAM Built over Point Clouds Matching for Robot Localization in Tunnels. *Sensors*, 21(16), 5340.

Shao, J., Zhang, W., Mellado, N., Wang, N., Jin, S., Cai, S., Luo, L., Lejemble, T., Yan, G., 2020: SLAM-aided forest plot mapping combining terrestrial and mobile laser scanning. *ISPRS Journal of Photogrammetry and Remote Sensing*, 163, 214-230.

Singandhupe, A., La, H. M., 2019: A review of SLAM techniques and security in autonomous driving. *2019 Third IEEE International Conference on Robotic Computing (IRC)*, IEEE.

Sonugür, G., 2023: A Review of quadrotor UAV: Control and SLAM methodologies ranging from conventional to innovative approaches. *Robotics and Autonomous Systems*, 161, 104342.

Tanduo, B., Martino, A., Balletti, C., & Guerra, F., 2022: New Tools for Urban Analysis: A SLAM-Based Research in Venice. *Remote Sensing*, *14*(17), 4325.

Torresani, A., Menna, F., Battisti, R., Remondino, F., 2021: A V-SLAM Guided and Portable System for Photogrammetric Applications. *Remote Sensing*, 13(12), 2351.

Trybała, P., Kasza, D., Wajs, J., Remondino, F., 2023a: Comparison of low-cost handheld LiDAR-based SLAM systems for mapping underground tunnels. *The International Archives of the Photogrammetry, Remote Sensing and Spatial Information Sciences*, XLVIII-1/W1-2023, 517–524.

Trybała, P., Szrek, J., Remondino, F., Kujawa, P., Wodecki, J., Balchowski, J., Zimroz, R., 2023b: MIN3D dataset: MultI-seNsor 3D mapping with an unmanned ground vehicle. *PFG – Journal of Photogrammetry, Remote Sensing and Geoinformation Science*, in press.

Wang, M., Long, X., Chang, P., Padlr, T., 2018: Autonomous robot navigation with rich information mapping in nuclear storage environments. *2018 IEEE International Symposium on Safety, Security, and Rescue Robotics (SSRR)*, IEEE, 1-6.

Welch, P., 1967: The use of the fast Fourier transform for the estimation of power spectra: A method based on time averaging over short, modified periodograms, *IEEE Trans. Audio Electroacoust.*, 15, 70-73.

Wróblewski, A., Trybała, P., Banasiewicz, A., Zawiślak, M., Walerysiak, N., Wodecki, J., 2023: Possibilities of 3D laser scanning data utilization for numerical analysis of airflow in mining excavations. *IOP Conference Series: Earth and Environmental Science*, 1189(1), 012009.